

**Preparation and characterization of ionic liquid
based microemulsions and their application
in catalysis**

Shaila Alam

December 2016

Preparation and characterization of ionic liquid based microemulsions and their application in catalysis

A Dissertation Submitted to University of Dhaka for the Partial Fulfillment of the Requirements of the Degree of Doctor of Philosophy in Chemistry

Submitted by

Shaila Alam

Registration No. 168

Session: 2011-2012



DEPARTMENT OF CHEMISTRY

PHYSICAL CHEMISTRY RESEARCH LABORATORY

University of Dhaka

Dhaka-1000, Bangladesh

December 2016

Dedicated

to

My Family and Supervisors

Abstract

Series of ionic liquid (IL) based microemulsions were prepared with ionic and nonionic surfactants. Hydrophilic and hydrophobic ILs were used instead of water and the oil phase, respectively. The structure of the ILs were systematically varied by varying the structure of the cation and the anion. The influence of both hydrophilic and hydrophobic ILs on the physicochemical properties of IL based microemulsions were extensively studied. Different microregions in IL based microemulsions depended on the polar phase (IL or water) to surfactant mole ratio (R or W_o) or the volume fraction of the polar phase (ϕ_{IL} or ϕ_w) in microemulsions were critically analyzed with the help of percolation theory. The catalytic activity of lipase in IL based microemulsions was also investigated. The lipase-catalyzed hydrolysis of 4-nitrophenyl butyrate (p -NPB) was used as a model reaction to characterize the catalytic behavior of lipase in the IL microemulsion.

IL based microemulsions were prepared by dissolving surfactants in ionic liquids. The surfactants used were nonionic surfactant, Triton X-100 (TX-100), anionic surfactant, sodium dodecyl sulfate (SDS), and cationic surfactant, cetyltrimethylammonium bromide (CTAB). Hydrophilic ILs, such as 1-ethyl-3-methylimidazolium ethyl sulfate ($[C_2mim][EtSO_4]$), 1-butyl-3-methylimidazolium methyl sulfate ($[C_4mim][MeSO_4]$), 1-ethyl-3-methylimidazolium methyl sulfate ($[C_2mim][MeSO_4]$), 1-ethyl-3-methylimidazolium tetrafluoroborate ($[C_2mim][BF_4]$) and 1-butyl-3-methylimidazolium tetrafluoroborate ($[C_4mim][BF_4]$) served as polar phases; while hydrophobic ILs, 1-ethyl-3-methylimidazolium bis(trifluoromethylsulfonyl)imide ($[C_2mim][TFSI]$), 1-ethyl-3-methylimidazolium hexafluorophosphate ($[C_2mim][PF_6]$) and 1-butyl-3-methylimidazolium hexafluorophosphate ($[C_4mim][PF_6]$) were used as non-polar phases. Conventional microemulsions with TX-100 and CTAB were also prepared to compare with IL based microemulsions. 1-Butanol was used as the cosurfactant to prepare CTAB based microemulsions. The IL to surfactant mole ratio (R) or water to surfactant mole ratio (W_o) was varied to prepare microemulsions of different compositions. Different types of microemulsions such as IL-in-oil (IL/o), oil-in-IL (o/IL), IL-in-water (IL/w), water-in-IL (w/IL) and bicontinuous were prepared by changing the composition and proportion of polar and nonpolar phases.

Physicochemical properties of TX-100 microemulsions based on hydrophilic and hydrophobic ILs and CTAB microemulsions based on hydrophilic ILs were studied with the variation of the anion or the cation of the IL. The conductivity, viscosity, density, and the droplet size of microemulsions changed interestingly with change in the structure of the ILs. The viscosity and density decreased with increasing temperature at $R = 0.2255$ and 1.5424 for TX-100 and CTAB microemulsions based on hydrophilic ILs respectively. The refractive index changed with R and temperature (at $R = 0.2255$) for TX-100 microemulsions based on hydrophilic ILs. The refractive index increased with R and temperature (at $R = 1.5424$) for CTAB based hydrophilic IL microemulsions. Surface tension changed with R for TX-100 and hydrophilic IL based microemulsions of CTAB. The conductivity first increased with W_o upto $W_o \approx$

8.0 and then decreased with increasing W_o for [C₂mim][TFSI] based microemulsion, decreased with increasing W_o for [C₂mim][PF₆] based microemulsion and first increased upto $W_o \approx 8.0$ and then decreased with increasing W_o for [C₄mim][PF₆] based microemulsion. The viscosity followed the reverse trend. The micelle droplet size increased with decreasing W_o for hydrophobic IL based TX-100 microemulsions. The density and refractive index decreased and the surface tension changed with increasing W_o for hydrophobic IL based microemulsions with TX-100. Absorption peaks in ultraviolet region was observed in the absorption spectra of Reichardt's Betaine dye (RBD) in microemulsions with TX-100 and CTAB at a fixed wavelength. If the ions of ILs in these microemulsions are weakly bonded, the conductivity shows the higher values and viscosity shows the lower values compared to the microemulsions where ions of ILs are strongly bonded. The weakly bonded ions of ILs can penetrate the surfactant layer easily and thus such microemulsions showed larger droplet size. Although ILs with spherical anions have strong Coulombic interaction between cations and anions, inductive and dispersive forces gradually increase and dominate the system with increasing cationic and anionic side chain length.

Different microregions were also established by applying percolation theory on conductivity results on TX-100 based microemulsions based on ILs with increasing volume fraction of water (ϕ_w) or volume fraction of IL (ϕ_{IL}) respectively. Composition percolation thresholds were obtained from the derived data of the density and refractive index. The phase transitions correspond to the structural change from IL/o to o/IL via bicontinuous microemulsions with increasing ϕ_{IL} and from w/IL to IL/w via bicontinuous microemulsions with increasing ϕ_w . For [C₂mim][MeSO₄] and [C₂mim][PF₆] based microemulsions with TX-100 only reverse micelle and micelle dominated microemulsions exist. Microstructures such as IL/o and bicontinuous microemulsions were identified by applying percolation theory on conductivity results for CTAB based hydrophilic IL microemulsions with increasing R which are in agreement with the change of the diameter of microemulsion droplets as a function of R .

Comparative study of physicochemical properties based on the viscosity, conductivity, density, and refractive index of different microemulsions was also made by varying polar phase, nonpolar phase, and surfactant. Gel formation occurred for conventional TX-100 based microemulsions at W_o ranging from 6.9385 to 12.3903. For CTAB based conventional microemulsions only micelle and reverse micelle dominated microemulsions exist. Viscosity increased with increasing W_o for both w/o and o/w microemulsions for TX-100/cyclohexane/water system. The viscosity slightly increased with increasing W_o for w/o microemulsions and viscosity initially increased and then decreased with increasing W_o for o/w microemulsions in CTAB/1-butanol/cyclohexane/water system. The conductivity and viscosity of TX-100/cyclohexane/[C₂mim][EtSO₄] microemulsions showed larger values compared to CTAB/1-butanol/cyclohexane/[C₂mim][EtSO₄] microemulsions.

The catalytic behavior of lipase in aqueous medium, w/o, w/C₄mim][PF₆] and bicontinuous [C₄mim][PF₆] microemulsions under optimum conditions was investigated using lipase catalyzed hydrolysis of *p*-NPB as a model reaction. Kinetic parameters of lipase catalyzed hydrolysis of *p*-NPB in aqueous medium were evaluated from Michaelis-Menten and Lineweaver-Burk plots. The bicontinuous [C₄mim][PF₆] microemulsion at $W_o = 4.20$ showed maximum catalytic activity among different reaction media.

Microemulsions with hydrophilic IL in place of water and hydrophobic IL instead of oil phase showed significantly different properties depending on their structure and selectivity, which may be fine tuned for desirable catalytic activity like enzyme catalysis.

Title of the thesis:

Preparation and characterization of ionic liquid based microemulsions and their application in catalysis

Submitted by:

Shaila Alam, Ph.D. Student, Department of Chemistry, University of Dhaka

Chapter 1: Introduction

Chapter 1 gives a brief account of the background research and reviews the available literature on IL based microemulsions. This also addresses the rationale of the work and describes the strategy to accomplish the objectives.

Chapter 2: Preparation of Conventional and Ionic Liquid Based Microemulsions

Chapter 2 describes the preparation of series of conventional and IL based microemulsions with ionic and noionic surfactants. The microemulsions prepared comprised cyclohexane, [C₂mim][TFSI], [C₂mim][PF₆] and [C₄mim][PF₆] as nonpolar phase and water, [C₂mim][EtSO₄], [C₄mim][MeSO₄], [C₂mim][MeSO₄], [C₂mim][BF₄] and [C₄mim][BF₄] as polar phase. Preparation of IL/o, o/IL, IL/w, w/IL and bicontinuous microemulsions with variation of R or W_o values have also been discussed. The necessity of the cosurfactant, 1-butanol for CTAB microemulsions based on ILs was also highlighted. The difficulty of preparation using anionic, SDS microemulsion based on ILs was noted and the dependence on the nature of surfactants for preparation of IL based microemulsions was discussed.

Chapter 3: Physicochemical Properties of TX-100 Microemulsions with Variation of the Structure of Ionic Liquids

Chapter 3 discusses physicochemical properties of different series of TX-100 microemulsions by the measurements of conductivity, density, viscosity, refractive index, surface tension, and droplet size. The physicochemical properties of TX-100/cyclohexane/hydrophilic IL microemulsions with the variation of the anion or the cation conductivity, viscosity and reverse micelle droplet size were analyzed. It has been shown that with the variation of IL anion in TX-100/hydrophobic IL/water microemulsions, the conductivity of [C₂mim][TFSI] based microemulsion first increases with W_o upto $W_o \approx 8.0$ and then decreases with increasing W_o and for [C₂mim][PF₆] based microemulsion the conductivity decreases with increasing W_o . The viscosity follows the reverse trend for [C₂mim][PF₆] and [C₂mim][TFSI] based microemulsions. The micelle droplet size was found to increase with decreasing W_o for both the systems. With the variation of IL cation in TX-100/hydrophobic IL/water

microemulsions, the conductivity of $[\text{C}_4\text{mim}][\text{PF}_6]$ based microemulsion first increases upto $W_o \approx 8.0$ and then decreases with increasing W_o and for $[\text{C}_2\text{mim}][\text{PF}_6]$ based microemulsion the conductivity decreases with increasing W_o . For $[\text{C}_2\text{mim}][\text{PF}_6]$ and $[\text{C}_4\text{mim}][\text{PF}_6]$ based microemulsions viscosity follows the reverse trend. The micelle droplet size increased with decreasing W_o for both the systems. This has been ascribed to a decrease in the electrostatic interaction and a competition between the electrostatic forces and the inductive, dispersive forces with increasing the nonpolar side chain of the cation or anion of the IL. The amount of IL dominated overall density of the microemulsions. With an increase of the amount of IL in microemulsions the density also increased. With increasing R for hydrophilic IL based microemulsions the density increased and with increasing W_o for hydrophobic IL based microemulsions the density decreased. The viscosity and the density decreased with temperature at $R = 0.2255$ for all the series. Refractive index decreased with increasing W_o for $[\text{C}_2\text{mim}][\text{PF}_6]$ and $[\text{C}_2\text{mim}][\text{TFSI}]$ based microemulsions. Different physicochemical properties have been systematically reported with variation of different parameters affecting TX-100 microemulsions based on different ILs.

Chapter 4: Physicochemical Properties of CTAB Microemulsions with Variation of the Structure of Ionic Liquids

Chapter 4 presents physicochemical properties of CTAB microemulsions where cyclohexane, hydrophilic ILs ($[\text{C}_2\text{mim}][\text{EtSO}_4]$, $[\text{C}_4\text{mim}][\text{MeSO}_4]$ and $[\text{C}_2\text{mim}][\text{MeSO}_4]$), and 1-butanol were used as nonpolar phase, polar phase and co-surfactant respectively. The change in viscosity, conductivity, density, refractive index, and reverse micelle droplet size was monitored with change in R . It was reported that When the cation is $[\text{C}_2\text{mim}]^+$, an increase in the the number of carbon atom in the anion, the electrostatic interaction decreases and when the anion is $[\text{MeSO}_4]$, an increase in the hydrophobic side chain in the cation, the electrostatic interaction also decreases. The viscosity and the density were found to decrease with temperature at $R = 1.5424$ for all the series.

Chapter 5: Analysis of Microregions of Ionic Liquid Based Microemulsions with Variation of Surfactants by Percolation Theory

Chapter 5 presents different microstructures of IL based microemulsions with TX-100 and CTAB by applying percolation theory on conductivity results. It was reported that excess volume, V^E vs. ϕ , excess refractive index, n^E vs. ϕ and excess molar refraction, R^E vs. ϕ profiles for TX-100 microemulsions and diameter, d (nm) of droplets vs. R profile for CTAB microemulsions also indicate the structural phase transitions which are in accordance with those obtained from conductivity measurements. For TX-100 microemulsions with hydrophilic IL, the phase transitions occurred from IL/o to o/IL via bicontinuous microemulsions with increasing ϕ_{IL} and for TX-100 microemulsion with hydrophobic IL, the phase transitions occurred from w/IL to IL/w via bicontinuous microemulsions with increasing ϕ_{w} . With increasing R , microstructures

such as IL/o and bicontinuous microemulsions could be identified by applying percolation theory on hydrophilic IL based microemulsions with CTAB.

Chapter 6: Comparative Study of Physicochemical Properties of Conventional Microemulsions with Ionic Liquid Based Microemulsions

Chapter 6 compares physicochemical properties of different microemulsions with variation of polar phase, non polar phase, and type of surfactant. Physicochemical properties of conventional TX-100 microemulsions were also compared with IL based TX-100 microemulsions where [C₂mim][EtSO₄] was used as the polar phase instead of water and [C₂mim][TFSI] was used as nonpolar phase instead of cyclohexane. Physicochemical properties were compared and contrasted and the microstructures have been analyzed to develop strategies to achieve desirable properties from IL based microemulsions.

Chapter 7: Catalytic Efficiency of Lipase in Aqueous Medium, Conventional, and [C₄mim][PF₆] Based Microemulsions of TX-100

Chapter 7 reports lipase catalyzed hydrolysis of *p*-NPB under optimum conditions in aqueous medium, w/o, w/C₄mim][PF₆] and bicontinuous [C₄mim][PF₆] based microemulsions to evaluate the catalytic efficiency of lipase. The W_o of the microemulsion was found to influence the catalytic activity of lipase. From Michaelis-Menten and Lineweaver-Burk plots, kinetic parameters of lipase catalyzed hydrolysis of *p*-NPB in aqueous medium were evaluated. Among the different reaction media, IL based microemulsion at $W_o = 4.20$ showed the highest catalytic activity because of the presence of bicontinuous phase. Volatile organic compound made the conventional microemulsions unstable and such system showed lower catalytic activity compared to aqueous medium.

Chapter 9: General Conclusions and Outlook

Chapter 9 summarizes the results for a general conclusion and discussed the future prospect of IL based microemulsions for development of suitable media to control the rate of reactions and stabilize reactive reagents or reaction intermediates.

CONTENTS

Chapter No.		Page No.
1.	General Introduction	1-39
1.1.	Background	2
1.2.	Supramolecular Chemistry	3
1.3.	Surfactant	5
1.3.1.	Basic Surfactant Classifications	5
1.3.2.	Thermodynamics of Micellization	6
1.3.3.	Micellar Structure and Shape	8
1.4.	Microemulsion	10
1.4.1.	Microstructures of Microemulsions	11
1.4.2.	Winsor Classification of Microemulsions	11
1.4.3.	Basics of Formation of Microemulsions	12
1.4.4.	Percolations in Microemulsions	13
1.5.	ILs	15
1.5.1.	Classification of ILs	17
1.5.2.	Walden Plot	19
1.6.	ILs in Microemulsion	20
1.7.	Applications of IL Based Microemulsions	20
1.8.	Enzyme Catalyzed Reaction	22
1.8.1.	Enzymatic Catalysis in Microemulsions	25
1.9.	Literature Review	26
1.10.	Objectives of the Work	30
1.11.	Present work	30
	References	32
2.	Preparation of Conventional and Ionic Liquid Based Microemulsions from Ionic and Nonionic Surfactants	40-53
	Abstract	41
2.1.	Introduction	41
2.2.	Experimental	43
2.2.1.	Materials and Equipments	43
2.3.	Preparation of Conventional Microemulsions	43
2.3.1.	Preparation of TX-100/Cyclohexane/Water Microemulsions	43
2.3.2.	Preparation of CTAB/1-Butanol/Cyclohexane/Water Microemulsions	44
2.4.	Preparation of IL Based Microemulsions	45
2.4.1.	Preparation of TX-100/Cyclohexane/IL Microemulsions where IL is Used as the Polar Phase	45
2.4.2.	Preparation of TX-100/IL/Water Microemulsions Using IL is Used as the oil Phase	47

2.4.3.	Preparation of CTAB/1-Butanol/Cyclohexane/IL Microemulsions	48
2.4.4.	Preparation of IL Based Microemulsions from SDS	50
2.5.	Stability of Microemulsions	50
2.5.1.	Stability of Microemulsions from TX-100	50
2.5.2.	Stability of Microemulsions from CTAB	50
2.6.	Preparation of Conventional and IL based Microemulsions with Different Surfactants	50
2.7.	Conclusions	51
	References	51
3.	Physicochemical Properties of TX-100 Microemulsions with Variation of the Structure of Ionic Liquids	54-103
	Abstract	55
3.1.	Introduction	55
3.2.	Experimental	58
3.2.1.	Materials	58
3.2.2.	Preparation of Microemulsions	58
3.2.3.	Measurements	58
3.3.	Results and Discussion	59
3.3.1.	Variation of Physicochemical Properties of TX-100 Microemulsions using ILs as the Polar or Nonpolar Phase with Variation of Anions of ILs	59
3.3.1.1.	Conductivity	60
3.3.1.1.1.	The Influence of R or W_o	60
3.3.1.1.2.	The Influence of IL Anion	62
3.3.1.1.2.1.	The Influence of IL Anion in TX-100/Cyclohexane/[C ₂ mim][MeSO ₄], TX-100/Cyclohexane/[C ₂ mim][EtSO ₄] and TX-100/Cyclohexane/[C ₂ mim][BF ₄] Microemulsions	62
3.3.1.1.2.2.	The Influence of IL Anion in TX-100/Cyclohexane/[C ₄ mim][MeSO ₄] and TX-100/Cyclohexane/[C ₄ mim][BF ₄] Microemulsions	63
3.3.1.1.2.3.	The Influence of IL Anion in TX-100/[C ₂ mim][TFSI]/Water and TX-100/[C ₂ mim][PF ₆]/Water Microemulsions	64
3.3.1.2.	Viscosity	65
3.3.1.2.1.	The Influence of R or W_o	65
3.3.1.2.2.	The Influence of IL Anion	66
3.3.1.2.2.1.	The Influence of IL Anion in TX-100/Cyclohexane/[C ₂ mim][MeSO ₄], TX-100/Cyclohexane/[C ₂ mim][EtSO ₄] and TX-100/Cyclohexane/[C ₂ mim][BF ₄] Microemulsions	66
3.3.1.2.2.2.	The Influence of IL Anion in TX-100/Cyclohexane/[C ₄ mim][MeSO ₄] and TX-100/Cyclohexane/[C ₄ mim][BF ₄] Microemulsions	67

3.3.1.2.2.3.	The Influence of IL Anion in TX-100/[C ₂ mim][TFSI]/Water and TX-100/[C ₂ mim][PF ₆]/Water Microemulsions	67
3.3.1.2.3.	Effect of Temperature on Viscosity	67
3.3.1.3.	Size and Size Distribution of Droplets	68
3.3.1.3.1.	Influence of IL Anion	68
3.3.1.3.1.1.	The Influence of IL Anion in (a) TX-100/Cyclohexane/[C ₂ mim][MeSO ₄], (b) TX-100/Cyclohexane/[C ₂ mim][EtSO ₄] and (c) TX-100/Cyclohexane/[C ₂ mim][BF ₄] Microemulsions	68
3.3.1.3.1.2.	The Influence of IL Anion in TX-100/Cyclohexane/[C ₄ mim][MeSO ₄] and TX-100/Cyclohexane/[C ₄ mim][BF ₄] Microemulsions	71
3.3.1.3.1.3.	The Influence of IL Anion in TX-100/[C ₂ mim][PF ₆]/Water and TX-100/[C ₂ mim][TFSI]/Water Microemulsions	72
3.3.1.4.	Density	73
3.3.1.4.1.	The Influence of <i>R</i> or <i>W</i> ₀	73
3.3.1.4.2.	Effect of Temperature on Density	74
3.3.1.5.	Refractive Index	74
3.3.1.5.1.	The Influence of <i>R</i> or <i>W</i> ₀	74
3.3.1.5.2.	Effect of Temperature on Refractive Index	76
3.3.1.6.	Polarity	76
3.3.1.7.	Surface Tension	77
3.3.2.	Effect of Nonpolar Chain Length of Anions of ILs on Physicochemical Properties of Microemulsions	78
3.3.3.	Variation of Physicochemical Properties of TX-100 Microemulsions using ILs as the Polar or Nonpolar Phase with Variation of Cations of ILs	80
3.3.3.1.	Conductivity	80
3.3.3.1.1.	The Influence of <i>R</i> or <i>W</i> ₀	80
3.3.3.1.2.	The Influence of IL Cation	82
3.3.3.1.2.1.	The Influence of Alkyl Side Chain Length of IL Cation in TX-100/ Cyclohexane/[C ₂ mim][MeSO ₄] and TX-100/Cyclohexane/[C ₄ mim][MeSO ₄] Microemulsion	82
3.3.3.1.2.2.	The Influence of IL Anion in TX-100/Cyclohexane/[C ₂ mim][BF ₄] and TX-100/Cyclohexane/[C ₄ mim][BF ₄] Microemulsion	83
3.3.3.1.2.2.1.	Walden Plot for TX-100/Cyclohexane/[C ₂ mim][BF ₄] and TX-100/Cyclohexane/[C ₄ mim][BF ₄] Microemulsion	83
3.3.3.1.2.3.	The Influence of IL Cation in TX-100/[C ₂ mim][PF ₆]/Water and TX-100/[C ₄ mim][PF ₆]/Water Microemulsions	84
3.3.3.1.2.3.1.	Walden Plot for TX-100/[C ₂ mim][PF ₆]/Water and TX-100/[C ₄ mim][PF ₆]/Water Microemulsions	84
3.3.3.2.	Viscosity	85
3.3.3.2.1.	The Influence of <i>R</i> or <i>W</i> ₀	85
3.3.3.2.2.	The Influence of IL Cation	86
3.3.3.2.2.1.	The Influence of IL Cation in TX-100/Cyclohexane/[C ₂ mim][MeSO ₄] and TX-100/Cyclohexane/[C ₄ mim][MeSO ₄] Microemulsions	86

3.3.3.2.2.2.	The Influence of IL Cation in TX-100/Cyclohexane/[C ₄ mim][BF ₄] and TX-100/Cyclohexane/[C ₂ mim][BF ₄] Microemulsions	87
3.3.3.2.2.3.	The Influence of IL Cation in TX-100/[C ₂ mim][PF ₆]/Water and TX-100/[C ₄ mim][PF ₆]/Water Microemulsions	87
3.3.3.2.3.	Effect of Temperature on Viscosity	87
3.3.3.3.	Size and Size Distribution of Droplets	88
3.3.3.3.1.	Influence of IL Cation	88
3.3.3.3.1.1.	The Influence of IL Cation in TX-100/Cyclohexane/[C ₂ mim][MeSO ₄] and TX-100/Cyclohexane/[C ₄ mim][MeSO ₄] Microemulsions	88
3.3.3.3.1.2.	The Influence of IL Cation in TX-100/Cyclohexane/[C ₂ mim][BF ₄] and TX-100/Cyclohexane/[C ₄ mim][BF ₄] Microemulsions	89
3.3.3.3.1.3.	The Influence of IL Anion in TX-100/[C ₂ mim][PF ₆]/Water and TX-100/[C ₄ mim][PF ₆]/Water Microemulsions	90
3.3.3.4	Density	91
3.3.3.4.1.	The Influence of R or W_0	91
3.3.3.4.2.	Effect of Temperature on Density	92
3.3.3.5.	Refractive Index	92
3.3.3.5.1.	The Influence of R or W_0	92
3.3.3.5.2.	Effect of Temperature on Refractive Index	93
3.3.3.6.	Polarity	94
3.3.3.7.	Surface Tension	95
3.3.4.	Effect of Nonpolar Chain Length of Cations of ILs on Physicochemical Properties of Microemulsions	96
3.3.5.	Interactions of Surfactant with Polar and Nonpolar Phase	97
3.3.6.	Probable Organization of Different Components in Microemulsion Systems	98
3.3.7.	Dispersive and Inductive Forces in ILs	100
3.4.	Conclusions	101
	References	101
4.	Physicochemical Properties of CTAB Microemulsions with Variation of the Structure of Ionic Liquids	104-122
	Abstract	105
4.1	Introduction	105
4.2.	Experimental	107
4.2.1.	Materials	107
4.2.2.	Preparation of Microemulsions	107
4.2.3.	Measurements	107
4.3.	Results and Discussion	107
4.3.1.	Physicochemical Properties of CTAB/1-Butanol/Cyclohexane/IL Microemulsions	107
4.3.1.1.	Conductivity	107
4.3.1.1.1.	The Influence of R	107

4.3.1.1.2.	The Influence of IL Anion	108
4.3.1.1.3.	The Influence of Alkyl Side Chain Length of Imidazolium Cation	109
4.3.1.2.	Viscosity	109
4.3.1.2.1.	The Influence of <i>R</i>	109
4.3.1.2.2.	The Influence of IL Anion	110
4.3.1.2.3.	The Influence of Alkyl Side Chain Length of Imidazolium Cation	110
4.3.1.2.4.	Effect of Temperature on Viscosity	111
4.3.1.3.	Size and Size Distribution of Droplets	111
4.3.1.3.1.	Influence of IL Anion	111
4.3.1.3.2.	Influence of Alkyl Side Chain Length of Imidazolium Cation	113
4.3.1.4.	Density	113
4.3.1.4.1.	Effect of Temperature on Density	114
4.3.1.5.	Refractive Index	114
4.3.1.5.1.	Effect of Temperature on Refractive Index	115
4.3.1.6.	Polarity	116
4.3.1.7.	Surface Tension	117
4.3.2.	Probable Organization of Different Components in IL/o Microemulsions	117
4.4.	Conclusion	119
	References	119
5.	Analysis of Microregions of Ionic Liquid Based Microemulsions with Variation of Surfactants by Percolation Theory	123-137
	Abstract	124
5.1.	Introduction	124
5.2.	Experimental	125
5.2.1.	Materials	125
5.2.2.	Preparation of Microemulsions	126
5.2.3.	Measurements	126
5.3.	Results and Discussion	126
5.3.1.	Analysis of Microregions of TX-100 Based Microemulsions by Composition Percolation Theory	126
5.3.1.1.	Conductivity	126
5.3.1.2.	Excess Volume from Density Results	128
5.3.1.3.	Excess Refractive Index from Refractive Index Results	129
5.3.1.4.	Excess Molar Refraction from Refractive Index Results	131
5.3.1.5.	Microstructures of Microemulsions	133
5.3.2.	Analysis of Microregions of CTAB Based Microemulsions by Composition Percolation Theory	134
5.3.2.1.	Conductivity	134
5.3.2.2.	Size of Droplets	135
5.3.2.3.	Microstructures of Microemulsions	136

5.4.	Conclusions	136
	References	136
6.	Comparative Study of Physicochemical Properties of Conventional Microemulsions with Ionic Liquid Based Microemulsions	138-152
	Abstract	139
6.1.	Introduction	139
6.2.	Experimental	141
6.2.1.	Materials	141
6.2.2.	Preparation of Microemulsions	141
6.2.3.	Measurements	141
6.3.	Results and Discussions	142
6.3.1.	Comparative Study of Physicochemical Properties of Conventional vs. IL Based Microemulsions of TX-100	142
6.3.1.1.	Viscosity	142
6.3.1.2.	Density	143
6.3.1.3.	Refractive Index	144
6.3.2.	Comparative Study of Physicochemical Properties of Conventional vs. IL Based Microemulsions of CTAB	145
6.3.2.1.	Viscosity	145
6.3.2.2.	Density	146
6.3.2.3.	Refractive Index	147
6.3.3.	Comparative Study of Physicochemical Properties of IL Based Microemulsions with TX-100 and CTAB	147
6.3.3.1.	Conductivity	147
6.3.3.2.	Viscosity	149
6.3.3.3.	Density	149
6.3.3.4.	Refractive Index	150
6.4.	Conclusions	151
	References	151
7.	Catalytic Efficiency of Lipase in Aqueous Medium, Conventional, and Ionic Liquid Based Microemulsions of TX-100	153-168
	Abstract	154
7.1.	Introduction	154
7.2.	Experimental	155
7.2.1.	Materials	155
7.2.2.	Preparation of Tris-HCl Buffer	155
7.2.3.	Preparation of Microemulsions	154
7.2.4.	Determination of the Catalytic Activity of Lipase	156
7.2.5.	Methods	157
7.3.	Results and Discussion	157

7.3.1.	Influence of Different Media on Lipase Catalyzed Hydrolysis of <i>p</i> -NPB	157
7.3.1.1.	Influence of Aqueous Medium on Lipase Catalyzed Hydrolysis of <i>p</i> -NPB	157
7.3.1.1.1.	Absorption Spectrum of Lipase Catalyzed Hydrolysis of <i>p</i> -NPB in Aqueous Medium	157
7.3.1.1.2.	Influence of the Concentration of <i>p</i> -NPB on the Catalytic Activity of Lipase in Aqueous Medium	158
7.3.1.1.3.	Kinetic Parameters of Lipase Catalyzed Hydrolysis of <i>p</i> -NPB in Aqueous Medium	159
7.3.1.2.	Influence of TX-100/Cyclohexane/Water Microemulsions on Lipase Catalyzed Hydrolysis of <i>p</i> -NPB	160
7.3.1.2.1.	Absorption Spectra of Lipase Catalyzed Hydrolysis of <i>p</i> -NPB in TX-100/Cyclohexane/Water Microemulsions	160
7.3.1.2.2.	Influence of W_o on the Catalytic Activity of Lipase in TX-100/Cyclohexane/Water Microemulsions	161
7.3.1.3.	Influence of TX-100/[C ₄ mim][PF ₆]/Water Microemulsions on Lipase Catalyzed Hydrolysis of <i>p</i> -NPB	162
7.3.1.3.1.	Absorption Spectrum of Lipase Catalyzed Hydrolysis of <i>p</i> -NPB in TX-100/[C ₄ mim][PF ₆]/Water Microemulsions	162
7.3.1.3.2.	Influence of W_o on the Catalytic Activity of Lipase in TX-100/[C ₄ mim][PF ₆]/Water Microemulsions	163
7.3.2.	Comparative Study of the Catalytic Activity of Lipase in Different Media	163
7.3.2.1.	Comparative Study of the Catalytic Activity of Lipase in Aqueous Medium and TX-100/Cyclohexane/Water Microemulsions	163
7.3.2.2.	Comparative Study of the Catalytic Activity of Lipase in TX-100/Cyclohexane/Water and TX-100/[C ₄ mim][PF ₆]/Water Microemulsions	164
7.3.2.3.	Comparative Study of the Catalytic Activity of Lipase in Aqueous Medium, TX-100/Cyclohexane/Water and TX-100/[C ₄ mim][PF ₆]/Water Microemulsion	166
7.3.3.	Probable Organization of Different Components in Bicontinuous TX-100/[C ₄ mim][PF ₆]/Water Microemulsion	166
7.4.	Conclusions	167
	References	168
8.	General Conclusions and Outlook	169-171
8.1.	General Conclusions	170
8.2.	Outlook	171
	Appendices	172-204
	List of Publications	205
	List of Attended Seminars	205
	List of Workshops Attended	206
	Abstracts Published as Contribution in the Scientific Meetings	206

LIST OF FIGURES

Figure No.	Title	Page No.
1.1.	Classification of surfactant function according to HLB scale	9
1.2.	Walden plot shows the classification of ILs	19
1.3.	(a) Determination of initial rates at different concentrations and (b) a plot of rate, v vs. substrate concentration, $[S]$ obeying Michaelis-Menten equation	24
1.4.	$1/v$ vs. $1/[S]$ obeying Lineweaver-Burk equation	25
3.3.1.	Variation of conductivity of (a) TX-100/cyclohexane/[C ₂ mim][MeSO ₄], TX-100/cyclohexane/[C ₂ mim][EtSO ₄] and TX-100/cyclohexane/[C ₂ mim][BF ₄], (b) TX-100/cyclohexane/[C ₄ mim][MeSO ₄] and TX-100/cyclohexane/[C ₄ mim][BF ₄], (c) TX-100/[C ₂ mim][TFSI]/water and TX-100/[C ₂ mim][PF ₆]/water microemulsions as a function of R or W_0 at 25 °C	60
3.3.2.	Variation of viscosity of (a) TX-100/cyclohexane/[C ₂ mim][MeSO ₄], TX-100/cyclohexane/[C ₂ mim][EtSO ₄] and TX-100/cyclohexane/[C ₂ mim][BF ₄], (b) TX-100/cyclohexane/[C ₄ mim][MeSO ₄] and TX-100/cyclohexane/[C ₄ mim][BF ₄], (c) TX-100/[C ₂ mim][TFSI]/water and TX-100/[C ₂ mim][PF ₆]/water microemulsions as a function of R or W_0 at 25 °C	65
3.3.3.	Effect of temperature on viscosity of (a) TX-100/cyclohexane/[C ₂ mim][MeSO ₄], TX-100/cyclohexane/[C ₂ mim][EtSO ₄] and TX-100/cyclohexane/[C ₂ mim][BF ₄], (b) TX-100/cyclohexane/[C ₄ mim][MeSO ₄] and TX-100/cyclohexane/[C ₄ mim][BF ₄] microemulsions at $R = 0.2255$	68
3.3.4.	Size and size distribution of droplets for (a) TX-100/cyclohexane/[C ₂ mim][MeSO ₄], (b) TX-100/cyclohexane/[C ₂ mim][EtSO ₄] and (c) TX-100/cyclohexane/[C ₂ mim][BF ₄] microemulsions at different R at 25 °C	69
3.3.5.	Size and size distribution of droplets for (d) TX-100/cyclohexane/[C ₄ mim][MeSO ₄] and (e) TX-100/cyclohexane/[C ₄ mim][BF ₄] microemulsions at different R at 25 °C	71
3.3.6.	Size and size distribution of droplets for (f) TX-100/[C ₂ mim][PF ₆]/water and (g) TX-100/[C ₂ mim][TFSI]/water microemulsions at different W_0 at 25 °C	72
3.3.7.	Density of (a) TX-100/cyclohexane/[C ₂ mim][MeSO ₄], TX-100/cyclohexane/[C ₂ mim][EtSO ₄] and TX-100/cyclohexane/[C ₂ mim][BF ₄], (b) TX-100/cyclohexane/[C ₄ mim][MeSO ₄] and TX-100/cyclohexane/[C ₄ mim][BF ₄], (c) TX-100/[C ₂ mim][TFSI]/water and TX-100/[C ₂ mim][PF ₆]/water microemulsions as a function of R or W_0 at 25 °C	73
3.3.8.	Effect of temperature on density of (a) TX-100/cyclohexane/[C ₂ mim][MeSO ₄], TX-100/cyclohexane/[C ₂ mim][EtSO ₄] and TX-100/cyclohexane/[C ₂ mim][BF ₄], (b) TX-100/cyclohexane/[C ₄ mim][MeSO ₄] and TX-100/cyclohexane/[C ₄ mim][BF ₄] microemulsions at $R = 0.2255$	74

3.3.9.	Refractive index of (a) TX-100/Cyclohexane/[C ₂ mim][MeSO ₄], TX-100/cyclohexane/[C ₂ mim][EtSO ₄] and TX-100/cyclohexane/[C ₂ mim][BF ₄], (b) TX-100/cyclohexane/[C ₄ mim][MeSO ₄] and TX-100/cyclohexane/[C ₄ mim][BF ₄], (c) TX-100/[C ₂ mim][TFSI]/water and TX-100/[C ₂ mim][PF ₆]/water microemulsions as a function of <i>R</i> or <i>W_o</i> at 25 °C	75
3.3.10.	Effect of temperature on refractive index of (a) TX-100/cyclohexane/[C ₂ mim][MeSO ₄], TX-100/cyclohexane/[C ₂ mim][EtSO ₄] and TX-100/cyclohexane/[C ₂ mim][BF ₄], (b) TX-100/cyclohexane/[C ₄ mim][MeSO ₄] and TX-100/cyclohexane/[C ₄ mim][BF ₄] microemulsions at <i>R</i> = 0.2255	76
3.3.11.	Absorption spectra of RBD in (a) TX-100/cyclohexane/[C ₂ mim][EtSO ₄], (b) TX-100/cyclohexane/[C ₂ mim][BF ₄] and (c) TX-100/[C ₂ mim][TFSI]/water microemulsions at different <i>R</i> or <i>W_o</i> at 25 °C	77
3.3.12.	Surface tension of (a) TX-100/cyclohexane/[C ₂ mim][EtSO ₄] and TX-100/cyclohexane/[C ₂ mim][MeSO ₄], (b) TX-100/[C ₂ mim][PF ₆]/water and TX-100/[C ₂ mim][TFSI]/water microemulsions as a function of <i>R</i> or <i>W_o</i> at 25 °C	78
3.3.13.	Conductivity of (a) TX-100/cyclohexane/[C ₂ mim][MeSO ₄] and TX-100/cyclohexane/[C ₄ mim][MeSO ₄], (b) TX-100/cyclohexane/[C ₂ mim][BF ₄] and TX-100/cyclohexane/[C ₄ mim][BF ₄], (c) TX-100/[C ₂ mim][PF ₆]/water and TX-100/[C ₄ mim][PF ₆]/water microemulsions as a function of <i>R</i> or <i>W_o</i> at 25 °C	81
3.3.14.	Walden plot for TX-100/cyclohexane/[C ₂ mim][BF ₄] and TX-100/cyclohexane/[C ₄ mim][BF ₄] microemulsions	84
3.3.15.	Walden plot for TX-100/cyclohexane/[C ₂ mim][PF ₆] and TX-100/cyclohexane/[C ₄ mim][PF ₆] microemulsions	85
3.3.16.	Viscosity of (a) TX-100/cyclohexane/[C ₂ mim][MeSO ₄] and TX-100/cyclohexane/[C ₄ mim][MeSO ₄], (b) TX-100/cyclohexane/[C ₂ mim][BF ₄] and TX-100/cyclohexane/[C ₄ mim][BF ₄] (c) TX-100/[C ₂ mim][PF ₆]/water and TX-100/[C ₄ mim][PF ₆]/water microemulsions as a function of polar phase (IL or water) to TX-100 mole ratio (<i>R</i> or <i>W_o</i>) at 25 °C	86
3.3.17.	Effect of temperature on viscosity of (a) TX-100/cyclohexane/[C ₂ mim][MeSO ₄] and TX-100/cyclohexane/[C ₄ mim][MeSO ₄], (b) TX-100/cyclohexane/[C ₂ mim][BF ₄] and TX-100/cyclohexane/[C ₄ mim][BF ₄] microemulsions at <i>R</i> = 0.2255	88
3.3.18.	Size and size distribution of droplets for (a) TX-100/cyclohexane/[C ₂ mim][MeSO ₄] and (d) TX-100/cyclohexane/[C ₄ mim][MeSO ₄] microemulsions at different <i>R</i> values at 25 °C	89
3.3.19.	Size and size distribution of droplets for (c) TX-100/cyclohexane/[C ₂ mim][BF ₄] and (e) TX-100/cyclohexane/[C ₄ mim][BF ₄] microemulsions at different <i>R</i> at 25 °C	89
3.3.20.	Size and size distribution of droplets for (f) TX-100/[C ₂ mim][PF ₆]/water and (h) TX-100/[C ₄ mim][PF ₆]/water microemulsions at different <i>W_o</i> values at 25 °C	90

3.3.21.	Density of (a) TX-100/cyclohexane/[C ₂ mim][MeSO ₄] and TX-100/cyclohexane/[C ₄ mim][MeSO ₄], (b) TX-100/cyclohexane/[C ₂ mim][BF ₄] and TX-100/cyclohexane/[C ₄ mim][BF ₄] (c) TX-100/[C ₂ mim][PF ₆]/water and TX-100/[C ₄ mim][PF ₆]/water microemulsions as a function of <i>R</i> or <i>W</i> ₀ at 25 °C	91
3.3.22.	Effect of temperature on density of (a) TX-100/cyclohexane/[C ₂ mim][MeSO ₄] and TX-100/cyclohexane/[C ₄ mim][MeSO ₄], (b) TX-100/cyclohexane/[C ₂ mim][BF ₄] and TX-100/cyclohexane/[C ₄ mim][BF ₄] microemulsions at <i>R</i> = 0.2255	92
3.3.23.	Refractive index of (a) TX-100/cyclohexane/[C ₂ mim][MeSO ₄] and TX-100/cyclohexane/[C ₄ mim][MeSO ₄], (b) TX-100/cyclohexane/[C ₂ mim][BF ₄] and TX-100/cyclohexane/[C ₄ mim][BF ₄] (c) TX-100/[C ₂ mim][PF ₆]/water and TX-100/[C ₄ mim][PF ₆]/water microemulsions as a function of <i>R</i> or <i>W</i> ₀ at 25 °C	93
3.3.24.	Effect of temperature on refractive index of (a) TX-100/cyclohexane/[C ₂ mim][MeSO ₄] and TX-100/cyclohexane/[C ₄ mim][MeSO ₄], (b) TX-100/cyclohexane/[C ₂ mim][BF ₄] and TX-100/cyclohexane/[C ₄ mim][BF ₄] at <i>R</i> = 0.2255	94
3.3.25.	Absorption spectra of RBD in (a) TX-100/cyclohexane/[C ₄ mim][BF ₄] and (b) TX-100/cyclohexane/[C ₂ mim][BF ₄] microemulsions as a function of <i>R</i> at 25 °C	95
3.3.26.	Surface tension of TX-100/[C ₂ mim][PF ₆]/water and TX-100/[C ₄ mim][PF ₆]/water microemulsions as a function of <i>W</i> ₀ at 25 °C	95
4.3.1.	Variation of conductivity of (a) CTAB/1-butanol/cyclohexane/[C ₂ mim][MeSO ₄] and CTAB/1-butanol/cyclohexane/[C ₂ mim][EtSO ₄] (b) CTAB/1-butanol/cyclohexane/[C ₂ mim][MeSO ₄] and CTAB/1-butanol/cyclohexane/[C ₄ mim][MeSO ₄] microemulsions as a function of <i>R</i> at 25 °C	108
4.3.2.	Variation of viscosity of (a) CTAB/1-butanol/cyclohexane/[C ₂ mim][MeSO ₄] and CTAB/1-butanol/cyclohexane/[C ₂ mim][EtSO ₄] (b) CTAB/1-butanol/cyclohexane/[C ₂ mim][MeSO ₄] and CTAB/1-butanol/cyclohexane/[C ₄ mim][MeSO ₄] microemulsions as a function of <i>R</i> at 25 °C	110
4.3.3.	Effect of temperature on viscosity of (a) CTAB/1-butanol/cyclohexane/[C ₂ mim][MeSO ₄] and CTAB/1-butanol/cyclohexane/[C ₂ mim][EtSO ₄] (b) CTAB/1-butanol/cyclohexane/[C ₂ mim][MeSO ₄] and CTAB/1-butanol/cyclohexane/[C ₄ mim][MeSO ₄] microemulsions at <i>R</i> = 1.5424	111
4.3.4.	Size and size distribution of droplets for (a) CTAB/1-butanol/cyclohexane/[C ₂ mim][MeSO ₄], (b) CTAB/1-butanol/cyclohexane/[C ₂ mim][EtSO ₄] and (c) CTAB/1-butanol/cyclohexane/[C ₄ mim][MeSO ₄], microemulsions at different <i>R</i> at 25 °C	112
4.3.5.	Density of (a) CTAB/1-butanol/cyclohexane/[C ₂ mim][MeSO ₄] and CTAB/1-butanol/cyclohexane/[C ₂ mim][EtSO ₄] (b) CTAB/1-butanol/cyclohexane/[C ₂ mim][MeSO ₄] and CTAB/1-butanol/cyclohexane/[C ₄ mim][MeSO ₄] microemulsions as a function of <i>R</i> at 25 °C	113

4.3.6.	Effect of temperature on density of (a) CTAB/1-butanol/cyclohexane/[C ₂ mim][MeSO ₄] and CTAB/1-butanol/cyclohexane/[C ₂ mim][EtSO ₄] (b) CTAB/1-butanol/cyclohexane/[C ₂ mim][MeSO ₄] and CTAB/1-butanol/cyclohexane/[C ₄ mim][MeSO ₄] microemulsions at $R = 1.5424$	114
4.3.7.	Refractive index of (a) CTAB/1-butanol/cyclohexane/[C ₂ mim][MeSO ₄] and CTAB/1-butanol/cyclohexane/[C ₂ mim][EtSO ₄] (b) CTAB/1-butanol/cyclohexane/[C ₂ mim][MeSO ₄] and CTAB/1-butanol/cyclohexane/[C ₄ mim][MeSO ₄] microemulsions as a function of R at 25 °C	115
4.3.8.	Effect of temperature on refractive index of (a) CTAB/1-butanol/cyclohexane/[C ₂ mim][MeSO ₄] and CTAB/1-butanol/cyclohexane/[C ₂ mim][EtSO ₄] (b) CTAB/1-butanol/cyclohexane/[C ₂ mim][MeSO ₄] and CTAB/1-butanol/cyclohexane/[C ₄ mim][MeSO ₄] microemulsions at $R = 1.5424$	116
4.3.9.	Absorption spectra of RBD in (a) CTAB/1-butanol/cyclohexane/[C ₄ mim][MeSO ₄] and (b) CTAB/1-butanol/cyclohexane/[C ₂ mim][EtSO ₄] microemulsions at different R values at 25 °C	116
4.3.10.	Surface tension of CTAB/1-butanol/cyclohexane/[C ₂ mim][EtSO ₄] ($R = 1.5424, 3.0849, 4.6273, 6.1697, 7.7121$), CTAB/1-butanol/cyclohexane/[C ₄ mim][MeSO ₄] ($R = 1.5424$) and CTAB/1-butanol/cyclohexane/[C ₂ mim][MeSO ₄] ($R = 1.5424$) as a function of R at 25 °C	117
5.3.1.	The $d\log\sigma/d\phi$ of (a) TX-100/cyclohexane/[C ₂ mim][EtSO ₄], TX-100/cyclohexane/[C ₂ mim][BF ₄], (b) TX-100/cyclohexane/[C ₄ mim][BF ₄], TX-100/cyclohexane/[C ₄ mim][MeSO ₄] , (c) TX-100/[C ₂ mim][TFSI]/water and (d) TX-100/[C ₄ mim][PF ₆]/water microemulsions as a function of ϕ at 25 °C	127
5.3.2.	The V^E of (a) TX-100/cyclohexane/[C ₂ mim][EtSO ₄], TX-100/cyclohexane/[C ₂ mim][BF ₄], (b) TX-100/cyclohexane/[C ₄ mim][BF ₄], TX-100/cyclohexane/[C ₄ mim][MeSO ₄] , (c) TX-100/[C ₂ mim][TFSI]/water and (d) TX-100/[C ₄ mim][PF ₆]/water microemulsions as a function of ϕ at 25 °C	128
5.3.3.	The n^E of (a) TX-100/cyclohexane/[C ₂ mim][EtSO ₄], TX-100/cyclohexane/[C ₂ mim][BF ₄], (b) TX-100/cyclohexane/[C ₄ mim][BF ₄], TX-100/cyclohexane/[C ₄ mim][MeSO ₄] , (c) TX-100/[C ₂ mim][TFSI]/water and (d) TX-100/[C ₄ mim][PF ₆]/water microemulsions as a function of ϕ at 25 °C	130
5.3.4.	The R^E of (a) TX-100/cyclohexane/[C ₂ mim][EtSO ₄], TX-100/cyclohexane/[C ₂ mim][BF ₄], (b) TX-100/cyclohexane/[C ₄ mim][BF ₄], TX-100/cyclohexane/[C ₄ mim][MeSO ₄] , (c) TX-100/[C ₂ mim][TFSI]/water and (d) TX-100/[C ₄ mim][PF ₆]/water microemulsions as a function of ϕ at 25 °C	132
5.3.5.	The $d\log\sigma/dR$ of (a) CTAB/1-butanol/cyclohexane/[C ₂ mim][MeSO ₄], CTAB/1-butanol/cyclohexane/[C ₂ mim][EtSO ₄] and (b) CTAB/1-butanol/cyclohexane/[C ₂ mim][MeSO ₄], CTAB/1-butanol/cyclohexane/[C ₄ mim][MeSO ₄] microemulsions as a function of R at 25 °C	134

5.3.6.	Diameter of droplets of (a) CTAB/1-butanol/cyclohexane/[C ₂ mim][MeSO ₄], butanol/cyclohexane/[C ₂ mim][EtSO ₄] and (b) CTAB/1-butanol/cyclohexane/[C ₂ mim][MeSO ₄], butanol/cyclohexane/[C ₄ mim][MeSO ₄] microemulsions as a function of <i>R</i> at 25 °C	135
6.3.1.	Viscosity of TX-100/cyclohexane/[C ₂ mim][EtSO ₄], TX-100/[C ₂ mim][TFSI]/water and TX-100/cyclohexane/water microemulsions (ME) as a function of <i>R</i> or <i>W</i> ₀ at 25 °C. <i>R</i> value at the top is for TX-100/cyclohexane/[C ₂ mim][EtSO ₄] microemulsions to understand clearly	142
6.3.2.	Density of TX-100/cyclohexane/[C ₂ mim][EtSO ₄], TX-100/[C ₂ mim][TFSI]/water and TX-100/cyclohexane/water microemulsions (ME) as a function of <i>R</i> or <i>W</i> ₀ at 25 °C. <i>R</i> value at the top is for TX-100/cyclohexane/[C ₂ mim][EtSO ₄] microemulsions to understand clearly	144
6.3.3.	Refractive index of TX-100/cyclohexane/[C ₂ mim][EtSO ₄], TX-100/[C ₂ mim][TFSI]/water and TX-100/cyclohexane/water microemulsions (ME) as a function of <i>R</i> or <i>W</i> ₀ at 25 °C. <i>R</i> value at the top is for TX-100/cyclohexane/[C ₂ mim][EtSO ₄] microemulsions to understand clearly	144
6.3.4.	Viscosity of CTAB/1-butanol/cyclohexane/[C ₂ mim][EtSO ₄] and CTAB/1-butanol/cyclohexane/water microemulsions (ME) as a function of polar phase to CTAB mole ratio at 25 °C. Viscosity at the right side is for CTAB/1-butanol/cyclohexane/water microemulsions to understand clearly	145
6.3.5.	Density of CTAB/1-butanol/cyclohexane/[C ₂ mim][EtSO ₄] and CTAB/1-butanol/cyclohexane/water microemulsions (ME) as a function of polar phase to CTAB mole ratio at 25 °C. Density at the right side is for CTAB/1-butanol/cyclohexane/water microemulsions to understand clearly	146
6.3.6.	Refractive index of CTAB/1-butanol/cyclohexane/[C ₂ mim][EtSO ₄] and CTAB/1-butanol/cyclohexane/water microemulsions (ME) as a function of polar phase to CTAB mole ratio at 25 °C	147
6.3.7.	Conductivity of TX-100/cyclohexane/[C ₂ mim][EtSO ₄] and CTAB/1-butanol/cyclohexane/[C ₂ mim][EtSO ₄] microemulsions (ME) as a function of <i>R</i> at 25 °C. Conductivity at the left and <i>R</i> value at the bottom is for TX-100/cyclohexane/[C ₂ mim][EtSO ₄] microemulsions	148
6.3.8.	Viscosity of TX-100/cyclohexane/[C ₂ mim][EtSO ₄] and CTAB/1-butanol/cyclohexane/[C ₂ mim][EtSO ₄] microemulsions (ME) as a function of <i>R</i> at 25 °C	149
6.3.9.	Density of TX-100/cyclohexane/[C ₂ mim][EtSO ₄] and CTAB/1-butanol/cyclohexane/[C ₂ mim][EtSO ₄] microemulsions (ME) as a function of <i>R</i> at 25 °C. Density at the left and <i>R</i> value at the bottom is for TX-100/cyclohexane/[C ₂ mim][EtSO ₄] microemulsions	150
6.3.10.	Refractive index of TX-100/cyclohexane/[C ₂ mim][EtSO ₄] and CTAB/1-butanol/cyclohexane/[C ₂ mim][EtSO ₄] microemulsions (ME) as a function of <i>R</i> at 25 °C. Conductivity at the left and <i>R</i> value at the bottom is for TX-100/cyclohexane/[C ₂ mim][EtSO ₄] microemulsions	150
7.3.1.	Absorption spectra of <i>p</i> -NP (10.87 mM) in aqueous medium at pH = 8.3 (50 mM Tris-HCl) at 37 °C	158
7.3.2.	(a) Absorbance as a function of <i>t</i> and (b) effect of the concentration of <i>p</i> -NPB on the <i>v</i> of the lipase catalyzed hydrolysis of <i>p</i> -NPB in aqueous medium at 37 °C. Conditions were: [lipase] = 2 mgmL ⁻¹ , pH = 8.3 (50 mM Tris-HCl), λ = 410 nm	158

7.3.3.	The ν as a function of $[p\text{-NPB}]$. Conditions were: $[\text{lipase}] = 2 \text{ mgmL}^{-1}$, $\text{pH} = 8.3$ (50 mM Tris-HCl), $\lambda = 410 \text{ nm}$	159
7.3.4.	The $1/\nu$ as a function of $1/[p\text{-NPB}]$. Conditions were: $[\text{lipase}] = 2 \text{ mgmL}^{-1}$, $\text{pH} = 8.3$ (50 mM Tris-HCl), $\lambda = 410 \text{ nm}$	160
7.3.5.	Absorption spectra of $p\text{-NP}$ (10.87 mM) in conventional microemulsion at $W_o = 4.20$, $\text{pH} = 8.3$ (50 mM Tris-HCl) at 37°C	161
7.3.6.	(a) Absorbance as a function of t and (b) effect of W_o on the ν of the lipase catalyzed hydrolysis of $p\text{-NPB}$ in conventional microemulsions at 37°C . Conditions were: $[\text{lipase}] = 2 \text{ mgmL}^{-1}$, $[p\text{-NPB}] = 10.87 \text{ mM}$, $\text{pH} = 8.3$ (50 mM Tris-HCl), $\lambda = 410 \text{ nm}$	161
7.3.7.	Absorption spectra of $p\text{-NP}$ (10.87 mM) in IL microemulsion at $W_o = 4.20$, $\text{pH} = 8.3$ (50 mM Tris-HCl) at 37°C	162
7.3.8.	(a) Absorbance as a function of t and (b) effect of W_o on the ν of the lipase catalyzed hydrolysis of $p\text{-NPB}$ in IL microemulsions at 37°C . Conditions were: $[\text{lipase}] = 2 \text{ mgmL}^{-1}$, $[p\text{-NPB}] = 10.87 \text{ mM}$, $\text{pH} = 8.3$ (50 mM Tris-HCl), $\lambda = 410 \text{ nm}$	163
7.3.9.	(a) Absorbance as a function of t of the lipase catalyzed hydrolysis of $p\text{-NPB}$ in aqueous medium (dark blue) and conventional microemulsion (dark red) at $W_o = 4.96$ and (b) ν for aqueous medium and conventional microemulsions with different W_o at 37°C . In Figure (a) absorbance in left side and t in bottom is for conventional microemulsion and absorbance in right side and t in top is for aqueous medium. Conditions were: $[\text{lipase}] = 2 \text{ mgmL}^{-1}$, $[p\text{-NPB}] = 10.87 \text{ mM}$, $\text{pH} = 8.3$ (50 mM Tris-HCl), $\lambda = 410 \text{ nm}$	164
7.3.10.	(a) Absorbance as a function of t of the lipase catalyzed hydrolysis of $p\text{-NPB}$ in conventional microemulsion (dark red) at $W_o = 4.96$ and IL microemulsion (dark yellow) at $W_o = 4.20$ and (b) ν for conventional and IL microemulsions with different W_o at 37°C . In Figure (a) absorbance in left side and t in bottom is for IL microemulsion and absorbance in right side and t in top is for conventional microemulsion. Conditions were: $[\text{lipase}] = 2 \text{ mgmL}^{-1}$, $[p\text{-NPB}] = 10.87 \text{ mM}$, $\text{pH} = 8.3$ (50 mM Tris-HCl), $\lambda = 410 \text{ nm}$	165
7.3.11.	(a) Absorbance as a function of t of the lipase catalyzed hydrolysis of $p\text{-NPB}$ in aqueous medium (dark blue), conventional microemulsion (dark red) at $W_o = 4.96$ and IL microemulsion (dark yellow) at $W_o = 4.20$ and (b) ν for aqueous medium, conventional and IL microemulsions with different W_o at 37°C . In Figure (a) absorbance in left side and t in bottom is for aqueous medium and IL microemulsion and absorbance in right side and t in top is for conventional microemulsion. Conditions were: $[\text{lipase}] = 2 \text{ mgmL}^{-1}$, $[p\text{-NPB}] = 10.87 \text{ mM}$, $\text{pH} = 8.3$ (50 mM Tris-HCl), $\lambda = 410 \text{ nm}$	166

LIST OF SCHEMES

Scheme No.	Caption	Page No.
1.1.	Schematic representation of (a) a surfactant and (b) orientation of surfactants at oil-water interface	5
1.2.	Classification of surfactant according to the composition of their head	6
1.3.	Schematic representation of the (a) formation of micelles and (b) physical properties of aqueous surfactant solution as a function of surfactant concentration	7
1.4.	Formation of self- assembly of surfactants	8
1.5.	Schematic structures of surfactant self assemblies for different values of critical packing parameter (CPP) and hydrophile-lipophile balance (HLB)	9
1.6.	Types of microemulsions	11
1.7.	Different types of Winsor structures	12
1.8.	Static and dynamic percolation processes	15
1.9.	Structure of NaCl and [C ₂ mim][Cl]	15
1.10.	Common cations and anions used in ILs	16
1.11.	Few examples of cations of PILs	17
1.12.	Concept of complex cation in solvate ILs	18
1.13.	Schematic model of the induced fit mechanism	23
1.14.	Structure of cations a) [C ₂ mim] ⁺ , b) [C ₄ mim] ⁺ , anions c) [MeSO ₄] ⁻ , d) [EtSO ₄] ⁻ , e) [BF ₄] ⁻ , f) [TFSI] ⁻ , g) [PF ₆] ⁻ , surfactants (h) TX-100 (nonionic), (i) CTAB (cationic), (j) SDS (anionic), cosurfactants (k) 1-butanol, (l) 1-pentanol, (m) 1-hexanol, dye (n) RBD, substrate (o) <i>p</i> -NPB	32
2.1.	Preparation of TX-100 microemulsions using different amounts of conventional polar (water) and non-polar (cyclohexane) phases	44
2.2.	Preparation of CTAB microemulsions using different amounts of conventional polar (water) and non-polar (cyclohexane) phases	45
2.3.	Preparation of TX-100/cyclohexane/IL microemulsions	46
2.4.	Preparation of TX-100/IL/water microemulsions	47
2.5.	Preparation of CTAB/1-butanol/cyclohexane/IL microemulsions	49
3.1.	Interaction and arrangement of ions of ILs in (a) IL/o microemulsion for TX-100/cyclohexane/[C ₂ mim][MeSO ₄], (b) IL/o, bicontinuous (BC) and o/IL microemulsions for TX-100/cyclohexane/[C ₂ mim][EtSO ₄] and (c) IL/o, bicontinuous (BC) and o/IL microemulsions for TX-100/cyclohexane/[C ₂ mim][BF ₄] systems	79
3.2.	Interaction and arrangement of ions of ILs in (a) IL/o microemulsion for TX-100/cyclohexane/[C ₂ mim][MeSO ₄] system and (b) IL/o, bicontinuous (BC) and o/IL microemulsions for TX-100/cyclohexane/[C ₄ mim][MeSO ₄] systems	96
3.3.	Interactions of TX-100 through different hydrogen bonding sites with (a) [C ₂ mim][BF ₄], (b) [C ₄ mim][MeSO ₄], (c) water and oil phase (d) [C ₂ mim][PF ₆], (e) [C ₂ mim][TFSI].	98
3.4.	Arrangement of substances in reverse micelle for (a) TX-100/cyclohexane/[C ₂ mim][BF ₄] and (c) TX-100/[C ₂ mim][TFSI]/water microemulsions and micelle droplets for (b) TX-100/cyclohexane/[C ₂ mim][BF ₄] and (d) TX-100/[C ₂ mim][TFSI]/water microemulsions	99
3.5.	Arrangement of the cations around spherical anions in IL	100

4.1.	Scheme of the interfacial film layer of inverse CTAB microemulsion droplets	118
4.2.	(a) Strong hydrophobic interaction of $[\text{EtSO}_4]^-$ anion compared to $[\text{MeSO}_4]^-$ anion with the CTAB tail group when the cation is $[\text{C}_2\text{mim}]^+$ (b) Strong hydrophobic interaction of $[\text{C}_4\text{mim}]^+$ cation compared to $[\text{C}_2\text{mim}]^+$ cation with the CTAB tail group when the anion is $[\text{MeSO}_4]^-$	119
5.1.	(a) Different microstructures of TX-100/cyclohexane/ $[\text{C}_2\text{mim}][\text{EtSO}_4]$, TX-100/cyclohexane/ $[\text{C}_2\text{mim}][\text{BF}_4]$, TX-100/cyclohexane/ $[\text{C}_4\text{mim}][\text{BF}_4]$, and TX-100/cyclohexane/ $[\text{C}_4\text{mim}][\text{MeSO}_4]$ microemulsions with increasing ϕ_{IL} and (b) TX-100/ $[\text{C}_2\text{mim}][\text{TFSI}]$ /water and TX-100/ $[\text{C}_4\text{mim}][\text{PF}_6]$ /water microemulsions with increasing ϕ_{w}	133
5.2.	Different microstructures of CTAB microemulsions with increasing R	136
7.1.	Preparation of (a) TX-100/cyclohexane/water and (b) TX-100/ $[\text{C}_4\text{mim}][\text{PF}_6]$ /water microemulsions at pH 8.3 (50 mM Tris-HCl)	156
7.2.	Schematic representation of the activating effect of $[\text{C}_2\text{mim}][\text{PF}_6]$ on lipase in presence of water in bicontinuous IL based microemulsion. Dark blue color represents polar (water) phase and dark yellow color represents oil ($[\text{C}_2\text{mim}][\text{PF}_6]$) phase	167

LIST OF TABLES

Table No.	Caption	Page No.
1.1.	Potential and current uses of ILs	16
2.1.	Preparation of TX-100/cyclohexane/water microemulsions	44
2.2.	Preparation of CTAB/1-butanol/cyclohexane/water microemulsions	45
2.3.	Preparation of TX-100/cyclohexane/IL microemulsions	46
2.4.	Preparation of TX-100/IL/water microemulsions	48
2.5.	Preparation of CTAB/1-butanol/cyclohexane/IL microemulsions	49
7.1.	Kinetic parameters of lipase-catalyzed hydrolysis of <i>p</i> -NPB in aqueous medium	160
A1.	The σ for TX-100/cyclohexane/[C ₂ mim][MeSO ₄], TX-100/cyclohexane/[C ₂ mim][EtSO ₄] and TX-100/cyclohexane/[C ₂ mim][BF ₄] microemulsions with increasing <i>R</i> at 25 °C	172
A2.	The σ for TX-100/cyclohexane/[C ₄ mim][MeSO ₄] and TX-100/cyclohexane/[C ₄ mim][BF ₄] microemulsions with increasing <i>R</i> at 25 °C	172
A3.	The values of σ for TX-100/[C ₂ mim][TFSI]/water and TX-100/[C ₂ mim][PF ₆]/water microemulsions with decreasing <i>W</i> ₀ at 25 °C	172
A4.	The η for TX-100/cyclohexane/[C ₂ mim][MeSO ₄], TX-100/cyclohexane/[C ₂ mim][EtSO ₄] and TX-100/cyclohexane/[C ₂ mim][BF ₄] microemulsions with increasing <i>R</i> at 25 °C	173
A5.	The η for TX-100/cyclohexane/[C ₄ mim][MeSO ₄] and TX-100/cyclohexane/[C ₄ mim][BF ₄] microemulsions with increasing <i>R</i> at 25 °C	173
A6.	The η for TX-100/[C ₂ mim][TFSI]/water and TX-100/[C ₂ mim][PF ₆]/water microemulsions with decreasing <i>W</i> ₀ at 25 °C	173
A7.	The η for TX-100/cyclohexane/[C ₂ mim][MeSO ₄], TX-100/cyclohexane/[C ₂ mim][EtSO ₄] and TX-100/cyclohexane/[C ₂ mim][BF ₄] microemulsions with increasing temperature (°C) at <i>R</i> = 0.2255	174
A8.	(b) The values of η for TX-100/cyclohexane/[C ₄ mim][MeSO ₄] and TX-100/cyclohexane/[C ₄ mim][BF ₄] microemulsions with increasing temperature (°C) at <i>R</i> = 0.2255	174
A9.	Diameter of droplets for TX-100/cyclohexane/[C ₂ mim][MeSO ₄], TX-100/cyclohexane/[C ₂ mim][EtSO ₄], TX-100/cyclohexane/[C ₂ mim][BF ₄], TX-100/cyclohexane/[C ₄ mim][MeSO ₄], TX-100/cyclohexane/[C ₄ mim][BF ₄], TX-100/[C ₂ mim][PF ₆]/water, TX-100/[C ₄ mim][PF ₆]/water and TX-100/[C ₂ mim][TFSI]/water microemulsions at different <i>R</i> or <i>W</i> ₀ at 25 °C	174
A10.	The ρ for TX-100/cyclohexane/[C ₂ mim][MeSO ₄], TX-100/cyclohexane/[C ₂ mim][EtSO ₄] and TX-100/cyclohexane/[C ₂ mim][BF ₄] microemulsions with increasing <i>R</i> at 25 °C	176
A11.	The ρ for TX-100/cyclohexane/[C ₄ mim][MeSO ₄] and TX-100/cyclohexane/[C ₄ mim][BF ₄] microemulsions with increasing <i>R</i> at 25 °C	176
A12.	The ρ for TX-100/[C ₂ mim][TFSI]/water and TX-100/[C ₂ mim][PF ₆]/water microemulsions with decreasing <i>W</i> ₀ at 25 °C	176

A13.	The ρ for TX-100/cyclohexane/[C ₂ mim][MeSO ₄], TX-100/cyclohexane/[C ₂ mim][EtSO ₄] and TX-100/cyclohexane/[C ₂ mim][BF ₄] microemulsions with increasing temperature (°C) at $R = 0.2255$	177
A14.	The ρ for TX-100/cyclohexane/[C ₄ mim][MeSO ₄] and TX-100/cyclohexane/[C ₄ mim][BF ₄] microemulsions with increasing temperature (°C) at $R = 0.2255$	177
A15.	The n for TX-100/cyclohexane/[C ₂ mim][MeSO ₄], TX-100/cyclohexane/[C ₂ mim][EtSO ₄] and TX-100/cyclohexane/[C ₂ mim][BF ₄] microemulsions with increasing R at 25 °C	177
A16.	The σ for n data of TX-100/cyclohexane/[C ₄ mim][MeSO ₄] and TX-100/cyclohexane/[C ₄ mim][BF ₄] microemulsions as a function of R at 25 °C	178
A17.	The n for TX-100/[C ₂ mim][TFSI]/water and TX-100/[C ₂ mim][PF ₆]/water microemulsions with decreasing W_o at 25 °C	178
A18.	The n for TX-100/cyclohexane/[C ₂ mim][MeSO ₄], TX-100/cyclohexane/[C ₂ mim][EtSO ₄] and TX-100/cyclohexane/[C ₂ mim][BF ₄] microemulsions with increasing temperature (°C) at $R = 0.2255$	178
A19.	The n for TX-100/cyclohexane/[C ₄ mim][MeSO ₄] and TX-100/cyclohexane/[C ₄ mim][BF ₄] microemulsions with increasing temperature (°C) at $R = 0.2255$	179
A20.	The γ for da TX-100/cyclohexane/[C ₂ mim][MeSO ₄] and TX-100/cyclohexane/[C ₂ mim][EtSO ₄] microemulsions with increasing R at 25 °C	179
A21.	The γ for TX-100/cyclohexane/[C ₂ mim][PF ₆] and TX-100/cyclohexane/[C ₂ mim][TFSI] microemulsions with decreasing W_o at 25 °C	179
A22.	The σ for TX-100/cyclohexane/[C ₂ mim][MeSO ₄] and TX-100/cyclohexane/[C ₄ mim][MeSO ₄] microemulsions with increasing R at 25 °C	180
A23.	The σ for TX-100/cyclohexane/[C ₂ mim][BF ₄] and TX-100/cyclohexane/[C ₄ mim][BF ₄] microemulsions with increasing R at 25 °C	180
A24.	(c) The σ for TX-100/[C ₂ mim][PF ₆]/water and TX-100/[C ₄ mim][PF ₆]/water microemulsions with decreasing W_o at 25 °C	180
A25.	Walden plot data of TX-100/cyclohexane/[C ₂ mim][BF ₄] and TX-100/cyclohexane/[C ₄ mim][BF ₄] microemulsions	181
A26.	Walden plot data of TX-100/[C ₂ mim][PF ₆]/water and TX-100/[C ₄ mim][PF ₆]/water microemulsions.	181
A27.	The η for TX-100/cyclohexane/[C ₂ mim][MeSO ₄] and TX-100/cyclohexane/[C ₄ mim][MeSO ₄] microemulsions with increasing R at 25 °C	181
A28.	The η for TX-100/cyclohexane/[C ₂ mim][BF ₄] and TX-100/cyclohexane/[C ₄ mim][BF ₄] microemulsions with increasing R at 25 °C	182
A29.	The η for TX-100/[C ₂ mim][PF ₆]/water and TX-100/[C ₄ mim][PF ₆]/water microemulsions with decreasing W_o at 25 °C	182
A30.	The η for TX-100/cyclohexane/[C ₂ mim][MeSO ₄] and TX-100/cyclohexane/[C ₄ mim][MeSO ₄] microemulsions with increasing temperature (°C) at $R = 0.2255$	182

A31.	The η for TX-100/cyclohexane/[C ₂ mim][BF ₄] and TX-100/cyclohexane/[C ₄ mim][BF ₄] microemulsions with increasing temperature (°C) at $R = 0.2255$	183
A32.	The ρ for TX-100/cyclohexane/[C ₂ mim][MeSO ₄] and TX-100/cyclohexane/[C ₄ mim][MeSO ₄] microemulsions with increasing R at 25 °C	183
A33.	The ρ for TX-100/cyclohexane/[C ₂ mim][BF ₄] and TX-100/cyclohexane/[C ₄ mim][BF ₄] microemulsions with increasing R at 25 °C	183
A34.	The ρ for TX-100/[C ₂ mim][PF ₆]/water and TX-100/[C ₄ mim][PF ₆]/water microemulsions with decreasing W_0 at 25 °C	184
A35.	The ρ for TX-100/cyclohexane/[C ₂ mim][MeSO ₄] and TX-100/cyclohexane/[C ₄ mim][MeSO ₄] microemulsions with increasing temperature (°C) at $R = 0.2255$	184
A36.	The ρ for TX-100/cyclohexane/[C ₂ mim][BF ₄] and TX-100/cyclohexane/[C ₄ mim][BF ₄] microemulsions with increasing temperature (°C) at $R = 0.2255$.	184
A37.	The n for TX-100/cyclohexane/[C ₂ mim][MeSO ₄] and TX-100/cyclohexane/[C ₄ mim][MeSO ₄] microemulsions with increasing R at 25 °C	185
A38.	The n for TX-100/cyclohexane/[C ₂ mim][BF ₄] and TX-100/cyclohexane/[C ₄ mim][BF ₄] microemulsions with increasing R at 25 °C	185
A39.	The n for TX-100/[C ₂ mim][PF ₆]/water and TX-100/[C ₄ mim][PF ₆]/water microemulsions with decreasing W_0 at 25 °C	185
A40.	The n for TX-100/cyclohexane/[C ₂ mim][MeSO ₄] and TX-100/cyclohexane/[C ₄ mim][MeSO ₄] microemulsions with increasing temperature (°C) at $R = 0.2255$.	186
A41.	The n for TX-100/cyclohexane/[C ₂ mim][BF ₄] and TX-100/cyclohexane/[C ₄ mim][BF ₄] microemulsions with increasing temperature (°C) at $R = 0.2255$	186
A42.	The γ for TX-100/[C ₂ mim][PF ₆]/water and TX-100/[C ₄ mim][PF ₆]/water microemulsions with decreasing W_0 at 25 °C	186
A43.	The σ for CTAB/1-butanol/cyclohexane/[C ₂ mim][MeSO ₄] and CTAB/1-butanol/cyclohexane/[C ₂ mim][EtSO ₄] microemulsions with increasing R at 25 °C	187
A44.	The σ for CTAB/1-butanol/cyclohexane/[C ₂ mim][MeSO ₄] and CTAB/1-butanol/cyclohexane/[C ₄ mim][MeSO ₄] microemulsions with increasing R at 25 °C	187
A45.	The η for CTAB/1-butanol/cyclohexane/[C ₂ mim][MeSO ₄] and CTAB/1-butanol/cyclohexane/[C ₂ mim][EtSO ₄] microemulsions with increasing R at 25 °C	187
A46.	The η for CTAB/1-butanol/cyclohexane/[C ₂ mim][MeSO ₄] and CTAB/1-butanol/cyclohexane/[C ₄ mim][MeSO ₄] microemulsions with increasing R at 25 °C	188
A47.	The η for CTAB/1-butanol/cyclohexane/[C ₂ mim][MeSO ₄] and CTAB/1-butanol/cyclohexane/[C ₂ mim][EtSO ₄] microemulsions with increasing temperature (°C) at $R = 1.5424$	188
A48.	The η for CTAB/1-butanol/cyclohexane/[C ₂ mim][MeSO ₄] and CTAB/1-butanol/cyclohexane/[C ₄ mim][MeSO ₄] microemulsions with increasing temperature (°C) at $R = 1.5424$	188
A49.	Diameter of droplets of CTAB microemulsions at different R at 25 °C	189
A50.	The ρ for CTAB/1-butanol/cyclohexane/[C ₂ mim][MeSO ₄] and CTAB/1-butanol/cyclohexane/[C ₂ mim][EtSO ₄] microemulsions with increasing R at 25 °C	189

A51.	The ρ for CTAB/1-butanol/cyclohexane/[C ₂ mim][MeSO ₄] and CTAB/1-butanol/cyclohexane/[C ₄ mim][MeSO ₄] microemulsions with increasing R at 25 °C	190
A52.	The ρ for CTAB/1-butanol/cyclohexane/[C ₂ mim][MeSO ₄] and CTAB/1-butanol/cyclohexane/[C ₂ mim][EtSO ₄] microemulsions with increasing temperature (°C) at $R = 1.5424$.	190
A53.	The ρ for CTAB/1-butanol/cyclohexane/[C ₂ mim][MeSO ₄] and CTAB/1-butanol/cyclohexane/[C ₄ mim][MeSO ₄] microemulsions with increasing temperature (°C) at $R = 1.5424$	190
A54.	The n for CTAB/1-butanol/cyclohexane/[C ₂ mim][MeSO ₄] and CTAB/1-butanol/cyclohexane/[C ₂ mim][EtSO ₄] microemulsions with increasing R at 25 °C	191
A55.	The n for CTAB/1-butanol/cyclohexane/[C ₂ mim][MeSO ₄] and CTAB/1-butanol/cyclohexane/[C ₄ mim][MeSO ₄] microemulsions with increasing R at 25 °C	191
A56.	The n for CTAB/1-butanol/cyclohexane/[C ₂ mim][MeSO ₄] and CTAB/1-butanol/cyclohexane/[C ₂ mim][EtSO ₄] microemulsions with increasing temperature (°C) at $R = 1.5424$	191
A57.	The n for CTAB/1-butanol/cyclohexane/[C ₂ mim][MeSO ₄] and CTAB/1-butanol/cyclohexane/[C ₄ mim][MeSO ₄] microemulsions with increasing temperature (°C) at $R = 1.5424$	192
A58.	The γ for CTAB/1-butanol/cyclohexane/[C ₂ mim][MeSO ₄], CTAB/1-butanol/cyclohexane/[C ₂ mim][EtSO ₄] and CTAB/1-butanol/cyclohexane/[C ₄ mim][MeSO ₄] microemulsions with increasing R at 25 °C.	192
A59.	The $d\log\sigma/d\phi$ for TX-100/cyclohexane/[C ₂ mim][EtSO ₄] and TX-100/cyclohexane/[C ₂ mim][BF ₄] microemulsions as a function of ϕ at 25 °C.	192
A60.	The $d\log\sigma/d\phi$ for TX-100/cyclohexane/[C ₄ mim][BF ₄] and TX-100/cyclohexane/[C ₄ mim][MeSO ₄] microemulsions as a function of ϕ at 25 °C	193
A61.	The $d\log\sigma/d\phi$ for TX-100/[C ₂ mim][TFSI]/water microemulsions as a function of ϕ at 25 °C	193
A62.	The $d\log\sigma/d\phi$ for TX-100/[C ₄ mim][PF ₆]/water microemulsions as a function of ϕ at 25 °C	193
A63.	The V^E for TX-100/cyclohexane/[C ₂ mim][EtSO ₄] and TX-100/cyclohexane/[C ₂ mim][BF ₄] microemulsions as a function of ϕ at 25 °C	194
A64.	The V^E for TX-100/cyclohexane/[C ₄ mim][BF ₄] and TX-100/cyclohexane/[C ₄ mim][MeSO ₄] microemulsions as a function of ϕ at 25 °C	194
A65.	The V^E for TX-100/[C ₂ mim][TFSI]/water microemulsions as a function of ϕ at 25 °C	194
A66.	The V^E for TX-100/[C ₄ mim][PF ₆]/water microemulsions as a function of ϕ at 25 °C	195
A67.	The n^E for TX-100/cyclohexane/[C ₂ mim][EtSO ₄] and TX-100/cyclohexane/[C ₂ mim][BF ₄] microemulsions as a function of ϕ at 25 °C	195
A68.	The n^E for TX-100/cyclohexane/[C ₄ mim][BF ₄] and TX-100/cyclohexane/[C ₄ mim][MeSO ₄] microemulsions as a function of ϕ at 25 °C	195
A69.	The n^E for TX-100/[C ₂ mim][TFSI]/water microemulsions as a function of ϕ at 25 °C	196
A70.	The values of n^E for TX-100/[C ₄ mim][PF ₆]/water microemulsions as a function of ϕ at 25 °C	196

A71.	The R^E for TX-100/cyclohexane/[C ₂ mim][EtSO ₄] and TX-100/cyclohexane/[C ₂ mim][BF ₄] microemulsions as a function of ϕ at 25 °C	196
A72.	The R^E for TX-100/cyclohexane/[C ₄ mim][BF ₄], TX-100/cyclohexane/[C ₄ mim][MeSO ₄] microemulsions as a function of ϕ at 25 °C	197
A73.	The values of R^E for TX-100/[C ₂ mim][TFSI]/water microemulsions as a function of ϕ at 25 °C	197
A74.	The R^E for TX-100/[C ₄ mim][PF ₆]/water microemulsions as a function of ϕ at 25 °C	197
A75.	The $\text{dlog}\sigma/\text{d}R$ for CTAB/1-butanol/cyclohexane/[C ₂ mim][MeSO ₄] and CTAB/1-butanol/cyclohexane/[C ₂ mim][EtSO ₄] microemulsions as a function of R at 25 °C	198
A76.	The $\text{dlog}\sigma/\text{d}R$ for CTAB/1-butanol/cyclohexane/[C ₂ mim][MeSO ₄] and CTAB/1-butanol/cyclohexane/[C ₄ mim][MeSO ₄] microemulsions as a function of R at 25 °C	198
A77.	Diameter of droplets for CTAB/1-butanol/cyclohexane/[C ₂ mim][MeSO ₄] and CTAB/1-butanol/cyclohexane/[C ₂ mim][EtSO ₄] microemulsions as a function of R at 25 °C	198
A78.	Diameter of droplets for CTAB/1-butanol/cyclohexane/[C ₂ mim][MeSO ₄], CTAB/1-butanol/cyclohexane/[C ₄ mim][MeSO ₄] microemulsions as a function of R at 25 °C	199
A79.	The η for TX-100/cyclohexane/[C ₂ mim][EtSO ₄], TX-100/[C ₂ mim][TFSI]/water and TX-100/cyclohexane/water microemulsions as a function of R or W_0 at 25 °C	199
A80.	The ρ for TX-100/cyclohexane/[C ₂ mim][EtSO ₄], TX-100/[C ₂ mim][TFSI]/water and TX-100/cyclohexane/water microemulsions as a function of R or W_0 at 25 °C	200
A81.	The n for TX-100/cyclohexane/[C ₂ mim][EtSO ₄], TX-100/[C ₂ mim][TFSI]/water and TX-100/cyclohexane/water microemulsions as a function of R or W_0 at 25 °C.	200
A82.	The η for CTAB/1-butanol/cyclohexane/[C ₂ mim][EtSO ₄] and CTAB/1-butanol/cyclohexane/water microemulsions as a function of R or W_0 at 25 °C	201
A83.	The ρ for CTAB/1-butanol/cyclohexane/[C ₂ mim][EtSO ₄] and CTAB/1-butanol/cyclohexane/water microemulsions as a function of R or W_0 at 25 °C	201
A84.	The n for CTAB/1-butanol/cyclohexane/[C ₂ mim][EtSO ₄] and CTAB/1-butanol/cyclohexane/water microemulsions as a function of R or W_0 at 25 °C	202
A85.	The σ for TX-100/cyclohexane/[C ₂ mim][EtSO ₄] and CTAB/1-butanol/cyclohexane/[C ₂ mim][EtSO ₄] microemulsions as a function of R at 25 °C	202
A86.	The η for TX-100/cyclohexane/[C ₂ mim][EtSO ₄] and CTAB/1-butanol/cyclohexane/[C ₂ mim][EtSO ₄] microemulsions as a function of R at 25 °C	202
A87.	The ρ for TX-100/cyclohexane/[C ₂ mim][EtSO ₄] and CTAB/1-butanol/cyclohexane/[C ₂ mim][EtSO ₄] microemulsions as a function of R at 25 °C	203
A88.	The n for TX-100/cyclohexane/[C ₂ mim][EtSO ₄] and CTAB/1-butanol/cyclohexane/[C ₂ mim][EtSO ₄] microemulsions as a function of R at 25 °C	203

A89.	The ν as a function of $[p\text{-NPB}]$ of the lipase catalyzed hydrolysis of $p\text{-NPB}$ in aqueous medium	203
A90.	The ν as a function of W_o of the lipase catalyzed hydrolysis of $p\text{-NPB}$ in conventional microemulsions	204
A91.	The ν as a function of W_o of the lipase catalyzed hydrolysis of $p\text{-NPB}$ in IL microemulsions	204
A92.	The ν for aqueous medium and conventional microemulsions as a function of W_o	204
A93.	The ν for conventional and IL microemulsions as a function of W_o	204
A94.	The ν for aqueous medium, conventional and IL microemulsions as a function of W_o	204

LIST OF SYMBOLS

Name	Symbol
IL to surfactant mole ratio	R
Water to surfactant mole ratio	W_o
Volume fraction of polar (IL) phase	ϕ_{IL}
Volume fraction of polar (water) phase	ϕ_w
Conductivity	σ
Viscosity	η
Density	ρ
Surface tension	γ
Diameter of droplet	d
Refractive index	n
Molar conductivity	Λ
Initial rate	ν
Substrate concentration	$[S]$
Michaelis constant	K_m
Number of substrate molecules handled by one active site per second.	k_{cat}
Maximum rate	V_m
Regression coefficient	r^2
Wavelength	λ

LIST OF ABBREVIATIONS

Elaborated Form	Abbreviated Form
Ionic liquid	IL
Oil-in-water	o/w
Water-in-oil	w/o
IL-in-oil	IL/o
Oil-in-IL	IL/o
water-in-IL	w/IL
IL-in-water	w/IL
Triton X-100	TX-100
Cetyltrimethylammonium bromide	CTAB
Sodium dodecyl sulfate	SDS
1-Ethyl-3-methylimidazolium bis(trifluoromethylsulfonyl)imide	[C ₂ mim][TFSI]
1-Ethyl-3-methylimidazolium hexafluorophosphate	[C ₂ mim][PF ₆]
1-Butyl-3-methylimidazolium hexafluorophosphate	[C ₄ mim][PF ₆]
1-Ethyl-3-methylimidazolium ethyl sulfate	[C ₂ mim][EtSO ₄]
1-Butyl-3-methylimidazolium methyl sulfate	[C ₄ mim][MeSO ₄]
1-Ethyl-3-methylimidazolium methyl sulfate	[C ₂ mim][MeSO ₄]
1-Ethyl-3-methylimidazolium tetrafluoroborate	[C ₂ mim][BF ₄]
1-Butyl-3-methylimidazolium tetrafluoroborate	[C ₄ mim][BF ₄]
Reichardt's Betaine dye	RBD
Tris(hydroxymethyl)aminomethane	Tris
4-Nitrophenylbutyrate	<i>p</i> -NPB
4-Nitrophenol	<i>p</i> -NP
Dynamic light scattering	DLS

1.1. Background

Microemulsions are thermodynamically stable liquid mixtures of two immiscible polar and nonpolar liquids and an amphiphilic component, surfactant is used with/without the assistance of a co-surfactant [1]. A monolayer between the two immiscible liquids is formed by the surfactant and under appropriate experimental conditions an isotropic and transparent phase is formed. Different types of microemulsions such as oil-in-water (o/w), water-in-oil (w/o) and bicontinuous microemulsions are formed depending on the amount of both polar and nonpolar component and the temperature. Microemulsions can solubilize both polar as well as nonpolar substances. They have low interfacial tension and large interfacial area. Spontaneous formation of different fine microstructures makes them excellent candidates for a variety of applications [2-5]. Synthesis of nanoparticles particularly in w/o type microemulsions is another important application where w/o droplets act as templates [5-7]. Polymer particles can be synthesized in both w/o and o/w microemulsions. Due to the formation of large interface between polar and nonpolar phase, microemulsions are very popular in pesticide formulation, extraction processes, templating, medical applications, cutting oils, cosmetics or as medium for chemical reactions in organic reaction and catalysis [8, 9].

Since microemulsions comprise both water and oil phase, eyes have been pointed on materials which can serve as alternative of either oil or water or both. Ionic liquids (ILs) are promising in this regard. An IL is a salt where the ions are coordinated poorly and these solvents are liquid below 100 °C or even at room temperature. Delocalized charge distribution exists at least in one ion in IL and one component is organic which prevents the formation of a stable crystal lattice. In the last decades, ILs have received much more attention because of their low volatility, high ionic conductivity, nonflammability, far higher liquidus range, non-corrosiveness, and their thermal and chemical stability [10–12]. Since the properties of the ILs are very much dependent on the constituent ions, various ILs can be designed using appropriate combination of the cationic and anionic constituents to obtain desired properties. Hydrophilic ILs may be used instead of water and hydrophobic ILs may be used instead of volatile organic oil phase to serve similar purposes. Environmentally benign solvent, IL can be used in various electronic applications (light-emitting materials, capacitors, batteries), organic reactions, separations electrochemical applications, polymers (synthesis and functionalization), molecular self-assemblies, nanomaterials (synthesis and stabilization) and separation [12-15]. As the polarities of ILs are very close to those of short-chain alcohols, ILs can be used as the polar cores of IL-in-oil (IL/o) microemulsions [16]. Traditional organic solvents can also be replaced by an IL to prepare water-in-IL (w/IL) microemulsions. Hydrophobic or hydrophilic IL nano domains can be used as reaction, separation or extraction media [17].

Recently, study on IL based microemulsions have received an upsurge of interest. Hydrophilic IL can be used as polar phase and hydrophobic IL can be used as oil

phase in IL based microemulsions which have both the advantages of ILs and microemulsions [18-20]. The nonaqueous IL based microemulsions are waterless and can find use in different field because all components are nonvolatile [21-27]. In conventional microemulsions oil phase is a volatile organic solvent that cannot be regarded as a green medium and water is used as a polar phase that cannot dissolve a wide range of chemicals. But in IL based microemulsions oil phase is a non volatile ILs that can be regarded as green medium and ILs is used as a polar phase that can dissolve a number of chemicals.

With a view to studying the microemulsions with both hydrophilic and hydrophobic ILs instead of water and oil phases respectively with different surfactants, it is necessary to explore microstructures in IL based microemulsions. IL based microemulsions show significant properties depending on their structure and selectivity. It is also interesting to investigate how these IL based microemulsions influence enzyme activity.

IL based microemulsions show several advantages in comparison with traditional surfactant based microemulsions. Firstly, strong attraction exists between the imidazolium ring and cosurfactants which facilitates the immobilization of the latter at the liquid/liquid interface and thus prevents its leakage into the conjugated water solution. Secondly, the wide imidazolium head shows a higher capability for solutes than the tertammonium cationic system. Thirdly, through π - π interaction, the imidazolium heads are strongly attracted to each other. Finally, the multitailed structures of ILs provide more than enough platform to explore the hydrophilic-lipophilic equilibrium in IL reverse micelles, which is a key to optimize the partitioning behaviors in microemulsions.

1.2. Supramolecular Chemistry

Supramolecular chemistry is defined as the chemistry of molecular assemblies and of the intermolecular bond [28]. It can be expressed as ‘chemistry beyond the molecule’. It can also be expressed as ‘the chemistry of the non-covalent bond’ and ‘non-molecular chemistry’. Supramolecular chemistry deals with molecular self-assembly, folding, molecular recognition, host-guest chemistry, mechanically-interlocked molecular architectures and dynamic covalent chemistry. Originally supramolecular chemistry was defined as the interaction between a ‘host’ and a ‘guest’ molecule which is non-covalent in nature to form a host-guest complex or supramolecule. The host with a central hole or cavity is an enzyme or synthetic cycle compound and the guest is monoatomic cation or simple inorganic anion. The guest is called a substrate in complex biological interactions. The substrate can be a food particle, hormone, pheromone or neurotransmitter. Supramolecular chemistry deals with the weaker and reversible non-covalent interactions between molecules. These forces include hydrogen bonding, metal coordination, hydrophobic forces, van der Waals forces, π - π interactions and electrostatic effects. The intermolecular interactions of species form a supramolecular assemblies by which molecules adopt a defined arrangement (such as

micelles, membranes, liquid crystals, microemulsions, vesicles, films, mesomorphic phase etc.) without guidance or arrangement from an outside source.

Supramolecular chemistry has opened a new way toward apprehending chemistry as an information science which can explain the concept of molecular information with the aim of gaining progressive control over the spatial (structural) and temporal (dynamic) features of matter and over its complexification through self organization, the drive to life [29, 30].

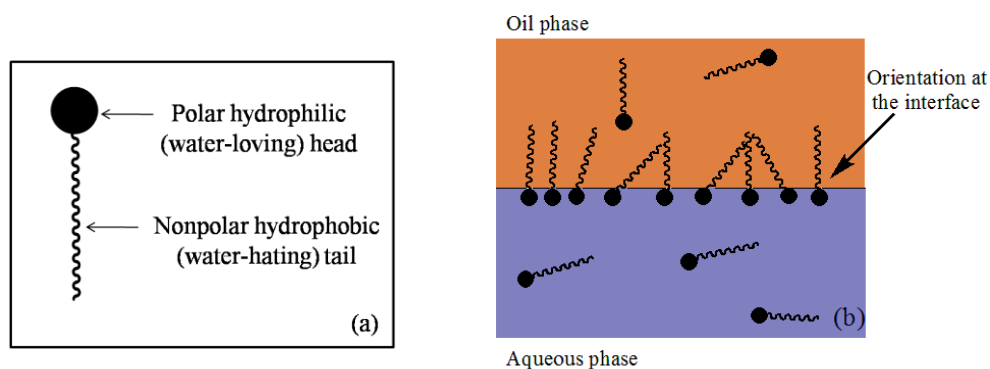
In the development of supramolecular chemistry, three overlapping phases may be considered [31].

- The first concerns of molecular recognition and its corollaries, supramolecular reactivity, catalysis and transport. It relies on design and preorganization and implements information storage and processing.
- The second is that of self-assembly and self-organization. It relies on design and implements programming and programmed systems.
- The third (emerging phase) introduces adaptation and evolution. It relies on self organization through selection in addition to design and implements chemical diversity and “informed” dynamics.

For supramolecular assemblies amphiphilicity is one of the molecular bases. The controllable self-assembly and disassembly can be realized by tuning the amphiphilicity of the building blocks which leads to fabricate a new functional supramolecular assemblies and materials. Not only the supramolecular assembly in solution but also the interfacial molecular assembly has shown increasing significance in fabricating organized thin films and devices. Amphiphiles (such as surfactants, amphiphile-like polymers or lipids) are synthetic or natural molecules with the characteristic self-assembly property and form wide variety of structures such as micelles, vesicles, nanotubes, nanofibers and lamellae. Due to the exceptional self-assembly ability, supramolecular systems based on surfactants have been used for different purposes such as solubilization of organic dye, drug delivery systems, development of switchable molecular devices, biological sensors etc. Amphiphiles with self-assembly property have been widely used in mimic biological systems (assembly of lipids and proteins). The integrated actions of amphiphiles allow the performance of highly specific cellular functions which has paved a way for bottom-up bio-nanotechnology.

1.3. Surfactant

Surfactants, also called surface active agent, are usually amphiphilic organic compounds that lower the surface tension (or interfacial tension) between two liquids or between a liquid and a solid. They can diffuse in water and adsorb at interfaces between air and water. They contain both hydrophobic tail groups and hydrophilic head groups (Scheme 1.1.). Therefore both a water-insoluble component and a water-soluble component exist in surfactant structure and can be soluble in both organic solvents and water. Hydrophobic tail group may extend out of the bulk water phase, into the air or into the oil phase, while the hydrophilic head group remains in the water or other polar phase (Scheme 1.1. (b)). It can be used as detergents, wetting agents, emulsifiers, foaming agents and dispersants.



Scheme 1.1. Schematic representation of (a) a surfactant and (b) orientation of surfactants at oil-water interface.

1.3.1. Basic Surfactant Classifications

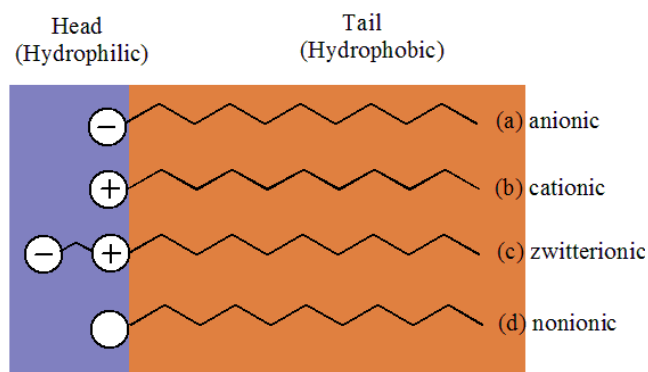
Surfactants can be classified into four classes defined as follows [32] (Scheme 1.2.):

(a) Anionic Surfactants

In anionic surfactant the hydrophilic part is a negatively charged group. They are in general an alkaline metal (Na^+ , K^+) or a quaternary ammonium. They include alkylbenzene sulfonates (detergents), sodium and potassium salts of straight chain fatty acids (soaps), coconut oil fatty acids and tall oil acids, lauryl sulfate (foaming agent), di-alkyl sulfosuccinate (wetting agent), lignosulfonates (dispersants), sulfated triglyceride oils, phosphoric and polyphosphoric acid esters etc.

(b) Cationic Surfactants

The hydrophilic part is a positively charged group. Large proportion of this class corresponds to nitrogen compounds such as long chain amines and their salts, diamines and polyamines and their salts, quaternary ammonium salts, polyoxyethylenated (POE) long chain amines, quaternized POE long-chain amines, amine oxides etc.



Scheme 1.2. Classification of surfactant according to the composition of their head.

(c) Zwitterionic (or amphoteric) Surfactants

The hydrophilic part contains both a negative charge and a positive charge. Some surfactants are insensitive to pH, whereas others are cationic in an acidic (at low pH) solution and anionic in an alkaline (at high pH) solution, with an amphoteric behavior at intermediate pH. They include betaines or sulfobetaines and natural substances such as aminoacids and phospholipids.

(d) Nonionic Surfactants

The hydrophilic part of the surfactant consists of a non-charged group. Their hydrophilic group is of a nondissociable type such as alcohol, phenol, ether, ester or amide which do not ionize in aqueous solution. The hydrophile derives its water solubility from highly polar groups such as a polyethylene glycol chain obtained by the polycondensation of ethylene oxide.

Moreover, polymeric surfactants, a new class of surface active substance draw attention which result from the association of one or several macromolecular structures exhibiting hydrophilic and lipophilic characters either as separated blocks or as grafts. They are used in cosmetics, paints, foodstuffs and petroleum production additives.

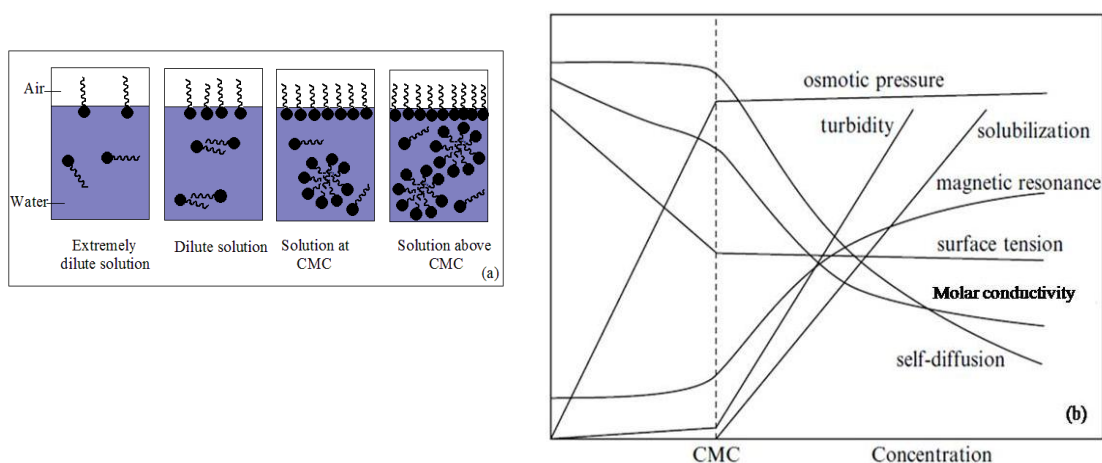
1.3.2. Thermodynamics of Micellization

Surfactants in aqueous solution seek the air/water and solid/water interfaces. As the hydrocarbon tail is repelled by water they orientate in such a fashion as to minimize the contact between their hydrophobic tail groups and the water. This process is known as 'adsorption' which change the interfacial properties. At low concentration of surfactant, it should be able to adsorb on the surface of air/liquid or interface between two immiscible phases (liquid-liquid, liquid-solid, solid-solid) to reduce the surface or interfacial excess free energy.

Monomeric (free or unassociated) form of surfactant exists in aqueous solution at low concentration which form monolayer at the interface and reduce surface and interfacial tension (Scheme 1.3). Formation of monolayer at the interface is highly

dynamic. Surfactants arrive and leave the interface very rapidly and the interaction of surfactants at the interface with the neighboring surfactants occurs very strongly that enables measurement of the rheological properties of the monolayer.

At high concentration of surfactants in aqueous solution, monomers of surfactant start accumulating in the solution because the available area at the surface for surfactant adsorption diminishes. Above certain aggregate concentration, the hydrophobic effect drives surfactant monomers to form self assembled aggregates known as micelles which exist in equilibrium with the surfactant monomers (Scheme 1.3. (a)). The critical aggregation concentration is called the critical micelle concentration (CMC) which is a property of the surfactants. In micelles the hydrophilic head regions are in contact with the surrounding water and the hydrophobic tail regions are directed at micelle centre. The surface active properties are at an optimum at CMC because monolayer adsorption is complete. Micelles have no surface activity. Any increase in the concentration of surfactant affects the structure of micelles but does not affect the number of monomers in the solution. The interaction between the hydrophilic heads and the hydrophobic tails of surfactant, temperature, the presence of electrolyte, existence of organic compound, concentration of salt within the solution, structure of surfactant and the presence of a second liquid have an effect on the CMC. Properties of the solution show sharp changes around the critical micelle concentration (Scheme 1.3. (b))



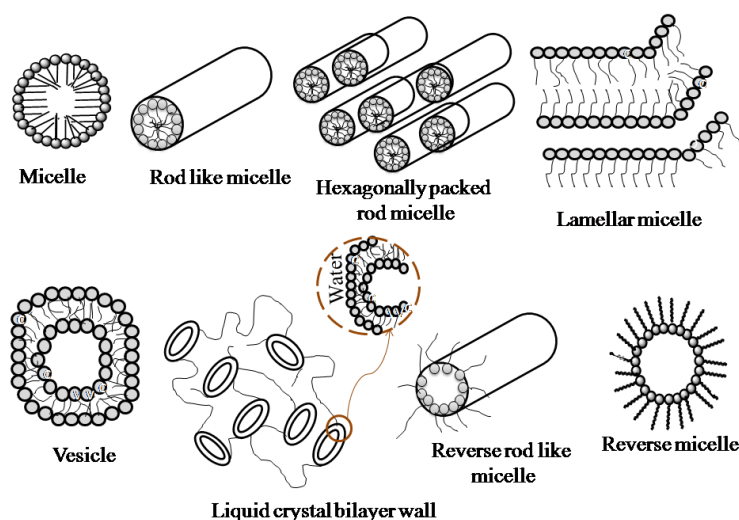
Scheme 1.3. Schematic representation of the (a) formation of micelles and (b) physical properties of aqueous surfactant solution as a function of surfactant concentration [32].

Self-assembly structures of surfactant (Scheme 1.4.) are building blocks of surfactant micelles and bilayers. The phase structures can be divided into two main groups:

- structures that are built of limited or discrete self-assemblies (such as spherical, prolate or cylindrical) and

- unlimited self-assembly structures in which the aggregates are connected over macroscopic distances in one, two or three dimensions. Hexagonal phase and lamellar phase are examples of one-dimensional and two-dimensional continuity respectively. Bicontinuous cubic phase and sponge phase are examples of three-dimensional continuity. Unlimited self-assembly structures in 1D, 2D or 3D are known as liquid crystalline structures.

Microstructures have a limited lifetime. For example the life time of spherically shaped micelle is about milliseconds. Physical forces of interactions between various microstructures become dominant as the energy difference between microstructures is small. Aggregates of surfactant can be transformed between several structures by small changes of temperature, concentration, pH or electrolyte strength.



Scheme 1.4. Formation of self- assembly of surfactants.

In highly non-polar solvents or water mixed with non-polar solvent the polar head groups of surfactants aggregate in such a way that they form the core with the tails extending out to the nonpolar solvent. Such aggregates structure is known as inverse or reverse micelles. Such structures are able to hold relatively large amount of water in their interior and forming a so called microwater pool. Depending on the concentration and composition of surfactants the shape of reverse micelle change from sphere-rod-hexagonal like structure.

1.3.3. Micellar Structure and Shape

Concentration of the surfactant in aqueous solution affects the shape and structure of the micelle. Hydrophile-lipophile balance (HLB) is an empirical expression for the relationship of the hydrophilic ("water-loving") and hydrophobic ("water-hating") parts of a surfactant. HLB is important in categorizing surfactants as solubilizing

agent, antifoaming agents, w/o emulsifier, o/w emulsifier, wetting and spreading agents, emulsifiers, detergents etc. (Figure 1.1).

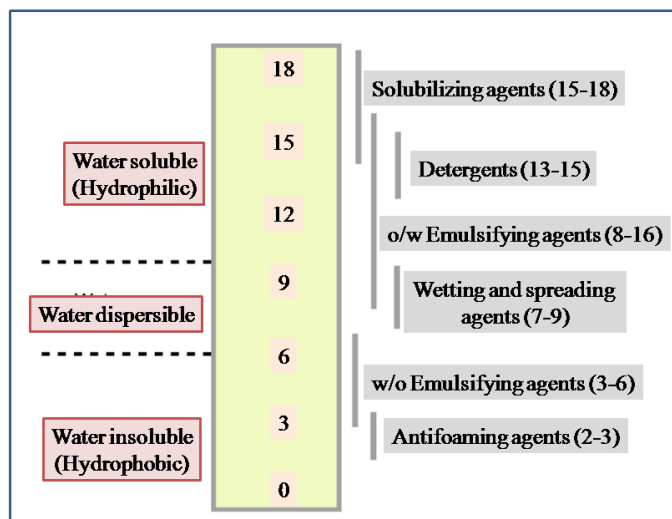







Figure 1.1. Classification of surfactant function according to HLB scale.

A simple dimensionless number, the critical packing parameter (CPP) governs the shape of micelles [33-37]. A surfactant with a tail volume, v , a head area, a and a tail length, l , the CPP can be calculated as, $CPP = v/al$. Scheme 1.5. shows the CPP and HLB of different aggregate structures.

Surfactant Shape	Critical Packing Parameter (CPP)	Surfactant Aggregates
 Cone	$< 1/3$	Spherical Micelle
 Truncated Cone	$1/3 - 1/2$	Cylindrical Micelle
 Truncated Cone	$1/2 - 1$	Vesicle
 Cylinder	1	Bilayer
 Inverted Truncated Cone	> 1	Reverse Micelle, Reverse Cylindrical Micelle

CPP	1/3	1/2	1	2	3
HLB	40	20	10	2	1

Scheme 1.5. Schematic structures of surfactant self assemblies for different values of critical packing parameter (CPP) and hydrophile-lipophile balance (HLB).

1.4. Microemulsion

Microemulsions are thermodynamically stable, isotropic transparent liquid mixtures of two immiscible polar and nonpolar liquids and an amphiphilic component, surfactant is used frequently in combination with a cosurfactant. The microheterogeneous environments present in microemulsions exhibit entirely different chemistry from that of homogeneous liquid solutions [38, 39]. The surfactant and/or co-surfactant form monolayers at the interface of the polar and non-polar phases with the hydrophilic parts directing to the polar phase and hydrophobic tails directing to the non-polar phase. Hoar and Schulman extensively work on microemulsions from 1943 [40]. The term microemulsion was first introduced by Schulman and coworkers in 1959 and they described microemulsion as optically isotropic transparent fluid systems consisting of water, oil, surfactant and medium chain alcohol as cosurfactant [41]. According to Danielsson and Lindmann, "A microemulsion is a system of water, oil and an amphiphile which is a single optically isotropic and thermodynamically stable liquid solution" [42]. The term "water" corresponds to a polar phase that can contain electrolytes and other additives. The word "amphiphile" from *amphi* (both sides) and *philos* (liking) was coined by Winsor to describe substances that has affinity towards both non-polar and polar phases [43]. Surfactants show the important amphiphilic character. The term "oil" refers to an volatile organic phase which is immiscible or partially miscible with the polar phase. *n*-Alkanes, hydrocarbons, partially or totally chlorinated or fluorinated hydrocarbons, single-chain alkanes, cyclic or aromatic hydrocarbons, triglyceride natural oils can be used as non-polar phases in microemulsions [44]. Definition of microemulsions according to IUPAC is, 'Dispersion made of water, oil, and surfactant(s) that is an isotropic and thermodynamically stable system with dispersed domain diameter varying approximately from 1 to 100 nm, usually 10 to 50 nm' [38].

Microemulsions have characteristic properties such as high capacity to solubilize polar and non-polar liquids, spontaneous formation, low interfacial tension, low viscosity, large interfacial area, fine microstructures, tunable microenvironment and physicochemical properties make them as excellent candidates for a variety of applications. As most single chain surfactants are incapable of reducing the interfacial tension of polar and nonpolar phase to form a microemulsion, cosurfactants (medium chain alcohols) are usually used with surfactants which reduce the tension and increase the entropy of the system [45].

The stability of microemulsions can be explained by interface science, chemical solubility theories or by thermodynamic explanations. According to thermodynamic explanation, a thermodynamically stable dispersion is formed when a net release of free energy is obtained with favourable entropic contributions from the mixing of small droplets in the continuous phase and the diffusion of surfactant in the interfacial layer that are larger than the unfavourable contribution of the reduction of surface

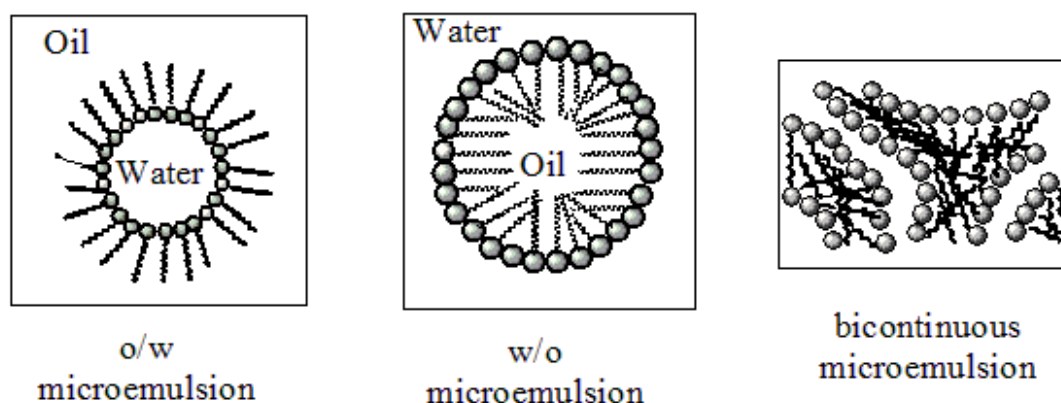
tension [46]. Microemulsions are also termed as nanoemulsions because the droplet diameter of microemulsion is usually within the range of 10-100 nm.

1.4.1. Microstructures of Microemulsions

In a micro-scale region, microemulsions are a class of micro heterogeneous systems and can exhibit different microstructures depending on the use of temperature, surfactant and cosurfactant concentration, water-oil ratios, polar phase, nonpolar phase and their relative concentrations etc. In a microemulsion one phase is dispersed in another phase depending on the relative percent amount of polar and nonpolar phase where the latter is called continuous phase and the dispersed phase is either globular or interconnected.

A well-known classification of microemulsions is represented in Scheme 1.6. and may be describes as given below:

1. In o/w microemulsion, water is the continuous phase where oil droplets are dispersed in the continuous phase.
2. In w/o microemulsion, oil is the continuous phase where water droplets are dispersed in the continuous phase.
3. Bicontinuous microemulsions are networks of oil and water nanodomains. They are separated and stabilized by a surfactant interfacial film. A net curvature close to zero can be found at almost equal amounts of water and oil.



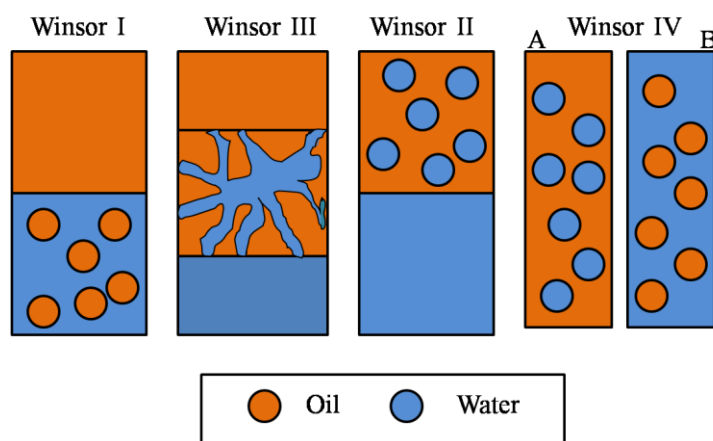
Scheme 1.6. Types of microemulsions.

1.4.2. Winsor Classification of Microemulsions

Winsor [47] classified four general types of phase equilibria in microemulsions (Scheme 1.7.):

- Type I: In a type I Winsor system, o/w microemulsion is in equilibrium with excess oil in the upper phase. Water is the continuous phase. The surfactant rich phase coexists with the oil phase with small non- aggregated amounts of surfactant.

- Type II: In a type II system, w/o microemulsion is in equilibrium with excess water in the lower phase. Oil is the continuous phase. The upper phase is the surfactant rich phase.
- Type III: Winsor Type III phases represent a three-phase microemulsion system which maintain equilibria with both oil and water phase. In this bicontinuous middle phase microemulsion both w/o and o/w dispersions remain simultaneously present.
- Type IV: Winsor IV microemulsion system which is not in equilibrium with either oil or water. This system is a true single phase where oil, water and surfactant are homogeneously mixed according to Schulman's definition of microemulsion.



Scheme 1.7. Different types of Winsor structures.

1.4.3. Basics of Formation of Microemulsions

The immiscibility of oil and water arises due to very high interfacial tension (IFT) between water and oil. According to thermodynamics, at a constant pressure and temperature, the IFT, $\gamma = (\delta G/\delta A)_{T,P}$. The Gibbs free energy change (δG) is positive when γ is positive and hence the mixing of oil and water fails. Addition of surfactant and cosurfactant helps to make the free energy change negative. The Gibbs free energy change of formation of microemulsion is as follows,

$$\Delta G = \Delta H - T\Delta S + \gamma\Delta A \dots\dots\dots(1.1)$$

Here ΔG , ΔH , ΔS , T and ΔA are the Gibbs free energy change, enthalpy change, entropy change, temperature in kelvin and change in interfacial area respectively. The enthalpy change is negligible when immiscible oil and water are mixed. There is a positive change in entropy ($T\Delta S \gg \gamma\Delta A$) occurs as the droplet size decreases and the system obtains a negative ΔG . Thus, the dispersion of micelle droplets in water continuous phase or reverse micelle droplets in oil continuous phase becomes spontaneous and stable. Originally, it was thought that the IFT becomes zero or even negative which imparts stability to microemulsion [48]. Now, it is accepted that by the action of surfactant the IFT between oil and water is reduced to a very low value. In many cases, surfactants cannot bring the IFT down to the required very low value.

The addition of a cosurfactant (short chain alcohols or amines) brings down the IFT further to a very low value for the formation of a stable microemulsion.

Change of IFT (γ) for a multicomponent system can be expressed by the relation

$$\partial\gamma = -\sum \Gamma_i d\mu_i = -\sum \Gamma_i RT d \ln C_i \dots\dots\dots(1.2)$$

where Γ_i , μ_i and C_i are the Gibbs surface excess, chemical potential and the concentration of the i^{th} component respectively. R is the universal gas constant (8.314 JK⁻¹ mol⁻¹) and T is the temperature in K.

The integrated form of equation (1.2) for a two component system is [49, 50]

$$\gamma - \gamma_o = -RT \left[\int_0^{C_1} \Gamma_1 d \ln C_1 - \int_0^{C_2} \Gamma_2 d \ln C_2 \right] \dots\dots\dots(1.3)$$

where Γ_1 and Γ_2 are the surface excesses of the component 1 and 2 respectively at their concentrations C_1 and C_2 and γ_o is the IFT between oil and water interface in absence of surfactant and cosurfactant.

Formation of microemulsion is controlled by the nature of surfactant, oil and temperature used. The mechanical agitation or even the order of component addition may affect microemulsification.

1.4.4. Percolations in Microemulsions

To have a systematic understanding of the structure and dynamics of microemulsions, it is necessary to clarify their microstructures and find efficient means to tune their properties. Percolation is very useful in this regard. Percolation is the process of movement and filtering of fluids through porous materials. It is a simple probabilistic model and exhibits a phase transition. Percolation threshold is the formation of long-range connectivity in random systems which is a mathematical concept related to percolation theory. A giant connected component does not exist below the threshold and a giant component of the order of the system size exists above the threshold.

Lagues [51-54] discussed about the dramatic increase in conductivity in terms of percolation model with volume fraction of water for w/o microemulsion. The physical situation was termed as stirred percolation, referring to Brownian motion of the medium. Useful information about micellar interactions could be obtained from the electrical conductivity measurements [55-57]. Water percolation threshold has determined using electrical conductivity measurements which is an indicator of microstructural transition from w/o to bicontinuous microemulsion [58, 59]. A sharp increase in electrical conductivity (σ) is observed as a function of water content (ϕ) or temperature (θ) occurs due to the change of the conductance medium as clustering of water droplets occur and changing to the continuous phase at water percolation

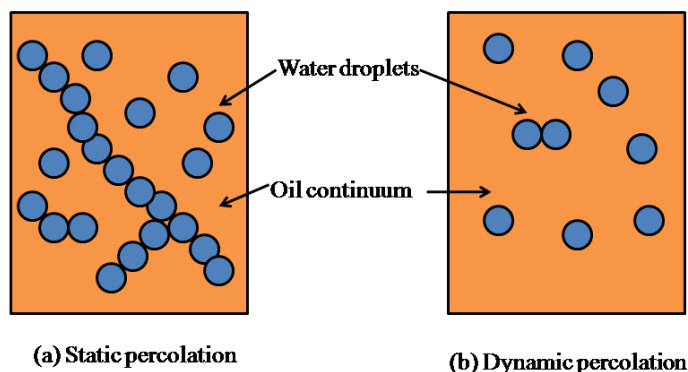
threshold [59-63]. Below the threshold the continuous medium is the oil phase that contributes very little to the conductance. At the threshold, the dispersed water phase percolates to form a continuous water phase which is highly conductive. Thus the formation of an infinite cluster of water droplets is responsible for increasing the conductivity in a dramatic nature. Hopping processes of surfactant ions between individual nanodroplets within the cluster is responsible for charge transport [64-67]. The charge exchange is caused by spontaneous opening and closing of droplet-droplet contacts in w/o microemulsions [68, 69]. The strong increase of conductivity is suggested to be due to the formation of a bicontinuous structure [70-72].

A similar percolation process with either ionic or onionic surfactants has been studied extensively for w/o microemulsions [59-62, 73, 74]. Theoretical models (effective medium theory and scaling law models) have been used to analyze the conductivity results [59, 61, 62, 73, 75-78]. Water-induced, ϕ_c and temperature-induced, θ_c water percolation thresholds of these w/o microemulsions have been obtained by numerical analysis of the models with adjustment by the least-squares method [73, 75-78]. The ϕ_c occurs when the water content (ϕ) increases at constant temperature and the θ_c occurs when the temperature (θ) increases at constant water content.

The percolation threshold value can also be obtained numerically from the maximum of $d(\log\sigma)/d\phi$ versus ϕ . The value obtained from this methodology is relatively close to the final predicted value from the fitting methodology [79-81]. Two approaches (static and dynamic) have been proposed for the conductivity (σ) along the oil dilution line which can be reproduced in terms of two separate asymptotic power laws having different exponents below and above the percolation threshold [1].

$$\begin{aligned}\sigma &= A(\phi_c - \phi)^{-s} \quad \text{where, } \phi < \phi_c \text{ (below percolation)} \\ \sigma &= B(\phi - \phi_c)^t \quad \text{where, } \phi_c < \phi \text{ (above percolation)}\end{aligned}$$

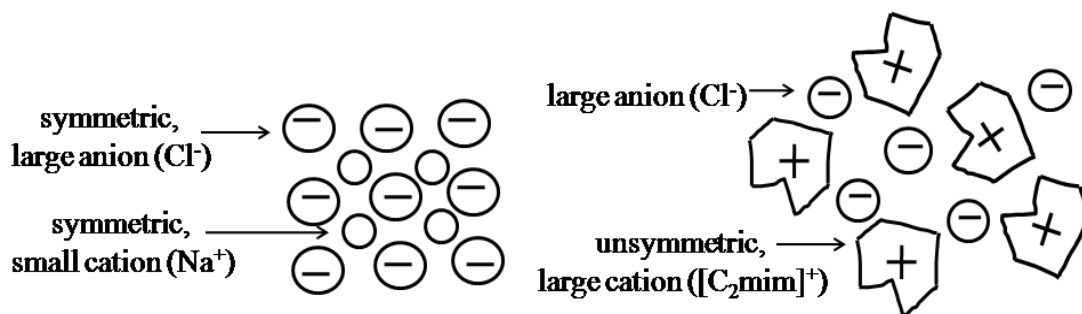
where A and B are free parameters, ϕ is the volume fraction and ϕ_c is the critical volume fraction of the conducting phase, s and t are critical exponents. From the slopes of the $\log\sigma$ versus $\log(\phi_c - \phi)$ plot for $\phi_c > \phi$ and the $\log\sigma$ versus $\log(\phi - \phi_c)$ for $\phi > \phi_c$ plot, the values of s and t can be obtained. The critical exponent t generally ranges between 1.5 and 2 and the exponent s allows the assignment of the time-dependent percolation regime. Thus, $s > 1$, generally around 1.3, describes a dynamic percolation regime which (Scheme 1.8. (b)) is connected to rapid process of fusion-fission among the droplets [51-54, 82-88]. The static percolation (Scheme 1.8. (a)) describes about the formation of bicontinuous microemulsions where conductivity increases sharply. The theoretical models (scaling law) are only valid close to the percolation threshold and cannot be applied for infinite dilution and immediate vicinity of the percolation threshold [57, 80, 81]. So, there are many restrictions in its application. Thus, the estimation of percolation threshold from the maximum of $d(\log\sigma)/d\phi$ versus ϕ plot was superior to the former one.



Scheme 1.8. Static and dynamic percolation processes [1].

1.5. ILs

ILs are liquid in which the ions are poorly coordinated. These are liquid below 100°C or even at room temperature. Stable crystal lattice does not form in ILs since at least one ion has a delocalized charge and one component is organic [89]. If a typical IL, e.g., 1-ethyl-3-methylimidazolium chloride, $[\text{C}_2\text{mim}][\text{Cl}]$ (melting point, 77 to 79 °C) and a typical inorganic salt, e.g., table salt, NaCl (melting point, 801 °C) are considered, the difference in structure between them is understood (Scheme 1.9.). IL has a significant lower symmetry and the charge of the cation and the anion are distributed over a larger volume of the molecule by resonance. So the solidification of IL will take place at lower temperatures. For some ILs (especially if long aliphatic side chains are present) a glass transition is observed instead of a melting point. Strong Coulombic interaction involve within these substances.

Scheme 1.9. Structure of NaCl and $[\text{C}_2\text{mim}][\text{Cl}]$.

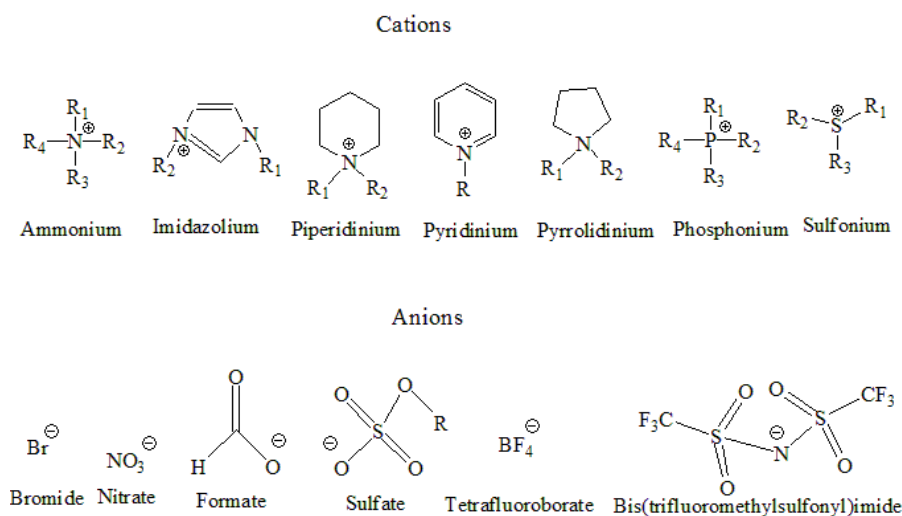
There is a still growing interest in ILs for the fascinating and outstanding properties and wide range of potential applications of ILs. ILs show large electrical conductivity due to their ionic nature. They are generally non-flammable. They have negligible vapour pressures, wider liquid ranges compared to molecular solvents, wide electrochemical window, and a wide range of solubilities and miscibilities. They are thermally, mechanically as well as electrochemically stable. ILs can be used as reaction media and/or catalysts for a wide variety of chemical reactions, for separations, and extractions of chemicals from aqueous and molecular solvents. They can be readily recycled following use as solvents and/or catalysts. For the

development of green chemistry and green technology the contribution of IL play an important role [89, 90]. ILs are called designer solvents as their physicochemical properties can be easily tuned by changing the structure of cations and anions. The Table 1.1. summarizes the potential and current uses of ILs.

Table 1.1. Potential and current uses of ILs.

Functions	Uses
Electrolytes	Polymer electrolyte fuel cells, dye sensitized solar cells, sensors, lithium ion batteries, supercapacitors, metal finishing, coating etc.
Thermal storage and heat transfer fluids	In thermal fluids
Liquid crystals	Displays, solar cells, optoelectronic devices etc.
Solvents	Bio-catalysis, organic reactions (such as Diels-Alder, Bails-Hillman, Heck Reaction, esterification, isomerization reactions and many coupling reactions) and catalysis, nano particle synthesis, polymerization etc.
Separation and extraction technology	Separate toxic metal ions and organic molecules, gas separations, extractive distillation, extraction, membranes etc.
Lubricants and additives	Lubricants, fuel additives, improved wear additives etc.
Electroelastic materials	Robotics, artificial muscles etc.
Analytics	Protein crystallization, Matrix Assisted Laser Desorption/Ionization-Time of Flight (MALDI-TOF) matrices, Gas Chromatography (GC) head space solvents etc.

Structures of widely used organic cations and organic/inorganic anions of ILs are shown in Scheme 1.10.



Scheme 1.10. Common cations and anions used in ILs.

1.5.1. Classification of ILs

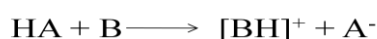
ILs have so far been classified in many different ways. The classification by Angell *et al.* [91] is the most recent and accepted one.

(a) Aprotic ILs (AILs):

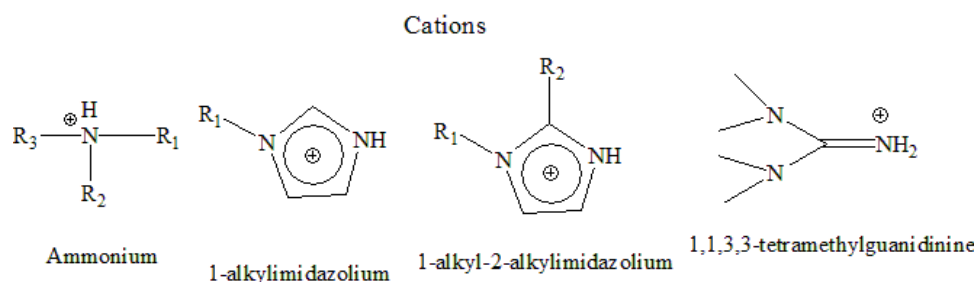
AILs consist solely of cations, which are not protonated and anions (Scheme 1.10.). The majority of the aprotic ILs are liquids in which the cations are organic molecular-ions. Resonance stabilized alkyl pyridinium and dialkylimidazolium cations are the examples of this class of ILs. Hurley and Weir [92] mixed *N*-substituted alkyl and aryl pyridinium halides with various metal chlorides and nitrates and obtained low-liquids which was used for electrochemical extractions and presented the first phase diagram on an aluminum chloride + organic cation halide system. This system showed the existence of stable ILs at temperatures of -40 °C. Cyclic and non-cyclic tetra alkyl ammonium salts like those with alkylpyrrolidinium cations and particularly those with ether oxygenated sidechains were also developed [93-95]. These kind of cations are usually charge-compensated by anions of oxidic character like nitrate perchlorate or more frequently fluorinated-oxidic character like triflate. Most common of the latter are the hexafluorophosphate, PF_6^- , tetrafluoroborate, $[\text{BF}_4]^-$, triflate (trifluoromethane sulfonate, $[\text{CF}_3\text{SO}_3]^-$) and bis(trifluoromethanesulfonyl)imide, ($[\text{CF}_3\text{SO}_2]_2\text{N}^-$ or $[\text{TFSI}]^-$) ions. Due to the viscosity-lowering reduction of the van der Waals interactions, fluorinated anions are prominent. Due to the two isoenergetic forms, large anion $[\text{TFSI}]^-$ can add an extra mode to the configurational entropy.

(b) Protic ILs (PILs):

PIL is formed by the proton transfer from a pure Brønsted acid (HA) to a pure Brønsted base (B). A proton potential in the liquid product is established for the nature and reversibility of the process that lends this class of ILs a special tunability.



A proton is available in all PILs for hydrogen bonding. Using stronger acids and/or stronger bases, proton-transfer process can be improved which leads to a greater driving force for the proton transfer. Structure of some organic cations of PILs are given in Scheme 1.11 [96]. A large variety of anions have been coupled with these cations. Cohesion force and fluidity of these liquids reduce when anion $[\text{TFSI}]^-$ is used.



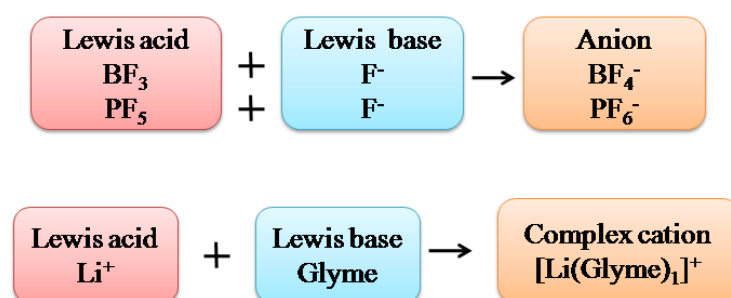
Scheme 1.11. Few examples of cations of PILs.

(c) Inorganic ILs

Inorganic ILs with low melting points are obtained in both aprotic and protic forms. Hydrazinium bromide, $[\text{N}_2\text{H}_5][\text{Br}]$ and hydrazinium nitrate, $[\text{N}_2\text{H}_5][\text{NO}_3]$ melt at 86.5 and 70 °C respectively. A binary mixture of lithium nitrate and ammonium nitrate, $\text{LiNO}_3\text{-NH}_4\text{NO}_3$ has a eutectic temperature of 98 °C. Protic molten salts, $[\text{NH}_4][\text{HF}_2]$ and $[\text{NH}_4][\text{HSO}_4]$ have melting point of 125 and 116 °C respectively [90]. Examples of aprotic molten salt is lithium chlorate with melting point of 115 °C and its glass forming eutectic with lithium perchlorate. Finally, the salts with inorganic molecular cations such as $[\text{PBr}_3\text{Cl}]^+$, $[\text{SCl}_3]^+$, $[\text{ClSO}_2\text{NH}_3]^+$ etc. with appropriate weak base anions are also the examples of low melting inorganic ILs.

(d) Solvate (chelate) ILs

Solvated ILs include multivalent cation salts that would not ordinarily be able to satisfy the criterion of melting point < 100 °C. The first recognized members of this class were molten salt hydrates, like $\text{Ca}(\text{NO}_3)_2 \cdot 4\text{H}_2\text{O}$. This concept is analogous to that for common complex anions of ILs such as $[\text{BF}_4]^-$, $[\text{PF}_6]^-$, and $[\text{AlCl}_4]^-$ [97]. These anions are the adducts of a Lewis acid and a Lewis base (Scheme 1.12.). Mixtures of molten salt hydrates with alkali metal salts were found to be almost ideal mixtures. Most of these ideal mixtures have liquidus temperatures well below ambient [98]. Certain equimolar mixtures of glymes (oligoethers) and certain Li salts (LiX , X = anion) yielded low melting or glass-forming complexes ($[\text{Li}(\text{glyme})_1]\text{X}$). Similarly, the Li^+ ions and the glymes are a Lewis acid and base respectively and form a complex $[\text{Li}(\text{glyme})_1]^+$ cation (Scheme 1.12) [97].



Scheme 1.12. Concept of complex cation in solvate ILs.

In this molten salt mixtures the lifetime of the water molecules in the cation coordination shell should be long with respect to the diffusion time scale for the ILs. Recently long lifetime is guaranteed because the ligating groups all belong to the same molecule. Thus instead of 4 water molecules, Tamura et al. used 4 alkoxy groups linked together (e.g. tetraglyme chelating the Li^+ cation) and found the salts with imide type anions to be ambient temperature liquids [99].

1.5.2. Walden Plot

P. Walden (1863–1957) suggested an empirical rule concerning ions in solutions that relates the molar conductivity, Λ of an ionically conducting liquid to its viscosity, η . According to this rule the product of the molar conductivity, Λ and the viscosity, η is approximately constant for the same ions in different solvents (Figure 1.2.). As different solvents hydrate the same ions differently so the viscosity change when the solvent is changed. This fact limits the validity of the rule.

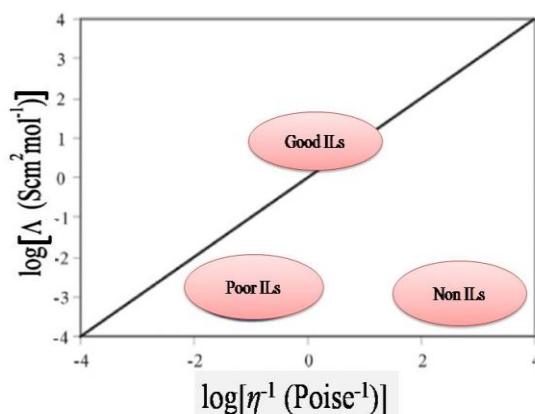


Figure 1.2. Walden plot shows the classification of ILs.

Not only in dilute aqueous solutions but also the Walden rule is applicable in nonaqueous electrolyte solutions and molten salts [100, 101]. According to Walden rule, a plot of $\log\Lambda$ vs $\log\eta$ predicts a straight line (reference line) that passes through the origin corresponds to a 0.01M aqueous KCl solution that exists as completely dissociated ions. Such plot give us information about the ionicity of the medium which is defined as the effective fraction of ions available to participate in conduction. Depending on the position in the Walden plot Angell *et al.* classified the ILs as either good or poor [102]. Components that lie close to this line are said to be ionic whereas poor ILs exist below this line (Figure 1.2).

Most ILs fall below the line. Many PILs fall well below the line because full ionization is not complete in those cases [103, 104]. Some AILs also fall well below this reference line suggesting that ion association occurs in their structure [105]. On the other hand it could be considered remarkable that so many ILs actually lie as close to (within 20 % of) the line. In such cases strong ion correlations during conductive motions occur in response to an electric field, to an extent that would not be present in the dilute electrolyte represented by the 0.01M KCl solution. Various effects such as relaxation effects and the impact of ion association which become significant as one moves from dilute aqueous salt solution to concentrated salt solutions have been very important [106-109]. Similar effects would be even more pronounced in the ILs where a single ion cannot possibly move without affecting or being affected by its surrounding ion neighbours.

1.6. ILs in Microemulsion

Conventional microemulsions consisting of water, oil, surfactant and/or cosurfactant where nonpolar volatile organic solvents cannot be regarded as green media and the solubility of different substances is limited in water which is used as polar phase. Now a days it has been demonstrated that the polar phase not necessarily has to be water and the non-polar phase not compulsorily oil. In non-aqueous microemulsions water can be replaced by glycerol, glycol or formamide [110-113]. Water can also be replaced by a mixture of molten salts (nitrate mixtures of ethylenediamine / ammonia / potassium) in a system composed of sodium dodecyl sulfate (SDS), 1-pentanol and decane [114]. Now a days ILs are being increasingly studied on the formulation of non-aqueous microemulsions where ILs are used as oil substitutes, water substitutes, cosurfactants and surfactants. Using as a polar phase, ILs can dissolve a large number of chemicals and ILs are regarded as green media when they are used as oil phase.

Microemulsions with AILs are almost entirely related to imidazolium based substances. IL, 1-butyl-3-methylimidazolium tetrafluoroborate ($[C_4mim][BF_4]$) as water substitute, non-ionic surfactant, Triton X-100 (TX-100) and any kind of oil as nonpolar phase are the most extensively studied microemulsions. The first microemulsion prepared by Gao et al., where water was replaced by $[C_4mim][BF_4]$ as polar phase, cyclohexane as nonpolar phase and TX- 100 as surfactant [21]. Atkin & Warr reported microemulsions composed of nonionic alkyl oligoethyleneoxide surfactants (CiEj), alkanes and PIL, ethylammonium nitrate ($[C_2NH_3][NO_3]$) as polar phase [115, 116].

PILs in microemulsions with IL surfactants have been reported as well. Microemulsions containing IL, 1-hexadecyl-3-methyl-imidazolium chloride ($[C_{16}mim][Cl]$) as surfactant, decanol as cosurfactant, dodecane as nonpolar phase and ILs ($[C_2NH_3][NO_3]$ and $[C_4mim][BF_4]$ respectively) as polar phase have been formulated by Zech et al.[117].

Cheng et al. used two types of ILs, the hydrophobic IL, 1-butyl-3-methylimidazolium hexafluorophosphate ($[C_4mim][PF_6]$) and the hydrophilic PIL propylammonium formate as nonpolar and polar phase respectively for the formation of nonaqueous microemulsions with the anionic surfactant sodium bis(2-ethylhexyl)sulfosuccinate (AOT) [118].

1.7. Applications of IL Based Microemulsions

Biocatalysis/Enzymatic Activity

IL based microemulsions have been found to be exceptional and versatile media for a variety of chemical reactions. This special microenvironment is called microreactor or nanoreactor which may be w/IL, IL/w as well as bicontinuous. The size of the microreactor can be controlled. The technological utility of enzymes can be enhanced greatly by their use in ILs. ILs are not only environmentally friendly alternatives to volatile organic solvents but also enzymes and substrate exhibit excellent selectivity

in such a solvent medium. In ILs enzymes can maintain very high thermal and operational stability. Moniruzzaman et. al. published the first report on the enzymatic activity of horseradish peroxidase (HRP) microencapsulated in w/IL microemulsions (AOT/1-hexanol/1-octyl-3-methyl imidazolium bis(trifluoromethylsulfonyl)amide, [C₈mim][TFSI] /water) where pyrogallol was used as substrate [119]. HRP retained almost 70 % of its initial activity after incubation at 28 °C for 30 h and HRP catalyzed oxidation of pyrogallol by hydrogen peroxide in IL based microemulsions is much more effective than in conventional AOT/water/isooctane microemulsion. Pavlidis et al. used w/IL microemulsion with a nonionic surfactant such as Tween-20 and TX-100 in 1-butyl-3-methylimidazolium hexafluorophosphate, [C₄mim][PF₆] to be a talented medium for biocatalytic processes. The lipases from *C. rugosa*, *C. viscosum* and *T. lanuginose* exhibit high catalytic performance in these IL based microemulsion systems in comparison to other microheterogeneous media [120].

Diels–Alder Reaction (DAR) Medium

Engberts et al. carried out several DAR kinetic measurements in micelles and microemulsions [121–123]. The rate of the reaction relatively improved compared to that in ordinary organic solvents [121, 124, 125]. In IL based microemulsions, the DAR between *N*-ethylmaleimide and 2,3-dimethyl-1,3-butadiene was studied. Using spectrophotometry the apparent second order rate constants were determined for IL based microemulsion and AOT microemulsion. They increased with both water content (molar ratio of IL aqueous solution to surfactant) and surfactant concentration in the IL based microemulsion systems. The effect of various solvents on the DAR rate was investigated. The rate constants k_2 in both AOT microemulsion and IL based microemulsion were roughly four to five times higher than that in the isooctane and the k_2 in pure IL were at least 10 times higher than that in the isooctane. High temperature accelerated the reaction. The apparent activation energy, E_a decreased with the increase of the water content.

Polymerization

IL based microemulsions have been used for the fabrication of polymer electrolyte membranes [126]. Nonaqueous proton conducting membranes can be prepared via the polymerization of microemulsions comprising PILs, surfactant and a polymerizable oil. This oil was a mixture of styrene and acetonitrile. Resulting polymers (vinyl polymers) were insoluble in the IL and the emerged nanodomains were found to be homogeneous, clear, and flexible. These proton conducting membranes have good mechanical properties. Thermally and chemically these membranes are stable. As connected PIL nanochannels preserved in the membrane, the conductivity of these membranes was up to 0.1 Sm⁻¹. Progressive release of the PIL may affect the long term stability of these new promising materials.

Synthesis of Nanoparticles

Zhao et al. used TX-100/benzene/[C₄mim][BF₄] microemulsions as template for the synthesis of silica nanoparticles under both basic and acidic conditions [127].

Ellipsoidal nanoparticles were formed under acidic conditions and hollow silica spheres were obtained under alkaline conditions by adjusting the reaction conditions. The size distribution of hollow silica spheres is narrow than that of the ellipsoidal nanoparticles. Li et al. studied the IL based microemulsion with TX-100 as surfactant and [C₄mim][PF₆] as continuous phase to fabricate porous silica microrods [128]. Traditional microemulsions with TX-100 as surfactant and cyclohexane as continuous phase only produce silica nanoparticles which is different from those microrods obtained by Li et al [128].

Medium for Drug Delivery

IL based microemulsions can provide an effective carrier for transdermal drug delivery. Solubility of several drugs is remarkably higher in ILs. Moniruzzaman et al. reported a policy for drug delivery in non-aqueous IL based microemulsions [129]. A large number of drugs are sparingly soluble in both water and most organic solvents.

1.8. Enzyme Catalyzed Reaction

Enzymes are large biological protein molecules that have catalytic functions obligatory to maintenance and activity of life. They are highly selective, effective, and active at optimum temperature. Every enzyme has a specific function and also have no side effects. They work like a key that fits in a lock and they have only one function. Only when the right enzyme finds the right material a biochemical reaction occur. Catalysts greatly accelerate both the rate and specificity of metabolic reactions from the digestion of food to the synthesis of DNA.

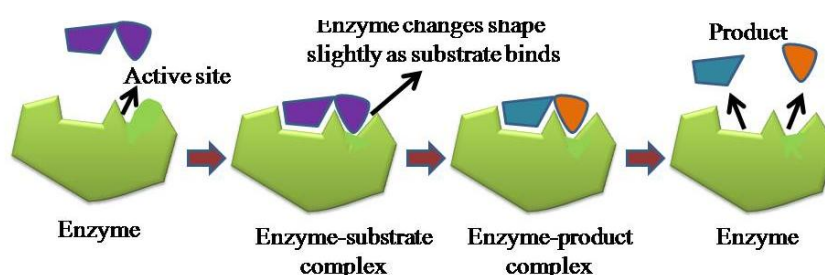
Enzymes are stable, biodegradable, and environmentally friendly than other chemicals or biological molecules. They work at low temperature and moderate pH. In a biochemical reaction they do not become part of the final product which they are catalyzing. At the end of a biochemical reaction, the enzyme is ready to effect the same reaction on another molecule again and again.

Like protein molecules, enzymes are made of amino acids. The greater part of enzymes are made of only 20 different kinds of amino acid. Each enzyme has its own unique sequence of amino acids and made up of between a hundred and up to a million amino acids placed like pearls on a string. In most enzymes a highly complex three dimensional structure is formed because the string of amino acids is coiled and folded thousands of times which is unique to each enzyme. Chemical bonds exist among the amino acid molecules in an enzyme. Order of the amino acids determine the structure and function of the enzyme.

In enzymatic reactions, substrates (the reactant molecules) are converted into different molecules, called products. As enzymes are selective for their substrates, metabolic pathways occur in a cell is determined by the set of enzymes present in that cell. Only a small part of a large enzyme molecule participates in the catalysis of biochemical reactions. This is called the active site of enzyme. Substrate binds to the enzyme which causes change in the distribution of electrons in the chemical bonds of the

substrate and ultimately causes the reactions that lead to the formation of products. From the enzyme surface, products are released to regenerate the enzyme for another reaction cycle. The active site specifically accommodates the shape of the biological substrate and only substrates with the right shape will be transformed by the enzyme. This makes enzymes specific in their action.

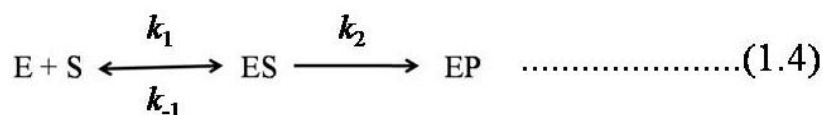
The Lock and Key theory first explains the specific action of an enzyme with a single substrate [130, 131]. According to this theory, only the correctly sized key (substrate) fits into the key hole (active site) of the lock (enzyme) (Scheme 1.13.). This model explains enzyme specificity. It cannot explain the stabilization of the enzyme. When substrate enters into the active site of an enzyme, the enzyme will change its shape slightly to match the substrate.



Scheme 1.13. Schematic model of the induced fit mechanism.

Daniel Koshland suggested a slight modification to the lock and key model. Koshland suggested was that since enzymes are so flexible, the active site is constantly being reshaped by its interaction with the substrate [132]. It is difficult for a substrate to simply bind to a rigid active site. The amino acid side-chains that are a part of the active site are molded into the specific positions that allows the enzyme to perform its catalytic role. This is known as induced fit theory.

In enzyme kinetics, the rate of reaction is measured. The effects of varying the conditions of the reaction can also be investigated. Michaelis–Menten kinetics is one of the well-known models for enzyme kinetics which explains the enzyme catalytic reactions by the following mechanism:



Where, enzyme (E) and substrate (S) bind to produce a product (P) and k_1, k_2, k_{-1} are rate constants.

According to this kinetics, an enzyme-substrate complex (Michaelis complex), ES is formed which is a fast and reversible process. Enzyme-substrate complex dissociates under liberation of the product, P. The second reaction is rate-limiting. At very high substrate concentration almost all enzyme is present as enzyme-substrate complex.

Under these conditions a steady state is reached, enzyme is steadily saturated by substrate and the initial rate is at a maximum (V_m).

The relation between substrate ($[S]$) concentration and reaction rate (v) can be expressed by the Michaelis-Menten equation:

$$v = \frac{V_m[S]}{K_m + [S]} \dots\dots\dots(1.5)$$

K_m is the Michaelis constant of the enzyme for the given substrate. K_m can be expressed as:

$$K_m = (k_{-1} + k_2)/k_1 \dots\dots\dots(1.6)$$

The significance of K_m becomes evident at $[S] = K_m$ when $v = V_m/2$. So K_m is the substrate concentration at which the reaction rate is half maximum (Figure 1.3.). The affinity between the substrate and the enzyme can be characterized by K_m . Rate, v can be calculated for each value of substrate concentration at known K_m and V_m . High affinity is reflected with a low K_m value. At low substrate concentrations, $[S] \ll K_m$, the reaction is first order and the rate is directly proportional to the substrate concentration; at high substrate concentration, $[S] \gg K_m$, the reaction (zero order reaction) is no longer dependent on the substrate concentration but only on the enzyme activity. Another useful and important constant is k_{cat} , which is the number of substrate molecules handled by one active site per second. The efficiency of an enzyme can be expressed in terms of k_{cat}/K_m .

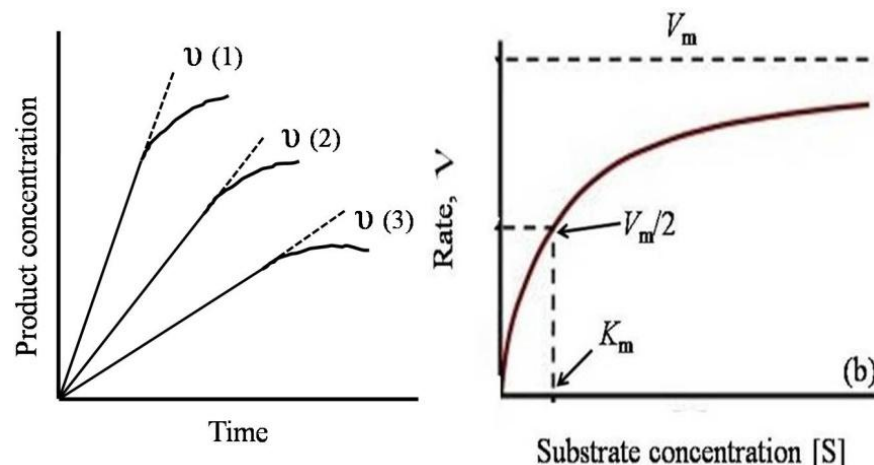


Figure 1.3. (a) Determination of initial rates at different concentrations and (b) a plot of rate, v vs. substrate concentration, $[S]$ obeying Michaelis-Menten equation [132].

To calculate kinetic parameters (K_m, V_m) easily it is advantageous to transform the Michaelis-Menten relation. From Lineweaver-Burk equation, containing the reciprocal values of v and $[S]$, we can get linear relationships (Figure 1.4.) between $[S]$ and v which can be evaluated graphically:

$$\frac{1}{v} = \frac{K_m}{V_m[S]} + \frac{1}{V_m} \dots\dots\dots(1.7)$$

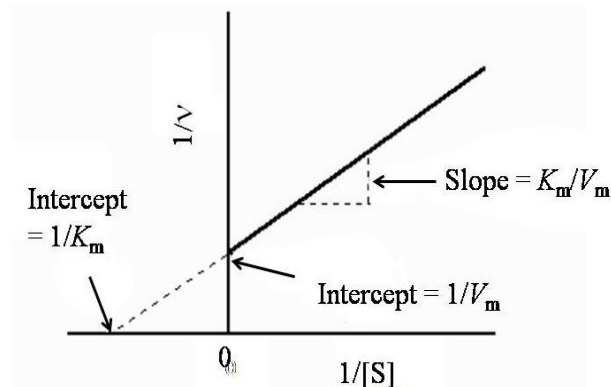


Figure 1.4. $1/v$ vs. $1/[S]$ obeying Lineweaver-Burk equation [132].

1.8.1. Enzymatic Catalysis in Microemulsions

Suitable reaction media is an important criterion for enzymatic conversion of hydrophobic substances. There are many improved techniques for exposing the enzymes to the organic solvents. Two methods are frequently used which deal with solid particles in which enzymes adsorbed on solid supports [133] or dry enzyme powder added directly to organic solvents [134] for enzymatic reaction. Involving solid particles in reaction, the rates can be restricted by diffusion limitations. Polar organic solvents can also be used as reaction media where all components can be solubilized and a homogeneous liquid phase is obtained in which both the substrate and the enzyme are soluble. But polar to intermediate polar solvents on the polar-apolar scale may deactivate enzymes [133, 135]. Microemulsions which are multicomponent isotropic liquids are useful as enzymatic reaction media. Reverse micellar systems are used for enzymatic catalysis in microemulsions [136, 137]. Microemulsions can be formed within a narrow temperature region under certain conditions. By a small change in temperature, a phase separation may induce where the microemulsion separates either an oil rich phase or a water rich phase. Depending on whether the temperature is increased or decreased, the surfactant has attraction either for the nonpolar or the polar phase and the surfactant is confined almost completely to one of the two phases. Membrane reactors are used to separate the products from the microemulsion [138, 139]. Forward and backward liquid-liquid extractions between a microemulsion and a water phase is another method for the extraction and separation of proteins [139-140]. Using this technique it is possible to reuse the enzyme and surfactant and to recover the product.

ILs can be used as a replacement for ordinary organic solvents to reduce volatile organic compound emissions which have exceptional properties discussed in Section 1.5. If pure IL is used as reaction media for enzymatic catalysis, one important drawback is that enzymes are not soluble in most ILs. Some ILs can dissolve enzymes through the weak hydrogen bonding interactions. In that case inactivation of enzyme

occurs because ILs often induce enzyme conformational changes. The insolubility of enzymes in ILs can be overcome by the use of w/IL microemulsions stabilized by a layer of surfactants. It is well recognized that enzymes can be solubilized in organic solvents by the use of w/o microemulsions without the loss of their catalytic activity [141-148]. At a very low surfactant concentrations enzymes can also be solubilized in organic solvents [149, 150]. The polar core of microemulsion systems has the ability to solubilize enzymes. In that case enzymes are protected from the unfavorable effect of organic solvents by the surfactant layer.

1.9. Literature Review

Non Aqueous IL Based microemulsions

In the preparation of nonaqueous IL based microemulsions, [C₄mim][BF₄] is the most frequently used IL, but a wide variety of other ILs are also used for the preparation of IL based microemulsions. Gao et al. reported the first microemulsion system where [C₄mim][BF₄] was used as polar phase [21]. They characterized TX-100/cyclohexane/[C₄mim][BF₄] microemulsions by phase behavior, conductivity measurement, DLS, freeze-fracturing transmission electron microscopy (FF-TEM) and ultraviolet–visible (UV–Vis) spectroscopy. Eastoe et al. carried out small-angle neutron scattering (SANS) experiments on TX-100/cyclohexane/[C₄mim][BF₄] microemulsions [17]. Regular swelling behavior was observed for the microemulsions with the addition of IL since the volume of the dispersed nanodomains is proportional to the amount of added IL. Chakrabarty et al. used the steady-state and picosecond time-resolved emission spectroscopy to study the effects of confinement of the IL on solvation dynamics and rotational relaxation of coumarin-15 (C-153) in TX-100/cyclohexane/[C₄mim][BF₄] microemulsions [151]. From dynamic light scattering (DLS) along with freeze-fracture transmission electron microscopy (FF-TEM) measurements Gao et al. concluded that the sizes of single microemulsion droplets vary with temperature [152, 153]. Similar systems were studied where [C₄mim][BF₄], TX-100 and toluene, *p*-xylene or benzene were used as the polar phase, surfactant and oil phase respectively [154–159]. The addition of a cosurfactant (alcohol) or small amounts of water changes the size and properties of TX-100/cyclohexane/[C₄mim][BF₄] microemulsions [160-162]. Gao et al. studied the effect of the polymer polyvinylpyrrolidone (PVP) on the microstructure of reverse TX-100/cyclohexane/[C₄mim][BF₄] microemulsions. The existence of region of the microemulsion state is remarkably decreased by the addition of PVP. The microemulsion droplets were gradually swollen by the addition of both [C₄mim][BF₄] and PVP and thereby the viscosity of the microemulsion was slightly increased [163]. However, the addition of a polymer, polyethylene glycol with a molecular weight of 400 (PEG-400) increases the size of the microemulsions which was revealed by DLS measurement [164]. Absorption solvatochromic shift experiments and kinetic studies on the aminolysis of 4-nitrophenyl laurate by *n*-decylamine show that the polarity at the interface of IL/o microemulsion for TX-100/cyclohexane/[C₄mim][BF₄] system is higher than at the interface of w/o microemulsion. But the polarity of [C₄mim][BF₄] is lower than the polarity of water. From proton nuclear magnetic resonance (¹H NMR)

experiments it was concluded that an increase in the IL content of the microemulsion led to an increase in the interaction between $[C_4mim][BF_4]$ and TX-100 [165]. In the reverse micellar system of TX-100/cyclohexane/ $[C_4mim][BF_4]$ microemulsion two silver salts, silver tetrafluoroborate ($AgBF_4$) and silver trifluoromethanesulfonate ($AgCF_3SO_3$) were dissolved. Pure reverse micellar system is characterized by DLS measurement to prepare stable silver nanoparticle solution without using any other auxiliary solvent in the whole process [166]. For the preparation of monodispersed palladium nanoparticle, TX-100/cyclohexane/ $[C_4mim][BF_4]$ microemulsions were recently used as a medium [167]. Different types of ILs can be also involved in the preparation of new IL based microemulsions. Small-angle X-ray scattering (SAXS), DLS, freeze-fracture electron microscopy (FFEM) or UV–Vis spectroscopy were used to characterize the aggregate size of TX-100/toluene/ $[C_4mim][PF_6]$ and TX-100/ethylene glycol/ $[C_4mim][PF_6]$ microemulsions [22, 23]. For the synthesis of poly(methyl methacrylate), $[C_4mim][PF_6]$ -based microemulsions is used as a reaction media [168, 169]. Polar organic solvent formamide (FA) and 1-butyl-3-methylimidazolium chloride $[C_4mim][Cl]$ and were used to form nonaqueous microemulsions where cyclohexane was used as oil phase and TX-100 was used as surfactant. Electrical conductivity measurement was used to identify the microstructures. DLS experiments confirmed the formation of reverse microemulsions of $[C_4mim][Cl]$ –FA in cyclohexane which was further confirmed by the UV–Vis studies with methyl orange (MO) and methylene blue (MB) as absorption probes [170]. TX-100/limonene/1-ethyl-3-methylimidazolium ethyl sulfate ($[C_2mim][EtSO_4]$) microemulsion was characterized by means of conductivity, viscosity and SAXS measurements from ambient temperature down to $-10\text{ }^\circ\text{C}$ [171]. DLS and picosecond time-resolved fluorescence spectroscopy were used to study TX-100/ cyclohexane/IL systems (IL = 1-ethyl-3-methylimidazolium butylsulfate, $[C_2mim][ButSO_4]$, 1-ethyl-3-methylimidazolium hexylsulfate, $[C_2mim][HexSO_4]$ and 1-ethyl-3-methylimidazolium octylsulfate $[C_2mim][OctSO_4]$) [172]. IL based microemulsions with $[C_2mim][ButSO_4]$ can form with the mixture of two nontoxic nonionic surfactants, polyoxyethylene (20) sorbitan monooleate (Tween-80) and sorbitan laurate (Span-20). Biological oil phase isopropyl myristate (IPM) was used [173]. TX-100/cyclohexane/*N,N,N*-trimethyl-*N*-propyl ammonium bis(trifluoromethanesulfonyl)imide ($[N_{3111}][TFSI]$) form nonaqueous microemulsions where $[N_{3111}][TFSI]$ was substituted for polar water. Different microregions such as IL/o, bicontinuous and o/IL were identified by electrical conductivity measurements. DLS revealed the formation of the IL based microemulsions. The size of the microemulsions increases with increasing the amount of $[N_{3111}][TFSI]$ [174]. TX-100/cyclohexane/ *N*-methyl-*N*-propylpyrrolidinium bis(trifluoromethanesulfonyl) imide, $[P_{13}][TFSI]$ also form nonaqueous microemulsions where $[P_{13}][TFSI]$ was substituted for polar water [175]. The phase behavior and DLS study showed that $[C_2mim][TFSI]$ /TX-100/cyclohexane microemulsion can be formed with $[C_2mim][TFSI]$ as polar core at suitable condition [176]. There are a wide range of other surfactants (nonionic, anionic, and cationic) that can form microemulsions. Nonionic surfactants (CiEj) can be also used in the preparation of microemulsions.

Traditional ILs, ethylammonium nitrate ($[\text{C}_2\text{NH}_3][\text{NO}_3]$) or propylammonium nitrate ($[\text{C}_3\text{NH}_3][\text{NO}_3]$) can be used as polar phase and alkanes (octane, decane, dodecane, tetradecane and hexadecane) can be used as oil phase in these systems [116, 177]. Falcone et al. studied IL based microemulsions with the anionic surfactant, sodium 1,4-bis(2-ethylhexyl) sulfosuccinate (NaAOT) and the cationic surfactant, benzyl-n-hexadecyldimethylammonium chloride (BHDC). DLS experiments reveal the formation of microemulsions with ILs 1-butyl-3-methylimidazolium trifluoromethanesulfonate ($[\text{C}_4\text{mim}][\text{CF}_3\text{SO}_3]$) and 1-butyl-3-methylimidazolium trifluoroacetate ($[\text{C}_4\text{mim}][\text{CF}_3\text{CO}_2]$) [178].

Aqueous IL Based microemulsions

In aqueous IL based microemulsions, IL is used as apolar phase. $[\text{C}_4\text{mim}][\text{PF}_6]$ is used mostly for the preparation of aqueous IL based microemulsions. Gao et al. reported IL based microemulsion, TX-100/ $[\text{C}_4\text{mim}][\text{PF}_6]$ /water. Different subregions such as w/IL, bicontinuous and IL/w were identified by cyclic voltammetry method using potassium ferrocyanide ($[\text{K}_4\text{Fe}(\text{CN})_6]$) as the electroactive probe. DLS study showed that the hydrodynamic diameter of the IL/w microemulsion is increased with increasing IL content due to the swelling of the micelles by the IL but nearly independent of water content [179]. A similar study was carried out for Tween-20/ $[\text{C}_4\text{mim}][\text{PF}_6]$ /water microemulsions and the phase behavior of the ternary system was investigated. Three subregions (w/IL, bicontinuous and IL/w) were identified by cyclic voltammetry method using $[\text{K}_4\text{Fe}(\text{CN})_6]$ as the electroactive probe. The polarity of the microemulsion environment was investigated by UV-Vis spectroscopy using MO as a probe. Tween-20/ $[\text{C}_4\text{mim}][\text{PF}_6]$ /water microemulsions could solubilize salt species into the microemulsion droplets by using the ionic compound potassium ferricyanide, $[\text{K}_3\text{Fe}(\text{CN})_6]$ in UV-Vis. measurements. UV-vis spectra also revealed the solubilization of riboflavin in the microemulsions [180]. The interaction of IL with water in TX-100/ $[\text{C}_4\text{mim}][\text{PF}_6]$ /water microemulsions i.e. IL/w microregions of the microemulsions has been studied by the dynamics of solvent and rotational relaxation of C-153 and coumarin 151 (C-151) [181]. Similar experiments were carried out later with C-153 and coumarin 490 (C-490) [182]. A broadband dielectric spectroscopy study on TX-100/ $[\text{C}_4\text{mim}][\text{PF}_6]$ /water microemulsions was performed where the phase behavior of microemulsion can be easily identified by its dielectric response [183]. Aqueous IL based microemulsions can be used for liquid-liquid extraction. A w/IL reverse microemulsion with AOT/ $[\text{C}_4\text{mim}][\text{PF}_6]$ /water system has been proved to entail selective extraction of hemoglobin from human whole blood. The hemoglobin might exist either in the bulk of IL phase or in the droplets of water of the microemulsion system. Electrostatic interaction is the main driving forces for the transfer of hemoglobin from aqueous phase into the microemulsion [184]. The catalytic activities of alcohol dehydrogenase in TX-100/ $[\text{C}_4\text{mim}][\text{PF}_6]$ /water microemulsions were found to be greatly improved as compared with those in pure $[\text{C}_4\text{mim}][\text{PF}_6]$ [185]. The catalytic activity of lignin peroxidase and laccase was studied in TX-100/ $[\text{C}_4\text{mim}][\text{PF}_6]$ /water microemulsions [186]. TX-100/ $[\text{C}_4\text{mim}][\text{PF}_6]$ /water microemulsions were used as enzyme catalyzed

reaction medium. The catalytic behavior and stability of lipases from *Candida rugosa*, *Chromobacterium viscosum* and *Thermomyces lanuginosa* were investigated in these microemulsions [187]. IL polymer materials incorporating enzymes can be used as active, stable and reusable biocatalysts. Lipase from *Candida rugosa* has been microencapsulated in surfactant aggregates formed in an IL monomer or the solution of an IL monomer/ IL and then incorporated into polymer frameworks through the free radical polymerization of (1-vinyl-3-ethylimidazolium bis(trifluoromethyl-sulfonyl)imide, [veim][TFSI]). Using lipase-catalyzed hydrolysis of *p*-PNB as a model reaction, the activity, stability and reusability of such IL polymer materials containing lipase were evaluated [188]. The IL based microemulsions (AOT/1-octyl-3-methylimidazolium bis(trifluoromethyl-sulfonyl)imide, [C₈mim][TFSI]/water) could have advantages over conventional microemulsions as reaction media for the hydrolysis of *p*-NPB catalyzed by lipase [189]. In the w/IL microemulsions stabilized by both AOT and TX-100, the lipase-catalyzed hydrolysis of *p*-NPB was investigated to evaluate the catalytic efficiency of lipase in this novel microemulsion [190].

Microemulsions with IL as Surfactant

ILs based on 1-alkyl-3-methylimidazolium cation [C_nmim]⁺ with a long alkyl chain can be used as surfactants in microemulsions. Microemulsions of 1-hexadecyl-3-methylimidazolium chloride, [C₁₆mim][Cl]/decanol/dodecane/IL were studied where [C₁₆mim][Cl] was used as the surfactant, decanol as the cosurfactant, dodecane as the continuous phase and ILs ([C₂NH₃][NO₃] and [C₄mim][BF₄] respectively) as polar microenvironment for the system. Hydrodynamic radius increases with the amount of IL, which indicates a swelling of the formed structures [117]. The hexagonal and lamellar phases formed in a ternary system of [C₁₆mim][Cl]/1-decanol/ water at 25 °C were characterized by SAXS and polarizing optical microscopy. The IL, [C₁₆mim][Cl] was used as surfactant. Liquid crystalline phases were formed from a hydrogen-bonded network comprised of an imidazolium ring, anion, 1-decanol, and water [191]. The lyotropic lamellar phase was formed in 1-octyl-3-methylimidazolium chloride [C₈mim][Cl]/alcohol (1-hexanol, 1-octanol, 1-decanol and 1-dodecanol)/water microemulsions by polarized optical microscopy and SAXS techniques [192]. An IL/o microemulsion could be formulated in [C₈mim][Cl]/[C₄mim][PF₆]/water system. DLS was used to confirm the formation of IL/o microemulsions with an average size of 3 nm [193]. The influence of an IL, [C₂mim][HexSO₄] was studied on the spontaneous formation of microemulsions with ionic surfactants, cetyltrimethylammonium bromide, CTAB and SDS. The results show a significant increase of the transparent phase region by replacing water by the IL. The w/o type microemulsions were formed which was confirmed by the use of NMR self-diffusion coefficients. A palisade layer was formed where the IL plays a similar role like a cosurfactant, changes the spontaneous curvature of the interfacial film and decreases the droplet size [194]. Recent studies have formulated IL/o microemulsions consisting of toluene as oil phase and two ILs, 1-butyl-3-methylimidazolium octylsulfate, [C₄mim][OctSO₄] and [C₂mim][EtSO₄] where [C₄mim][OctSO₄] take over the role of a surfactant in the spontaneous interfacial film

formation process. Conductometric, cyclic voltammetric and rheological measurements were used to study the isotropic phase region [195]. The ternary system composed of the IL, 1-butyl-3-methylimidazolium dodecylsulfate, [C₂mim][DodSO₄] as surfactant, [C₂mim][EtSO₄] as polar phase and toluene as oil phase was investigated. Conductometric experiments revealed the presence of oil/IL, bicontinuous and IL/o microemulsions [196]. Ternary system, 1-butyl-3-methylimidazolium 1,4-bis(2-ethylhexyl) sulfosuccinate, [C₄mim][AOT]/benzene/ILs was characterized by phase behavior study, DLS measurements and ¹H NMR spectroscopy measurements. The area of single phase region increases with increase in alkyl chain length of cation of ILs and follows the trend [C₆mim][TFSI] > [C₄mim][TFSI] > [C₂mim][TFSI], while the area increases with decrease in cation anion interaction strength of added ILs and follows the trend [C₄mim][TFSI] > [C₄mim][PF₆] > [C₄mim][BF₄] [197].

1.10. Objectives of the Work

IL based microemulsions may be very interesting since the advantageous properties of both microemulsions and ILs may be exploited. The properties of IL based microemulsions may be controlled by changing the structure of the cation and anion of IL and the nature and composition of the microemulsions. This gives the option to fine tune the properties of IL based microemulsions for manifold applications like the study of catalytic activity of enzymes.

The work was initiated to accomplish following objectives:

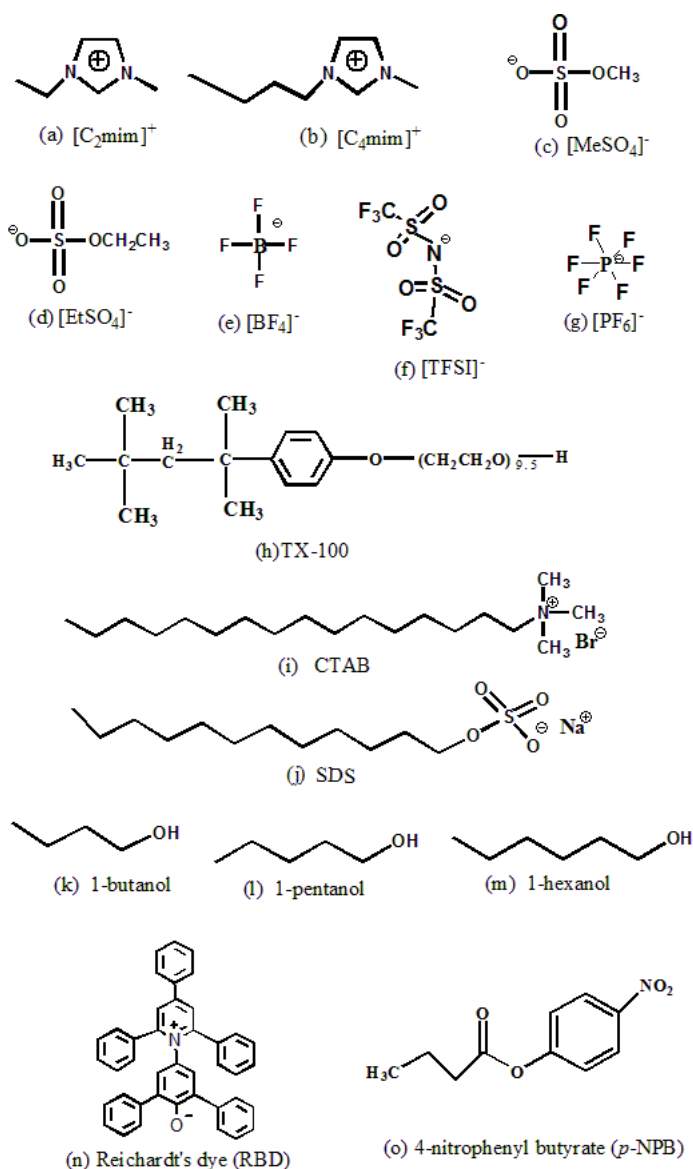
- To prepare and characterize IL based microemulsions and to study how the nature of surfactants (anionic, cationic and nonionic) and ILs (hydrophilic and hydrophobic) influence the physicochemical properties of IL based microemulsions.
- To analyze the nature of interactions of different components in these IL based microemulsions and to analyze the microstructures in the light of percolation theory.
- To study the catalytic activity of lipase in these IL based microemulsions. using hydrolysis of *p*-NPB as a model reaction.
- To correlate the physicochemical properties of IL based microemulsions with conventional microemulsions to develop the strategy to tune and enhance the catalytic activity of enzymes in IL based microemulsions.

1.11. Present Work

In this work, series of IL based microemulsions have been prepared with different surfactants such as nonionic surfactant, Triton X-100 (TX-100), cationic surfactant, cetyltrimethylammonium bromide (CTAB) and anionic surfactant, sodium dodecyl

sulfate (SDS) with the variation of polar phase (IL or water) to surfactant molar ratio (R or W_o). Both hydrophilic and hydrophobic ILs influence the physicochemical properties of IL based microemulsions. Cyclohexane and hydrophobic ILs, 1-ethyl-3-methylimidazolium bis(trifluoromethylsulfonyl)imide ($[\text{C}_2\text{mim}][\text{TFSI}]$), 1-ethyl-3-methylimidazolium hexafluorophosphate ($[\text{C}_2\text{mim}][\text{PF}_6]$) and 1-butyl-3-methylimidazolium hexafluorophosphate ($[\text{C}_4\text{mim}][\text{PF}_6]$) have been used as nonpolar phase where water and hydrophilic ILs, 1-ethyl-3-methylimidazolium ethyl sulfate ($[\text{C}_2\text{mim}][\text{EtSO}_4]$), 1-butyl-3-methylimidazolium methyl sulfate ($[\text{C}_4\text{mim}][\text{MeSO}_4]$), 1-ethyl-3-methylimidazolium methyl sulfate ($[\text{C}_2\text{mim}][\text{MeSO}_4]$), 1-ethyl-3-methylimidazolium tetrafluoroborate ($[\text{C}_2\text{mim}][\text{BF}_4]$) and 1-butyl-3-methylimidazolium tetrafluoroborate ($[\text{C}_4\text{mim}][\text{BF}_4]$) have been used as polar phase to prepare IL based microemulsions (Scheme 1.14.). Cosurfactants (1-butanol, 1-pentanol, 1-hexanol) have been used in these IL based microemulsions. Different microregions in IL based microemulsions depend on polar phase (IL or water) to surfactant mole ratio (R or W_o) or volume fraction of polar phase (ϕ_{IL} or ϕ_{W}) in microemulsions. The catalytic activity of lipase in IL based microemulsions will also be investigated. The lipase-catalyzed hydrolysis of 4-nitrophenyl butyrate (p -NPB) is used as a model reaction to characterize the catalytic behavior of lipase in the IL based microemulsion.

Physicochemical properties such as conductivity, viscosity, density, refractive index, polarity, surface tension and droplet sizes have been studied. Droplet sizes of microemulsions were determined by DLS measurements. Absorption spectra of Reichardt's Betaine dye, RBD (2, 6-diphenyl-4-(2, 4, 6-triphenyl-N-pyridino)phenolate) in these microemulsions were monitored for polarity estimation (Scheme 1.1). Different types of microstructures in these IL based microemulsions depending on volume fraction of polar phase (ϕ_{IL} or ϕ_{W}) have been determined by applying percolation theory on conductivity results. The physicochemical properties of IL based microemulsions were also compared with conventional microemulsions. The lipase catalyzed hydrolysis of 4-nitrophenyl butyrate (p -NPB) is used as a model reaction to characterize the catalytic behavior of lipase in IL based microemulsions.



Scheme 1.14. Structure of cations a) $[\text{C}_2\text{mim}]^+$, b) $[\text{C}_4\text{mim}]^+$, anions c) $[\text{MeSO}_4]^-$, d) $[\text{EtSO}_4]^-$, e) $[\text{BF}_4]^-$, f) $[\text{TFSI}]^-$, g) $[\text{PF}_6]^-$, surfactants (h) TX-100 (nonionic), (i) CTAB (cationic), (j) SDS (anionic), cosurfactants (k) 1-butanol, (l) 1-pentanol, (m) 1-hexanol, dye (n) RBD, substrate, and (o) *p*-NPB.

References

- [1] Fanun M. *Microemulsions: properties and applications*, CRC press, Surfactant science series 144.
- [2] Wormuth, K.; Lade, O.; Lade, M.; Schomäcker, R. *Microemulsions, Handbook of Applied Surface and Colloid Chemistry*, ed. Holmberg, K. Wiley: U.K. **2002**, vol. 2.
- [3] Rees, G. D.; Robinson, B. H. *Adv. Mater.* **1993**, *5*, 608-619.
- [4] Paul, B. K.; Moulik, S. P. *Current Sci.* **2001**, *80*, 990-1001.

- [5] Solans, C.; Kunieda, H. *Industrial applications of microemulsions*, Surfactant Science Series, Dekker: New York, **1997**, vol. 66.
- [6] Schwuger, M. J.; Stickdorn, K.; Schömäcker, R. *Chem. Rev.* **1995**, 95, 849-864.
- [7] Eastoe, J.; Warne, B. *Curr. Opin. Colloid Interface Sci.* **1996**, 1, 800-805.
- [8] Porada, J. H.; Mansueto, M.; Laschat, S.; Stubenrauch, C. *Soft Matter* **2011**, 7, 6805–6810.
- [9] *Microemulsions: Background, New Concepts, Applications, Perspectives*, ed. Stubenrauch, C. John Wiley & Sons, Ltd, **2009**.
- [10] Himmler, S.; Hormann, S.; van Hal, R.; Schulz, P. S.; Wasserscheid, P. *Green Chem.* **2006**, 8, 887-894.
- [11] Fei, Z.; Goldbach, T. J.; Zhao, D.; Dyson, P. J. *Chem. Eur. J.* **2006**, 12, 6762-6775.
- [12] Welton, T. *Chem. Rev.* **1999**, 99, 2071–2083.
- [13] Huddleston, J. G.; Willauer, H. D.; Swatloski, R. P.; Visser, A. E.; Rogers, R. D. *Chem. Commun.* **1998**, 1765–1766.
- [14] Dickinson, E. V.; Williams, M. E.; Hendrickson, S. M.; Masui, H.; Murray, R. W. *J. Am. Chem. Soc.* **1999**, 121, 613–616.
- [15] Nakashima, T.; Kimizuka, N. *Chem. Lett.* **2002**, 1018–1019.
- [16] Aki, S. N. V. K.; Brennecke, J. F.; Samanta, A. *Chem. Commun.* **2001**, 413–414.
- [17] Eastoe, J.; Gold, S.; Rogers, S. E.; Paul, A.; Welton, T.; Heenan, R. K.; Grillo, I. *J. Am. Chem. Soc.* **2005**, 127, 7302–7303.
- [18] Qiu, Z.; Texter, J. *Curr. Opin. Colloid Interface Sci.* **2008**, 13, 252-262.
- [19] Gao, Y.; Han, S.; Han, B.; Li, G.; Shen, D.; Li, Z.; Du, J.; Hou, W.; Zhang, G. *Langmuir* **2005**, 21, 5681-5684.
- [20] Gao, Y.; Li, N.; Zheng, L.; Zhao, X.; Zhang, S.; Han, B.; Hou, W.; Li, G. *Green Chem.* **2006**, 8, 43.
- [21] Gao, H.; Li, J.; Han, B.; Chen, W.; Zhang, J.; Zhang, R.; Yan, D. *Phys. Chem. Chem. Phys.* **2004**, 6, 2914-2916.
- [22] Li, J.; Zhang, J.; Gao, H.; Han, B.; Gao, L. *Colloid Polym. Sci.* **2005**, 283, 1371-1375.
- [23] Cheng, S.; Fu, X.; Liu, J.; Zhang, J.; Zhang, Z.; Wei, Y.; Han, B. *Colloids Surf. A: Physicochem. Eng. Aspects* **2007**, 302, 211-215.
- [24] Gao, Y.; Zhang, J.; Xu, H.; Zhao, X.; Zheng, L.; Li, X.; Yu, L. *Chem. Phys. Chem.* **2006**, 7, 1554.
- [25] Zheng, Y.; Eli, W. *J. Dispers. Sci. Technol.* **2009**, 30, 698-703.
- [26] Zheng, Y.; Eli, W.; Li, G. *Colloid Polym. Sci.* **2009**, 287, 871-876.
- [27] Li, N.; Zhang, S.; Li, X.; Yu, L.; Zheng, L. *Colloid Polym. Sci.* **2009**, 287, 103-108.
- [28] Oshovsky, G. V.; Reinhoudt, D. N.; Verboom, W. *Angew. Chem. Int. Ed.*, **2007**, 46, 2366-2393.
- [29] Eigen, M. *Naturwissenschaften* **1971**, 58, 465–523.
- [30] Brackmann, S. *Biophys. Chem.* **1997**, 66, 133–143.
- [31] Lehn, J. M. *Pro. Nat.l Acad. Sci.* **2002**, 99, 4763–4768.
- [32] Salager, J. -L. *Surfactant Types and Uses*, firp booklet E300-A, Teaching aid in Surfactant Science & engineering. Universidad de Los Andes, Versión 2, Mérida-Venezuela, **2002**.
- [33] Milton, J. R. *Surfactants and Interfacial Phenomena*, 3rd Ed., A John Wiley and Sons, **2004**.

- [34] Moroi, Y. *Micelles, Theoretical and Applied Aspects*, Plenum Press, New York, **1992**.
- [35] Myers, D. *Surfactant Science and Technology*, VCH, New York, **1988**.
- [36] Holmberg, K.; Jönsson, B.; Kronberg, B.; Lindman, B. *Surfactants and Polymers in Aqueous Solution*, 2nd Ed., Wiley, Chichester, **2003**.
- [37] Tadros, T. F. *Applied Surfactants: Principles and Applications*, Wiley, New York, **2005**.
- [38] Dwars, T.; Paetzold, E.; Oehme, G. *Angew. Chem.* **2005**, 117, 7338–7364.
- [39] Crans, D. C.; Trujillo, A. M.; Bonetti, S.; Rithner, C. D.; Baruah, B.; Levinger, N. E. *J. Org. Chem.* **2008**, 73, 9633–9640.
- [40] Hoar, T. P.; Schulman, J. H. *Nature*, **1943**, 152, 102-103.
- [41] Schulman, J. H.; Stoeckenius, W.; Prince, L. M. *J. Phys. Chem.* **1959**, 63, 1677-1680.
- [42] Danielsson, I.; Lindmann, B. *Colloids Surf.* **1981**, 3, 391-392.
- [43] Winsor, P. A. *Solvent properties of amphiphilic compounds*, Butterworth: London, **1954**.
- [44] Salager, J. -L.; Antón, R. E. *Handbook of Microemulsions Science and Technology, Ionic microemulsions*, eds. Kumar, P.; Mittal, K. L. Dekker: New York, **1999**.
- [45] Lawrence, M. J.; Rees, G.D. *Adv. Drug Deliv. Rev.* **2000**, 45, 89-121.
- [46] Lawrence, M. J. *Eur. J. Drug Metab. Pharmacokinet.* **1994**, 3, 257–269.
- [47] Winsor, P. A. *J. Chem. Soc. Faraday Trans.* **1948**, 44, 376-382.
- [48] Prince, L. M. *Microemulsions: Theory and Practice*, New York, Academic Press, **1977**.
- [49] Friberg, S. E.; Bothorel, P. *Microemulsions: Structure and Dynamics*, CRC Press, Boca Raton, **1987**.
- [50] Moulik, S. P.; Pal, B. K. *Adv. Colloid Interf. Sci.* **1998**, 78, 99–195.
- [51] Lagues, M.; Ober, R.; Taupin, C. *Phys. (France) Lett.* **1978**, 39, L487–L491.
- [52] Lagues, M.; *J. Phys. Lett.* **1979**, 40, 331–333.
- [53] Lagues, M.; Sauterey, C. *J. Phys. Chem.* **1980**, 84, 1532–1535.
- [54] Lagues, M.; Sauterey, C. *J. Phys. Chem.* **1980**, 84, 3503–3508.
- [55] García-Río, L.; Leis, J. R.; López-Fontán, J. L.; Mejuto, J. C.; Mosquera, V.; Rodríguez-Dafonte, P. *J. Colloid Interface Sci.* **2005**, 289, 521-529.
- [56] van Bommel, A.; MacIsaac, G.; Livingstone, N.; Palepu, R. *Fluid Phase Equilib.* **2005**, 237, 59-67.
- [57] Fanun, M. *J. Dispersion Sci. Technol.* **2008**, 29, 1426-1434.
- [58] Mehta, S. K.; Kaur, G.; Mutneja, R.; Bhasin, K. K. *J. Colloid Interface Sci.* **2009**, 338, 542-549.
- [59] Fanun, M. *J. Colloid Interface Sci.* **2010**, 343, 496-503.
- [60] Paul, B. K.; Mitra, R. K. *J. Colloid Interface Sci.* **2006**, 295, 230-242.
- [61] Fanun, M. *J. Mol. Liq.* **2009**, 150, 25-32.
- [62] Li, X.; He, G.; Zheng, W.; Xiao, G. *Colloid Surface A* **2010**, 360, 150-158.
- [63] Paul, B. K.; Mitra, R. K.; Moulik, S. P. Microemulsions: percolation of conductance and thermodynamics of droplet clustering. In *Encyclopedia of Surface and Colloid Science*, ed. Somasundaran, P. Taylor & Francis: New York, **2006**.
- [64] Boned, C.; Peyrelasse, J.; Saidi, Z. *Phys. Rev. E* **1993**, 47, 468.
- [65] Hilfiker, R.; Eicke, H. F.; Geiger, S.; Furler, S. *J. Coll. Int. Sci.* **1985**, 105, 378-387.
- [66] Van Dijk, M. A.; Joosten, J. G. H.; Levine, Y. K.; Bedeaux, D. *J. Phys.*

- Chem.* **1989**, 93, 2506-2512.
- [67] Maitra, A.; Mathew, C.; Varshney, M. *J. Phys. Chem.* **1990**, 94, 5290-5292.
- [68] Hamilton, R. T.; Billman, J. F.; Kaler, E. W. *Langmuir* **1990**, 6, 1696-1700.
- [69] Clark, S.; Fletcher, P. D. I.; Ye, X. *Langmuir* **1990**, 6, 1301-1309.
- [70] Chen, S. H.; Rouch, J.; Tartaglia P. *J. Non-Cryst. Solids* **1991**, 131-133, 275-281.
- [71] Chatenay, D.; Urbach, W.; Cazabat, A. M.; Langevin, D. *Phys. Rev. Lett.* **1985**, 54, 2253
- [72] Matsen, M. W.; Schick, M.; Sullivan, D. E. *J. Chem. Phys.* **1993**, 98, 2341-2352.
- [73] Hattori, Y.; Ushiki, H.; Engl, W.; Courbin, L.; Panizza, P. *Physica A* **2005**, 353, 29-37.
- [74] Cid-Samamed, A.; García-Río, L.; Fernández-Gándara, D.; Mejuto, J. C.; Morales, J.; Pérez-Lorenzo, M. *J. Colloid Interface Sci.* **2008**, 318, 525-529.
- [75] Safran, S. A.; Grest, G. S.; Bug, A.; Webman, I. Percolation in interacting microemulsions. In *Microemulsion Systems*; Rosano, H.; Clause, M. eds. Marcel Dekker: New York, **1987**.
- [76] Pal, S.; Bisal, S. R.; Moulik, S. P. *J. Phys. Chem.* **1992**, 96, 896-901.
- [77] Garboczi, E. J.; Berryman, J. G. *Concrete Sci. Eng.* **2000**, 2, 88-96.
- [78] Weissker, H. Ch.; Furthmiller, J.; Bechstedt, F. *Phys. Rev. B* **2003**, 67, 165322-165325.
- [79] Mehta, S. K.; Bala, K. *Fluid Phase Equilib.* **2000**, 172, 197-209.
- [80] Fanun, M. *J. Mol. Liq.* **2008**, 139, 14-22.
- [81] Fanun, M. *J. Mol. Liq.* **2008**, 142, 103-110.
- [82] Bug, A. L. R.; Safran, S. A.; Grest, G. S.; Webman, I. *Phys Rev Lett* **1985**, 55, 1896-1899.
- [83] Safran, S. A.; Webman, I.; Grest, G. S. *Phys Rev A* **1986**, 32, 506-511.
- [84] Grest, G. S.; Webman, I.; Safran, S. A.; Bug, A. L. R. *Phys Rev A* **1986**, 33, 2842-2845.
- [85] Boned, C.; Peyrelasse, J.; Saidi, Z. *Phys Rev E* **1993**, 47, 5732-5737.
- [86] Cametti, C.; Codastefno, P.; Tartaglia, P.; Chen, S.; Rouch, J. *Phys Rev A* **1992**, 45, R5358-R5361.
- [87] Straley, J. P. *Phys Rev B* **1977**, 15, 5733-5737.
- [88] Bhattacharya, S.; Stokes, J. P.; Kim, M. W.; Huang, J. S. *Phys Rev Lett* **1985**, 55, 1884-1887.
- [89] Freemantle M. *Chem. Eng. News* **1998**, 76, 32-37.
- [90] Freemantle, M. *An Introduction to Ionic Liquids*, RSC publishers, Cambridge UK, **2010**.
- [91] Angell, C. A.; Ansari, Y.; Zhao, Z. *Faraday Discuss.* **2012**, 154, 9-27.
- [92] Hurley, F. H.; Wier, T. P.; *J. Electrochem. Soc.* **1951**, 98, 203-206.
- [93] MacFarlane, D. R.; Forsyth, S. A.; Golding, J.; Deacon, G. B. *Green Chem.* **2002**, 4, 444-448.
- [94] Sun, J.; Forsyth, M.; MacFarlane, D. R. *J. Phys. Chem. B* **1998**, 102, 8858-8864.
- [95] Cooper, E. I.; Angell, C. A. *Solid State Ionics* **1983**, 9-10, 617-622.
- [96] Greaves, T. L.; Drummond, C. J. *Chem. Rev.* **2008**, 108, 206-237.
- [97] Angell, C. A. *J. Electrochem. Soc.* **1965**, 112, 1224-1227.
- [98] Tamura, T.; Hachida, T.; Yoshida, K.; Tachikawa, N.; Dokko, K.; Watanabe, M. *J. Power Sources* **2010**, 195, 6095-6100.
- [99] Mandai, T.; Yoshida, K.; Ueno, K.; Dokko, K.; Watanabe, M. *Phys. Chem*

- Chem. Phys.* **2014**, 16, 8761-8772.
- [100] Adams, W. A.; Laidler, K. J. *Can. J. Chem.* **1968**, 46, 1977-2011.
- [101] Campbell, A. N.; van der Kouwe, E. T. *Can. J. Chem.* **1968**, 46, 1294-1298.
- [102] Angell, C. A.; Byrne, N.; Belieres, J. P. *Acc. Chem. Res.* **2007**, 40, 1228-1236.
- [103] Yoshizawa, M.; Xu, W.; Angell, C. A. *J. Am. Chem. Soc.* **2003**, 125, 15411-15419.
- [104] Zhao, C.; Burrell, G.; Torriero, A. A. J.; Separovic, F.; Dunlop, N. F.; MacFarlane, D. R.; Bond, A. M. *J. Phys. Chem. B* **2008**, 112, 6923-6936.
- [105] Fraser, K. J.; Izgorodina, E. I.; Forsyth, M.; Scott, J. L.; MacFarlane, D. R. *Chem. Commun.* **2007**, 3817-3819.
- [106] Angell, C. A. *Aust. J. Chem.* **1970**, 23, 929-937.
- [107] Angell, C. A. *J. Phys. Chem.* **1972**, 76, 3244.
- [108] Smedley, S. I.; MacFarlane, D. R. *J. Electroanal. Chem.* **1981**, 118, 445-452.
- [109] Smedley, S. I. *The Interpretation of Ionic Conductivity in Liquids*, Plenum Press, New York, 1980.
- [110] Friberg, S. E.; Podzimek, M. *Colloid Polym. Sci.* **1984**, 262, 252.
- [111] Rico, I.; Lattes, A. *New J. Chem.* **1984**, 8, 429-431.
- [112] Saidi, Z.; Mathew, C.; Peyrelasse, J.; Boned, C. *Phys. Rev. A* **1990**, 42, 872-876.
- [113] Ray, S.; Moulik, S. P. *Langmuir* **1994**, 10, 2511-2515.
- [114] Chang, D. R. *Langmuir* **1990**, 6, 1132-1135.
- [115] Atkin, R.; Warr, G. G. *J. Am. Chem. Soc.* **2005**, 34, 11940-11941.
- [116] Atkin, R.; Warr, G. G. *J. Phys. Chem. B* **2007**, 111, 9309-9316.
- [117] Zech, O.; Thomaier, S.; Bauduin, P.; Rück, T.; Touraud, D.; Kunz, W. *J. Phys. Chem. B* **2009**, 113, 465-473.
- [118] Cheng, S.; Zhang, J.; Zhang, Z.; Han, B. *Chem. Commun.* **2007**, 43, 2497-2499.
- [119] Moniruzzaman, M.; Kamiya, N.; Goto, M. *Langmuir* **2009**, 25, 977-982.
- [120] Pavlidis, I. V.; Gournis, D.; Papadopoulos, G. K.; Stamatidis, H. *J. Mol. Cat B* **2009**, 60, 50-56.
- [121] Rispen, T.; Engberts, J. B. F. N. *J. Org. Chem.* **2002**, 67, 7369-7371.
- [122] Engberts, J. B. F. N.; Fernández, E.; García-Río, L.; Leis, J. R. *J. Org. Chem.* **2006**, 71, 4111-4117.
- [123] Engberts, J. B. F. N.; Fernández, E.; García-Río, L.; Leis, J. R. *J. Org. Chem.* **2006**, 71, 6118-6123.
- [124] Gayet, F.; Kalamouni, C. E.; Lavedan, P.; Marty, J. D.; Brûlet, A.; Viguerie, N. L. *Langmuir* **2009**, 25, 9741-9750.
- [125] Liu, L.; Bauduin, P.; Zemb, T.; Eastoe, J.; Hao, J. *Langmuir* **2009**, 25, 2055-2059.
- [126] Yan, F.; Yu, S.; Zhang, X.; Qiu, L.; Chu, F.; You, J.; Lu, J. *Chem. Mater.* **2009**, 21, 1480-1484.
- [127] Zhao, M.; Zheng, L.; Bai, X.; Li, N.; Yu, L. *Colloid Surface A* **2009**, 346, 229-236.
- [128] Li, Z.; Zhang, J.; Du, J.; Han, B.; Wang, J. *Colloid Surface A* **2006**, 286, 117-120.
- [129] Moniruzzaman, M.; Tahara, Y.; Tamura, M.; Kamiya, N.; Goto, M. *Chem. Commun.* **2010**, 46, 1452-1454.
- [130] Fischer, E. *Ber. Dtsch. Chem. Ges.* **1890**, 23, 2611-2624.

- [131] Fischer, E. *Ber. Dtsch. Chem. Ges.* **1894**, 27, 2985-2993.
- [132] Koshland, D. E. *Proc. Natl. Acad. Sci. U.S.A.* **1958**, 44, 98-104.
- [133] Reslow, M.; Adlercreutz, P.; Mattiasson, B. *Eur. J. Biochem.* **1988**, 172, 573-578.
- [134] Zaks, A.; Russel, A. J. *J. Biotechnol.* **1988**, 8, 259-269.
- [135] Laane, C.; Boeren, S.; Vos, K.; Veeger, C. *Biotechnol. Bioeng.* **1987**, 30, 81-87.
- [136] Luisi, P. L.; Giomini, M.; Pileni, M. P.; Robinson, B. H. *Biochim Biophys. Acta* **1988**, 947, 209-246.
- [137] Martinek, K.; Berezin, I. V.; Khmelnitski, Y. L.; Klyachko, N. L.; Levashov, A. V. *Biocatalysis* **1987**, 1, 9-15.
- [138] Luisi, P. L.; Liithi, P.; Tomka, I.; Prenosil, J.; Pande, P. *Ann. N. Y. Acad. Sci.* **1984**, 434, 549-557.
- [139] Eggers, D. K.; Blanch, H. W. *Bioprocess Eng.* **1988**, 3, 83-91.
- [140] Leser, M. E.; Wei, G.; Luisi, P. L.; Maestro, M. *Biochem. Biophys. Res. Commun.* **1986**, 135, 629-635.
- [141] Martinek, K.; Levashov, A. V.; Khmelnitskii Y. L.; Klyachko, N. L.; Berezin, I. V. *Science* **1982**, 218, 889-891.
- [142] Luisi, P. L.; Magid, I. J. *CRC Crit. Rev. Biochem.* **1986**, 20, 409-474.
- [143] Rees, G. D.; Robinson, B. H.; Stephenson, G. R. *Biochim. Biophys. Acta* **1995**, 1257, 239-248.
- [144] Han, D.; Walde, P.; Luisi, P. L. *Biocatalysis* **1990**, 4, 153-161.
- [145] Fletcher, P. D. I.; Robinson, B. H. *J. Chem. Soc., Faraday Trans. 1* **1985**, 81, 2667-2679.
- [146] Das, D.; Roy, S.; Mitra, R. N.; Dasgupta, A.; Das, P. K. *Chem. Eur. J.* **2005**, 11, 488-4889.
- [147] Satianegara, G.; Rogers, P. L.; Rosche, B. *Biotechnol. Bioeng.* **2006**, 94, 1189-1195.
- [148] Shome, A.; Roy, S.; Das, P. K. *Langmuir* **2007**, 23, 4130-4136.
- [149] Paradkar, V. M.; Dordick, J. S. *J. Am. Chem. Soc.* **1994**, 116, 5009-5010.
- [150] Paradkar, V. M.; Dordick, J. S. *Biotechnol. Bioeng.* **1994**, 43, 529-540.
- [151] Chakrabarty, D.; Seth, D.; Chakraborty, A.; Sarkar, N. *J. Phys. Chem. B* **2005**, 109, 5753-5758.
- [152] Gao, Y.; Li, N.; Hilfert, L.; Zhang, S.; Zheng, L.; Yu, L. *Langmuir* **2009**, 25, 1360-1365.
- [153] Gao, Y. A.; Vogit, A.; Hilfert, L.; Sundmacher, K. *ChemPhysChem* **2008**, 9, 1603-1609.
- [154] Gao, Y.; Wang, S.; Zheng, L.; Han, S.; Zhang, X.; Lu, D.; Yu, L.; Ji, Y.; Zhang, G. *J. Colloid Interface Sci.* **2006**, 301, 612-616.
- [155] Gao, Y.; Zhang, J.; Xu, H.; Zhao, X.; Zheng, L.; Li, X.; Yu, L. *ChemPhysChem* **2006**, 7, 1554-1561.
- [156] Gao, Y.; Li, N.; Zheng, L.; Bai, X.; Yu, L.; Zhao, X.; Zhang, J.; Zhao, M.; Li, Z. *J. Phys. Chem. B* **2007**, 111, 2506-2513.
- [157] Gao, Y.; Li, N.; Zheng, L.; Zhao, X.; Zhang, J.; Cao, Q.; Zhao, M.; Li, Z.; Zhang, G. *Chem. Eur. J.* **2007**, 13, 2661-2670.
- [158] Li, N.; Gao, Y.; Zheng, L.; Zhang, J.; Yu, L.; Li, X. *Langmuir* **2007**, 23, 1091-1097.
- [159] Gao, Y.; Li, N.; Zhang, S.; Zheng, L.; Li, X.; Dong, B.; Yu, L. *J. Phys. Chem. B* **2009**, 113, 1389-1395.

- [160] Cheng, S.; Han, F.; Wang, Y.; Yan, J. *Colloid Surface A* **2008**, 317, 457–461.
- [161] Gao, Y.; Hilfert, L.; Voigt, A.; Sundmacher, K. *J. Phys. Chem. B* **2008**, 112, 3711–3719.
- [162] Pramanik, R.; Sarkar, S.; Ghatak, C.; Setua, P.; Rao, V. G.; Sarkar, N. *Chem. Phys. Lett.* **2010**, 490, 154–158.
- [163] Gao, Y.; Voigt, A.; Hilfert, L.; Sundmacher, K. *Colloid Surface A* **2008**, 329, 146–152.
- [164] Pramanik, R.; Sarkar, S.; Ghatak, C.; Setua, P.; Sarkar, N. *Phys. Chem. Chem. Phys.* **2010**, 12, 3878–3886.
- [165] Andújar-Matalobos, M.; García-Río, L.; López-García, S.; Rodríguez-Dafonte, P. *J. Colloid Interface Sci.* **2011**, 363, 261–267.
- [166] Setua, P.; Pramanik, R.; Sarkar, S.; Ghatak, C.; Rao, V. G.; Sarkar, N.; Das, S. K. *J. Mol. Liq.* **2011**, 162, 33–37.
- [167] Banerjee, C.; Mandal, S.; Ghosh, S.; Kuchlyan, J.; Sarkar, N. *Chem. Phys. Lett.* **2013**, 580, 88–93.
- [168] Wang, G. -X.; Lu, M.; Wu, H. *Polymer* **2012**, 53, 1093–1097.
- [169] Wang, G. -X.; Lu, M.; Liu, L. -C.; Wu, H.; Zhong, M. *J. Appl. Polym. Sci.* **2013**, 128, 3077–3083.
- [170] Wei, J.; Su, B.; Liang, R.; Xing, H.; Bao, Z.; Yang, Q.; Yang, Y.; Ren, Q. *Colloid Surface A* **2012**, 414, 82–87.
- [171] Harrar, A.; Zech, O.; Hartl, R.; Bauduin, P.; Zemb, T.; Kunz, W. *Langmuir* **2011**, 27, 1635–1642.
- [172] Ghosh, S.; Banerjee, C.; Mandal, S.; Rao, V. G.; Sarkar, N. *J. Phys. Chem. B* **2013**, 117, 5886–5897.
- [173] Mandal, S.; Ghosh, S.; Banerjee, C.; Kuchlyan, J.; Banik, D.; Sarkar, N. *J. Phys. Chem. B* **2013**, 117, 3221–3231.
- [174] Pramanik, R.; Sarkar, S.; Ghatak, C.; Rao, V. G.; Setua, P.; Sarkar, N. *J. Phys. Chem. B* **2010**, 114, 7579–7586.
- [175] Pramanik, R.; Sarkar, S.; Ghatak, C.; Rao, V. G.; Sarkar, N. *J. Phys. Chem. B* **2011**, 115, 2322–2330.
- [176] Sarkar, S.; Pramanik, R.; Ghatak, C.; Rao, V. G.; Sarkar, N. *J. Chem. Phys.* **2011**, 134, 074507/1–074507/11.
- [177] Atkin, R.; Bobillier, S. M. C.; Warr, G. G. *J. Phys. Chem. B* **2010**, 114, 1350–1360.
- [178] Blach, D.; Silber, J. J.; Correa, N. M.; Falcone, R. D. *Phys. Chem. Chem. Phys.* **2013**, 15, 16746–16757.
- [179] Gao, Y.; Han, S.; Han, B.; Li, G.; Shen, D.; Li, Z.; Du, J.; Hou, W.; Zhan, G. *Langmuir* **2005**, 21, 5681–5684.
- [180] Gao, Y.; Li, N.; Zheng, L.; Zhao, X.; Zhang, S.; Han, B.; Houa, W.; Li, G. *Green Chem.* **2006**, 8, 43–49.
- [181] Seth, D.; Chakraborty, A.; Setua, P.; Sarkar, N. *Langmuir* **2006**, 22, 7768–7775.
- [182] Seth, D.; Chakraborty, A.; Setua, P.; Sarkar, N. *J. Chem. Phys.* **2007**, 126, 224512/1–224512/12.
- [183] Chen, Z.; Nozaki, R. *J. Chem. Phys.* **2012**, 136, 244505/1–244505/10.
- [184] Shu, Y.; Cheng, D.; Chen, X.; Wang, J. *Sep. Purif. Technol.* **2008**, 64, 154–159.
- [185] Zhang, Y.; Huang, X. R.; Li, Y. Z. *J. Chem. Technol. Biotechnol.* **2008**, 83, 1230–1235.

- [186] Zhou, G. P.; Zhang, Y.; Huang, X. R.; Shi, C. H.; Liu, W. F.; Li, Y. Z.; Qu, Y. B.; Gao, P. J. *Colloid Surf. B Biointerfaces* **2008**, 66, 146–149.
- [187] Pavlidis, I. V.; Gouris, D.; Papadopoulos, G. K.; Stamatis, H. *J. Mol. Catal. B* **2009**, 60, 50–56.
- [188] Moniruzzaman, M.; Ino, K.; Kamiya, N.; Goto, M. *Org. Biomol. Chem.* **2012**, 10, 7707–7713.
- [189] Moniruzzaman, M.; Kamiya, N.; Nakashima, K.; Goto, M. *Green Chem.* **2008**, 10, 497–500.
- [190] Xue, L.; Li, Y.; Zou, F.; Lu, L.; Zhao, Y.; Huang, X.; Qu, Y. *Colloid Surf. B Biointerfaces* **2012**, 92, 360–366.
- [191] Zhang, G.; Chen, X.; Xie, Y.; Zhao, Y.; Qiu, H. *J. Colloid Interface Sci.* **2007**, 315, 601–606.
- [192] Zhang, G.; Chen, X.; Zhao, Y.; Xie, Y.; Qiu, H. *J. Phys. Chem. B* **2007**, 111, 11708–11713.
- [193] Safavi, A.; Maleki, N.; Farjami, F. *Colloids Surface A* **2010**, 355, 61–66.
- [194] Rojas, O.; Koetz, J.; Kosmella, S.; Tiersch, B.; Wacker, P.; Kramer, M. *J. Coll. Interface Sci.* **2009**, 333, 782–790.
- [195] Rojas, O.; Tiersch, B.; Frasca, S.; Wollenberger, U.; Koetz, J. *Colloids Surf. A* **2010**, 369, 82–87.
- [196] Rojas, O.; Tiersch, B.; Rabe, C.; Stehle, R.; Hoell, A.; Arlt, B.; Koetz, J. *Langmuir* **2013**, 29, 6833–6839.
- [197] Rao, V. G.; Mandal, S.; Ghosh, S.; Banerjee, C.; Sarkar N. *J. Phys. Chem. B* **2013**, 117, 1480–1493.

Abstract

Conventional and IL based microemulsions have been prepared from TX-100 and CTAB surfactants with the variation of R and/or W_o . Cyclohexane, [C₂mim][TFSI], [C₂mim][PF₆] and [C₄mim][PF₆] were used as the nonpolar phase, and water, [C₂mim][EtSO₄], [C₄mim][MeSO₄], [C₂mim][MeSO₄], [C₂mim][BF₄] and [C₄mim][BF₄] were used as the polar phase,. For TX-100 based microemulsions the surfactant could be dissolved in both polar and nonpolar phases, whereas for CTAB based microemulsions a cosurfactant was required in addition to the surfactant to obtain optically clear microemulsions. Microemulsions from TX-100 and CTAB were stable for pretty long time; up to one year and three years respectively.

2.1. Introduction

Conventional approach for the preparation of microemulsions is to utilize phase diagrams. Friberg et al. reported this technique and extensive used for preparation of microemulsions [1-4]. But construction of the phase diagram is time-consuming which is the major drawback of this approach especially when one has a variety of surfactants, cosurfactants and oils for estimation. Recently, automated systems have been commercialized to balance the difficult titrations for the determination of various phases. But the cost as well as accuracy of the measurements is the major drawbacks of such systems at present.

H. L. Rosano [5] suggested an alternative simpler approach in which one can determine the minimum amount of primary surfactant needed for the preparation of microemulsions. In this theoretical calculation, for preparing microemulsions the minimum amount of primary surfactant required is calculated by determining the mono-molecular interfacial film area needed to form between the dispersed phase and the continuous phase. From the simple calculation one can get the idea of the minimum amount of surfactant necessary to cover the interface. However, it does not take into account the amount of surfactant that is dispersed in both the polar and nonpolar phases and other aggregates that can form in solution. As the viscosity levels are always low, a coarse emulsion of dispersed phase in continuous phase is formed from the estimated amounts of surfactants by simple mixing equipment. As most cosurfactants are liquids, a cosurfactant can be added by titration to the coarse emulsion followed by gentle mixing. The system can be considered unacceptable if it does not turn clear after adding the cosurfactant in an amount equivalent to that of the primary surfactant. The components of the system must be altered. As cosurfactant (usually alcohols are used) is commonly the nonspecific component, it is first altered with a different hydrocarbon chain length. The cosurfactants need to be chosen as they do not prefer either the continuous or dispersed phase. A proper cosurfactant will migrate to the oil-water interface and form a mixed surfactant/cosurfactant film.

If the microemulsion does not form with the selected cosurfactant, one should consider a new primary surfactant. The amount of the new surfactant is recalculated

and the process is carried out again. If the selection of surfactant and cosurfactant fail, the dispersed phase should rather be altered, in a logical manner.

In order to combine the unique properties of ILs [6] with the unique nanostructures of microemulsions, this designer solvent (IL) can be used as either the polar [7-19] or the nonpolar [20-24] phase in microemulsions. In order to replace water as the polar phase to prepare microemulsions, IL can be used for the development of high-temperature microemulsions stable at temperatures above the boiling point of water [16,18-19]. They can also be used as the nonpolar solvents in IL based microemulsions as a nalternative for oil which is volatile and flammable.

Gao et al. extensively studied IL based TX-100 microemulsions where different volatile organic solvents were used as the nonpolar phase and [C₄mim][BF₄] ionic liquid was used as the polar phase [25-29]. Microemulsions ([C₄mim][BF₄]/o) in TX-100/*p*-xylene/[C₄mim][BF₄] system were prepared by Gao et al. where the initial TX-100 weight fractions were kept constant at 0.8000 and 0.5500 for different series of microemulsions [25]. For preparation of the cyclohexane based microemulsion TX-100/cyclohexane/[C₄mim][BF₄], the weight ratio of the components was 1.1000:0.9000:0.2000. The molar ratio of [C₄mim][BF₄]/TX-100 was 0.5300 [26]. o/[C₄mim][BF₄] microemulsions were also prepared by Gao et al. using TX-100. In these works, toluene, cyclohexane, benzene, and *p*-xylene were used as the oil phases. Weight fraction, *F* of organic solvent ($F = W_{oil}/(W_{oil} + W_{TX-100} + W_{IL})$) was varied at different initial weight fraction of TX-100, *R* ($R = W_{TX-100}/(W_{TX-100} + W_{IL})$) [27]. Gao et al. also prepared reverse microemulsion ([C₄mim][BF₄]/o) where [C₄mim][BF₄]/TX-100 molar ratio (*R*) was 0.5300 with 49.9000 % wt TX-100, 40.8000 % wt cyclohexane and 9.3000 % wt [C₄mim][BF₄] [28]. Li et al. prepared IL/o microemulsion from TX-100/toluene/[C₄mim][BF₄] system with [C₄mim][BF₄] to TX-100 molar ratio (*R*) was varied at 1.1300, 1.4700, 181.0000, 2.1500 to 2.5000. Initial weight fraction of TX-100 here was 0.4500 [29].

Cheng et al. studied IL/IL microemulsions where a hydrophobic IL, [C₄mim][PF₆] was dispersed in a hydrophilic IL, PAFcontaining NaAOT surfactant. The [C₄mim][PF₆] to NaAOT molar ratio were varied at 0.2000, 0.5000, 0.7500 and 1.0000 respectively and the weight fraction of AOT in the microemulsions was kept constant at 0.1600 [30]. Moniruzzaman et al. prepared IL based reverse micelles where a desired amount of AOT was dissolved in the IL, [C₈mim][TFSI] using 10.0000 vol% of cosurfactant (1-hexanol). Reverse micelles were prepared by injecting an appropriate amount of water to vary the molar ratio of water to NaAOT. Vortex mixing was carried out until an optically transparent solution was obtained. From the total amount of water used the independently known amount of water soluble in the pure IL without surfactant was subtracted to calculate the values of *W*_o [31]. Using the ILs [C₄mim][BF₄] and [C₄mim][TFSI] (1-butyl-3-methylimidazolium bis(trifluoromethylsulfonyl)imide) as the polar domain, reverse micelles of TX-100/benzene and BHDC/benzene were prepared by Falcon et al. [32] At a fixed surfactant concentration ([BHDC] = 0.3000 M and [TX-100] = 0.7000 M)

with different [IL]/[surfactant] ratios the micellar systems were studied. Ferreyra et al. prepared BHDC/chlorobenzene/[C₄mim][TFSI] and NaAOT/chlorobenzene/[C₄mim][TFSI] reverse micelles at different [IL]/[surfactant] ratios with [surfactant] = 0.1000 M [33]. Toluene, pentanol, CTAB and [C₂mim][EtSO₄] or [C₂mim][HexSO₄] ILs were used to prepare microemulsions by Rabe et al. with a CTAB:toluene:IL mass ratio of 0.1000:0.5000:0.4000 which were titrated at 25 °C by toluene:pentanol mixtures (5:1 for [C₂mim][EtSO₄] and 20.0000:1.0000 for [C₂mim][HexSO₄] [34]. Rojas et al. used ILs, [C₂mim][EtSO₄] as the polar phase and toluene as the oil phase using [C₄mim][OctSO₄] as surfactant to prepare microemulsions [35]. Rao et al. prepared [C₄mim][AOT]/benzene/IL microemulsions with the variation of *R* from different ILs [36]. Despite numerous studies, studies on systematic variation of the structure of the cations and anions of ILS and nature of surfactants and compositions for preparation of microemulsions are scarcely reported.

The aim of this work is therefore to study the role of the surfactant structure and IL structure as polar and nonpolar phase on the stability of microemulsions. For this work both conventional and IL based microemulsions have been prepared by using three different types of surfactants; non-ionic, cationic and anionic (TX-100, CTAB and SDS respectively), polar (water or IL) and nonpolar (cyclohexane or IL) phases in a wide range of compositions.

2.2. Experimental

2.2.1. Materials and Equipments

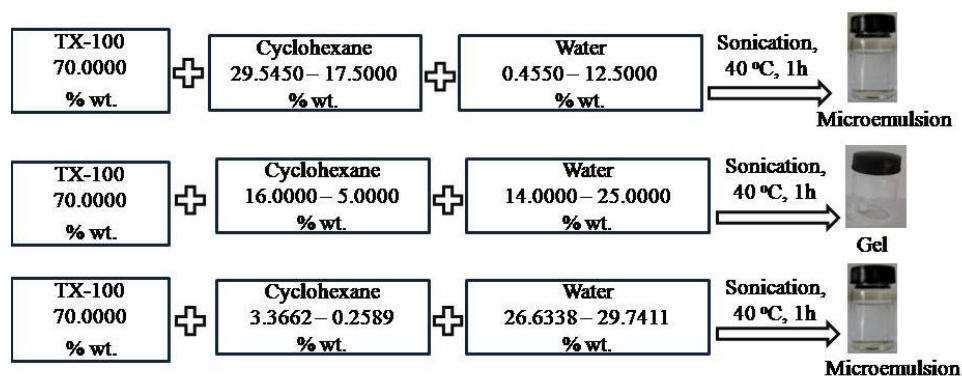
The surfactants (TX-100, CTAB and SDS), cyclohexane, cosurfactants (1-butanol, 1-pentanol, 1-hexanol) and the ILs, [C₂mim][EtSO₄], [C₂mim][BF₄], [C₂mim][MeSO₄], [C₄mim][BF₄], [C₄mim][MeSO₄], [C₂mim][PF₆], [C₄mim][PF₆] and [C₂mim][TFSI] were obtained from Sigma-Aldrich and used without further purification. The elaborated forms of the abbreviations have been given in Section 1.11. of Chapter 1. De-ionized water (conductivity: 0.0550 μS cm⁻¹ at 25 °C), collected from HPLC grade water purification system (BOECO, BOE 8082060 Germany), was used for preparing all the microemulsions.

Mass of the individual components of microemulsions were taken by using analytical balance, UB-110/0.0001 g, UNILAB, and the mixtures were sonicated by UNILAB UET-1080 digital ultrasonic bath.

2.3. Preparation of Conventional Microemulsions

2.3.1. Preparation of TX-100/Cyclohexane/Water Microemulsions

Conventional TX-100 microemulsions were prepared by mixing a fixed mass of TX-100 surfactant and varying that of cyclohexane and water, which were used as the nonpolar and polar phases respectively and the total mass of the mixture being the same in all cases. Clear, transparent microemulsions with a single phase were obtained after 1 day of mixing different components. The scheme for preparation of different microemulsions is represented below (Scheme 2.1) and compositions of different microemulsions thus prepared are listed in Table 2.1.



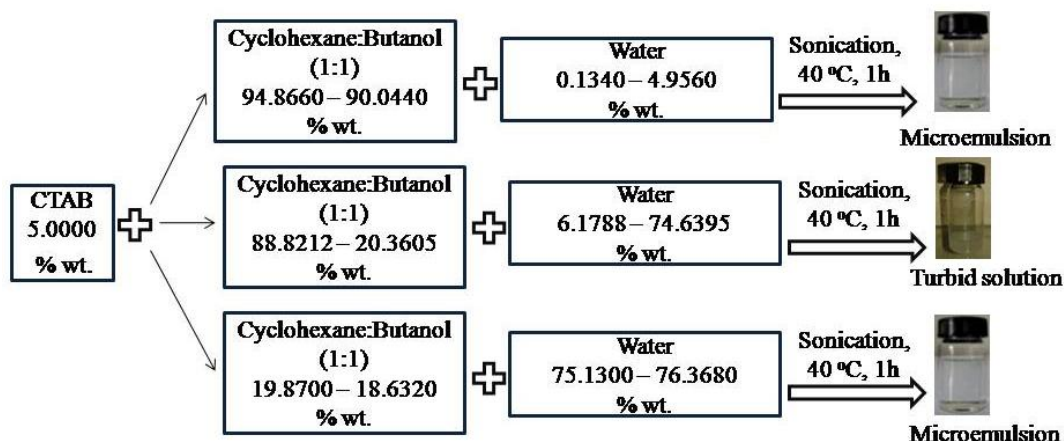
Scheme 2.1. Preparation of TX-100 microemulsions using different amounts of conventional polar (water) and non-polar (cyclohexane) phases.

Table 2.1. Preparation of TX-100/cyclohexane/water microemulsions.

Composition	TX-100, % wt	Water, % wt	Cyclohexane, % wt	W_o
1.	70.0000	0.4550	29.5450	0.2255
2.	70.0000	1.1300	28.8700	0.5600
3.	70.0000	1.4930	28.5070	0.7400
4.	70.0000	1.8200	28.1800	0.9020
5.	70.0000	5.0000	25.0000	2.4781
6.	70.0000	10.0000	20.0000	4.9562
7.	70.0000	12.5000	17.5000	6.1953
8.	70.0000	26.6338	3.3662	13.1999
9.	70.0000	28.1875	1.8125	13.9700
10.	70.0000	28.8735	1.1265	14.3100
11.	70.0000	29.5393	0.4607	14.6399
12.	70.0000	29.7411	0.2589	14.7400

2.3.2. Preparation of CTAB/1-Butanol/Cyclohexane/Water Microemulsions

Conventional CTAB microemulsions were prepared at a fixed CTAB composition containing cyclohexane, water and 1-butanol as nonpolar, polar phases and cosurfactant respectively. Mole ratio of cyclohexane and 1-butanol was always maintained at 1:1. Optically clear microemulsions were found after 1 day of mixing different components. The scheme for preparation of different microemulsions is shown below in Scheme 2.2. and compositions of microemulsions are given in Table 2.2.



Scheme 2.2. Preparation of CTAB microemulsions using different amounts of conventional polar (water) and non-polar (cyclohexane) phases

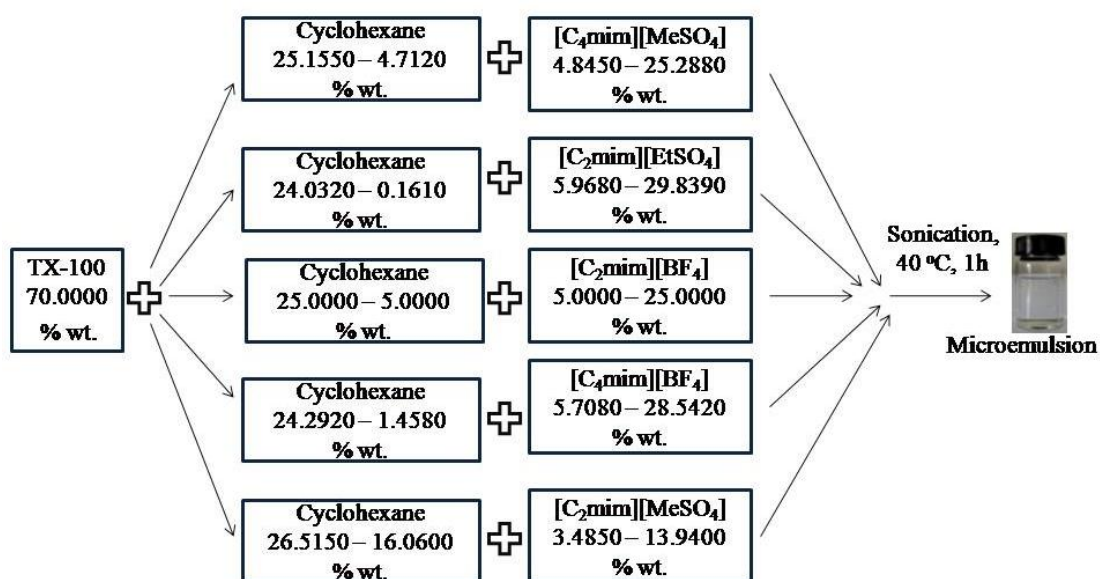
Table 2.2. Preparation of CTAB/1-butanol/cyclohexane/water microemulsions.

Composition	CTAB, % wt	Water, % wt	Cyclohexane:Butanol (1:1), % wt	W_o
1.	5.0000	0.1340	94.8660	0.5424
2.	5.0000	1.1440	93.8560	4.6273
3.	5.0000	1.9060	93.0940	7.7121
4.	5.0000	2.6684	92.3320	10.7970
5.	5.0000	3.4310	91.5690	13.8818
6.	5.0000	4.1930	90.8070	16.9667
7.	5.0000	4.9560	90.0440	20.0515
8.	5.0000	75.1300	19.8700	304.0000
9.	5.0000	75.3800	19.6200	305.0000
10.	5.0000	75.8740	19.1260	307.0000
11.	5.0000	76.3680	18.6320	309.0000

2.4. Preparation of IL Based Microemulsions

2.4.1. Preparation of TX-100/Cyclohexane/IL Microemulsions, where IL is Used as the Polar Phase

IL based microemulsions were prepared using a fixed amount of TX-100 along with various amounts of cyclohexane and hydrophilic ILs as the nonpolar and polar phases respectively. Optically transparent microemulsions were formed within 1-2 days after mixing of different components, while some of the microemulsions based on $[C_2mim][MeSO_4]$ and $[C_2mim][BF_4]$ took 10-15 days to form clear microemulsions. The scheme and compositions for preparation of different microemulsions are displayed in Scheme 2.3 and Table 2.3 respectively.



Scheme 2.3. Preparation of TX-100/cyclohexane/IL microemulsions.

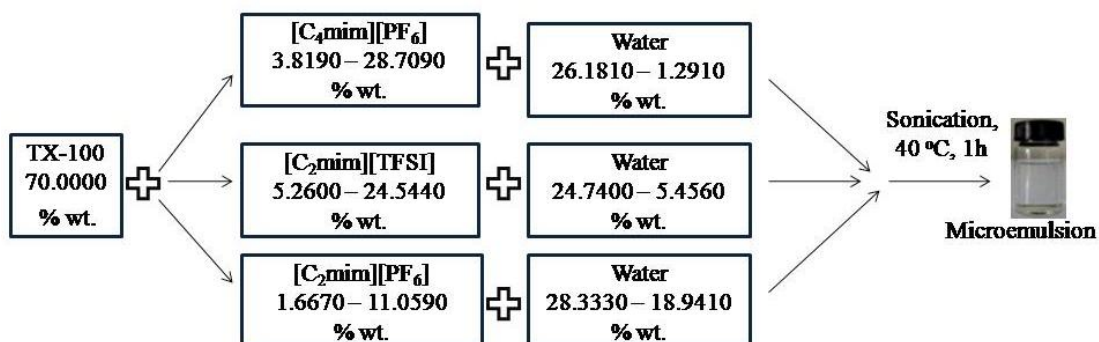
Table 2.3. Preparation of TX-100/cyclohexane/IL microemulsions

Composition	TX-100, % wt	[C ₄ mim][MeSO ₄], % wt	Cyclohexane, % wt	<i>R</i>	ϕ_{IL}
1.	70.0000	4.8450	25.1550	0.1728	0.0394
2.	70.0000	6.3220	23.6780	0.2255	0.0517
3.	70.0000	12.6440	17.3560	0.4510	0.1065
4.	70.0000	15.7000	14.3000	0.5600	0.1342
5.	70.0000	18.9660	11.0340	0.6765	0.1647
6.	70.0000	20.7470	9.2530	0.7400	0.1817
7.	70.0000	25.2880	4.7120	0.9020	0.2264
Composition	TX-100, % wt	[C ₂ mim][EtSO ₄], % wt	Cyclohexane, % wt	<i>R</i>	ϕ_{IL}
1.	70.0000	5.9680	24.0320	0.2255	0.0479
2.	70.0000	11.9350	18.0650	0.4510	0.0983
3.	70.0000	14.8200	15.1800	0.5600	0.1237
4.	70.0000	17.9030	12.0970	0.6765	0.1518
5.	70.0000	19.5840	10.4160	0.7400	0.1674
6.	70.0000	23.8710	6.1290	0.9020	0.2086
7.	70.0000	29.8390	0.1610	1.1275	0.2690
Composition	TX-100, % wt	[C ₂ mim][BF ₄], % wt	Cyclohexane, % wt	<i>R</i>	ϕ_{IL}
1.	70.0000	5.0000	25.0000	0.2255	0.0385
2.	70.0000	10.0000	20.0000	0.4510	0.0789
3.	70.0000	12.4170	17.5830	0.5600	0.0992
4.	70.0000	15.0000	15.0000	0.6765	0.1215
5.	70.0000	15.5200	14.4800	0.7000	0.1256

6.	70.0000	20.0000	10.0000	0.9020	0.1663
7.	70.0000	25.0000	5.0000	1.1275	0.2137
Composition	TX-100, % wt	[C ₄ mim][BF ₄], % wt	Cyclohexane, % wt	<i>R</i>	ϕ_{IL}
1.	70.0000	5.7080	24.2920	0.2255	0.0469
2.	70.0000	11.4170	18.5830	0.4510	0.0963
3.	70.0000	14.1760	15.8240	0.5600	0.1211
4.	70.0000	17.1250	12.8750	0.6765	0.1483
5.	70.0000	18.7330	11.2670	0.7400	0.1635
6.	70.0000	22.8330	7.1670	0.9020	0.2032
7.	70.0000	28.5420	1.4580	1.1275	0.2612
Composition	TX-100, % wt	[C ₂ mim][MeSO ₄], % wt	Cyclohexane, % wt	<i>R</i>	
1.	70.0000	3.4850	26.5150	0.1400	
2.	70.0000	4.3020	25.6980	0.1728	
3.	70.0000	4.9790	25.0210	0.2000	
4.	70.0000	5.6130	24.3870	0.2255	
5.	70.0000	7.1070	22.8930	0.2855	
6.	70.0000	11.2270	18.7730	0.4510	
7.	70.0000	13.9400	16.0600	0.5600	

2.4.2. Preparation of TX-100/IL/Water Microemulsions Using IL as the Oil Phase

IL based microemulsions were prepared from a constant amount of TX-100, while the amount of water and hydrophobic ILs, i.e. the polar and nonpolar phases, were varied to keep the total weight of the mixture constant. It took 2-3 days to obtain clear microemulsions after mixing the components. The preparation scheme of different microemulsions is demonstrated below (Scheme 2.4) and the amounts of different components required for preparing microemulsions are shown in Table 2.4.



Scheme 2.4. Preparation of TX-100/IL/water microemulsions.

Table 2.4. Preparation of TX-100/IL/water microemulsions

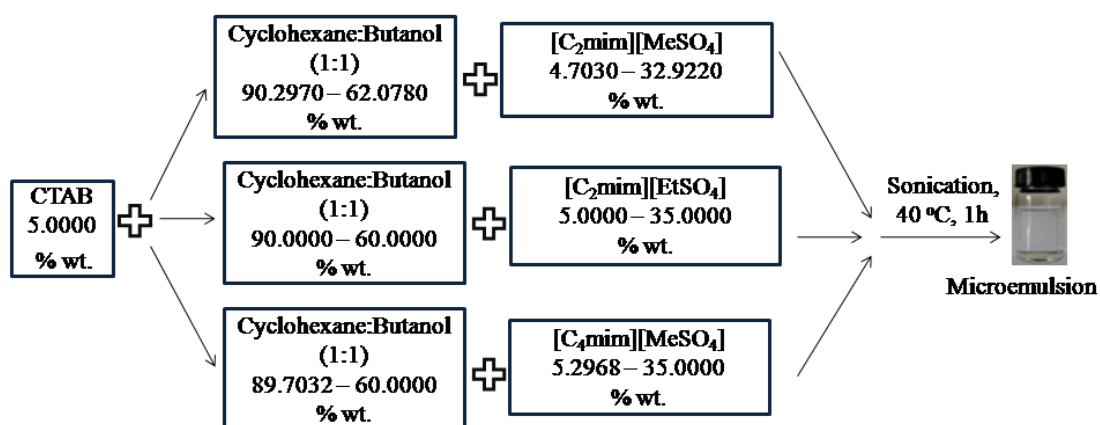
Composition	TX-100, % wt	[C ₄ mim][PF ₆], % wt	Water, % wt	<i>R</i>	<i>W</i> _o	ϕ_w
1.	70.0000	3.8190	26.1810	0.1200	12.9756	0.2779
2.	70.0000	7.1770	22.8230	0.2255	11.3113	0.2447
3.	70.0000	10.1850	19.8150	0.3200	9.8205	0.2143
4.	70.0000	14.3550	15.6450	0.4510	7.7538	0.1713
5.	70.0000	17.8240	12.1760	0.5600	6.0346	0.1347
6.	70.0000	21.5320	8.4680	0.6765	4.1968	0.0947
7.	70.0000	23.5530	6.4470	0.7400	3.1952	0.0726
8.	70.0000	28.7090	1.2910	0.9020	0.6398	0.0148

Composition	TX-100, % wt	[C ₂ mim][TFSI], % wt	Water, % wt	<i>R</i>	<i>W</i> _o	ϕ_w
1.	70.0000	5.2600	24.7400	0.1200	12.2614	0.2648
2.	70.0000	7.5720	22.6800	0.1728	11.2404	0.2442
3.	70.0000	9.8840	20.1160	0.2255	9.9697	0.2191
4.	70.0000	11.9560	18.0440	0.2728	8.9428	0.1980
5.	70.0000	14.0240	15.9760	0.3200	7.9179	0.1767
6.	70.0000	16.8960	11.0400	0.3855	5.4715	0.1264
7.	70.0000	19.7640	10.2360	0.4510	5.0731	0.1157
8.	70.0000	24.5440	5.4560	0.5600	2.7041	0.0629

Composition	TX-100, % wt	[C ₂ mim][PF ₆], % wt	Water, % wt	<i>R</i>	<i>W</i> _o
1.	70.0000	1.6670	28.3330	0.0581	14.0421
2.	70.0000	3.4420	26.5580	0.1200	13.1624
3.	70.0000	4.8767	25.1233	0.1700	12.4514
4.	70.0000	6.4670	23.5310	0.2255	11.6622
5.	70.0000	7.8260	22.1740	0.2728	10.9897
6.	70.0000	9.1800	20.8200	0.3200	10.3186
7.	70.0000	11.0590	18.9410	0.3855	9.3874

2.4.3. Preparation of CTAB/1-Butanol/Cyclohexane/IL Microemulsions

IL based microemulsions were prepared using CTAB of a constant weight with varying amounts of nonpolar and polar phases and cosurfactant, namely cyclohexane, water and 1-butanol respectively. Microemulsions formed 1 day after mixing different components. The schematic representation of the preparation of different microemulsions and compositions of the microemulsions are given in Scheme 2.5 and Table 2.5, respectively.



Scheme 2.5. Preparation of CTAB/1-butanol/cyclohexane/IL microemulsions.

Table 2.5. Preparation of CTAB/1-butanol/cyclohexane/IL microemulsions.

Composition	CTAB, % wt	[C ₂ mim][MeSO ₄], % wt	Cyclohexane:Butanol, % wt (1:1 mole ratio)	R
1.	5.0000	4.7030	90.2970	1.5424
2.	5.0000	9.4060	85.5940	3.0849
3.	5.0000	14.1090	80.8910	4.6273
4.	5.0000	18.8120	76.1880	6.1697
5.	5.0000	23.5150	71.4850	7.7121
6.	5.0000	28.2190	66.7810	9.2546
7.	5.0000	32.9220	62.0780	10.7970
Composition	CTAB, % wt	[C ₂ mim][EtSO ₄], % wt	Cyclohexane:Butanol, % wt (1:1 mole ratio)	R
1.	5.0000	5.0000	90.0000	1.5424
2.	5.0000	10.0000	85.0000	3.0849
3.	5.0000	15.0000	80.0000	4.6273
4.	5.0000	20.0000	75.0000	6.1697
5.	5.0000	25.0000	70.0000	7.7121
6.	5.0000	30.0000	65.0000	9.2546
7.	5.0000	35.0000	60.0000	10.7970
Composition	CTAB, % wt	[C ₄ mim][MeSO ₄], % wt	Cyclohexane:Butanol, % wt (1:1 mole ratio)	R
1.	5.0000	5.2968	89.7032	1.5424
2.	5.0000	10.5939	84.4061	3.0849
3.	5.0000	15.0000	80.0000	4.3679
4.	5.0000	21.1875	73.8125	6.1697
5.	5.0000	25.0000	70.0000	7.2800
6.	5.0000	30.0000	65.0000	8.7359
7.	5.0000	35.0000	60.0000	10.1918

2.4.4. Preparation of IL Based Microemulsions from SDS

Attempt was taken to prepare microemulsions from the anionic surfactant, SDS by varying the amount (% wt) of hydrophilic ILs ([C₂mim][EtSO₄], [C₂mim][BF₄], [C₂mim][MeSO₄], [C₄mim]BF₄] and [C₄mim][MeSO₄]) and fixing the mole ratio of cyclohexane to cosurfactant (1-butanol, 1-pentanol and 1-hexanol) at 1:1, amount (% wt) of SDS (5 % wt, 10 % wt, 20 % wt, 30 % wt, 40 % wt, 50 % wt, 60 % wt and 70 % wt) being kept constant. However, no clear and optically transparent microemulsions could be observed for any of the compositions from SDS. Electrostatic attractions between the anionic sulfate head groups and the cation of IL reduce the range of SDS microemulsions [37].

2.5. Stability of Microemulsions

2.5.1. Stability of Microemulsions from TX-100

Both conventional and IL based microemulsions with TX-100 were stored at room temperature for more than one year and they were thermodynamically stable up to one year.

2.5.2. Stability of Microemulsions from CTAB

Both conventional and IL based microemulsions with CTAB were stored at room temperature for more than three years and they were thermodynamically stable up to three years.

2.6. Preparation of Conventional and IL based Microemulsions with Different Surfactants:

Both conventional and IL based microemulsions could be prepared using different type of surfactants. Surfactants stabilize the microemulsion thermodynamically by reducing interfacial tension between two immiscible liquids. There exists no electrostatic repulsion among nonionic surfactants. So a wide range of microemulsions with TX-100 were easily formed. The surfactant film could be stabilized much better by the incorporation of IL into the interfacial region and a so-called palisade layer was formed.

Microemulsions could be prepared for any of the compositions from SDS. In fact, the study of IL based SDS microemulsions is limited. This may be due to the fact that the electrostatic attractions between the anionic sulfate head groups and the cation of IL reduce the range of microemulsion. Rojas et al. reported that by adding more surfactant like water soluble IL, for example, by using [C₂mim][HexSO₄], in the presence of SDS, a broad isotropic phase channel can be formed [38]. Water soluble ILs play the role of the polar solvent as well as the role of a stabilizer of the interfacial film to form a palisade layer surrounding the microemulsion droplets. The bicontinuous sponge phase can be clearly identified by Cryo-SEM micrographs. ¹H NMR diffusion coefficient measurements give information about the existence of reverse microemulsions.

Series of microemulsions could be prepared based on CTAB, although the study of CTAB based IL/o microemulsions is also limited due to the necessity of high temperature and cosurfactants for microemulsion formation and stability [34]. In fact, there exists electrostatic repulsion among cationic ammonium head group of CTAB surfactants. The use of cosurfactants helped to reduce this electrostatic repulsion. Rabe et al. studied CTAB/toluene/pentanol/IL microemulsions and concluded that by increasing the temperature or by using more surfactant like IL, that is, by replacing [C₂mim][EtSO₄] with [C₂mim][HexSO₄], isotropic phase region increased. The temperature treatment is important for the better solubility of surfactant and the IL in the oil phase. For the formation of bicontinuous microemulsions, a cosurfactant is required in combination with [C₂mim][EtSO₄], in contrast with the [C₂mim][HexSO₄], where the hexylsulfate anion can serve this purpose.

2.7. Conclusion

Series of clear and transparent microemulsions, both conventional and IL based, could be prepared by using TX-100 and CTAB surfactants at varying R or W_o . For IL based microemulsions, hydrophilic and hydrophobic ILs were used as the alternatives for water and volatile organic phases respectively. Conventional microemulsions with TX-100 were formed at W_o ranging from 0.2255 to 6.1953 and then from 13.2000 to 14.4700, where gel formation occurred at W_o values from 6.9385 to 12.3903. Conventional microemulsions with CTAB were formed for W_o values from 0.5424 to 20.0515 and again from 304.0000 to 309.0000. IL based microemulsions from TX-100 and [C₄mim][MeSO₄], [C₂mim][EtSO₄], [C₂mim][BF₄], [C₄mim][BF₄] and [C₂mim][MeSO₄] were formed when the values of R were varied from 0.1728 to 0.9020, 0.2255 to 1.1275, 0.2255 to 1.1275, 0.2255 to 1.1275 and 0.1400 to 0.5600 respectively. Microemulsions from CTAB could be prepared with [C₄mim][PF₆], [C₂mim][TFSI] and [C₂mim][PF₆] at W_o ranging between 0.6398 to 12.9756, 2.7041 to 12.2614 and 9.3874 to 14.0421 respectively.

References

- [1] Friberg, S.; *Chem Technology* **1976**, 6, 124-127.
- [2] Zana R.; Lans, J. *Dynamics of microemulsion, Microemulsions: Structure and Dynamics*, CRC, Boca Raton, FL, **1987**, pp. 153-172.
- [3] Bellocq, A.; Roux, D. *Phase diagram and critical behavior of a quaternary microemulsion system, Microemulsion: Structure and Dynamics*, CRC, Boca Raton, FL, **1987**, pp. 33-77.
- [4] Friberg, S.; Bothorel, P. *Microemulsions: Structure and Dynamics*, CRC, Boca Raton, FL, **1987**, p. 219.
- [5] Rosano, H. L.; *J. Colloid Interface Sci.* **1973**, 44, 242.
- [6] Freemantle, M.; *An Introduction to Ionic Liquids*, RSC publishers, Cambridge UK, **2010**.
- [7] Atkin, R.; Warr, G. G. *J. Phys. Chem. B* **2007**, 111, 9309–9316.
- [8] Chakrabarty, D.; Seth, D.; Chakraborty, A.; Sarkar, N. *J. Phys. Chem. B* **2005**, 109, 5753–5758.

- [9] Eastoe, J.; Gold, S.; Rogers, S. E.; Paul, A.; Welton, T.; Heenan, R. K.; Grillo, I. *J. Am. Chem. Soc.* **2005**, 127, 7302–7303.
- [10] Gao, H.; Li, J.; Han, B.; Chen, W.; Zhang, J.; Zhang R.; Yan, D. *Phys. Chem. Chem. Phys.* **2004**, 6, 2914–2916.
- [11] Gao, Y.; Li, N.; Zheng, L. Q.; Zhao, X. Y.; Zhang, J.; Cao, Q.; Zhao, M. W.; Li, Z.; G. Y. Zhang, G. Y. *Chem. Eur. J.* **2007**, 13, 2661–2670.
- [12] Gao, Y.; Zhang, J.; Xu, H. Y.; Zhao, X. Y.; Zheng, L. Q.; X. W. Li, X. W.; Yu, L. *ChemPhysChem* **2006**, 7, 1554–1561.
- [13] Li, J.; Zhang, J.; Gao, H.; Han, B.; Gao, L. *Colloid Polym. Sci.* **2005**, 283, 1371–1375.
- [14] Li, N.; Gao, Y. A.; Zheng, L. Q.; Zhang, J.; Yu, L.; Li, X. W. *Langmuir* **2007**, 23, 1091–1097.
- [15] Li, N.; Zhang, S. H.; Zheng, L. Q.; Gao, Y.; Yu, L. *Langmuir* **2008**, 24, 2973–2976.
- [16] Zech, O.; Bauduin, P.; Palatzky, P.; Touraud, D.; Kunz, W. *Energy Environ. Sci.* **2010**, 3, 846–851.
- [17] Zech, O.; Thomaier, S.; Bauduin, P.; Ruck, T.; Touraud, D.; Kunz, W. *J. Phys. Chem. B* **2009**, 113, 465–473.
- [18] Zech, O.; Thomaier, S.; Kolodziejski, A.; Touraud, D.; Grillo, I.; Kunz, W. *Chem. Eur. J.*, **2010**, 16, 783–786.
- [19] Zech, O.; Thomaier, S.; Kolodziejski, A.; Touraud, D.; Grillo, I.; Kunz, W. *J. Colloid Interface Sci.* **2010**, 347, 227–232.
- [20] Anjum, N.; Guedeau-Boudeville, M. A.; Stubenrauch, C.; Mourchid, A. *J. Phys. Chem.* **2009**, 113, 239–244.
- [21] Behera, K.; Kumar, V.; Pandey, S. *ChemPhysChem* **2010**, 11, 1044–1052.
- [22] Gao, Y.; Han, S.; Han, B.; Li, G.; Shen, D.; Li, Z.; Du, J.; Hou, W.; Zhang, G. *Langmuir* **2005**, 21, 5681–5684.
- [23] Gao, Y.; Li, N.; Zheng, L. Q.; Zhao, X. Y.; Zhang, S. H.; Han, B. X.; Hou, W. G.; Li, G. Z. *Green Chem.* **2006**, 8, 43–49.
- [24] Xue, L. Y.; Qiu, H. J.; Li, Y.; Lu, L.; Huang, X. R.; Qu, Y. B.; *Colloids Surf. B* **2011**, 82, 432–437.
- [25] Gao, Y.; Zhang, J.; Xu, H.; Zhao, X.; Zheng, L.; Li, X.; Yu, L. *ChemPhysChem* **2006**, 7, 1554–1561.
- [26] Gao, Y.; Li, N.; Hilfert, L.; Zhang, S.; Zheng, L.; Yu, L. *Langmuir* **2009**, 25, 1360–1365.
- [27] Gao, Y.; Li, N.; Zhang, S.; Zheng, L.; Li, X.; Dong, B.; Yu, L. *J. Phys. Chem. B* **2009**, 113, 1389–1395.
- [28] Gao, Y.; Hilfert, L.; Voigt, A.; Sundmacher, K. *J. Phys. Chem. B* **2008**, 112, 3711–3719.
- [29] Li, N.; Gao, Y.; Zheng, L.; Zhang, J.; Yu, L.; Li, X. *Langmuir* **2007**, 23, 1091–1097.
- [30] Cheng, S.; Zhang, J.; Zhang, Z.; Han, B. *Chem. Commun.* **2007**, 2497.
- [31] Moniruzzaman, M.; Kamiya, N.; Nakashima, K.; Goto, M. *ChemPhysChem* **2008**, 9, 689–692.
- [32] Falcone, R. D.; Correa, N. M.; Silber, J. J. *Langmuir* **2009**, 25, 10426–10429.
- [33] Ferreyra, D. D.; Correa, N. M.; Silber, J. J.; Falcone, R. D. *Phys. Chem. Chem. Phys.* **2012**, 14, 3460–3470.
- [34] Rabe, C.; Koetz, J. *Colloids Surf., A* **2010**, 354, 261–267.
- [35] Rojas, O.; Tiersch, B.; Frasca, S.; Wollenberger, U.; Koetz, J. *Colloids Surf., A* **2010**, 369, 82–87.

- [36] Rao, V.G.; Mandal, S.; Ghosh, S.; Banerjee, C.; Sarkar, N. *J. Phys. Chem. B* **2013**, 117, 1480–1493.
- [37] Behera, K.; Kumar, V.; and Siddharth Pandey, S. *ChemPhysChem* **2010**, 11, 1044–1052
- [38] Rojas, O.; Koetz, J.; Kosmella, S.; Tiersch, B.; Wacker, P.; Kramer, M. *J. Colloid Interface Sci.* 2009, **333**, 782–790.

Abstract

Physicochemical properties of series of TX-100 microemulsions were prepared by using cyclohexane or hydrophobic ILs, [C₂mim][TFSI], [C₄mim][PF₆] and [C₂mim][PF₆], as the nonpolar phase and water or hydrophilic ILs, [C₂mim][EtSO₄], [C₄mim][MeSO₄], [C₂mim][MeSO₄], [C₂mim][BF₄] and [C₄mim][BF₄], as the polar phase. Effect of the structure of the cation or anion of the ILs, weight ratio of the polar phase to surfactant on the physicochemical properties of the microemulsions have been extensively investigated. For TX-100/cyclohexane/hydrophilic IL microemulsions, conductivity, viscosity, and hydrodynamic sizes of reverse micelle droplets have been found to increase with increasing *R*. Conductivity and droplet size of microemulsions containing [C₂mim]⁺ cations decrease in the order [C₂mim][BF₄] > [C₂mim][EtSO₄] > [C₂mim][MeSO₄], while viscosity follows the increasing trend of [C₂mim][BF₄] < [C₂mim][EtSO₄] < [C₂mim][MeSO₄]. Conductivity, droplet size, and viscosity of microemulsions based on ILs containing [C₄mim]⁺ cation also show a similar trend. Studies of physicochemical properties by varying the structure of the cation of the ILs in microemulsions show that conductivity and droplet size of microemulsions based on [C₄mim][MeSO₄] are higher than those from [C₂mim][MeSO₄] ILs, whereas viscosity of the latter is found higher than the former. Similar observations were found in the case of [C₂mim][BF₄] and [C₄mim][BF₄] based microemulsions. For TX-100/hydrophobic IL/water microemulsions, the conductivity of [C₂mim][TFSI] based microemulsion first increases upto a value of ≈8.0 and then decreases with increasing *W*₀, while for [C₂mim][PF₆] based microemulsion, the conductivity decreases with increasing *W*₀. Viscosities of these microemulsions follow the opposite trend. The droplet size of the micelles increases with decreasing *W*₀ for both [C₂mim][PF₆] and [C₂mim][TFSI] based microemulsions. Study of the conductivity and viscosity of microemulsions based on the ILs having [C₂mim]⁺ cation and different anions, [PF₆]⁻ and [TFSI]⁻ specifies higher values for [C₂mim][PF₆] than [C₂mim][TFSI] based microemulsions, while viscosity of [C₂mim][TFSI] is found higher than [C₂mim][PF₆]. Micelle droplet size increases with decreasing *W*₀ for both [C₂mim][PF₆] and [C₄mim][PF₆] based microemulsions. When the anion is [PF₆]⁻ in combination with different cations, [C₂mim]⁺ and [C₄mim]⁺ in ILs, conductivity and viscosity follow the trend [C₂mim][PF₆] > [C₄mim][PF₆]. Refractive index of [C₂mim][PF₆] and [C₂mim][TFSI] based microemulsions decrease with increasing *W*₀. The variation in the physicochemical properties have been explained in terms of the transition of the microemulsion structure from reverse micelle to micelle dominated system via bicontinuous microemulsions. The structural variations of cations and anions have also been taken into consideration for understanding the change in physicochemical properties.

3.1. Introduction

Microemulsions are one of the different kinds of self organized media formed by a surfactant. They have received considerable attention till date due to their potential applications in pharmaceutical, analytical, industrial, chemical as well as electrochemical processes [1, 2]. Such media exhibit many special properties such as

low viscosity, low interfacial tension and high solubilization capacity of both polar and nonpolar substances. The physicochemical properties of microemulsions are of great importance as they are used in drug delivery systems and synthesis of nanomaterials [3-6]. Different experimental techniques such as measurement of conductivity [7-23], viscosity [8-21], refractive index [24], interfacial tension [12], density [17, 18], polarity [9], turbidity [13-16], DLS [9], cyclic voltammetry [9, 10] etc. have therefore been used to characterize microemulsions. Freeze fracture electron microscopy [FEM] [25, 26] has been used to characterize the size and shape of aggregates in microemulsions. The sizes of microemulsion droplets and connectivity of the water and oil rich domains could be analyzed properly by small angle x-ray scattering(SAXS), small angle neutron scattering (SANS) and NMR-self diffusion [27]. The free and bound water in different types of microemulsions could be identified by differential scanning calorimetry measurement [28, 29].

Conductivity and viscosity measurements are commonly used to measure the transport properties of microemulsions. From the knowledge of transport property different microstructures (Section 1.4.1. of Chapter 1) of microemulsion can be determined. In conventional o/w microemulsion, the conductance is fairly high as water is the continuous phase, whereas a quite opposite situation occurs for o/w microemulsion where oil is the continuous phase. Ion transport in w/o microemulsions with increasing water to surfactant mole ratio (W_o) or volume fraction of water (ϕ_w) can be explained by two mechanisms. Firstly, the reverse micelle droplets join together and surfactant ions hop from droplet to droplet which results in large increase in conductance. Secondly, two or more reverse micelle droplets coalesce or fuse to make small channels and transfer of ions of surfactant or salt take place in such channels followed by fission of associated droplets.

Microemulsions are usually Newtonian fluids with low viscosity. The viscosity of microemulsion increases with temperature and ϕ_w due to the increased hydrophobic-hydrophobic interactions among reverse micelle droplets. Viscosity of microemulsion can be properly described by the rigid sphere hypothesis at low temperature. When temperature approaches a critical value, this hypothesis fails and viscosity increase with volume fraction of dispersed phase is much more pronounced [30, 31].

The polarity of IL and IL based microemulsions etc. cannot be directly measured by measurement of dielectric constant because of the high conductivity of the media. However, solvatochromism have been efficiently used to estimate polarity by describing the pronounced change in position and sometimes intensity and shape of a UV-visible absorption band. A red (bathochromic) shift and a blue (hypsochromic) shift with increasing solvent polarity are called positive and negative solvatochromism, respectively. The polarity of a medium is generally characterized by a polarity scale, E_T (30) based on Equation 3.1, which describes the electronic transition energy of a probe dye (such as, Reichardt's dye 30 (Scheme 1.14. (n) of Chapter 1)) in the medium with a change in the color with a change in polarity. The

λ_{\max} is the wavelength for absorption maxima for intramolecular charge transfer π - π^* absorption band of the zwitterionic RBD.

$$E_T(30) (\text{kcalmol}^{-1}) = 28591 / \lambda_{\max} \dots \dots \dots (3.1)$$

Polarities of the ground and excited state of a dye are different. RBD is polar in the ground state and nonpolar in the excited state. So, a change in the polarity of a medium will lead to different stabilization of the ground and excited states which results in a change in the energy gap between electronic states. Intramolecular π - π^* charge transfer transition may occur in ILs. In the presence of RBD in IL based microemulsion, the intensity and shape of a UV-visible absorption band may be changed. As IL and the ground state of RBD are polar, specific stabilization of the ground state can be occurred. But in some cases no significant observation in the UV-visible absorption band is occurred. As in IL/o and IL/w microemulsions, IL is trapped in the core of the microemulsion droplets, the interaction with RBD may not be possible.

ILs are now a days, used both as polar and nonpolar phases for preparing microemulsions due to their unique properties and advantages over conventional microemulsions. ILs were earlier used instead of water since they can dissolve a large variety of chemicals. In contrast to conventional microemulsions, IL based microemulsions contain highly conductive polar or non-polar phase that undergoes variety of specific interactions with the components of microemulsion (Section 1.9. of Chapter 1). The IL/o system can be useful in applications where waterless conditions are required. Moreover, due to the absence of water, thermal stability range can be expanded in such microemulsions. In IL/o microemulsion, with increasing R or ϕ_{IL} , two or more reverse micelle droplets coalesce or fuse to make small channels. The ions of IL can transfer easily in such channels resulting in a large increase in conductance compared to the conventional w/o microemulsions. In addition, the use of volatile organic compounds in preparing microemulsions can be avoided when ILs are used as the oil phase (Section 1.9. of Chapter 1). Recently, there have been successful attempts to prepare aqueous microemulsions containing IL as the nonpolar phase. Nonionic surfactants have been promising in this regard.

Physicochemical properties of microemulsions play an important role to identify different microstructures as a result of the phase transition with varying ϕ_w or ϕ_{IL} . For specific applications in multidisciplinary areas these microstructures can play a vital role. Therefore, the goal of this research is to study the physicochemical properties of IL based microemulsions by varying R or W_o using nonionic TX-100 microemulsions where IL is used as both polar and nonpolar phases. Several ILs have been used for this purpose, having same cation with different anions and same anion with different cations. Such microemulsions were characterized by measuring several physicochemical properties such as conductivity, density, viscosity, refractive index

polarity, and surface tension. Droplet sizes of TX-100 microemulsions were measured from DLS measurements. From the analysis of physicochemical properties, the interactions involved in different components in microemulsion were also investigated. Attempts have also been made to distinguish different microstructures with phase transition with variation of ϕ_W or ϕ_{IL} by systematic analysis of the physicochemical properties of microemulsions.

3.2. Experimental

3.2.1. Materials

TX-100, cyclohexane and the ILs, [C₂mim][EtSO₄], [C₂mim][BF₄], [C₂mim][MeSO₄], [C₄mim]BF₄, [C₄mim][MeSO₄], [C₂mim][PF₆], [C₄mim][PF₆] and [C₂mim][TFSI] were obtained from Sigma-Aldrich. De-ionized water was collected from HPLC grade water purification system. RBD was received from Sigma Aldrich. Reagent grade ethanol was used to prepare stock solution of RBD. All the chemicals were used as received without further purification. Further details have been reported in in Section 1.11. of Chapter 1.

3.2.2. Preparation of Microemulsions

Microemulsions were prepared with a constant amount of TX-100 (70 % wt.) with variation of the polar and the nonpolar phases to keep the total weight of the microemulsion constant. Sections 2.4.1. and 2.4.2. of Chapter 2 describe the methodology for the preparation of the microemulsions and the details of the composition of TX-100/cyclohexane/hydrophilic IL and TX-100/hydrophobic IL/water microemulsions Sections 2.4.1. and 2.4.2. of Chapter 2.

3.2.3. Measurements

Conductivity of different CTAB microemulsions was measured with a digital conductivity meter (JENWAY, Model 4510, UK) equipped with a dip-type pre-calibrated cell at 25 °C.

Density of the microemulsions was measured with an Anton Paar (Model no. DMA 4500) vibrating tube density meter. The accuracy was 0.000005 gcm⁻³ and repeatability was 0.00001 gcm⁻³ of density measurement. The meter was calibrated with nano-pure water and with dry air at atmospheric pressure. A small amount of sample (about 2 mL) was injected to a U-shaped borosilicate glass tube. The density values were directly taken from the digital display. After each measurement, the U-shaped tube was cleaned with ethanol and nano-pure water and dried well. The temperature of the apparatus was controlled by a built-in Peltier device.

Viscosity of the microemulsions was measured with an Anton-Paar (Lovis-2000M/ME) falling ball automated viscometer with an accuracy of $\pm 10^{-6}$ mPa.s. A capillary with diameter 1.59 mm and a steel ball were used for the measurements. The supplied standard oil was used to calibrate the capillary and the ball. The measuring angle was 55°. Temperature was controlled by means of a built-in Peltier thermostat within ± 0.01 K.

Refractive index of the microemulsions was measured by using an Anton-Paar Abbemat-300 automated refractometer with high resolution optical sensor. The temperature was controlled by means of a built-in Peltier thermostat within ± 0.01 K.

The size and size distribution of droplets of different microemulsions were determined using a Zetasizer Nano ZS90 (ZEN3690, Malvern Instruments Ltd, UK) by DLS measurements at 25 °C. A He-Ne laser beam of 632.8 nm wavelength was used as the light source. The refractive index and viscosity data were used for interpretation of DLS data. All the measurements were made at a fixed scattering angle of 90°. The particle size detection limit was about 0.3 nm-5 μ m. To obtain the size and size distribution of the scattered data in microemulsion, the scattering intensity data were analyzed. The accuracy of the size determined by DLS measurement has been $\pm 2\%$. A measuring glass cell of 10 mm diameter was used. Before starting the measurements the laser light was illuminated for about 30 min to stabilize the system. The temperature was controlled by means of a built-in Peltier thermostat within ± 0.01 K. At least 3 measurements, each of 50 runs were carried out for each sample and the run time was set at 20 s for each sample.

Surface tension of microemulsions was measured by a sigma force tensiometer (Model: Attension Sigma-701, KSB Instruments, Finland) with a platinum Wilhelmy plate. The accuracy of the measurements was ± 0.1 mNm⁻¹ which was checked by replicate experiments and by frequent measurement of the interfacial tension of pure water.

Spectral studies were carried out using a double beam Shimadzu UV-visible spectrophotometer (Model: UVD 3500, Labomed, USA). It was equipped with a thermoregulated compartment and spectral data processing facilities. A rectangular quartz cell of path length 1 cm was used throughout the investigation. The UV-visible spectra of RBD in different microemulsions were recorded, where the concentration of dye in [C₄mim][MeSO₄] and [C₂mim][EtSO₄] based microemulsions were 8.93×10^{-5} M and 1.25×10^{-4} M respectively.

3.3. Results and Discussion

3.3.1. Variation of Physicochemical Properties of TX-100 Microemulsions using ILs as the Polar or Nonpolar Phase with Variation of Anions of ILs

Different physicochemical properties such as conductivity, viscosity, density, refractive index, polarity, and surface tension of the microemulsions were measured for IL based microemulsions. Droplet sizes were measured by DLS method. The effects of the variations of R or W_0 and anions of ILs on the physicochemical properties of microemulsions were investigated. Different types of combinations for ILs, such as [MeSO₄]⁻, [EtSO₄]⁻ and [BF₄]⁻ anions with [C₂mim]⁺ cation and [MeSO₄]⁻ and [BF₄]⁻ anions with [C₄mim]⁺ cation were used to observe the effect of ion structures on the physicochemical properties when IL was the polar phase. To observe the effect on physicochemical properties with the variation of the anions of ILs,

anions $[\text{TFSI}]^-$ and $[\text{PF}_6]^-$ were used with $[\text{C}_2\text{mim}]^+$ cation when IL was the nonpolar phase.

3.3.1.1. Conductivity

3.3.1.1.1. Influence of R or W_0

Figure 3.3.1 shows the change of conductivity of different series of TX-100 microemulsions with increasing R or W_0 at 25 °C while the anion of the ILs were also varied (Appendices Tables A1-3.). From Figure 3.3.1 (a, b) where ILs are used as the polar phase, it can be seen that the conductivity of the microemulsions increases with increasing R for all the systems and from Figure 3.3.1. (c), where ILs are used as the nonpolar phase, it is seen that for TX-100/ $[\text{C}_2\text{mim}][\text{TFSI}]/\text{water}$ system the conductivity initially increases and after reaching a maximum value, decreases with increasing W_0 , while for TX-100/ $[\text{C}_2\text{mim}][\text{PF}_6]/\text{water}$ system conductivity monotonically decreases with increasing W_0 .

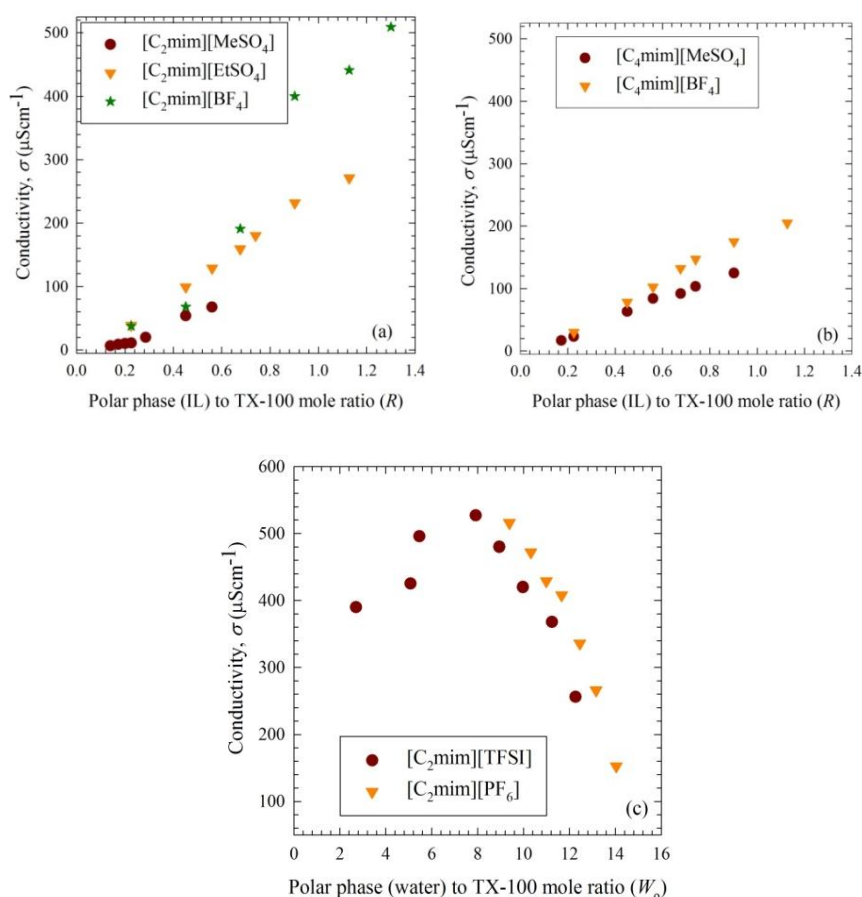


Figure 3.3.1. Variation of conductivity of (a) TX-100/cyclohexane/ $[\text{C}_2\text{mim}][\text{MeSO}_4]$, TX-100/cyclohexane/ $[\text{C}_2\text{mim}][\text{EtSO}_4]$ and TX-100/cyclohexane/ $[\text{C}_2\text{mim}][\text{BF}_4]$, (b) TX-100/cyclohexane/ $[\text{C}_4\text{mim}][\text{MeSO}_4]$ and TX-100/cyclohexane/ $[\text{C}_4\text{mim}][\text{BF}_4]$, (c) TX-100/ $[\text{C}_2\text{mim}][\text{TFSI}]/\text{water}$ and TX-100/ $[\text{C}_2\text{mim}][\text{PF}_6]/\text{water}$ microemulsions as a function of R or W_0 at 25 °C.

For TX-100/cyclohexane/[C₂mim][EtSO₄] and TX-100/cyclohexane/[C₂mim][BF₄] microemulsions (Figure 3.3.1 (a)), with increasing R the structure of the microemulsions systems is likely to change from IL/o to o/IL microemulsions via bicontinuous microemulsions. When R is low, nonpolar cyclohexane is the continuous medium of the reverse micelle dominated microemulsions (IL/o) and thus the conductivity is low. With increasing R , sticky droplets experience collision with one another and clustering of microemulsion droplets due to the hydrophobic interactions of the tail parts of surfactants [32-36]. By fusion, mass exchange and fission, the charge particles (cations and anions of IL) can easily move through the small channels, leading to increased conductivity. With further increase of R , formation of bicontinuous complex microemulsions start to take place. Since ions of IL can move easily through the channels of bicontinuous structures, conductivity of the microemulsions increases. When the system changes from reverse micelle dominated microemulsions (IL/o) to micelle dominated microemulsions (o/IL) with R increasing to even higher values, IL now exists in the bulk and cyclohexane molecules are encapsulated in the core of micelles. In the bulk, movement of the ions of IL is much easier compared to that inside the core of reverse micelles which causes the highest conductivity at high R regions. For TX-100/cyclohexane/[C₂mim][MeSO₄] system may be only IL/o microemulsions are formed. At very low IL content, reverse micelle is the dominant species and IL resides in the core of reverse micelle of [C₂mim][MeSO₄] based microemulsions (Figure 3.3.1. (a)).

For TX-100/cyclohexane/[C₄mim][MeSO₄] and TX-100/cyclohexane/[C₄mim][BF₄] microemulsions (Figure 3.3.1. (b)), the increase in conductivity with increasing R may be attributed to the same phenomenon associated with structure of microemulsions changing from IL/o to o/IL microemulsions via bicontinuous microemulsions.

For TX-100/[C₂mim][TFSI]/water microemulsions where ILs serve as the nonpolar phase, with increasing W_o the system changes from w/IL to IL/w microemulsions via bicontinuous microemulsions. At low W_o , due to the non-polar aggregation of the IL continuous medium in the reverse micelle dominated microemulsions (w/IL), the conductivity is low (Figure 3.3.1(c)) [33, 35, 36]. With increasing W_o , the increasing amount of water dissociates the aggregated IL more and more in the bulk, thus facilitating the movement of ions of IL and hence, conductivity. With increasing W_o , the size of the water pool also increases at the same time. After a certain value of W_o , clustering of water droplets in microemulsions occur and the ions of IL can now easily move through the small channels of the bicontinuous structure. Conductivity shows the highest value at this point due to the formation of bicontinuous complex microemulsions which allows the most favorable condition for the movement of IL ions. As the system changes from reverse micelle dominated to micelle dominated microemulsions (IL/w) with further increase in W_o , water starts to accumulate in the bulk and IL now becomes encapsulated in the core of micelles. Inside the core, movement of ions of IL is restricted and conductivity thus continually decreases with increasing W_o . For TX-100/cyclohexane/[C₂mim][PF₆] system, homogeneous

microemulsions could be prepared only when W_o values are greater than 8 (discussed in Chapter 2). Conductivity of such microemulsions consistently decrease with increasing W_o , possibly due to the same reason as discussed above. The persistent decrease in conductivity above a certain value of W_o , which is almost the same as for the TX-100/[C₂mim][TFSI]/water microemulsion system, indicates that the microemulsions might have a micelle dominated system here above this W_o due to the high water content. Consistent with the observation for TX-100/[C₂mim][TFSI]/water microemulsion, with decreasing R , number of free ions of IL decreases and conductivity decreases in parallel.

3.3.1.1.2. The Influence of IL Anion

The structures of the cations and anions of [C₂mim][EtSO₄], [C₂mim][BF₄], [C₂mim][MeSO₄], [C₄mim][BF₄], [C₄mim][MeSO₄], [C₂mim][PF₆] and [C₂mim][TFSI] ILs are shown in Scheme 1.14 in Chapter 1. In the next two sections, the effect of the structures of the cations and anions of ILs on their different physicochemical parameters will be discussed based on Figure 3.3.1.

3.3.1.1.2.1. The Influence of IL Anion in TX-100/Cyclohexane/[C₂mim][MeSO₄], TX-100/Cyclohexane/[C₂mim][EtSO₄] and TX-100/Cyclohexane/[C₂mim][BF₄] Microemulsions

Figure 3.3.1 (a) shows different series of IL (polar phase) based microemulsions with identical [C₂mim]⁺ cation, but different anions, namely [EtSO₄]⁻, [MeSO₄]⁻ and [BF₄]⁻. Conductivity of IL based microemulsions with [C₂mim]⁺ cation follows the trend as [C₂mim][BF₄] > [C₂mim][EtSO₄] > [C₂mim][MeSO₄] based microemulsions.

Relatively low anionic donacity exists in [BF₄]⁻. The negative charge of the anion is equally distributed on the small, spherical inorganic [BF₄]⁻ ion. Due to this highly symmetric distribution of negative charge on fluorine atoms, specific interacting sites of [BF₄]⁻ is relatively low. The electrostatic attraction of [BF₄]⁻ anion towards imidazolium cation is thus not so high, as the negative charge is highly centered on [BF₄]⁻ [37]. This causes easier dissociation of the ions from the IL and thereby, increased conductivity. The smaller size of [BF₄]⁻ anion than [EtSO₄]⁻ and [MeSO₄]⁻ anions might also be responsible for the high conductivity of these microemulsions than the other two. Between the [C₂mim][EtSO₄] and [C₂mim][MeSO₄] based microemulsions, the interaction between the cation and anion in [C₂mim][EtSO₄] is comparatively lower due to the longer hydrophobic carbon chain in [EtSO₄]⁻ than in [MeSO₄]⁻ in [C₂mim][MeSO₄]. The unit negative charge is less homogeneously distributed around [EtSO₄]⁻ anion due to its more asymmetric nature which results in less electrostatic attraction in [C₂mim][EtSO₄] compared to [C₂mim][MeSO₄]. On the other hand, in [MeSO₄]⁻ the negative charge density is higher due to the less asymmetric structure. So, the negative charge is more centered around [MeSO₄]⁻, resulting in stronger electrostatic attraction and strong packing between [C₂mim]⁺ and [MeSO₄]⁻ ions.

When IL is incorporated in TX-100 reverse micelle core, anions of ILs are attracted to the head group of TX-100 (Scheme 3.1) and can interact with hydrogen of head group terminal hydroxide of TX-100. As number of specific interacting sites of inorganic $[\text{BF}_4]^-$ are low due to the highly symmetric distribution of negative charge on fluorine atoms, $[\text{BF}_4]^-$ from $[\text{C}_2\text{mim}][\text{BF}_4]$ can move faster than the organic $[\text{EtSO}_4]^-$ and $[\text{MeSO}_4]^-$ ions from $[\text{C}_2\text{mim}][\text{EtSO}_4]$ and $[\text{C}_2\text{mim}][\text{MeSO}_4]$ to the inner interface of TX-100 to form hydrogen bonds among fluorine atoms of $[\text{BF}_4]^-$ and hydrogen atoms of terminal -OH group in TX-100 head group. Cations stay close to the anions. Therefore, high mobility of $[\text{BF}_4]^-$ anion is thus the main factor for the high conductivity of reverse micelle dominated TX-100/Cyclohexane/ $[\text{C}_2\text{mim}][\text{BF}_4]$ microemulsions. Organic $[\text{EtSO}_4]^-$ ions from $[\text{C}_2\text{mim}][\text{EtSO}_4]$ can move faster than organic $[\text{MeSO}_4]^-$ from $[\text{C}_2\text{mim}][\text{MeSO}_4]$ to the inner interface of TX-100 to form hydrogen bonds between oxygen atoms of $[\text{EtSO}_4]^-$ and hydrogen atoms of terminal OH group of TX-100 head group. Weaker electrostatic attraction exists in $[\text{C}_2\text{mim}][\text{EtSO}_4]$ than in $[\text{C}_2\text{mim}][\text{MeSO}_4]$ due to longer hydrophobic carbon chain of $[\text{EtSO}_4]^-$. Mobility of $[\text{EtSO}_4]^-$ therefore is the principal reason for the higher conductivity of TX-100/Cyclohexane/ $[\text{C}_2\text{mim}][\text{EtSO}_4]$ than TX-100/Cyclohexane/ $[\text{C}_2\text{mim}][\text{MeSO}_4]$ microemulsions in the reverse micelle dominated systems

With increasing R , as the bicontinuous microemulsions start to form, due to the formation of three dimensional channels conductivity further increases due to the increased mobility of both the cations and anions of IL in all the three microemulsion systems.

With further increasing R , the mobility of cations becomes the main factor for determining conductivity in the micelle dominated TX-100/cyclohexane/ $[\text{C}_2\text{mim}][\text{EtSO}_4]$ microemulsions. The nonpolar part of $[\text{EtSO}_4]^-$ experiences hydrophobic attraction to the tail part of TX-100 inside micelle core (Scheme 3.1 (b)). Thus, exposure of $[\text{EtSO}_4]^-$ in the bulk becomes increasingly difficult. Mobility of both the cations and anions may thus be the required factors for increasing conductivity in micelle dominated TX-100/cyclohexane/ $[\text{C}_2\text{mim}][\text{BF}_4]$ microemulsions (Scheme 3.1 (c)).

3.3.1.1.2.2. The Influence of IL Anion in TX-100/Cyclohexane/ $[\text{C}_4\text{mim}][\text{MeSO}_4]$ and TX-100/Cyclohexane/ $[\text{C}_4\text{mim}][\text{BF}_4]$ Microemulsions

Figure 3.3.1 (b) shows different series of IL based microemulsions containing the same cation, $[\text{C}_4\text{mim}]^+$, but different anions, $[\text{MeSO}_4]^-$ and $[\text{BF}_4]^-$. TX-100/cyclohexane/ $[\text{C}_4\text{mim}][\text{BF}_4]$ microemulsions show higher conductivity than TX-100/cyclohexane/ $[\text{C}_4\text{mim}][\text{MeSO}_4]$ microemulsions.

Due to the reduced specific interacting sites and consequent weaker electrostatic attraction between the ions in $[\text{BF}_4]^-$, this anion can easily dissociate from and associate with $[\text{C}_4\text{mim}]^+$ cation, while for the small hydrophobic carbon chain in $[\text{MeSO}_4]^-$ strong electrostatic interaction exists between $[\text{C}_4\text{mim}]^+$ and $[\text{MeSO}_4]^-$.

As $[\text{BF}_4]^-$ dissociates easily from $[\text{C}_4\text{mim}]^+$, when $[\text{C}_4\text{mim}][\text{BF}_4]$ is inside the TX-100 reverse micelle core, $[\text{BF}_4]^-$ ions move to the head groups of TX-100 rapidly. On the other hand, due to the strong electrostatic attraction between $[\text{C}_4\text{mim}]^+$ and $[\text{MeSO}_4]^-$, organic $[\text{MeSO}_4]^-$ from $[\text{C}_4\text{mim}][\text{MeSO}_4]$ dissociate and move slowly to the inner interface of TX-100 reverse micelles.

With increasing R , due to the formation of three dimensional channels, conductivity further increases which is attributed to the mobility of both the cations and anions of IL in the two systems.

With further increase of R , the mobility of cations becomes the dominating factor for deciding conductivity in micelle dominated compositions of TX-100/cyclohexane/ $[\text{C}_4\text{mim}][\text{MeSO}_4]$ microemulsions. The nonpolar part of $[\text{MeSO}_4]^-$ forms hydrophobic interaction with the tail part of TX-100 in micelle core making it difficult for $[\text{MeSO}_4]^-$ ions to get exposed in the bulk. Mobility of both the cations and anions may thus be the deciding factor for conductivity in micelle dominated TX-100/ cyclohexane/ $[\text{C}_2\text{mim}][\text{BF}_4]$ / microemulsions.

3.3.1.2.2.3. The Influence of IL Anion in TX-100/ $[\text{C}_2\text{mim}][\text{TFSI}]$ /Water and TX-100/ $[\text{C}_2\text{mim}][\text{PF}_6]$ /Water Microemulsions

Figure 3.3.1 (c) shows different series of IL based microemulsions (IL working as the nonpolar phase) with a fixed cation $[\text{C}_2\text{mim}]^+$, but different anions $[\text{TFSI}]^-$ and $[\text{PF}_6]^-$.

Relatively low anionic donacity exists in the $[\text{PF}_6]^-$ anion. The negative charge of the anion is equally distributed on the fluorine atoms of spherical inorganic anion $[\text{PF}_6]^-$. Due to this highly symmetric distribution of negative charge on the fluorine atoms, number of specific interacting sites of $[\text{PF}_6]^-$ are small. $[\text{PF}_6]^-$ can therefore easily dissociate from and associate with $[\text{C}_2\text{mim}]^+$. On the contrary, in $[\text{C}_2\text{mim}][\text{TFSI}]$, the hydrogen atom bonded with the C_2 atom in $[\text{TFSI}]$ has the highest electron density and thereby maintains close contact with the $-\text{N}$ or $-\text{SO}_2$ group of $[\text{TFSI}]$ [37], making the dissociation of the IL difficult.

The number of free $[\text{C}_2\text{mim}]^+$ and $[\text{TFSI}]^-$ ions in the bulk increases with increasing W_o in TX-100/ $[\text{C}_2\text{mim}][\text{TFSI}]$ /water reverse micelle dominated microemulsions. Mobility of both cation and anion is the main factor here for the increase in conductivity in reverse micelle dominated microemulsions.

At $W_o \approx 8.0$ and 9.0 , due to the formation of three dimensional channels in the bicontinuous structures, conductivity shows the highest values for $[\text{C}_2\text{mim}][\text{TFSI}]$ and $[\text{C}_2\text{mim}][\text{PF}_6]$ based microemulsions respectively. Mobility of cation and anion may thus be considered as the main factor for highest conductivity in bicontinuous microemulsions.

Further increase in W_o induces encapsulation of IL in the micelle core. As $[\text{PF}_6]^-$ can dissociate easily from $[\text{C}_2\text{mim}]^+$, when $[\text{C}_2\text{mim}][\text{PF}_6]$ is trapped in reverse micelle core of TX-100, $[\text{PF}_6]^-$ ions are rapidly attracted to the head group of TX-100,

compared to [TFSI]⁻. In the micelle dominated region, the conductivity values are slightly higher for TX-100/[C₂mim][PF₆]/water system compared to TX-100/[C₂mim][TFSI]/water system. With increasing W_0 i.e. decreasing R , number of free ions decreases and thus conductivity decreases.

3.3.1.2. Viscosity

3.3.1.2.1. The Influence of R or W_0

Figure 3.3.2 shows the variation of viscosity of different series of TX-100 microemulsions with increasing R or W_0 at 25 °C (Appendices Tables A4-6.). From Figure 3.3.2 (a, b) (IL as the polar phase), it can be seen that the viscosity of the microemulsions increase with increasing R for all the systems; whereas from Figure 3.3.2 (c) (IL as the nonpolar phase), viscosity of the TX-100/[C₂mim][TFSI]/water system initially decreases and after reaching a minimum value, again increases with increasing W_0 in a similar fashion as for TX-100/[C₂mim][PF₆]/water system.

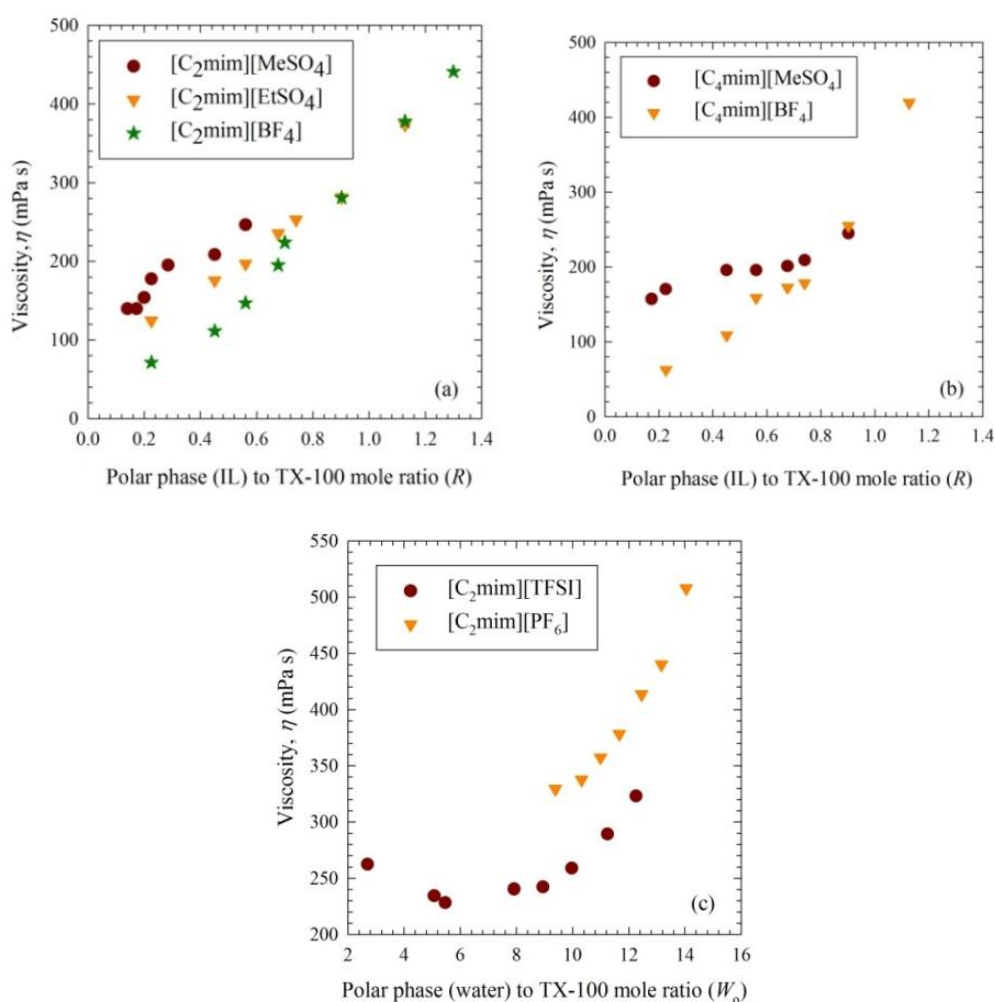


Figure 3.3.2. Variation of viscosity of (a) TX-100/cyclohexane/[C₂mim][MeSO₄], TX-100/cyclohexane/[C₂mim][EtSO₄] and TX-100/cyclohexane/[C₂mim][BF₄], (b) TX-100/cyclohexane/[C₄mim][MeSO₄] and TX-100/cyclohexane/[C₄mim][BF₄], (c) TX-100/[C₂mim][TFSI]/water and TX-100/[C₂mim][PF₆]/water microemulsions as a function of R or W_0 at 25 °C.

At low R for IL/o microemulsions, viscosity property mainly depends on the continuous medium which is the nonpolar cyclohexane (. Viscosity increases monotonically with increasing R due to the addition of more viscous IL and simultaneously decreasing cyclohexane (Figure 3.3.2 (a, b)). Increasing R increases the size of reverse micelle droplets. As R is further increased, for TX-100/cyclohexane/[C₂mim][EtSO₄], TX-100/cyclohexane/[C₂mim][BF₄], TX-100/cyclohexane/[C₄mim][MeSO₄], and TX-100/cyclohexane/[C₄mim][BF₄] microemulsions, viscosity increases due to the formation of channels among TX-100 droplet clusters in three dimensions at a given temperature. When the above systems change from reverse micelle dominated to micelle dominated microemulsions (o/IL) at even higher values of R , the viscous IL starts to accumulate in the bulk and cyclohexane is now encapsulated in the core of micelles causing viscosity to be increased furthermore.

For TX-100/[C₂mim][TFSI]/water microemulsions, with increasing W_o , the system undergoes change from w/IL to IL/w microemulsions via bicontinuous microemulsions (Figure 3.3.2 (c)). At low W_o , due to the aggregated IL clusters in the continuous media of reverse micelle dominated microemulsions (w/IL), the viscosity is high. As W_o is increased, water dissociates the aggregated IL clusters present in the bulk, thus liberating free ions from IL, increasing movement of ions of IL and consequently, decreasing viscosity. At the same time, clustering of water droplets in microemulsions occur and the ions of IL can easily move through the small channels. At this point, viscosity shows the lowest value due to the formation of bicontinuous complex microemulsions with increasing W_o . As the system changes to micelle dominated microemulsions (IL/w) from reverse micelle dominated ones (w/IL) with increasing W_o , water exists in the bulk and ILs are gradually entrapped in the core of micelles. In the micelle core, movement of ions of IL decreases. Further increasing W_o i.e. increasing water in the bulk results in increasing H-bonds among water molecules, causing viscosity to increase furthermore. For TX-100/cyclohexane/[C₂mim][PF₆] system, with increasing W_o i.e. decreasing R , number of free ions of IL decreases and thus, viscosity increases.

3.3.1.2.2. The Influence of IL Anion

3.3.1.2.2.1. The Influence of IL Anion in TX-100/Cyclohexane/[C₂mim][MeSO₄], TX-100/Cyclohexane/[C₂mim][EtSO₄] and TX-100/Cyclohexane/[C₂mim][BF₄] Microemulsions

ILs with fixed [C₂mim]⁺ cation and different anions [EtSO₄]⁻, [MeSO₄]⁻ and [BF₄]⁻ were used for preparing different series of IL based microemulsions (Figure 3.3.2 (a)). As seen in Figure 3.3.2 (a), viscosity of IL based microemulsions with [C₂mim]⁺ cation follows the increasing order [C₂mim][BF₄] < [C₂mim][EtSO₄] < [C₂mim][MeSO₄] which shows just the opposite trend of conductivity. These two trends can be correlated by visualizing that, increasing conductivity indicates one layer of a microemulsion system can flow easily with the other layers resulting in a lower viscosity. As TX-100/cyclohexane/[C₂mim][MeSO₄] system shows the lowest

conductivity due to the encapsulated ions in reverse micelle droplets, the viscosity of this system exhibits the highest values for IL/o microemulsions. Same situation occurs for TX-100/cyclohexane/[C₂mim][EtSO₄] and TX-100/cyclohexane/[C₂mim][BF₄] systems. With increasing *R*, these systems change from IL/o to o/IL microemulsions via bicontinuous microemulsions. In bicontinuous microemulsions three dimensional channeling and clustering among the droplets occur which results in increasing viscosity. In o/IL microemulsions more viscous IL exists in bulk leading to the highest attained viscosity.

3.3.1.2.2.2. The Influence of IL Anion in TX-100/Cyclohexane/[C₄mim][MeSO₄] and TX-100/Cyclohexane/[C₄mim][BF₄] Microemulsions

ILs with [C₄mim]⁺ cation with different anions [MeSO₄]⁻ and [BF₄]⁻ were used for different series of IL based microemulsions (Figure 3.3.2 (b)). TX-100/cyclohexane/[C₄mim][BF₄] microemulsions show the lower viscosity values than TX-100/cyclohexane/[C₄mim][MeSO₄] microemulsions which shows the opposite results of conductivity.

3.3.1.2.2.3. The Influence of IL Anion in TX-100/[C₂mim][TFSI]/Water and TX-100/[C₂mim][PF₆]/Water Microemulsions

ILs containing a fixed cation, [C₂mim]⁺ and different anions [TFSI]⁻ and [PF₆]⁻ were used for verifying the effect of IL anions on the viscosity of different series of IL based microemulsions (Figure 3.3.2. (c)). Of the two, TX-100/[C₂mim][TFSI]/water microemulsions show the lower and TX-100/[C₂mim][PF₆]/water microemulsions show the higher viscosity values. Spherical anions like [PF₆]⁻ can easily dissociate and associate with the cations. With increasing *W*_o, the mobility of ions of IL increases sharply for w/IL microemulsions due to the dissociation of IL clusters in the bulk induced by water. But at the same time, channel formation occurs rapidly and viscosity increases due to this complex three dimensional network of channel. That is why, TX-100/[C₂mim][PF₆]/water microemulsions show the highest viscosity and conductivity values.

3.3.1.2.3. Effect of Temperature on Viscosity

Figure 3.3.3 (a, b) shows the effect of temperature on viscosity of different series of TX-100 microemulsions at *R* = 0.2255 (Appendices Tables A7-8.). From Figure 3.3.3 (a, b), it can be seen that the viscosity of the microemulsions decrease with increasing temperature for *R* = 0.2255.

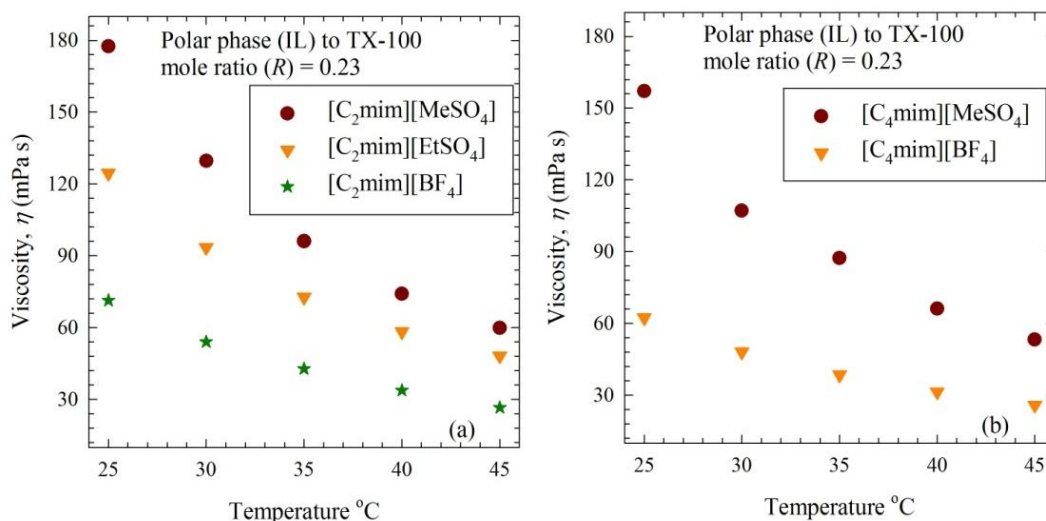


Figure 3.3.3. Effect of temperature on the viscosity of (a) TX-100/cyclohexane/[C₂mim][MeSO₄], TX-100/cyclohexane/[C₂mim][EtSO₄] and TX-100/cyclohexane/[C₂mim][BF₄], (b) TX-100/cyclohexane/[C₄mim][MeSO₄] and TX-100/cyclohexane/[C₄mim][BF₄] microemulsions at $R = 0.2255$.

With increasing temperature, attractive interactions among the droplets is reduced and mobility of different layers in microemulsion due to enhanced kinetic energy increases which causes the viscosity to decrease.

3.3.1.3. Size and Size Distribution of Droplets

The size of the reverse micelle droplets increase with increasing R as hydrophilic ILs can encapsulate in the core of reverse micelle droplets to a certain level [38-44]. The curvature parameter of surfactant depends on the IL concentration, anion structure and alkyl side-chain length of cation of IL [45]. The sizes of micelle droplets increase with decreasing W_o . In this case the hydrophobic ILs can be encapsulated in the core of micelle droplets to a certain level.

3.3.1.3.1. Influence of IL Anion

3.3.1.3.1.1. The Influence of IL Anion in (a) TX-100/Cyclohexane/[C₂mim][MeSO₄], (b) TX-100/Cyclohexane/[C₂mim][EtSO₄] and (c) TX-100/Cyclohexane/[C₂mim][BF₄] Microemulsions

Figure 3.3.4 shows the variation in size and size distributions of the reverse micelle droplets in three different microemulsion systems with increasing R at 25 °C where the ILs are (a) [C₂mim][MeSO₄], (b) [C₂mim][EtSO₄] and (c) [C₂mim][BF₄] (Appendices Table A9)

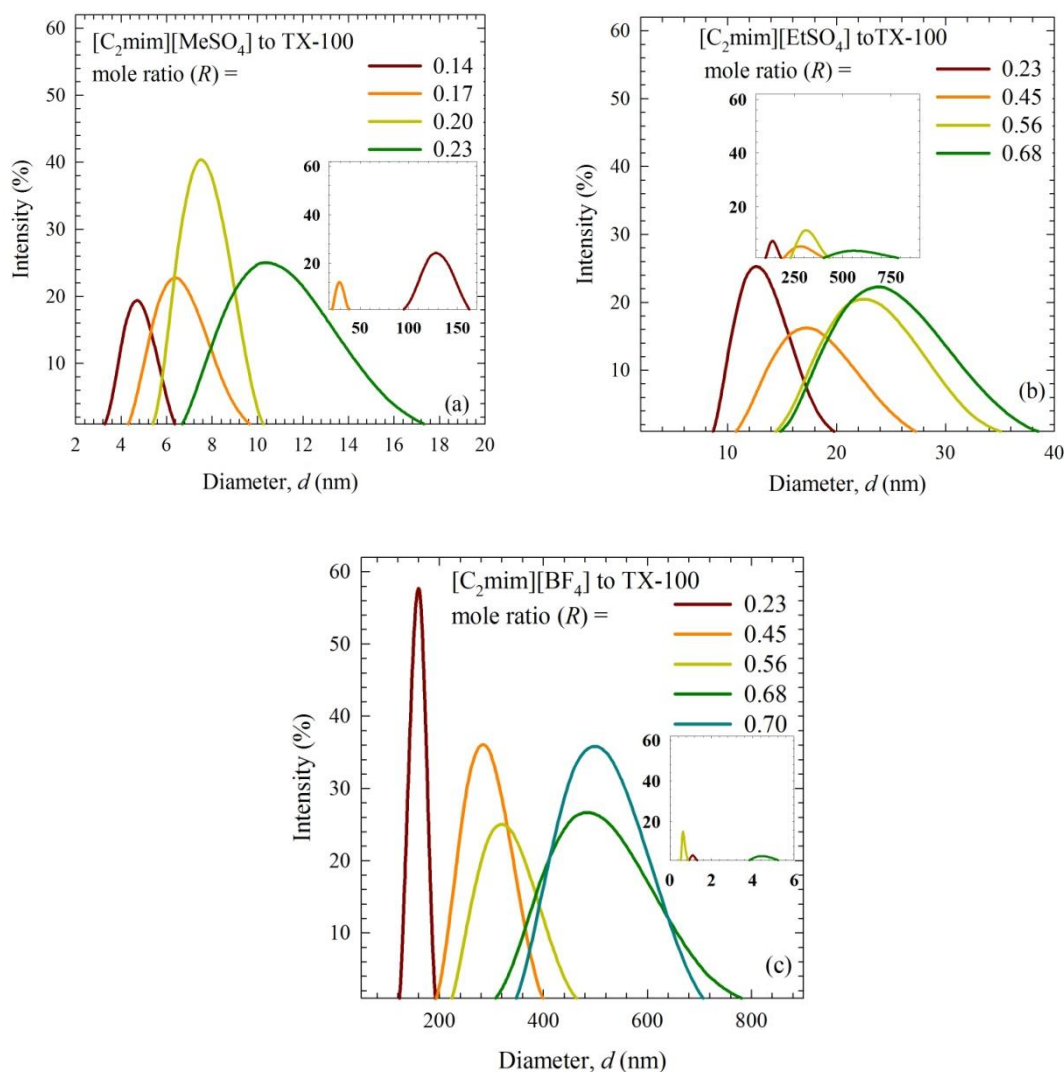


Figure 3.3.4. Size and size distribution of droplets in (a) TX-100/cyclohexane/[C₂mim][MeSO₄], (b) TX-100/cyclohexane/[C₂mim][EtSO₄] and (c) TX-100/cyclohexane/[C₂mim][BF₄] microemulsions at different R at 25 °C.

Sizes of the reverse micelle droplets increase approximately from 5 nm to 11 nm with increasing R values from 0.1400 to 0.2255 for [C₂mim][MeSO₄] based microemulsions; where sizes of the IL clusters are obtained for $R = 0.1400$ and 0.1728 to be approximately 130 and 29 nm respectively (Appendices Table A9.). For [C₂mim][EtSO₄] based microemulsions, sizes of the reverse micelle droplets increase approximately from 13 nm to 24 nm with increasing R from 0.2255 to 0.6765, while size of clusters are obtained for $R = 0.2255$ to 0.6765 to give the values at approximately 142, 295, 308 and 555 nm (Appendices Table A9.). Sizes of the reverse micelle droplets increase approximately from 164 nm to 503 nm with increasing values of R from 0.2255 to 0.7000 for [C₂mim][BF₄] based microemulsions. Small droplets are additionally obtained for $R = 0.2255$, 0.5600 and 0.6765 and the droplets are of approximately 1, 0.62 and 4 nm respectively (Appendices Table A9.). At higher R values for all the systems, size of the droplets

cannot be measured accurately because complex three-dimensional structure formation occurs.

With increasing R i.e. with the addition of IL in all the three systems, ILs become more and more encapsulated into the core of reverse micelle droplets and thus the sizes of droplets increase. The width of the size distribution curves also increases with increasing R . Although the droplets are considered to be spherical for DLS measurements, with increasing IL content the droplets actually aggregate to form large clusters. Therefore, the laser beam generally detects both spherical droplets and the clusters which may give hexagonal, cylindrical, rod shape, ellipsoidal, cone-shaped and other patterns as well. Because of these different structures of the large aggregated clusters, the hydrodynamic diameters show some additional larger values. For [C₂mim][BF₄] based microemulsions, small droplets ranges from 0.62 to 4 nm since ILs or surfactants may aggregate in the system.

The droplet sizes of the reverse micelles in IL based microemulsions follow the decreasing trend [C₂mim][BF₄] > [C₂mim][EtSO₄] > [C₂mim][MeSO₄] based microemulsions. At $R = 0.2255$, the average size of the reverse micelle droplets for [C₂mim][MeSO₄] based microemulsion shows the smallest and for [C₂mim][BF₄] based microemulsion shows the largest value. At $R = 0.2255, 0.4510, 0.5600$ and 0.6765 , [C₂mim][BF₄] based microemulsion system shows larger particle size values compared to [C₂mim][EtSO₄] based microemulsion system.

When ILs are encapsulated in the cores of reverse micelle droplets, different types of interactions exist between TX-100 and the cations and anions of ILs. Hydrogen bonding exists between the hydrogen atoms adjacent to the C₂ atoms of [C₂mim]⁺ ions and the lone pairs of oxygen atoms of the ethylene oxide groups in TX-100, between anions of ILs and hydrogen atoms of TX-100 hydroxyl terminals, in addition, dipole-induced dipole type of interaction exists between TX-100 phenyl π electron cloud and [C₂mim]⁺ ions.

As the cations and anions of [C₂mim][BF₄] can easily dissociate due to the spherical shape of [BF₄]⁻ anion, ions from this IL can easily move to the inner interface of TX-100 reverse micelles and also can exist between surfactants. So the sizes of reverse micelle droplets for [C₂mim][BF₄] based microemulsion system shows the largest values (Appendices Table A9.). On the other hand, strong electrostatic interaction exists between the ions of [C₂mim][MeSO₄]. So dissociation of ILs into cations and anions is not likely to occur unlike [C₂mim][BF₄]. The droplets sizes for [C₂mim][MeSO₄] based microemulsion system thus show the lowest values. For [C₂mim][EtSO₄] based microemulsion system cations and anions of ILs are comparatively loosely bound due to the longer nonpolar ethyl chain present in [EtSO₄]⁻. So the droplets sizes for [C₂mim][EtSO₄] based microemulsionsystem shows higher values than those for [C₂mim][MeSO₄] based microemulsion system albeit lower values than [C₂mim][BF₄] based microemulsion system.

3.3.1.3.1.2. The Influence of IL Anion in TX-100/Cyclohexane/[C₄mim][MeSO₄] and TX-100/Cyclohexane/[C₄mim][BF₄] Microemulsions

Figure 3.3.5 shows the variation of size and size distributions of the reverse micelle droplets for two different microemulsion systems with increasing R at 25 °C where the ILs are (d) [C₄mim][MeSO₄] and (e) [C₄mim][BF₄] (Appendices Table A9)

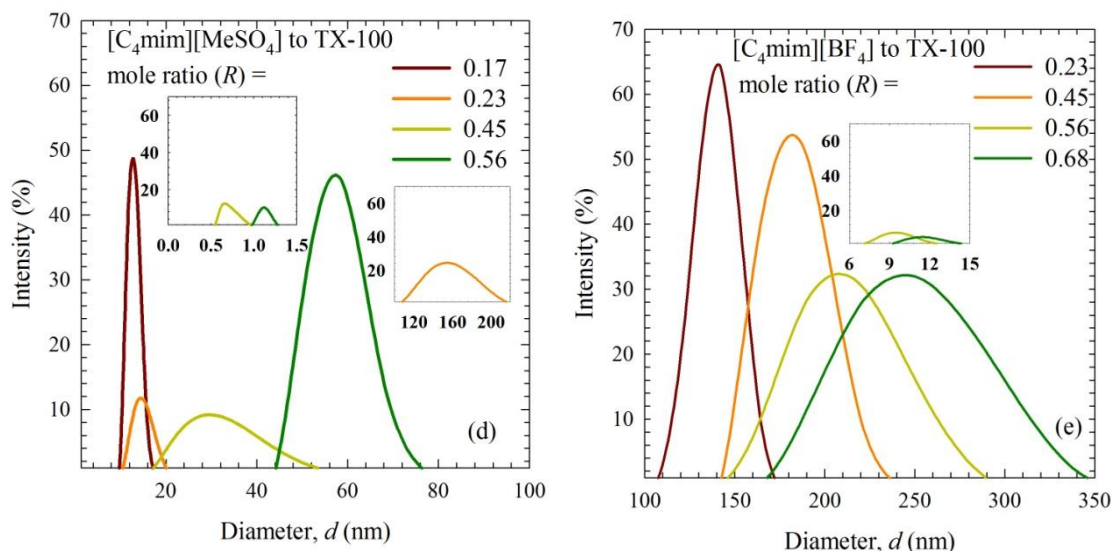


Figure 3.3.5. Size and size distribution of droplets in (d) TX-100/cyclohexane/[C₄mim][MeSO₄] and (e) TX-100/cyclohexane/[C₄mim][BF₄] microemulsions at different R at 25 °C.

Size of the reverse micelle droplets increases from approximately 13 nm to 58 nm with increasing R from 0.1728 to 0.5600 for [C₄mim][MeSO₄] based microemulsions. The size of the cluster is obtained for $R = 0.2255$, which is approximately 155 nm. Additional small droplets are obtained for $R = 0.4510$ and 0.5600 with sizes approximately 0.7 and 1 nm respectively (Appendices Table A9.).

For [C₄mim][BF₄] based microemulsions, sizes of the droplets increase from 142 nm to 245 nm with increasing R from 0.2255 to 0.6765. Small droplets are also obtained for $R = 0.5600$ and 0.6765 with sizes approximately 10, and 12 nm respectively (Appendices Table A9.).

ILs become gradually encapsulated into the core of droplets with increasing R and thus, the sizes of the droplets increase. With increasing R , an increasing trend in the widths of the peaks are also observed due to the increased inhomogeneity in sizes due to aggregation of droplets. Some ILs or surfactants may aggregate in the microemulsion system resulting in small droplets (0.7 and 1 nm) in [C₄mim][MeSO₄] based microemulsions.

At $R = 0.2255, 0.4510$ and 0.5600 , $[\text{C}_4\text{mim}][\text{BF}_4]$ based microemulsion system shows the larger droplet sizes compared to $[\text{C}_4\text{mim}][\text{MeSO}_4]$ based microemulsion system. At higher R values, size of the droplets cannot be measured for both the microemulsions systems.

As the cations and anions of $[\text{C}_4\text{mim}][\text{BF}_4]$ can easily dissociate due to the spherical shape of $[\text{BF}_4]^-$ and consequent homogeneous charge density over the spherical anion, ions from this IL can easily move inside the inner interface of TX-100 reverse micelle cores and also can exist between the surfactants. So the droplets sizes for $[\text{C}_4\text{mim}][\text{BF}_4]$ based microemulsion system show larger values (Table 3.4). On the other hand, strong electrostatic interaction occurs between the ions of $[\text{C}_4\text{mim}][\text{MeSO}_4]$. So, unlike $[\text{C}_4\text{mim}][\text{BF}_4]$, dissociation of cation and anion does not easily take place. The droplets size for $[\text{C}_4\text{mim}][\text{MeSO}_4]$ based microemulsion system thus shows smaller values.

3.3.1.3.1.3. The Influence of IL Anion in TX-100/ $[\text{C}_2\text{mim}][\text{PF}_6]$ /Water and TX-100/ $[\text{C}_2\text{mim}][\text{TFSI}]$ /Water Microemulsions

Figure 3.3.6 shows the variation of sizes and size distributions of micelle droplets for two different microemulsion systems with decreasing W_o at 25°C , where the ILs are $[\text{C}_2\text{mim}][\text{PF}_6]$ and $[\text{C}_2\text{mim}][\text{TFSI}]$ (Appendices Table A9.)

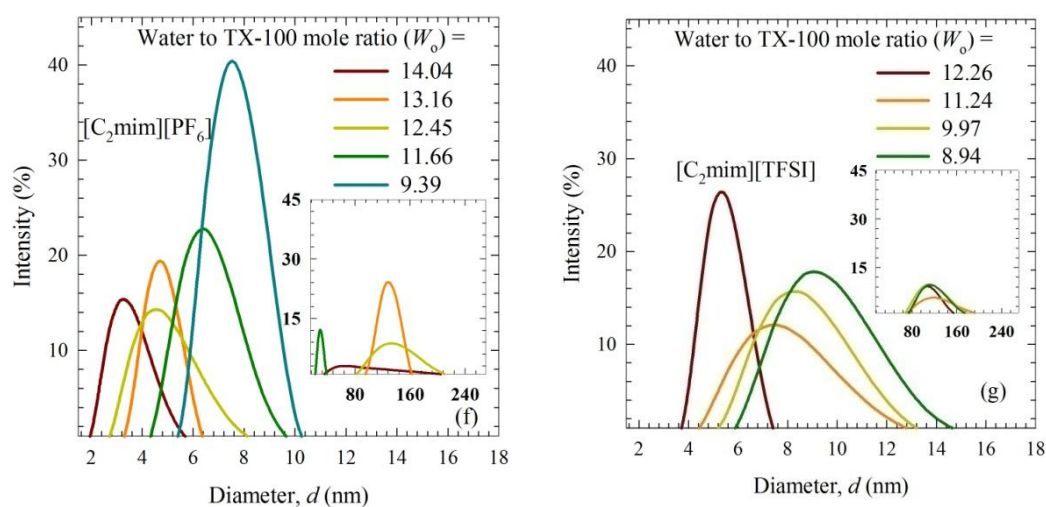


Figure 3.3.6. Size and size distribution of droplets in (f) TX-100/ $[\text{C}_2\text{mim}][\text{PF}_6]$ /water and (g) TX-100/ $[\text{C}_2\text{mim}][\text{TFSI}]$ /water microemulsions at different W_o at 25°C .

Sizes of the micelle droplets increase from approximately 3 nm to 8 nm with decreasing W_o from 14.0421 to 9.3874 for $[\text{C}_2\text{mim}][\text{PF}_6]$ based microemulsions, where for $W_o = 14.0421, 13.1624, 12.4514$ and 11.6622 , the size of clusters are also obtained to be approximately 59, 130, 132 and 29 nm respectively (Appendices Table A9.). For $[\text{C}_2\text{mim}][\text{TFSI}]$ based microemulsions, sizes of the micelle droplets increase approximately from 5 nm to 9 nm with decreasing W_o from 12.2614 to 8.9428, while the sizes of large clusters are also obtained for $W_o = 12.2614, 11.2404, 9.9697$ and

8.9428 and they were approximately 106, 120, 110 and 113 nm respectively (Appendices Table A9.).

With decreasing W_o , sizes of the droplets increase because ILs are gradually encapsulated into the micelle cores and the width of the distribution also increases due to the formation of clusters of variable sizes.

3.3.1.4. Density

3.3.1.4.1. The Influence of R or W_o

Figure 3.3.7 shows the change of density of different series of TX-100 microemulsions, where ILs have been used either as the polar or the nonpolar phase, with increasing R or W_o at 25 °C (Appendices Tables A10-12.). From Figure 3.3.7. (a, b) it can be seen that the density of the microemulsions increase with increasing R for all the systems due to the addition of IL and from Figure 3.3.7. (c) it can be seen that the density of the microemulsions decreases with increasing W_o for all the systems due to the addition of water.

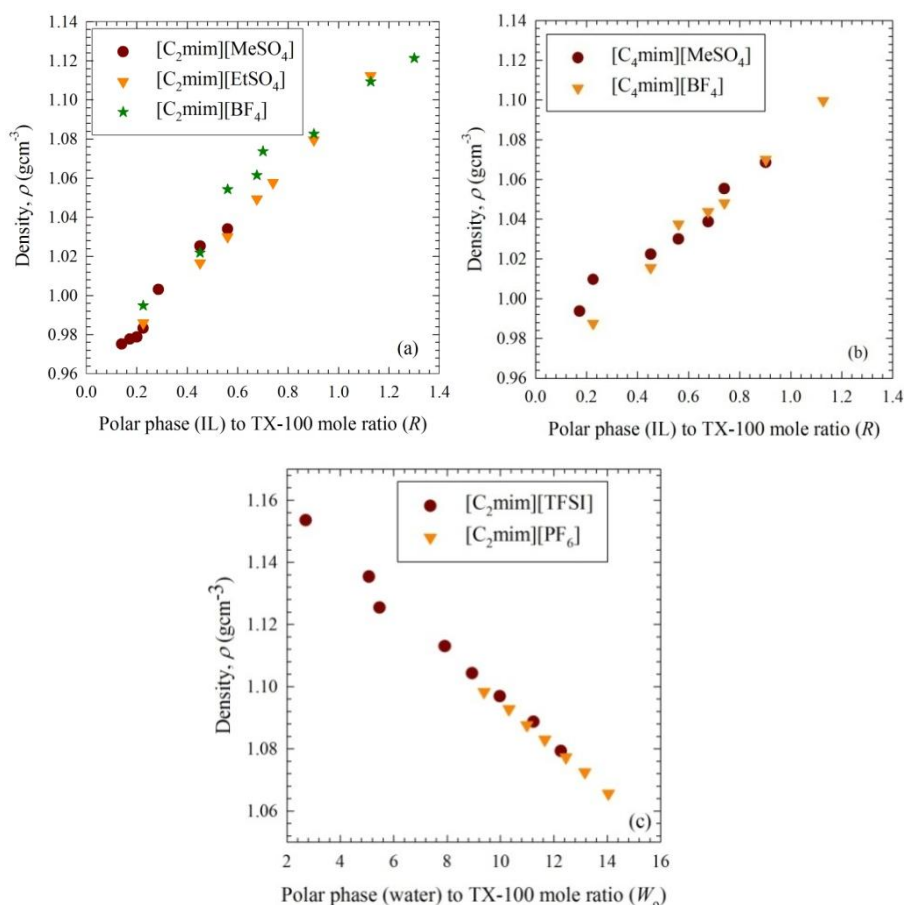


Figure 3.3.7. Density of (a) TX-100/cyclohexane/ $[\text{C}_2\text{mim}][\text{MeSO}_4]$, TX-100/cyclohexane/ $[\text{C}_2\text{mim}][\text{EtSO}_4]$ and TX-100/cyclohexane/ $[\text{C}_2\text{mim}][\text{BF}_4]$, (b) TX-100/cyclohexane/ $[\text{C}_4\text{mim}][\text{MeSO}_4]$ and TX-100/cyclohexane/ $[\text{C}_4\text{mim}][\text{BF}_4]$, (c) TX-100/ $[\text{C}_2\text{mim}][\text{TFSI}]$ /water and TX-100/ $[\text{C}_2\text{mim}][\text{PF}_6]$ /water microemulsions as a function of R or W_o at 25 °C.

For the four microemulsion systems in Figure 3.3.7 (a, b), IL and cyclohexane are the polar and nonpolar phases respectively. When the amount of IL is increased, the amount of cyclohexane is simultaneously decreased to keep the total mass of microemulsion constant. As density of IL is higher compared to cyclohexane, the addition of IL contributes more to the density and dominates the system; resulting in increasing density of the microemulsions as the amount of IL increases. In Figure 3.3.7 (c), the polar phase is water and the nonpolar phase is IL in the microemulsions. Here, as the amount of water is increased, that of IL is decreased and eventually, density of the system is decreased.

3.3.1.4.2. Effect of Temperature on Density

Figure 3.3.8 (a, b) shows the effect of temperature on the density of different series of TX-100 microemulsions using ILs as the polar phase at $R = 0.2255$ (Appendices Tables A13-14). From Figure 3.3.8 (a, b), it can be seen that the densities of the microemulsions decrease with increasing temperature for $R = 0.2255$.

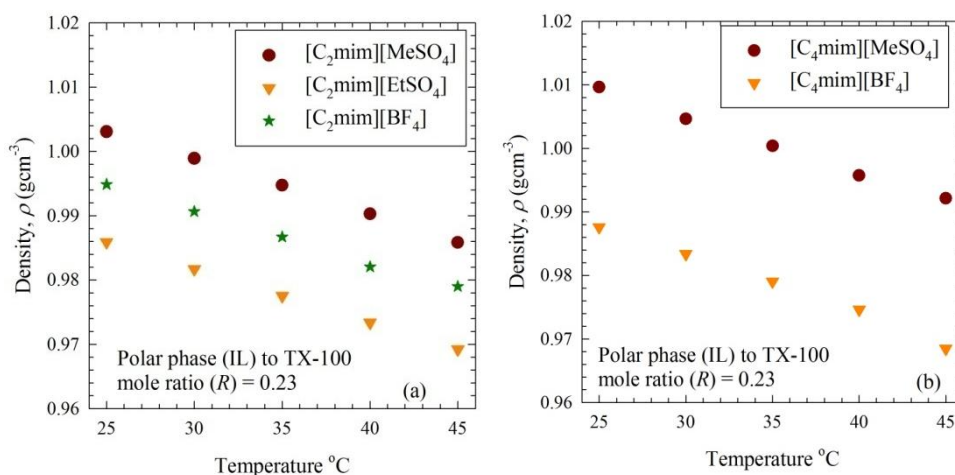


Figure 3.3.8. Effect of temperature on the densities of (a) TX-100/cyclohexane/ $[\text{C}_2\text{mim}][\text{MeSO}_4]$, TX-100/cyclohexane/ $[\text{C}_2\text{mim}][\text{EtSO}_4]$ and TX-100/cyclohexane/ $[\text{C}_2\text{mim}][\text{BF}_4]$, (b) TX-100/cyclohexane/ $[\text{C}_4\text{mim}][\text{MeSO}_4]$ and TX-100/cyclohexane/ $[\text{C}_4\text{mim}][\text{BF}_4]$ microemulsions at $R = 0.2255$.

Volume of the dispersed phase (cyclohexane) of microemulsions increases with increasing temperature, thus the density accordingly decreases.

3.3.1.5. Refractive Index

3.3.1.5.1. The Influence of R or W_0

Figure 3.3.9 shows the change of refractive index of different series of TX-100 microemulsions with increasing R or W_0 at 25°C (Appendices Tables A15-17). It can be seen from Figure 3.3.9 (a, b) that the refractive index follow irregular patterns with increasing R and from Figure 3.3.9 (c), the refractive index of the microemulsions decreases with increasing W_0 for all the microemulsion systems, where ILs serve as the nonpolar phase.

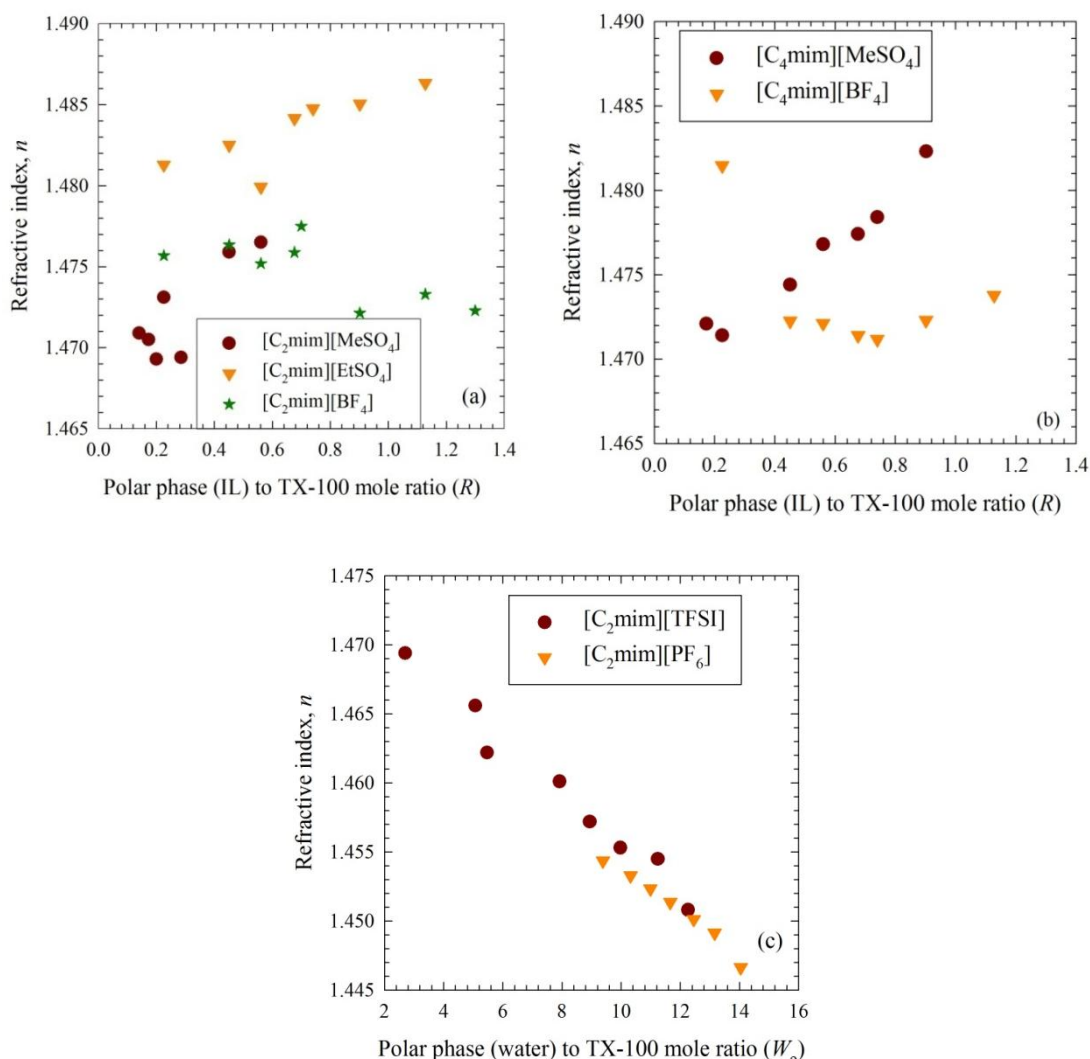


Figure 3.3.9. Refractive index of (a) TX-100/cyclohexane/ $[C_2mim][MeSO_4]$, TX-100/cyclohexane/ $[C_2mim][EtSO_4]$ and TX-100/cyclohexane/ $[C_2mim][BF_4]$, (b) TX-100/cyclohexane/ $[C_4mim][MeSO_4]$ and TX-100/cyclohexane/ $[C_4mim][BF_4]$, (c) TX-100/ $[C_2mim][TFSI]$ /water and TX-100/ $[C_2mim][PF_6]$ /water microemulsions as a function of R or W_o at 25 °C.

For TX-100/cyclohexane/ $[C_2mim][EtSO_4]$ and TX-100/cyclohexane/ $[C_4mim][BF_4]$ microemulsions (Figure 3.3.9 (a), (b)) with increasing R , the system undergoes transition from reverse micelle dominated to micelle dominated via bicontinuous microemulsions. The microemulsion changes from IL/o to bicontinuous and from bicontinuous to o/IL microemulsions.

For TX-100/ $[C_2mim][TFSI]$ /water microemulsion system, the reverse micelle dominated microemulsion converts to micelle dominated one via bicontinuous one with increasing W_o and for TX-100/ $[C_2mim][PF_6]$ /water microemulsion system, only the micelle dominated microemulsions exist at the homogeneous compositions (Figure 3.3.9 (c)). In the reverse micelle dominated microemulsions (i.e. at low W_o), IL exists in the bulk and water exists in the core of the reverse micelles and in micelle

dominated microemulsions, water exists in the bulk and IL exists in the core of micelles. The change in the microstructure brings about the change in refractive indices.

3.3.1.5.2. Effect of Temperature on Refractive Index

Figure 3.3.10 (a, b) shows the effect of temperature on the refractive index of different series of TX-100 microemulsions where IL is the polar phase at $R = 0.2255$ (Appendices Tables A18-19.). From Figure 3.3.10 (a), it can be seen that the refractive index of the microemulsions decreases with increasing temperature upto 35 °C and then increases slightly for TX-100/cyclohexane/[C₂mim][BF₄] microemulsions. On the contrary, for TX-100/cyclohexane/[C₂mim][MeSO₄] and TX-100/cyclohexane/[C₂mim][EtSO₄] microemulsions, refractive index consistently decreases with increasing temperature.

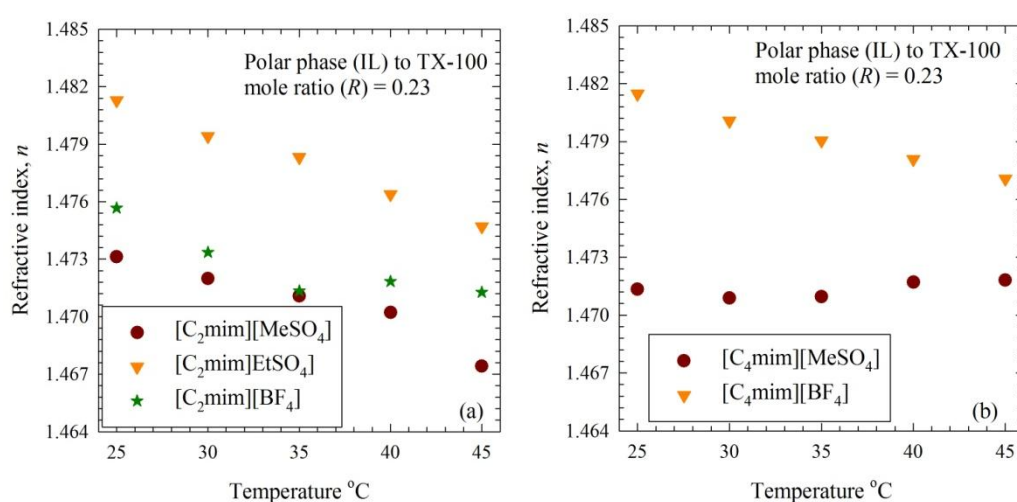


Figure 3.3.10. Effect of temperature on the refractive index of (a) TX-100/cyclohexane/[C₂mim][MeSO₄], TX-100/cyclohexane/[C₂mim][EtSO₄] and TX-100/cyclohexane/[C₂mim][BF₄], (b) TX-100/cyclohexane/[C₄mim][MeSO₄] and TX-100/cyclohexane/[C₄mim][BF₄] microemulsions at $R = 0.2255$.

The mobility of the droplets of the microemulsions increases with increasing temperature. Phase transition from IL/o to bicontinuous microemulsion may be approximated. For TX-100/cyclohexane/[C₂mim][BF₄] and TX-100/cyclohexane/[C₂mim][MeSO₄] microemulsions it occurs at around 35 °C and 45 °C respectively (Figure 3.3.10 (a)) and for TX-100/cyclohexane/[C₄mim][MeSO₄] microemulsions at around 35 °C (Figure 3.3.10 (b)).

3.3.1.6. Polarity

Figure 3.3.11 shows the UV-visible absorption spectra for RBD in the (a) TX-100/cyclohexane/[C₂mim][EtSO₄], (b) TX-100/cyclohexane/[C₂mim][BF₄], and (c) TX-100/[C₂mim][TFSI]/water microemulsions at different R or W_0 at 25 °C where the concentration of RBD was 1.54×10^{-4} M, 1.25×10^{-4} M and 1.25×10^{-4} M respectively. From Figure 3.3.11, only a slight change in λ_{\max} is observed in the

visible range of absorption spectra of RBD in all the TX-100 microemulsions (Section 3.1.).

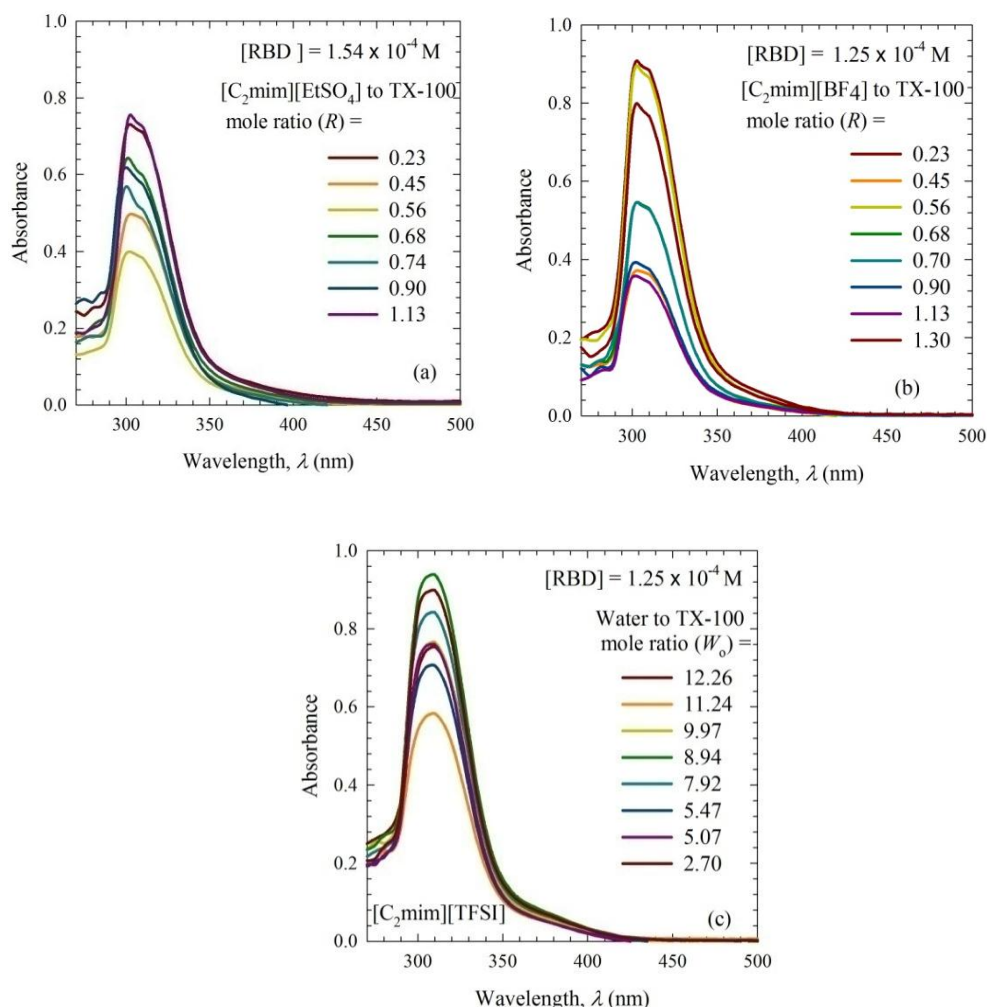


Figure 3.3.11. UV-visible absorption spectra of RBD in (a) TX-100/cyclohexane/[C₂mim][EtSO₄], (b) TX-100/cyclohexane/[C₂mim][BF₄] and (c) TX-100/[C₂mim][TFSI]/water microemulsions at different *R* or *W*₀ at 25 °C.

Both IL based microemulsions and IL exhibit intramolecular π - π^* charge transfer transition. The dye is zwitterionic in the ground state and upon excitation electron transfer occurs from oxygen to the Ag⁺ and RBD-Ag complex is formed which prevents the intramolecular π - π^* charge transfer transition. During synthesis of IL, metathesis of a halide salt with silver salt of the desired anion is carried out and trace amount of silver ions thus can remain as residue in ILs after purification.

3.3.1.7. Surface Tension

Figure 3.3.12 shows the variation of surface tension of TX-100/cyclohexane/[C₂mim][EtSO₄] (*R* = 0.1728, 0.2255, 0.4510, 0.5600, 0.6765), TX-100/cyclohexane/[C₂mim][MeSO₄] (*R* = 0.2255), TX-100/[C₂mim][PF₆]/water (*W*₀ = 14.0421, 13.1624, 11.6622, 10.9897, 10.3186, 9.9697) and TX-

100/[C₂mim][TFSI]/water ($W_o = 9.9697$) microemulsions as a function of R or W_o at 25 °C (Appendices Tables A20-21.).

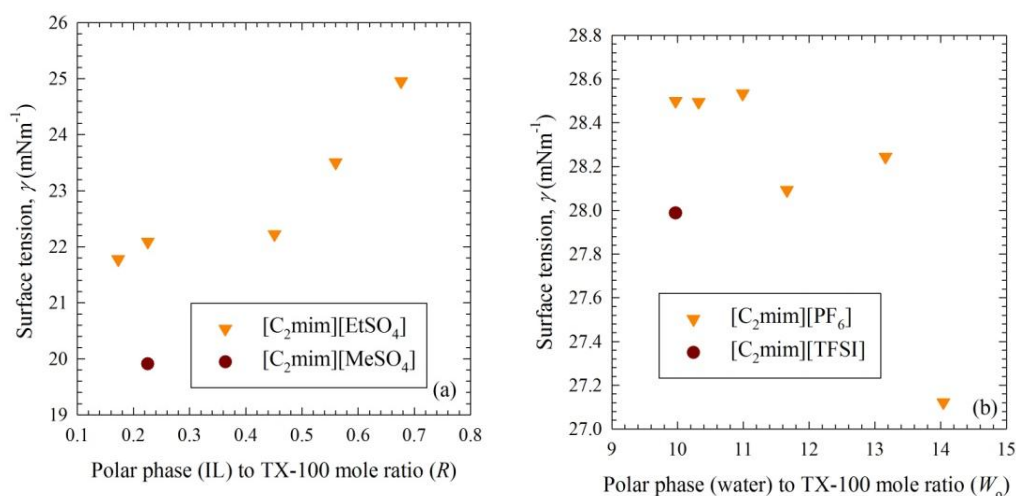
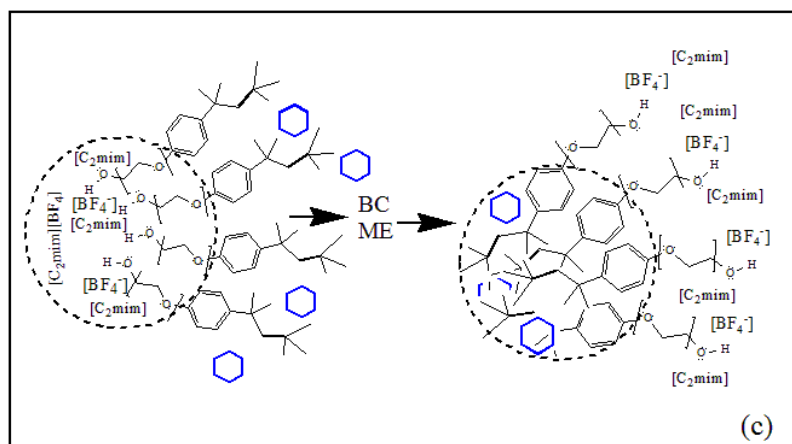
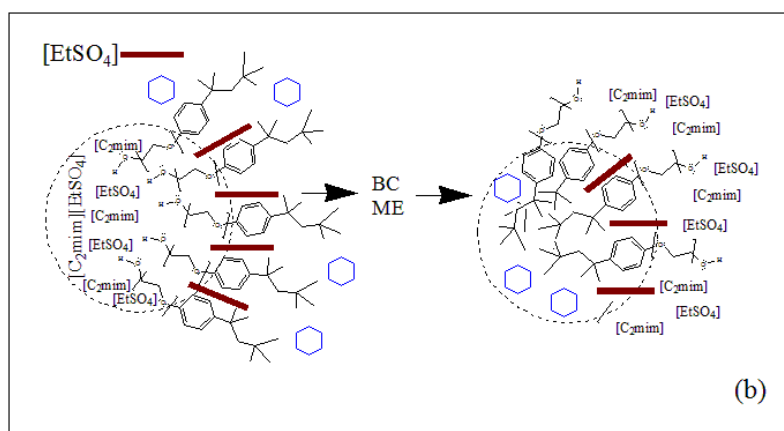
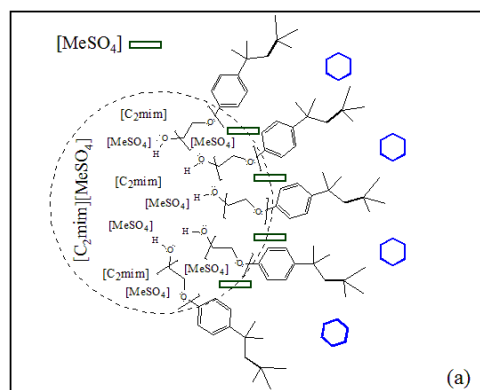


Figure 3.3.12. Surface tension of (a) TX-100/cyclohexane/[C₂mim][EtSO₄] and TX-100/cyclohexane/[C₂mim][MeSO₄], (b) TX-100/[C₂mim][PF₆]/water and TX-100/[C₂mim][TFSI]/water microemulsions as a function of R or W_o at 25 °C.

Surface tension of [C₂mim][EtSO₄] based microemulsions with $R = 0.1728, 0.2255, 0.4510, 0.5600, 0.6765$ show the values of 21.777, 22.088, 22.222, 23.503, and 24.951 mNm^{-1} respectively and of [C₂mim][MeSO₄] based microemulsion with $R = 0.2255$ shows the value of 19.907 mN m^{-1} (Figure 3.3.12 (a)). Surface tension of [C₂mim][PF₆] based microemulsions with $W_o = 14.0421, 13.1624, 11.6622, 10.9897, 10.3186, 9.9697$ show the values of 27.122, 28.245, 28.092, 28.534, 28.495 and 27.987 mN m^{-1} respectively and that of [C₂mim][TFSI] based microemulsion with $W_o = 9.9697$ shows the value of 27.987 mN m^{-1} (Figure 3.3.12 (b)).

3.3.2. Effect of Nonpolar Chain Length of Anions of ILs on Physicochemical Properties of Microemulsions

When the ions of IL in IL/o microemulsion (TX-100/cyclohexane/[C₂mim][MeSO₄], TX-100/cyclohexane/[C₂mim][EtSO₄] and TX-100/cyclohexane/[C₂mim][BF₄]) migrate from reverse micelle core to the interfacial layer, both the nonpolar group of anions and the nonpolar side chain of cations experience hydrophobic interactions with the tail part of TX-100 (Scheme 3.1). The more carbon atoms are attached with the nonpolar group of anions and the nonpolar side chain of cations, the more hydrophobic interactions exist with the tail part of TX-100. The more the hydrophobic interaction of nonpolar groups of ions of IL with the TX-100 tail part, the higher the number of ions that transfer to the bulk. Cyclohexane which exists in the bulk creates hydrophobic interactions with the tail part of TX-100 in reverse micelle dominated microemulsions.



Scheme 3.1. Interaction and arrangement of ions of ILs in (a) IL/o microemulsion for TX-100/cyclohexane/[C₂mim][MeSO₄], (b) IL/o, bicontinuous (BC) and o/IL microemulsions for TX-100/cyclohexane/[C₂mim][EtSO₄], and (c) IL/o, bicontinuous (BC) and o/IL microemulsions for TX-100/cyclohexane/[C₂mim][BF₄] systems.

The results of conductivity (Figure 3.3.1 (a)) droplet sizes (Figure 3.3.3 (a)) of IL based microemulsions with $[\text{C}_2\text{mim}]^+$ cation follows the order $[\text{C}_2\text{mim}][\text{BF}_4] > [\text{C}_2\text{mim}][\text{EtSO}_4] > [\text{C}_2\text{mim}][\text{MeSO}_4]$, while viscosity follows the trend $[\text{C}_2\text{mim}][\text{BF}_4] < [\text{C}_2\text{mim}][\text{EtSO}_4] < [\text{C}_2\text{mim}][\text{MeSO}_4]$ (Figure 3.3.2 (a)). In TX-100/cyclohexane/ $[\text{C}_2\text{mim}][\text{BF}_4]$ microemulsions, the spherical anion $[\text{BF}_4]^-$ in $[\text{C}_2\text{mim}][\text{BF}_4]$ can easily associate with or dissociate from the imidazolium cation (Scheme 3.2 (c)), thus conductivity of these microemulsions shows the highest values. Due to increasing mobility of ions, these systems show the lowest viscosity values (Figure 3.3.2 (a)). As the spherical $[\text{BF}_4]^-$ anions dissociate easily from cations, $[\text{BF}_4]^-$ can move to the interfacial layer faster in $[\text{C}_2\text{mim}][\text{BF}_4]$ based microemulsions than the other anions in microemulsions with $[\text{C}_2\text{mim}][\text{EtSO}_4]$ and $[\text{C}_2\text{mim}][\text{MeSO}_4]$ and the imidazolium cations can also move to the interface along with the anions. Penetration of ions in the interface is easy. So the reverse micelle droplets for $[\text{C}_2\text{mim}][\text{BF}_4]$ based microemulsions show the biggest size (Table 3.4)

For TX-100/cyclohexane/ $[\text{C}_2\text{mim}][\text{MeSO}_4]$ and TX-100/cyclohexane/ $[\text{C}_2\text{mim}][\text{EtSO}_4]$ microemulsions, as the nonpolar $-\text{Et}$ group of anion $[\text{EtSO}_4]^-$ is larger compared to that of $[\text{MeSO}_4]^-$, the hydrophobic-hydrophobic interaction is stronger between the nonpolar groups of $[\text{EtSO}_4]^-$ and TX-100 tail part (Scheme 3.2 (a,b)). $[\text{EtSO}_4]^-$ anion can expose to bulk easily. The conductivity of TX-100/cyclohexane/ $[\text{C}_2\text{mim}][\text{EtSO}_4]$ system is higher (Figure 3.3.1 (a)), viscosity is lower (Figure 3.3.2 (a)) and reverse micelle droplets are bigger compared to TX-100/cyclohexane/ $[\text{C}_2\text{mim}][\text{MeSO}_4]$ system. In the reverse micelle dominated system the anions might play as the important factor for increasing the conductivity. For micelle dominated microemulsions in TX-100/cyclohexane/ $[\text{C}_2\text{mim}][\text{EtSO}_4]$ system the cations are assumed to play important role for increasing the conductivity (Scheme 3.2 (b)). In the case of TX-100/cyclohexane/ $[\text{C}_4\text{mim}][\text{MeSO}_4]$, TX-100/cyclohexane/ $[\text{C}_4\text{mim}][\text{BF}_4]$ (Figure 3.3.1 (b)), and TX-100/ $[\text{C}_2\text{mim}][\text{TFSI}]$ /water, TX-100/ $[\text{C}_2\text{mim}][\text{PF}_6]$ /water (Figure 3.3.1 (c)) microemulsions, the same situation occurs.

3.3.3. Variation of Physicochemical Properties of TX-100 Microemulsions using ILs as the Polar or Nonpolar Phase with Variation of Cations of ILs

3.3.3.1. Conductivity

3.3.3.1.1. The Influence of R or W_o

Figure 3.3.13 shows the change of conductivity of different series of TX-100 microemulsions with increasing R or W_o at 25 °C (Appendices Tables A22-24.). From Figure 3.3.13 (a, b), it can be seen that the conductivity of the microemulsions increase with increasing R for all the systems and from Figure 3.3.13 (c), it is seen that for TX-100/ $[\text{C}_4\text{mim}][\text{PF}_6]$ /water system, conductivity initially increases and after reaching a maximum value at $W_o = 8$, the conductivity decreases with further increasing W_o and for TX-100/ $[\text{C}_2\text{mim}][\text{PF}_6]$ /water system conductivity decreases with increasing W_o .

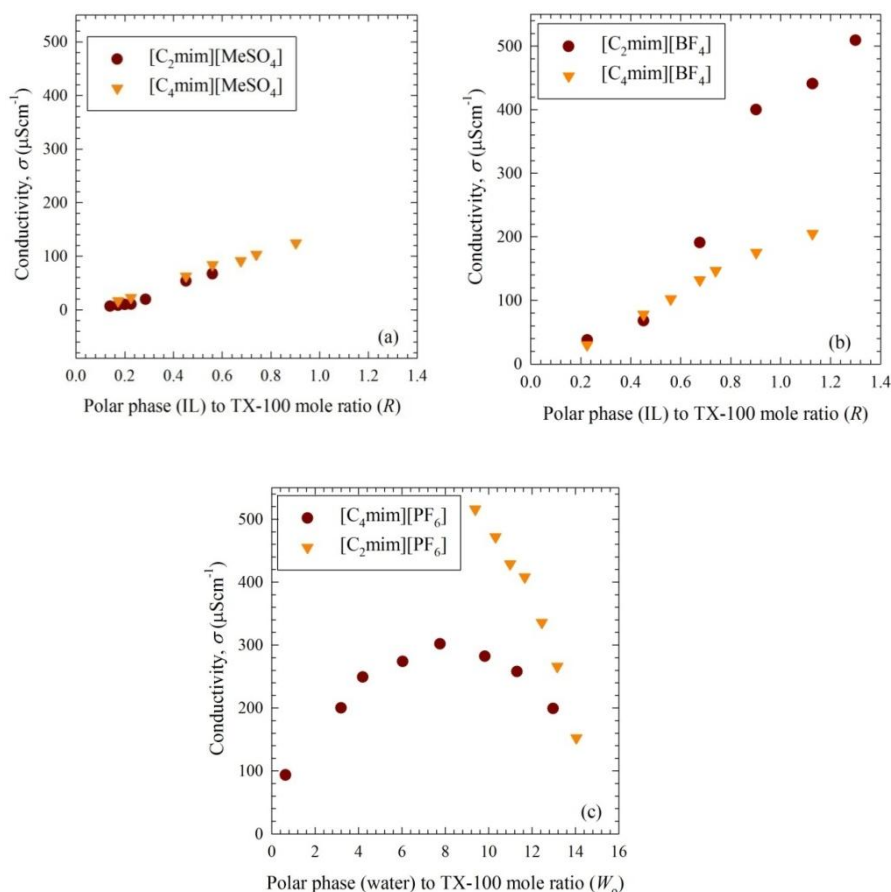


Figure 3.3.13. Variation of conductivity of (a) TX-100/cyclohexane/ $[\text{C}_2\text{mim}][\text{MeSO}_4]$ and TX-100/cyclohexane/ $[\text{C}_4\text{mim}][\text{MeSO}_4]$, (b) TX-100/cyclohexane/ $[\text{C}_2\text{mim}][\text{BF}_4]$ and TX-100/cyclohexane/ $[\text{C}_4\text{mim}][\text{BF}_4]$, (c) TX-100/ $[\text{C}_2\text{mim}][\text{PF}_6]$ /water and TX-100/ $[\text{C}_4\text{mim}][\text{PF}_6]$ /water microemulsions as a function of R or W_0 at 25 °C.

Figure 3.3.13 (a) shows that for TX-100/cyclohexane/ $[\text{C}_4\text{mim}][\text{MeSO}_4]$ microemulsions, with increasing R the system changes from IL/o to o/IL microemulsions via bicontinuous microemulsions. At low R , for the reverse micelle dominated microemulsions (IL/o) the continuous medium is cyclohexane. The low conductivity at this region is attributed to this nonpolar continuous medium. With increasing R , clustering of droplets in IL/o microemulsions occur due to the hydrophobic interactions of the tail parts of surfactants [32-36]. Cations and anions of IL can easily move through the small channels by fusion, mass exchange and subsequent fission. Conductivity further increases due to the formation of bicontinuous complex microemulsions with further increasing R . In o/IL microemulsions IL exists in the bulk and cyclohexane is encapsulated in the core of micelles. Cations and anions of IL can freely move in the bulk, thereby increasing the conductivity. In TX-100/cyclohexane/ $[\text{C}_2\text{mim}][\text{MeSO}_4]$, only IL/o microemulsions may have been formed due to the low IL content.

For TX-100/cyclohexane/[C₂mim][BF₄] and TX-100/cyclohexane/[C₄mim][BF₄] microemulsions, with increasing *R* both the systems are likely to change from IL/o to o/IL microemulsions via bicontinuous microemulsions (Figure 3.3.1 (b)).

In Figure 3.3.1 (c), for TX-100/[C₄mim][PF₆]/water microemulsions, with increasing *W*₀ the system changes from w/IL to IL/w microemulsions via bicontinuous microemulsions. The conductivity is low at low *W*₀ for w/IL microemulsions due to the non-polar aggregation of the IL continuous medium. Since water dissociates the aggregated IL in bulk and thereby increases the number and movement of free ions from IL, with increasing *W*₀ conductivity increases. Cations and anions of IL can easily move through the small channels which are formed due to the clustering of water droplets in microemulsions. When the bicontinuous complex microemulsions are formed with increasing *W*₀, conductivity shows the highest value. In IL/w microemulsions, water exists in the bulk and ILs are encapsulated in the core of micelles. Conductivity decreases because ions of IL are now encapsulated in the core of micelle droplets. Number of ions of IL decreases with further increasing *W*₀ and conductivity further decreases. In TX-100/cyclohexane/[C₂mim][PF₆] microemulsions only IL/w systems are formed as the IL content is very low in these microemulsions.

3.3.3.1.2. The Influence of IL Cation

The structures of the cation and anion of [C₂mim][MeSO₄], [C₄mim][MeSO₄], [C₂mim][BF₄], [C₄mim]BF₄, [C₂mim][PF₆] and [C₄mim][PF₆] have been shown in Scheme 1.14.

3.3.3.1.2.1. The Influence of Alkyl Side Chain Length of IL Cation in TX-100/Cyclohexane/[C₂mim][MeSO₄] and TX-100/Cyclohexane/[C₄mim][MeSO₄] Microemulsions

Electrostatic interaction between the cation and anion of [C₄mim][MeSO₄] is comparatively lower than those of [C₂mim][MeSO₄] due to the bulky size of [C₄mim]⁺ cation with longer alkyl side chains. Due to the longer butyl side chain of [C₄mim]⁺, asymmetric nature increases i.e. the unit positive charge is less centered around [C₄mim]⁺. Moreover, the positive charge density is lower in [C₄mim]⁺ cation due to the attachment of the electron releasing longer butyl side chain, which is responsible for the weaker electrostatic attraction between [C₄mim]⁺ and [MeSO₄]⁻ ions. Thus, as the *R* increases, ions of [C₄mim][MeSO₄] become more easily available compared to the ions of [C₂mim][MeSO₄] in the reverse micelle dominated microemulsions. So the conductivities of [C₄mim][MeSO₄] based microemulsions are larger than [C₂mim][MeSO₄] based microemulsions (Figure 3.3.13 (a)).

When IL is incorporated in TX-100 reverse micelle core, anions of ILs are attracted to the head groups of TX-100 (Scheme 3.3). Anions of ILs can interact with the hydrogen atoms of terminal hydroxide head groups of TX-100, while the cations stay close to the anions. For TX-100/cyclohexane/[C₄mim][MeSO₄] and TX-100/cyclohexane/[C₂mim][MeSO₄] systems as the nonpolar group of [C₄mim]⁺ is larger compared to [C₂mim]⁺, hydrophobic-hydrophobic interaction is stronger

between the nonpolar groups of $[\text{C}_4\text{mim}]^+$ cation and TX-100 tail part. $[\text{C}_4\text{mim}]^+$ can therefore expose to the bulk more easily, making the conductivity of TX-100/cyclohexane/ $[\text{C}_4\text{mim}][\text{MeSO}_4]$ system higher (Figure 3.3.13 (a)). In the reverse micelle dominated system, the cation therefore plays important role for increasing the conductivity. In the bicontinuous microemulsions conductivity further increases. As stated earlier, the mobility of anion may be the main factor for increasing conductivity in micelle dominated microemulsions for TX-100/cyclohexane/ $[\text{C}_4\text{mim}][\text{MeSO}_4]$ microemulsions (Scheme 3.3.).

3.3.3.1.2.2. The Influence of IL Cation in TX-100/Cyclohexane/ $[\text{C}_2\text{mim}][\text{BF}_4]$ and TX-100/Cyclohexane/ $[\text{C}_4\text{mim}][\text{BF}_4]$ Microemulsion

Figure 3.3.13 (b) shows different series of IL based microemulsions with the same anion $[\text{BF}_4]^-$, but different cations $[\text{C}_2\text{mim}]^+$ and $[\text{C}_4\text{mim}]^+$. The electrostatic attraction between $[\text{BF}_4]^-$ and imidazolium based cations is high, because negative charge is highly centered on spherical $[\text{BF}_4]^-$.

The positive charge on $[\text{C}_2\text{mim}]^+$ and $[\text{C}_4\text{mim}]^+$ is located mainly on the $\text{C}_2\text{-H}$ side of imidazolium ring. On the other hand, $[\text{BF}_4]^-$ has close contact with $\text{C}_4\text{-H}$ and $\text{C}_5\text{-H}$ of the imidazolium ring [37]. In determining the formation of ionic aggregates both the magnitude and the directionality of the interaction energy plays important roles. The relatively localized distribution of cationic charge as well as the aromatic plane structure allows the close contact of the cation with the anion.

If the symmetry in $[\text{C}_2\text{mim}]^+$ and $[\text{C}_4\text{mim}]^+$ structure is considered, it is observed that more asymmetry is involved in structure of $[\text{C}_4\text{mim}]^+$ due to the longer alkyl side chain. Probably due to this longer side chain, the dispersion force and steric hindrance in $[\text{C}_4\text{mim}][\text{BF}_4]$ are higher [46, 55]. From Figure 3.3.13 (b), the conductivity of $[\text{C}_2\text{mim}][\text{BF}_4]$ based microemulsion system seems higher compared to $[\text{C}_4\text{mim}][\text{BF}_4]$ based microemulsion system. IL with bulky cation $[\text{C}_4\text{mim}]^+$ is more viscous than IL with smaller, more mobile cation $[\text{C}_2\text{mim}]^+$. Moreover, for the longer side chain in $[\text{C}_4\text{mim}]^+$, dispersion force may play an important role in enhancing the ionic association. Those are why, hydrophobic-hydrophobic interaction is stronger between the nonpolar groups of imidazolium ion and TX-100 tail part in $[\text{C}_4\text{mim}]^+$ than in $[\text{C}_2\text{mim}]^+$. $[\text{C}_2\text{mim}]^+$ can therefore expose to the bulk more easily compared to $[\text{C}_4\text{mim}]^+$.

3.3.3.1.2.2.1. Walden Plots for TX-100/Cyclohexane/ $[\text{C}_2\text{mim}][\text{BF}_4]$ and TX-100/Cyclohexane/ $[\text{C}_4\text{mim}][\text{BF}_4]$ Microemulsions

Figure 3.3.14 shows the Walden plots (Section 1.5.2. of Chapter 1) for TX-100/cyclohexane/ $[\text{C}_2\text{mim}][\text{BF}_4]$ and TX-100/cyclohexane/ $[\text{C}_4\text{mim}][\text{BF}_4]$ microemulsions (Appendices Table A25).

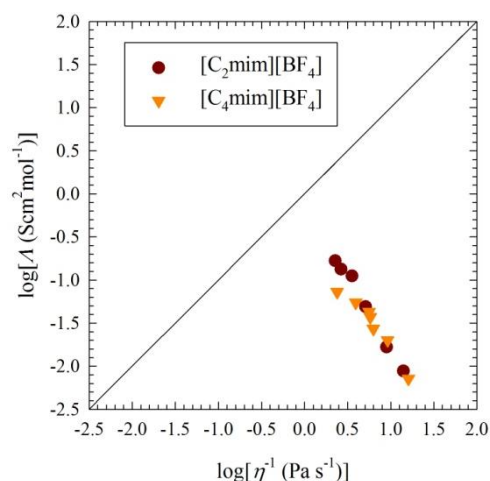


Figure 3.3.14. Walden plots for TX-100/cyclohexane/[C₂mim][BF₄] and TX-100/cyclohexane/[C₄mim][BF₄] microemulsions.

From Walden plot it can be seen that the mobility of ions of IL in TX-100/cyclohexane/[C₂mim][BF₄] microemulsions is higher compared to that of ions of IL in TX-100/cyclohexane/[C₄mim][BF₄] microemulsion, which is consistent to the previous observations.

3.3.3.1.2.3. The Influence of IL Cation in TX-100/[C₂mim][PF₆]/Water and TX-100/[C₄mim][PF₆]/Water Microemulsions

Figure 3.3.13 (c) shows different series of IL based microemulsions with the same anion [PF₆]⁻, but different cations [C₂mim]⁺ and [C₄mim]⁺.

The positive charge is located mainly on the C₂-H side of the imidazolium ring of [C₂mim]⁺ and [C₄mim]⁺. [PF₆]⁻ has close contact with C₄-H and C₅-H of the imidazolium ring [37]. The degree of asymmetry, dispersion force and steric hindrance are higher in [C₄mim]⁺ than in [C₂mim]⁺ due to the longer alkyl butyl side chain.

From Figure 3.3.13 (c), it is seen that the conductivity of [C₂mim][PF₆] based microemulsion is higher compared to [C₄mim][PF₆] based microemulsion system. [C₄mim][PF₆] with longer butyl side chain [C₄mim]⁺ is more viscous than [C₂mim][PF₆]. The longer butyl side chain in [C₄mim]⁺ may induce higher dispersion force, enhancing the ionic association. [C₂mim]⁺ can expose to the bulk more easily than [C₄mim]⁺ because hydrophobic-hydrophobic interaction between butyl side chain of [C₄mim]⁺ and TX-100 tail part is stronger. The conductivity for TX-100/cyclohexane/[C₂mim][PF₆] system is thus higher as shown in Figure 3.3.1 (a).

3.3.3.1.2.3.1. Walden Plots for TX-100/[C₂mim][PF₆]/Water and TX-100/[C₄mim][PF₆]/Water Microemulsions

Figure 3.3.15 shows the Walden plots for TX-100/cyclohexane/[C₂mim][PF₆] and TX-100/cyclohexane/[C₄mim][PF₆] microemulsions (Appendices Table A26).

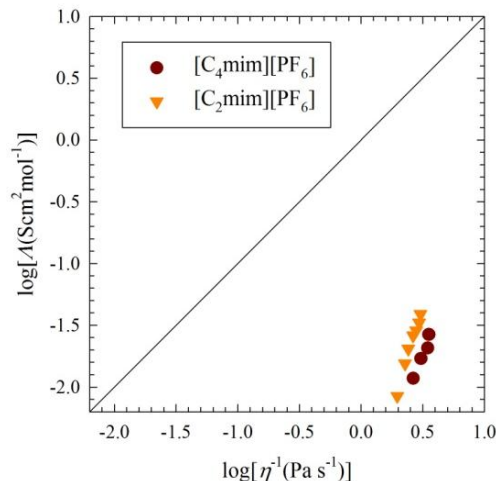


Figure 3.3.15. Walden plots for TX-100/cyclohexane/[C₂mim][PF₆] and TX-100/cyclohexane/[C₄mim][PF₆] microemulsions.

From Walden plots it can be seen that the mobility of ions of IL in TX-100/cyclohexane/[C₂mim][PF₆] microemulsions is higher compared to that of ions of IL in TX-100/cyclohexane/[C₄mim][PF₆] microemulsions.

3.3.3.2. Viscosity

3.3.3.2.1. The Influence of R or W_o

Figure 3.3.16 shows the change of viscosity of different series of TX-100 microemulsions with increasing polar phase (IL or Water) to surfactant mole ratio (R or W_o) at 25 °C (Appendices Tables A27-29.). As shown in Figure 3.3.16 (a, b), the viscosity of the microemulsions increase with increasing R for all the systems and in Figure 3.3.16. (c), TX-100/[C₄mim][PF₆]/water system viscosity initially decreases and after reaching a minimum value viscosity increases with increasing W_o and for TX-100/[C₂mim][PF₆]/water system viscosity increases with increasing W_o .

Increasing W_o , TX-100/[C₄mim][PF₆]/water system may changes from w/IL to IL/w microemulsions via bicontinuous microemulsions (Figure 3.3.16. (c)). In reverse micelle dominated microemulsions (w/IL) with low W_o , the continuous medium is aggregated IL and thus the viscosity is high. Mobility of ions of IL increases with increasing W_o because addition of water dissociates the aggregated IL in the bulk, one layer of microemulsion can easily flow with the other layers and viscosity decreases. Increasing W_o , clustering of water droplets in microemulsions occur and the charge particles of IL can easily move through the small channels. When bicontinuous microemulsion is formed viscosity shows the lowest value. In micelle dominated microemulsions (IL/w) with increasing W_o , water is the continuous medium and IL exists in the core of micelles. Mobility of ions of IL decreases in the core of micelle. H-bonding among water molecules in the bulk increasing and the micelle size decreases with further increases W_o and viscosity increases. Change of viscosity of other microemulsions have been discussed in Section 3.3.1.2.1.

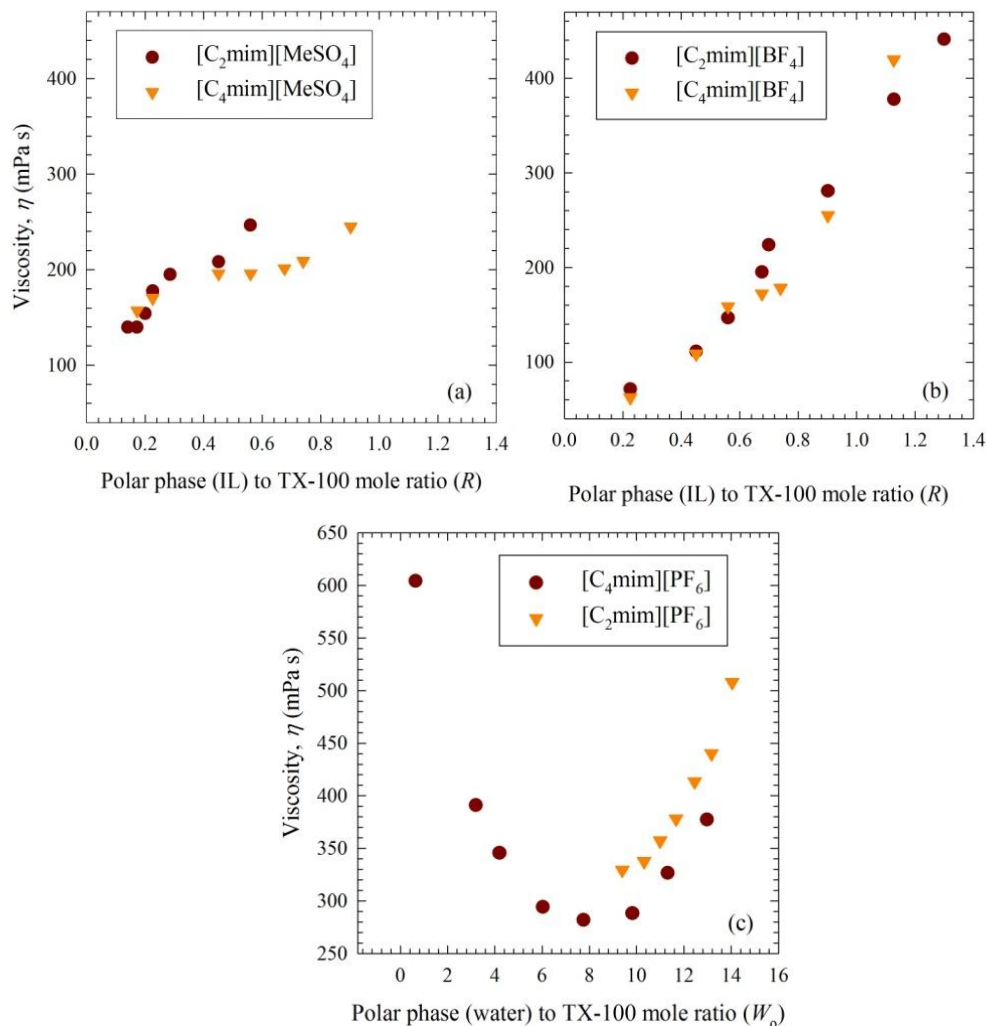


Figure 3.3.16. Variation of viscosity of (a) TX-100/cyclohexane/[C₂mim][MeSO₄] and TX-100/cyclohexane/[C₄mim][MeSO₄], (b) TX-100/cyclohexane/[C₂mim][BF₄] and TX-100/cyclohexane/[C₄mim][BF₄] (c) TX-100/[C₂mim][PF₆]/water and TX-100/[C₄mim][PF₆]/water microemulsions as a function of polar phase (IL or water) to TX-100 mole ratio (R or W_0) at 25 °C.

3.3.3.2.2. The Influence of IL Cation

3.3.3.2.2.1. The Influence of IL Cation in TX-100/Cyclohexane/[C₂mim][MeSO₄] and TX-100/Cyclohexane/[C₄mim][MeSO₄] Microemulsions

Different cations [C₂mim]⁺ and [C₄mim]⁺ with anion [MeSO₄]⁻ were used for different series of IL based microemulsions (Figure 3.3.16 (a)). TX-100/cyclohexane/[C₄mim][MeSO₄] microemulsions show the lower and TX-100/cyclohexane/[C₂mim][MeSO₄] microemulsions show the higher viscosity values which shows the opposite results of conductivity (Figure 3.3.1 (a)). Increasing conductivity shows decreasing trend in viscosity. For TX-100/cyclohexane/[C₄mim][MeSO₄] microemulsions, with increasing R value, the systems may change from IL/o to o/IL microemulsions via bicontinuous microemulsions. Three dimensional complex channeling occur in bicontinuous

microemulsions which results in increase in viscosity. In o/IL microemulsions, continuous medium is viscous IL.

3.3.3.2.2. The Influence of IL Cation in TX-100/Cyclohexane/[C₄mim][BF₄] and TX-100/Cyclohexane/[C₂mim][BF₄] Microemulsions

The cations [C₂mim]⁺ and [C₄mim]⁺ with anion [BF₄]⁻ were used for different series of IL based microemulsions (Figure 3.3.16. (b)). Dissociation and association of spherical anions with the cations occur easily. TX-100/cyclohexane/[C₄mim][BF₄] and TX-100/cyclohexane/[C₂mim][BF₄] microemulsions show the same trend as conductivity. The values of both conductivity and viscosity data of TX-100/cyclohexane/[C₂mim][BF₄] microemulsions in most of the *R* values are higher than TX-100/cyclohexane/[C₄mim][BF₄] microemulsions. As the mobility of ions of TX-100/cyclohexane/[C₂mim][BF₄] microemulsions is comparatively higher, this system can easily form three dimensional complex channel structure. So the viscosity of this system is also higher compared to TX-100/cyclohexane/[C₄mim][BF₄] microemulsions.

3.3.3.2.3. The Influence of IL Cation in TX-100/[C₂mim][PF₆]/Water and TX-100/[C₄mim][PF₆]/Water Microemulsions

ILs with different cations, [C₂mim]⁺ and [C₄mim]⁺ with anion [PF₆]⁻ were used for different series of IL based microemulsions. Spherical anions can easily dissociate from and associate with the cations. Each viscosity series shows the opposite trend of conductivity. But the values of both conductivity and viscosity data of TX-100/[C₂mim][PF₆]/water microemulsions are higher than TX-100/cyclohexane/[C₄mim][PF₆] microemulsions (Figure 3.3.16 (c)). As the mobility of ions of TX-100/cyclohexane/[C₂mim][PF₆] microemulsions is comparatively higher, this system can form three dimensional complex channel structure. So the viscosity of this system is also higher compared to TX-100/Cyclohexane/[C₄mim][PF₆] microemulsions.

3.3.3.2.3. Effect of Temperature on Viscosity

Figure 3.3.17 (a, b) shows the effect of temperature on viscosity of different series of TX-100 microemulsions at *R* = 0.2255 (Appendices Tables A30-31.). From Figure 3.3.17 (a, b), it can be seen that the viscosities of the microemulsions decrease with increasing temperature for *R* = 0.2255. Mobility of different layers in microemulsion increases with increasing temperature. Increasing temperature enhances kinetic energy and consequently lowers the attractive interaction among droplets in microemulsion and decreases viscosity.

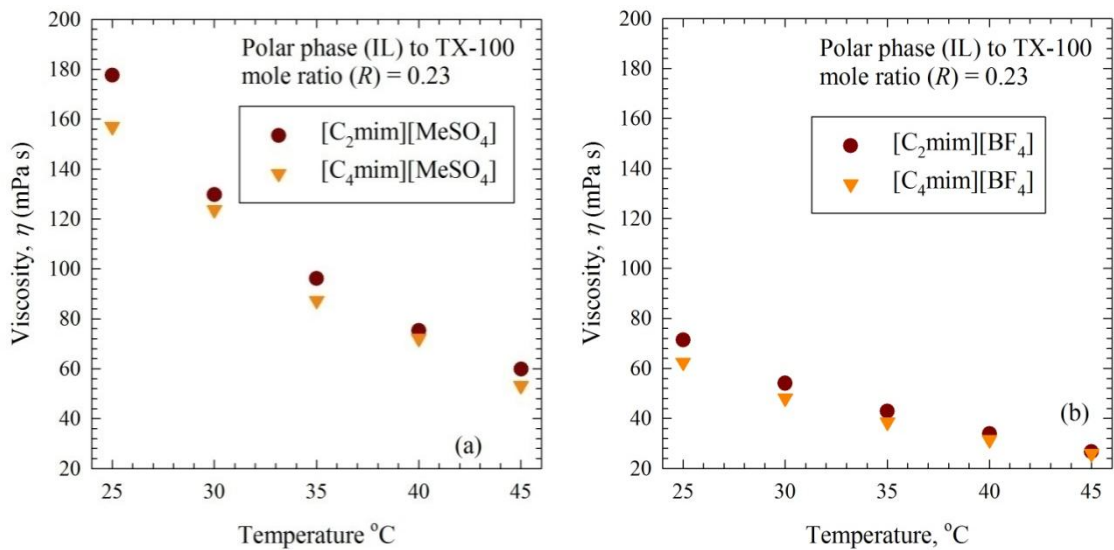


Figure 3.3.17. Effect of temperature on viscosity of (a) TX-100/cyclohexane/ $[\text{C}_2\text{mim}][\text{MeSO}_4]$ and TX-100/cyclohexane/ $[\text{C}_4\text{mim}][\text{MeSO}_4]$, (b) TX-100/cyclohexane/ $[\text{C}_2\text{mim}][\text{BF}_4]$ and TX-100/cyclohexane/ $[\text{C}_4\text{mim}][\text{BF}_4]$ microemulsions at $R = 0.2255$.

3.3.3.3. Size and Size Distribution of Droplets

3.3.3.3.1. Influence of IL Cation

3.3.3.3.1.1. The Influence of IL Cation in TX-100/Cyclohexane/ $[\text{C}_2\text{mim}][\text{MeSO}_4]$ and TX-100/Cyclohexane/ $[\text{C}_4\text{mim}][\text{MeSO}_4]$ Microemulsions

Figure 3.3.18 shows the size distributions and variation of size of reverse micelle droplets for different microemulsion systems with increasing R at 25 °C where ILs are $[\text{C}_2\text{mim}][\text{MeSO}_4]$ and $[\text{C}_4\text{mim}][\text{MeSO}_4]$ (Appendices Table A9.).

The change of the droplet sizes in TX-100/cyclohexane/ $[\text{C}_2\text{mim}][\text{MeSO}_4]$ and TX-100/cyclohexane/ $[\text{C}_4\text{mim}][\text{MeSO}_4]$ microemulsions with increasing R is described briefly in Section 3.3.1.3.1.1. and 3.3.1.3.3.2 respectively. Comparatively strong electrostatic interaction is involved between the ions of IL in TX-100/cyclohexane/ $[\text{C}_2\text{mim}][\text{MeSO}_4]$ microemulsion than TX-100/cyclohexane/ $[\text{C}_4\text{mim}][\text{MeSO}_4]$ microemulsion system. In the cation of $[\text{C}_4\text{mim}][\text{MeSO}_4]$, longer nonpolar butyl chain is attached. When the ions of $[\text{C}_4\text{mim}][\text{MeSO}_4]$ move to the inner interface of TX-100 reverse micelle, strong hydrophobic hydrophobic interaction prevails between $[\text{C}_4\text{mim}]^+$ and TX-100 tail group because of longer hydrophobic butyl side chain in $[\text{C}_4\text{mim}]^+$. Penetration of $[\text{C}_4\text{mim}]^+$ in the interface of TX-100 occur easily. Therefore, the droplets sizes for $[\text{C}_4\text{mim}][\text{MeSO}_4]$ based microemulsion system are larger than $[\text{C}_2\text{mim}][\text{MeSO}_4]$ based microemulsion system.

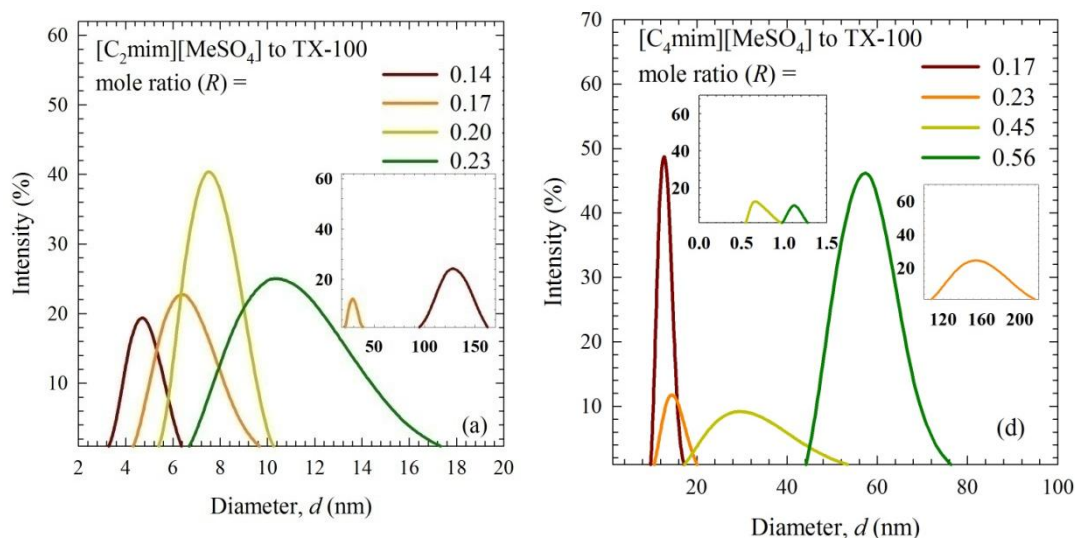


Figure 3.3.18. Size and size distribution of droplets for (a) TX-100/cyclohexane/[C₂mim][MeSO₄] and (d) TX-100/cyclohexane/[C₄mim][MeSO₄] microemulsions at different R values at 25 °C.

3.3.3.3.1.2. The Influence of IL Cation in TX-100/Cyclohexane/[C₂mim][BF₄] and TX-100/Cyclohexane/[C₄mim][BF₄] Microemulsions

Figure 3.3.19 shows the size distributions and variation of size of IL reverse micelle droplets for two different microemulsion systems with increasing R at 25 °C where ILs are [C₂mim][BF₄] and [C₄mim][BF₄] (Appendices Table A9).

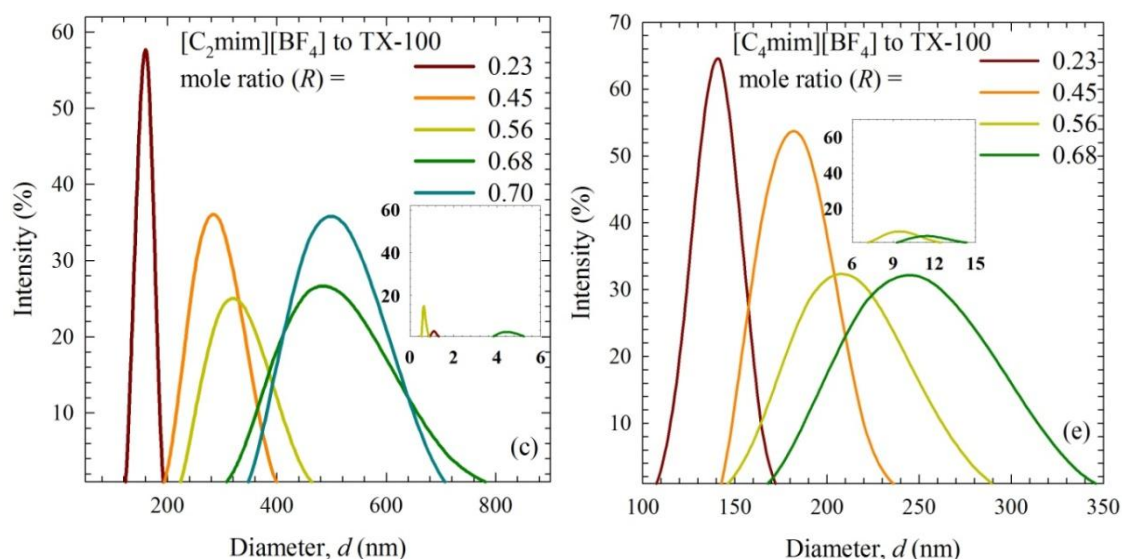


Figure 3.3.19. Size and size distribution of droplets for (c) TX-100/cyclohexane/[C₂mim][BF₄] and (e) TX-100/cyclohexane/[C₄mim][BF₄] microemulsions at different R at 25 °C.

The change of the droplet sizes in TX-100/cyclohexane/[C₂mim][BF₄] and TX-100/cyclohexane/[C₄mim][BF₄] microemulsions with increasing R is described

briefly in Section 3.3.1.3.1.1. and 3.3.1.3.3.2 respectively. Dispersion force in IL of TX-100/cyclohexane/[C₄mim][BF₄] microemulsion is larger due to longer hydrophobic butyl chain in the cation compared to the dispersion force in IL of TX-100/cyclohexane/[C₂mim][BF₄] microemulsion where ethyl side chain is attached with [C₂mim]⁺ in [C₂mim][BF₄]. Dissociation of ions of [C₂mim][BF₄] in TX-100/cyclohexane/[C₂mim][BF₄] microemulsion occurs with ease compared to [C₄mim][BF₄] in TX-100/cyclohexane/[C₄mim][BF₄] microemulsion. When [C₂mim]⁺ and [BF₄]⁻ move to the inner interface of TX-100 reverse micelle, strong hydrophobic hydrophobic interaction takes place between [C₂mim]⁺ and TX-100 tail group due to the ethyl side chain in [C₂mim]⁺. Penetration of [C₂mim]⁺ in the interface of TX-100 occur easily. Droplets size for [C₂mim][BF₄] based microemulsion system are larger than [C₄mim][BF₄] based microemulsion system.

3.3.3.3.1.3. The Influence of IL Anion in TX-100/[C₂mim][PF₆]/Water and TX-100/[C₄mim][PF₆]/Water Microemulsions

Figure 3.3.20 shows the size distributions and variation of size of IL micelle droplets for different microemulsion systems with decreasing W_o at 25 °C where ILs are [C₂mim][PF₆] and [C₄mim][PF₆] (Appendices Table A9.).

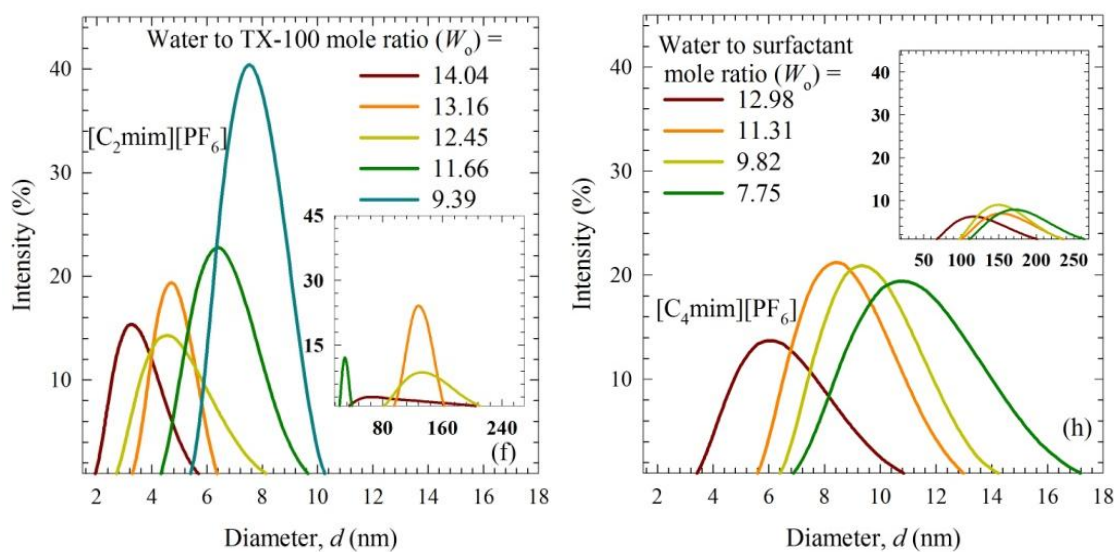


Figure 3.3.20. Size and size distribution of droplets for (f) TX-100/[C₂mim][PF₆]/water and (h) TX-100/[C₄mim][PF₆]/water microemulsions at different W_o values at 25 °C.

The change of the droplet sizes in TX-100/[C₂mim][PF₆]/water microemulsions with increasing W_o has been described in Section 3.3.1.3.1.3. Size of the micelle droplets increases from approximately 6 nm to 11 nm with decreasing W_o values from 12.9756 to 7.7538 for [C₄mim][PF₆] based microemulsion system. Size of clusters are obtained for $W_o = 12.9756, 11.3113, 9.8205,$ and 7.7538 and the size of the clusters are approximately 118, 153, 149, and 169 nm respectively (Appendices Table A9.). Increasing trend in the width of the peaks are observed with decreasing W_o because cluster formation occur.

3.3.3.4. Density

3.3.3.4.1. The Influence of R or W_o

Figure 3.3.21 shows the change of density of different series of TX-100 microemulsions with R or W_o at 25 °C (Appendices Tables A32-34.). From Figure 3.3.21 (a, b) it can be seen that the density of the microemulsions increase with increasing R for all the systems due to the addition of IL. From Figure 3.3.21 (c) it is seen that the density of the microemulsions decreases with increasing W_o for all the systems due to the addition of water.

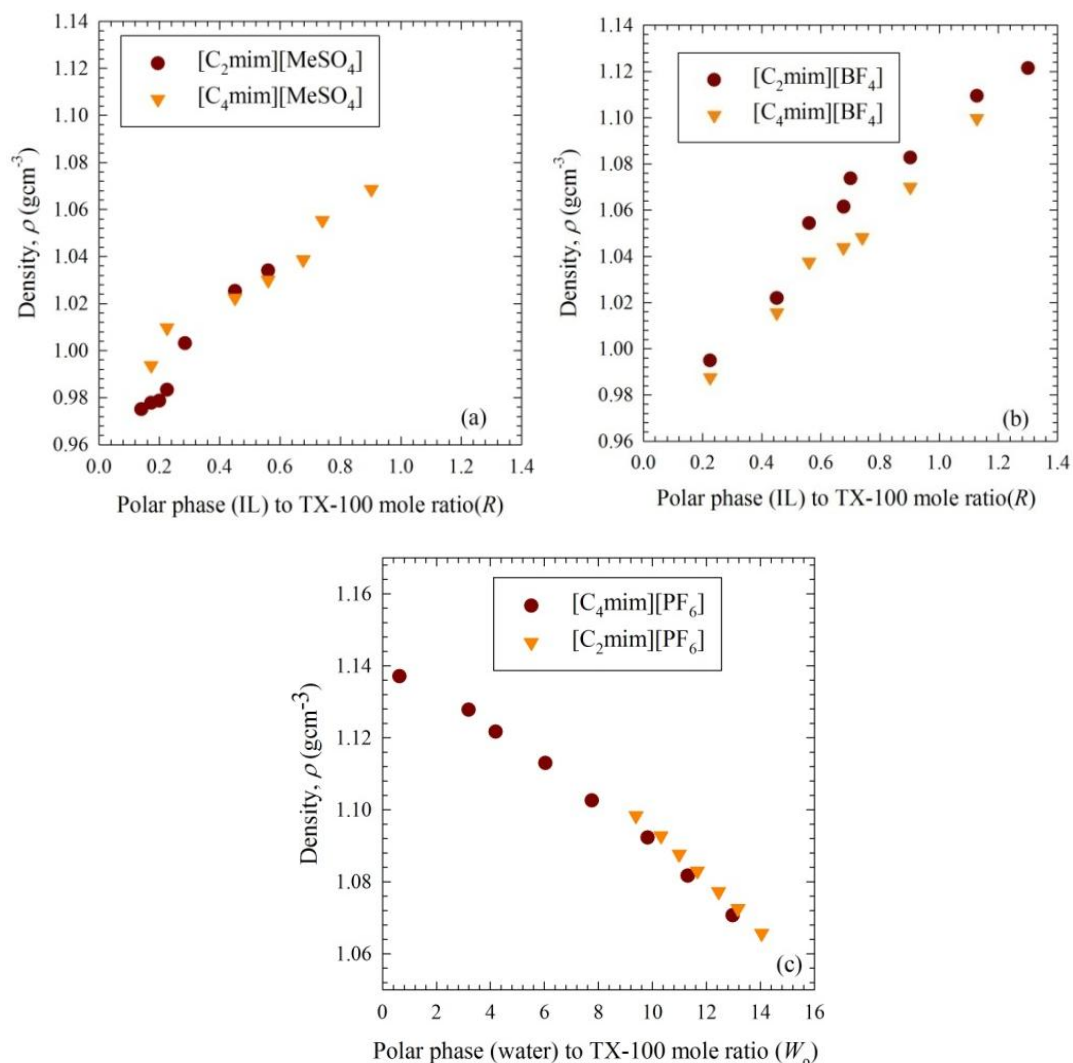


Figure 3.3.21. Density of (a) TX-100/cyclohexane/[C₂mim][MeSO₄] and TX-100/cyclohexane/[C₄mim][MeSO₄], (b) TX-100/cyclohexane/[C₂mim][BF₄] and TX-100/cyclohexane/[C₄mim][BF₄] (c) TX-100/[C₂mim][PF₆]/water and TX-100/[C₄mim][PF₆]/water microemulsions as a function of R or W_o at 25 °C.

In the microemulsions when polar phase is IL and nonpolar phase is cyclohexane (Figure 3.3.21 (a, b)), the density of IL plays an important role for the microemulsion systems. Density of ILs are higher compared to cyclohexane. For these four systems

the total mass of microemulsion was kept constant. With increasing R the amount of IL increases and simultaneously the amount of cyclohexane decreases to keep the total mass constant. Thus increasing R increases density. When the polar phase is water and nonpolar phase is IL (Figure 3.3.21 (c)), increasing W_o results in decreasing density since density of water is lower than IL.

3.3.3.4.2. Effect of Temperature on Density

Figure 3.3.22 (a, b) shows the effect of temperature on density for different series of TX-100 microemulsions at $R = 0.2255$ (Appendices Tables A35-36.). From Figure 3.3.22 (a, b), it can be seen that the density of the microemulsions decrease with increasing temperature for $R = 0.2255$.

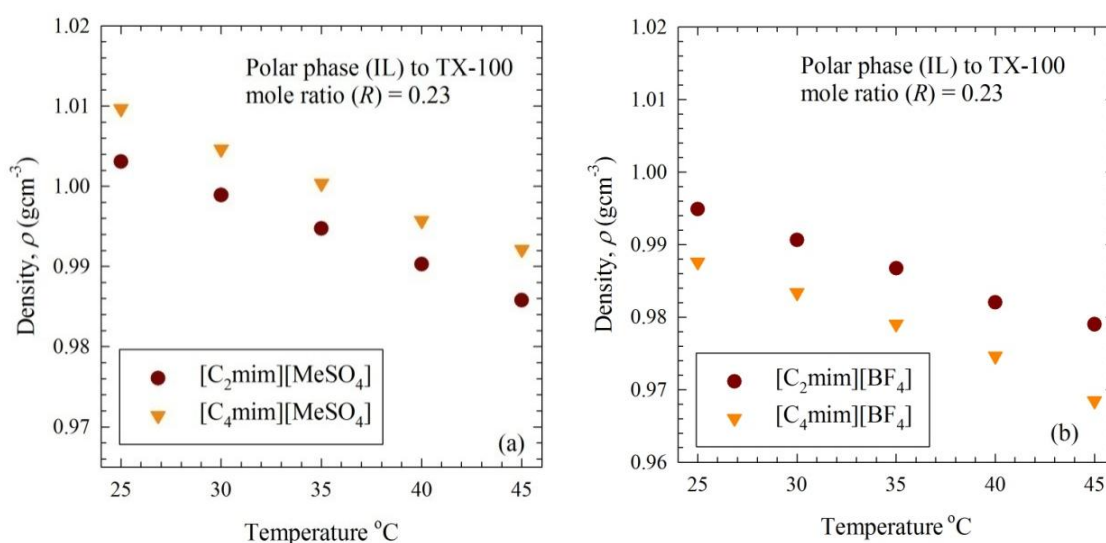


Figure 3.3.22. Effect of temperature on density of (a) TX-100/cyclohexane/[C₂mim][MeSO₄] and TX-100/cyclohexane/[C₄mim][MeSO₄], (b) TX-100/cyclohexane/[C₂mim][BF₄] and TX-100/cyclohexane/[C₄mim][BF₄] microemulsions at $R = 0.2255$.

For all the four series of microemulsions, the density decreases with increasing temperature since volume of the dispersed phase (cyclohexane) increases as temperature increases.

3.3.3.5. Refractive Index

3.3.3.5.1. The Influence of R or W_o

Figure 3.3.23 shows the change of refractive index of different series of TX-100 microemulsions with increasing R or W_o at 25 °C (Appendices Tables A37-39.). Change of refractive index with increasing R or W_o value follow different patterns for the six different microemulsion series.

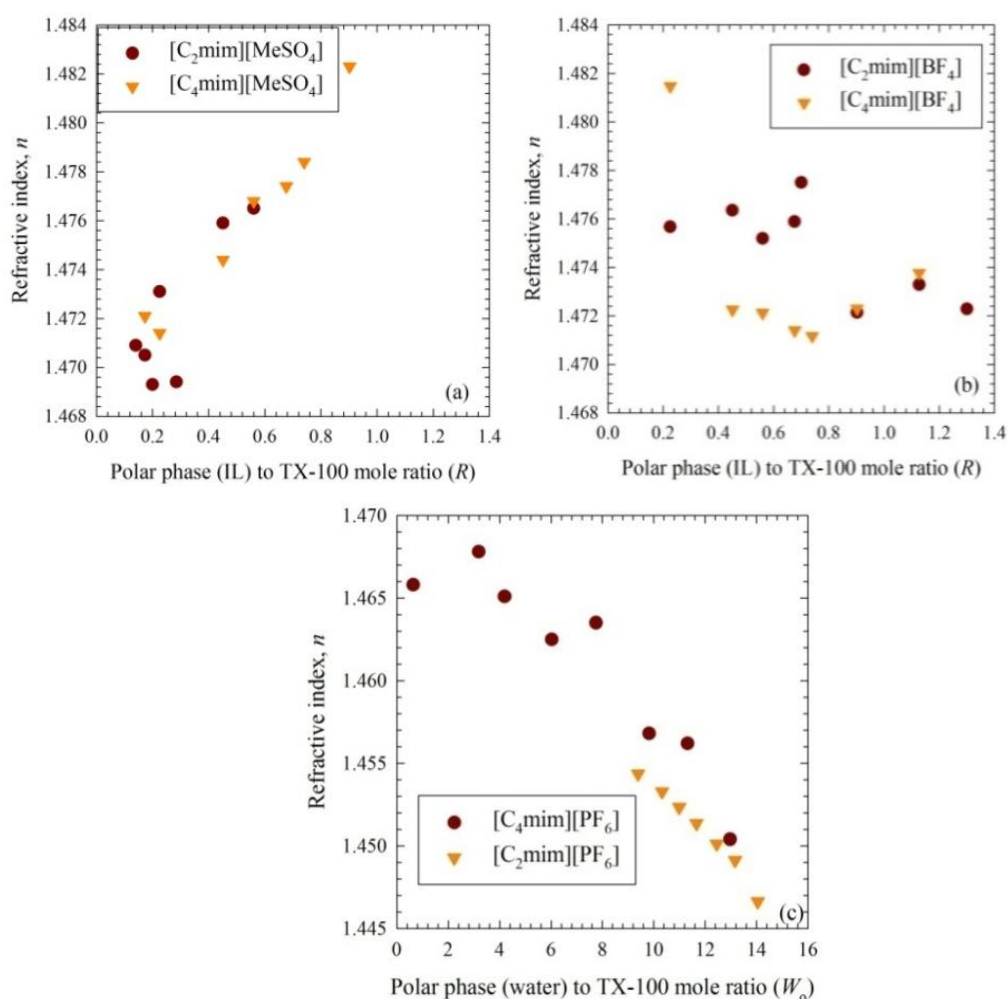


Figure 3.3.23. Refractive index of (a) TX-100/cyclohexane/ $[C_2mim][MeSO_4]$ and TX-100/cyclohexane/ $[C_4mim][MeSO_4]$, (b) TX-100/cyclohexane/ $[C_2mim][BF_4]$ and TX-100/cyclohexane/ $[C_4mim][BF_4]$ (c) TX-100/ $[C_2mim][PF_6]$ /water and TX-100/ $[C_4mim][PF_6]$ /water microemulsions as a function of R or W_o at 25 °C.

Increasing W_o , refractive index shows almost decreasing trend in TX-100/ $[C_4mim][PF_6]$ /water microemulsion (Figure 3.3.23. (c)). Change of refractive index with W_o for other microemulsion series is similar to that observed for other microemulsions as discussed in Section 3.3.1.5.1.

3.3.3.5.2. Effect of Temperature on Refractive Index

Figure 3.3.24 (a, b) shows the effect of temperature on refractive index of different series of TX-100 microemulsions at $R = 0.2255$ (Appendices Tables A40-41.). From Figure 3.3.24 (a), it can be seen that the refractive index of the microemulsions decreases with increasing temperature up to 30 °C and remain almost constant up to 35 °C and then again increases up to 40 °C and remain almost constant up to 45 °C for TX-100/cyclohexane/ $[C_4mim][MeSO_4]$ microemulsions. Refractive index of the microemulsions decreases with increasing temperature for TX-100/cyclohexane/ $[C_2mim][MeSO_4]$ microemulsions. From Figure 3.3.24 (b), it can be

seen that the refractive index of the microemulsions decreases with increasing temperature for TX-100/cyclohexane/[C₄mim][BF₄] microemulsions. Refractive index of the microemulsions decreases with increasing temperature upto 35 °C and then increases upto 40 °C and then again decreases upto 45 °C for TX-100/cyclohexane/[C₂mim][MeSO₄] microemulsions.

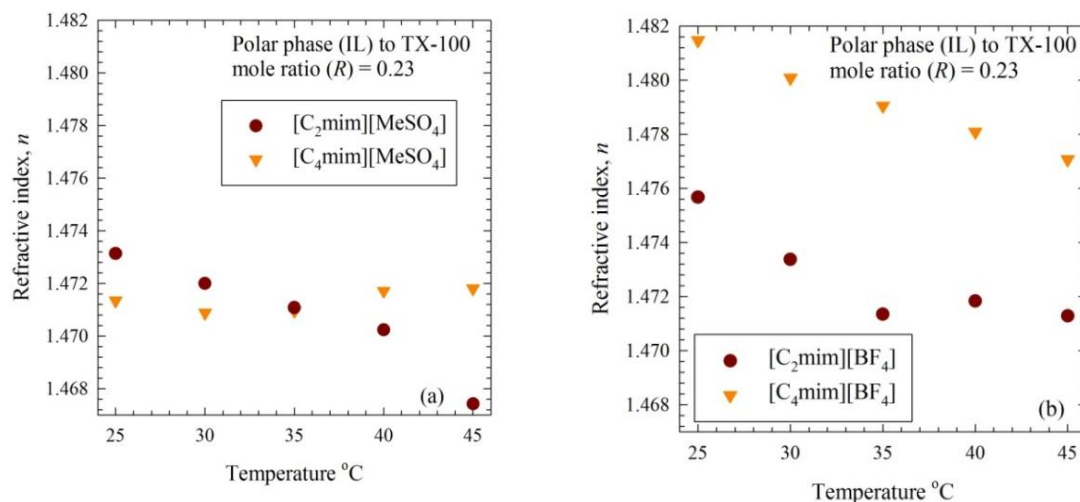


Figure 3.3.24. Effect of temperature on refractive index of (a) TX-100/cyclohexane/[C₂mim][MeSO₄] and TX-100/cyclohexane/[C₄mim][MeSO₄], (b) TX-100/cyclohexane/[C₂mim][BF₄] and TX-100/cyclohexane/[C₄mim][BF₄] at $R = 0.2255$.

Near temperature 40 °C, 35 °C and 35 °C for TX-100/cyclohexane/[C₂mim][MeSO₄], TX-100/cyclohexane/[C₄mim][MeSO₄] and TX-100/cyclohexane/[C₂mim][BF₄] microemulsions respectively, phase transition might have occurred from IL/o to bicontinuous microemulsion.

3.3.3.6. Polarity

Figure 3.3.25 shows the observed λ_{max} values in UV-visible absorption spectrum for zwitterionic RBD dye for (a) TX-100/cyclohexane/[C₄mim][BF₄] and (b) TX-100/cyclohexane/[C₂mim][BF₄] microemulsions at different R at 25 °C where the concentration of RBD was 1.25×10^{-4} M. No significant change in absorption is observed in the visible range of absorption spectra of RBD in TX-100 microemulsions.

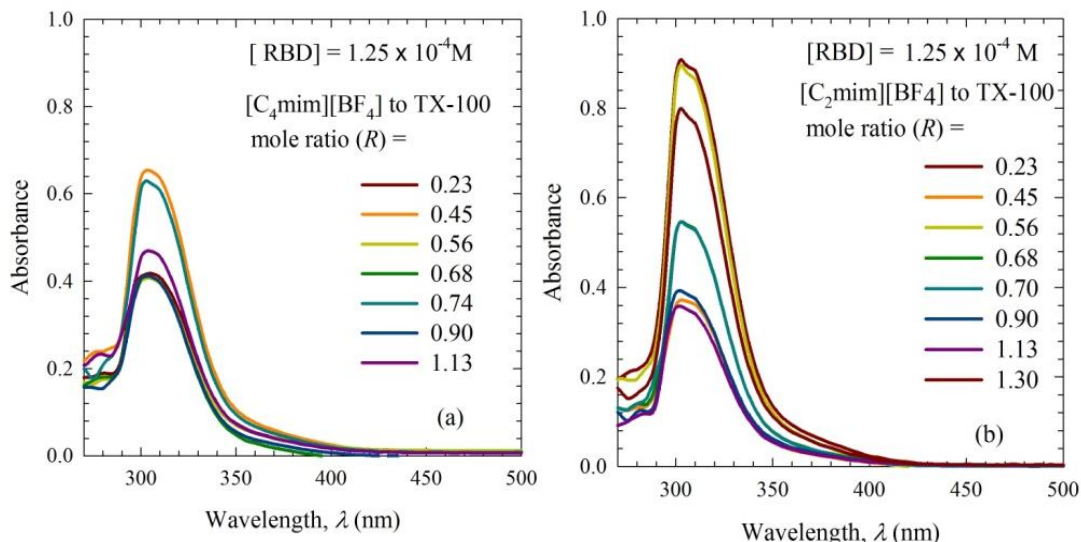


Figure 3.3.25. Absorption spectra of RBD in (a) TX-100/cyclohexane/[C₄mim][BF₄] and (b) TX-100/cyclohexane/[C₂mim][BF₄] microemulsions at different R at 25 °C

3.3.3.7. Surface Tension

Figure 3.3.26 shows the change of surface tension of TX-100/[C₂mim][PF₆]/water ($W_o = 14.0421, 13.1624, 11.6622, 10.9897, 10.3186, 9.9697$) and TX-100/[C₄mim][PF₆]/water ($W_o = 11.3113$) microemulsions as a function of W_o at 25 °C (Appendices Table A42.).

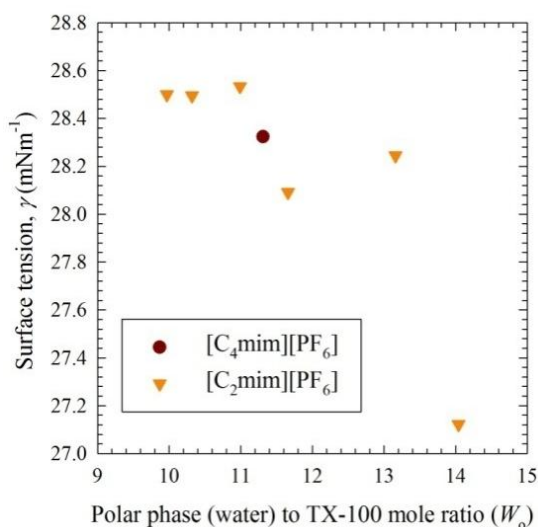
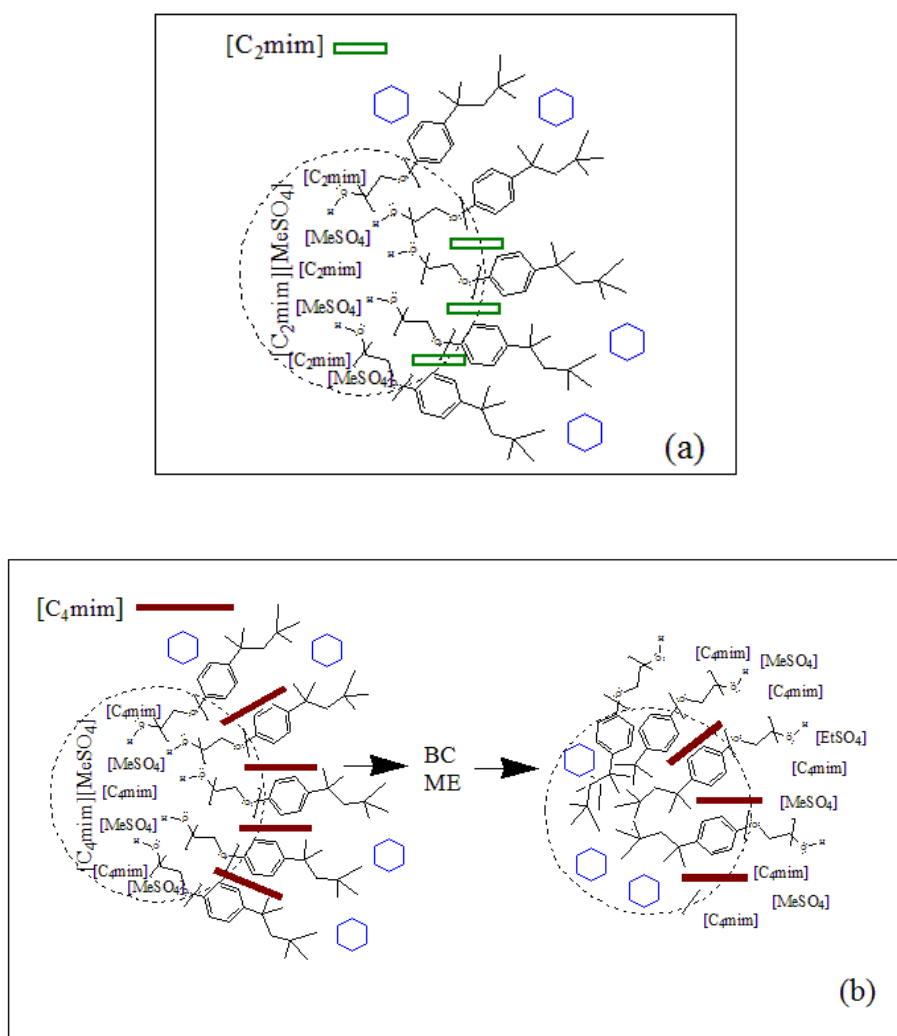


Figure 3.3.26. Surface tension of TX-100/[C₂mim][PF₆]/water and TX-100/[C₄mim][PF₆]/water microemulsions as a function of W_o at 25 °C.

Surface tension of [C₂mim][PF₆] based microemulsions with $W_o = 14.0421, 13.1624, 11.6622, 10.9897, 10.3186, 9.9697$ shows the value of 27.122, 28.245, 28.092, 28.534, 28.495, and 28.500 mN m⁻¹ respectively and for [C₄mim][PF₆] based microemulsions with $W_o = 11.3113$ shows the value of 28.324 mN m⁻¹.

3.3.4. Effect of Nonpolar Chain Length of Cations of ILs on Physicochemical Properties of Microemulsions

When the ions of IL in IL/o microemulsions move from reverse micelle core to the interfacial layer of surfactant, the nonpolar side chain of the cations experience hydrophobic interactions with the tail part of TX-100 (Scheme 3.2). This means, the more carbon atoms present in the nonpolar side chain of cations, the stronger hydrophobic interactions is formed with the tail part of TX-100. If strong hydrophobic interaction exists between hydrophobic side chain of cations and TX-100 tail group, the cations prefer to be exposed to the bulk.



Scheme 3.2. Interaction and arrangement of ions of ILs in (a) IL/o microemulsion for TX-100/cyclohexane/[C₂mim][MeSO₄] system and (b) IL/o, bicontinuous (BC) and o/IL microemulsions for TX-100/cyclohexane/[C₄mim][MeSO₄] systems.

In IL/o microemulsions like TX-100/cyclohexane/[C₂mim][MeSO₄] and TX-100/cyclohexane/[C₄mim][MeSO₄] systems, as the nonpolar side chain of [C₄mim]⁺ is longer compared to [C₂mim]⁺, hydrophobic-hydrophobic interaction is stronger between the side chain of [C₄mim]⁺ and TX-100 tail part (Scheme 3.3). So, [C₄mim]⁺ can expose to the bulk easily, resulting in higher conductivity and droplet size of reverse micelles and lower viscosity for TX-100/cyclohexane/[C₄mim][MeSO₄] (Figure 3.3.13 (a), 3.3.16 (a) and 3.3.18) compared to TX-100/cyclohexane/[C₂mim][MeSO₄] system. Unlike the reverse micelle dominated system where cation plays the important role for increasing the conductivity, for micelle dominated microemulsions in TX-100/cyclohexane/[C₄mim][MeSO₄] system, anion plays the important role for the same.

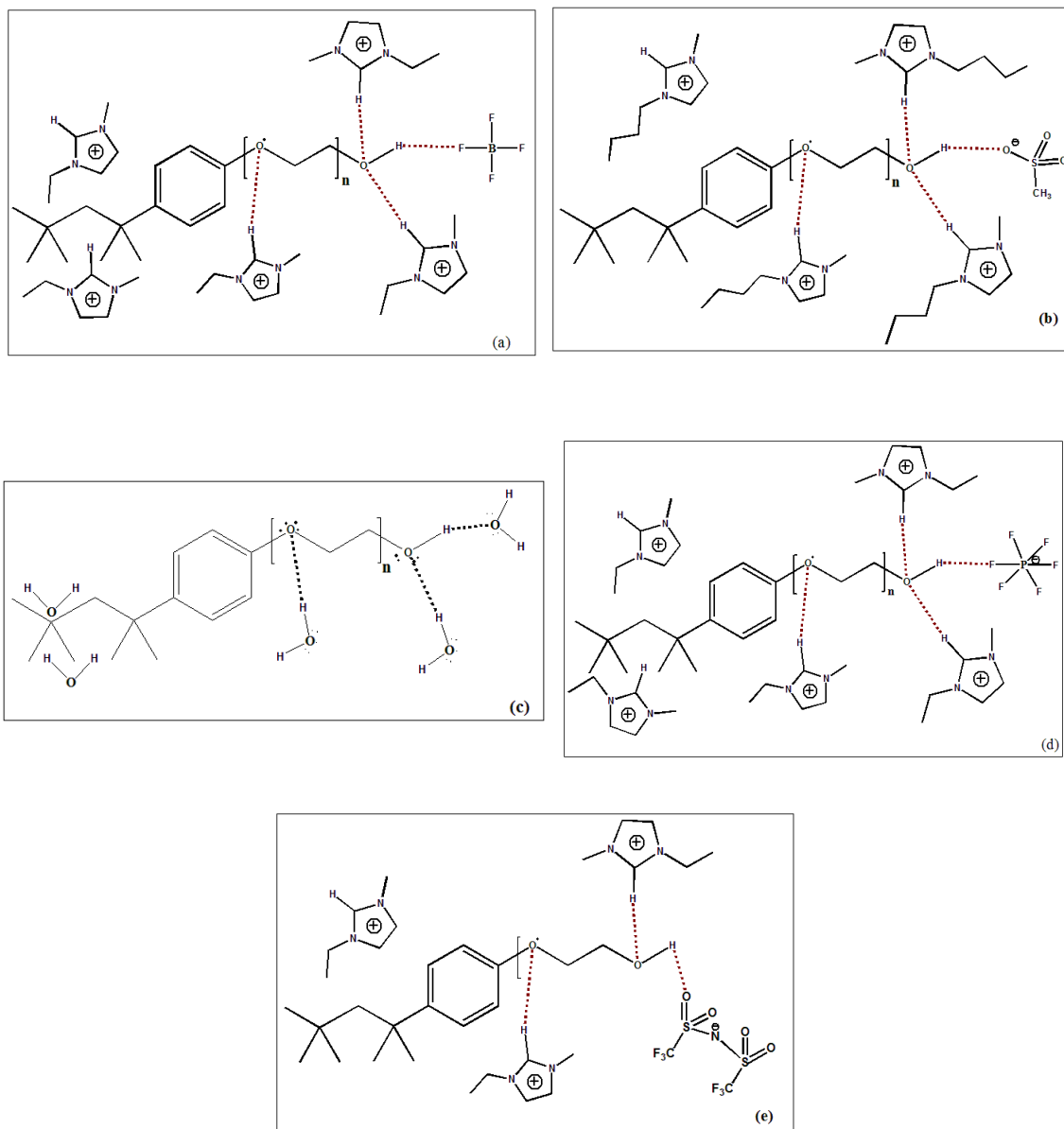
3.3.5. Interactions of Surfactant with Polar and Non-polar Phase of Microemulsions

Cations and anions of hydrophilic ([C₂mim][EtSO₄], [C₂mim][BF₄], [C₄mim][BF₄], [C₂mim][MeSO₄], and [C₄mim][MeSO₄]) can have electrostatic attraction, and tendency to form H-bond and van der Waals interaction with TX-100 which has hydrophobic tail part and hydrophilic head part [47-50]. For example, fluorine atoms of [BF₄]⁻ in [C₂mim][BF₄] or oxygen atoms of [MeSO₄]⁻ or [EtSO₄]⁻ can form hydrogen bonds with the hydrogen atoms of terminal -OH group from polyethylene oxide of TX-100 and the hydrogen atoms adjacent to the C-2 carbon of [C₂mim]⁺ can form hydrogen bonds with the oxygen atoms of polyethylene oxide of TX-100. Hydrophobic-hydrophobic interaction occurs between the long side chain (containing ethyl and methyl groups) of the imidazolium cation and tail part of TX-100 (Scheme 3.3 (a) and (b)). When hydrophilic IL is used as the polar phase, the oil phase is cyclohexane which can form hydrophobic-hydrophobic interaction with the tail part of TX-100.

When hydrophobic IL is used as the oil phase, polar phase is water. Some water molecules can be entrapped in the tail part of TX-100. Hydrogen bonds can be formed between the head group of TX-100 and water. Oxygen atoms in water can form hydrogen bonds with the hydrogen atoms of terminal -OH group of polyethylene oxide and hydrogen atoms in water can form hydrogen bonds with the oxygen atoms from the polyethylene oxide chain of TX-100 (Scheme 3.3 (c)).

Cations and anions of hydrophobic ILs ([C₂mim][TFSI], [C₂mim][PF₆] and [C₄mim][PF₆]) thus can form bond with TX-100 in many ways [51,52]. Fluorine atoms of [PF₆]⁻ in [C₂mim][PF₆] can form hydrogen bonds with the hydrogen atoms from the terminal -OH groups of polyethylene oxide of TX-100 (Scheme 3.3 (d)).

Again, oxygen atoms from [TFSI]⁻ in [C₂mim][TFSI] can form hydrogen bonds with the hydrogen atoms from the terminal -OH groups of polyethylene oxide of TX-100 (Scheme 3.3 (e)). A resonance structure of [TFSI]⁻ may exist due to the delocalization of electrons over the sulfur-nitrogen π -bonding [53].

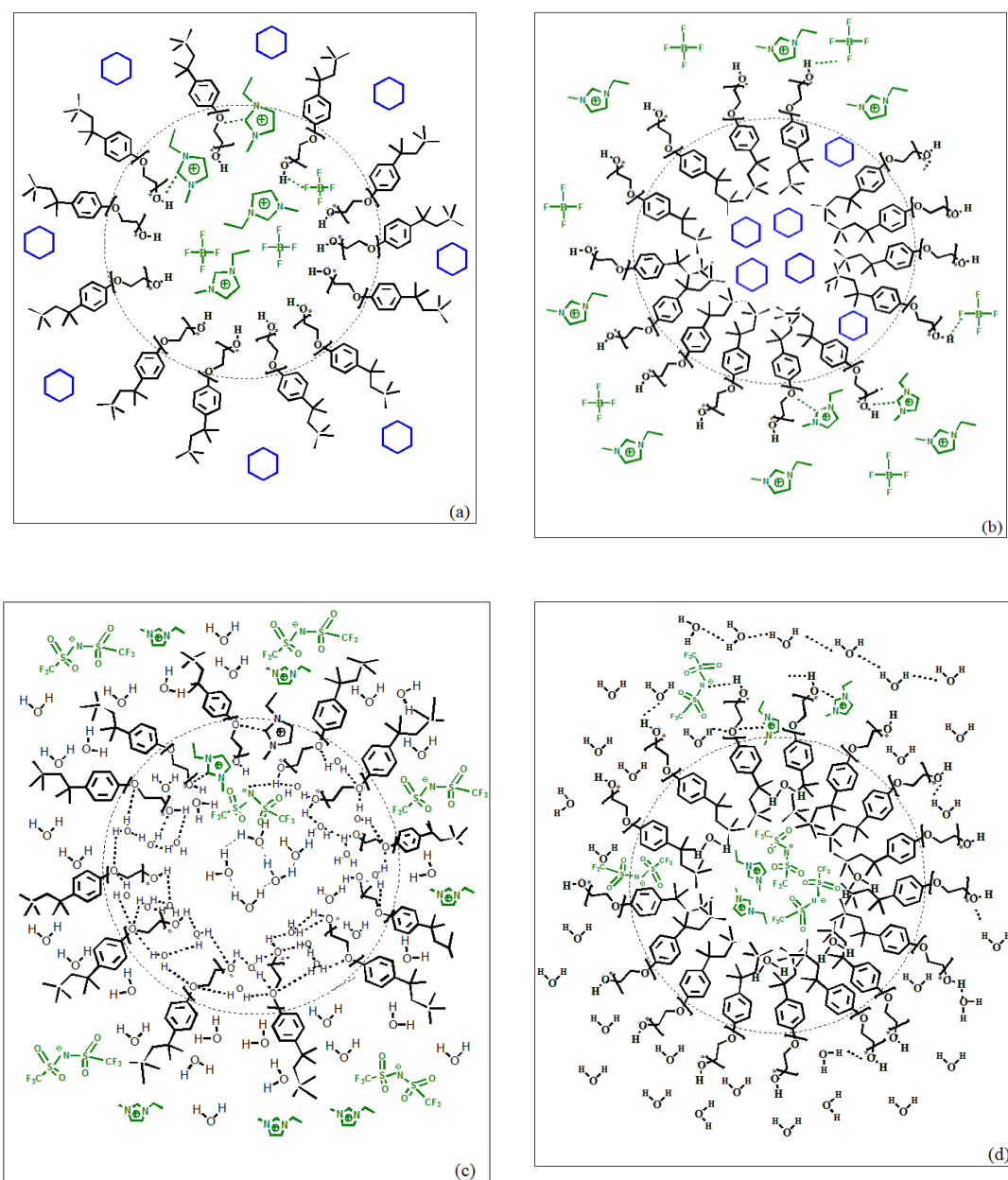


Scheme 3.3. Interactions of TX-100 through different hydrogen bonding sites with (a) [C₂mim][BF₄], (b) [C₄mim][MeSO₄], (c) water and oil phase (d) [C₂mim][PF₆], (e) [C₂mim][TFSI].

3.3.6. Probable Organization of Different Components in Microemulsion Systems

For hydrophilic IL based microemulsions like TX-100/cyclohexane/[C₂mim][EtSO₄], TX-100/cyclohexane/[C₂mim][BF₄], TX-100/cyclohexane/[C₄mim][BF₄] and TX-100/cyclohexane/[C₄mim][MeSO₄], at low R , the polar phase (IL) is trapped into the cores of reverse micelle droplets, while the nonpolar phase (i.e. cyclohexane) resides in the bulk as the continuous medium (Scheme 3.4 (a)). With increasing R , the systems undergo transition from IL/o to o/IL via bicontinuous microemulsions. In o/IL microemulsions, IL exists in the bulk and cyclohexane is now encapsulated inside

the core of micelle droplets (Scheme 3.4 (b)). For TX-100/cyclohexane/[C₂mim][MeSO₄] microemulsion, only the reverse micelle dominated microemulsions exist.



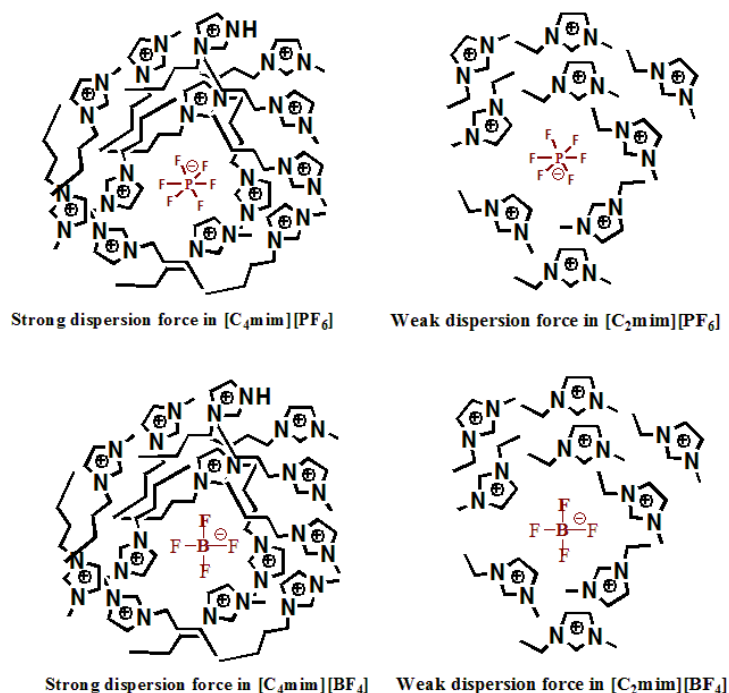
Scheme3.4. Arrangement of substances in reverse micelle droplets for (a) TX-100/cyclohexane/[C₂mim][BF₄] and (c) TX-100/[C₂mim][TFSI]/water microemulsions and micelle droplets for (b) TX-100/cyclohexane/[C₂mim][BF₄] and (d) TX-100/[C₂mim][TFSI]/water microemulsions.

On the contrary, for hydrophobic IL based microemulsions like TX-100/[C₂mim][TFSI]/water, at low W_o , the polar phase (i.e. water) is trapped inside the core of reverse micelle droplets and the nonpolar phase (IL) exists as the continuous medium (Scheme 3.4 (c)). As W_o increases, the systems convert from o/IL to IL/o via

bicontinuous microemulsions. Water now accumulates in the bulk and ILs become encapsulated inside the cores of micelle droplets (Scheme 3.4 (d)). For TX-100/[C₂mim][PF₆]/water microemulsion, only the micelle dominated microemulsion exists.

3.3.7. Dispersive and Inductive Forces in ILs

While strong Coulombic interaction exists between cations and anions of IL, hydrogen bonding, dispersive and inductive forces also play important roles in their bonding nature. ILs with spherical anions possess strong Coulombic interaction between the cations and anions. As a result of increasing hydrophobic side chain length of the cation, a competition arises between the Coulombic forces and the dispersive and inductive forces [46]. Relaxation of the Coulombic force occurs with increasing side chain length. But inductive and dispersive forces gradually increase and start to dominate the system as the length of the side chain increases. Therefore, dispersive and inductive forces between [C₄mim]⁺ and [PF₆]⁻ is stronger than those between [C₂mim]⁺ and [PF₆]⁻ (Scheme 3.5). Association of the cations with anions is much easier when the anions are spherical in shape. Thus, [C₄mim]⁺ ions around the spherical [PF₆]⁻ ions have stronger dispersive and inductive forces due to the longer butyl side chain in [C₄mim]⁺. So, the dissociation of [C₄mim]⁺ from [PF₆]⁻ is more difficult compared to [C₂mim]⁺ from [PF₆]⁻. Thus the conductivity of TX-100/[C₂mim][PF₆]/water microemulsion is higher than that of TX-100/[C₄mim][PF₆]/water microemulsion (Figure 3.3.13 (c)). Same explanation applies for [C₂mim][BF₄] and [C₂mim][BF₄] ILs in TX-100/cyclohexane/[C₂mim][BF₄] and TX-100/cyclohexane/[C₄mim][BF₄] microemulsion systems.



Scheme 3.5. Arrangement of the cations around spherical anions in IL.

3.4. Conclusions

The physicochemical properties of series of microemulsions with variation of polar and nonpolar phases, i.e. TX-100/cyclohexane/hydrophilic IL and TX-100/hydrophobic IL/water microemulsions, were found to change with changing R or W_o values. Conductivity, reverse micelle droplet size, and viscosity of TX-100/cyclohexane/hydrophilic IL microemulsions increase with increasing R , during variation of both cations and anions. The conductivity of TX-100/[C₂mim][TFSI]/water microemulsions first increases with W_o upto $W_o \approx 8.0$ and then decreases with increasing W_o , while viscosity shows an opposite trend. Conductivities and viscosities of TX-100/[C₂mim][PF₆]/water microemulsions decrease and increase respectively with increasing W_o . The micelle droplet size was found to increase with increasing W_o for these microemulsions. Variation of those physicochemical properties were explained considering the fact that the electrostatic interaction between the cation and anion of IL decreases with increasing length of nonpolar side chain of the cation or anion. Moreover, cations of IL can easily associate with or dissociate from anions if the latter have spherical shapes. Dispersive and inductive forces increase as the nonpolar side chain length of cation around the spherical anion ([PF₆]⁻, [BF₄]⁻) of IL increases. These properties of IL play an important role in determining the physicochemical properties of microemulsions.

References

- [1] Lawrence, M. J.; Rees, G. D. *Adv. Drug Deliv. Rev.* **2000**, *45*, 89-121.
- [2] Bhargava, H. N.; Narukar, A.; Lieb, L. M. *Pharm. Technol.* **1987**, *11*, 46-52.
- [3] Shukla, A.; Kiselev, M. A.; Hoell, A.; Neubert, R., H. *J. Phys.* **2004**, *63*, 291-295.
- [4] Mitra, D.; Chakraborty, I.; Bhattacharya, S.C.; Moulik, S.P. *J. Phys. Chem. B* **2006**, *110*, 11314-11426.
- [5] Paul, S.; Panda, A. K. *J. Surfact. Deterg.* **2011**, *14*, 473-486.
- [6] Zhang W.; Qiao, X.; Chen, J. *Mat. Chem. Phys.* **2008**, *109*, 411-416.
- [7] Sripriya, R.; Raja, K. M.; Santhosh, G; Chandrasekaran, M.; Noel, M. *J. Colloid Interface Sci.* **2007**, *314*, 712-717.
- [8] Ruiz, C. C. *Colloid. Polym. Sci.* **1995**, *273*, 1033-1040.
- [9] Saha, R.; Rakshit, S.; Mitra, R. ; Pal, S. K. *Langmuir* **2012**, *28*, 8309-8317.
- [10] Yang, C. J.; Zeng, Q. R.; Yang, H. J.; Zou, Chin, M. Y. *J. Anal. Chem.* **2006**, *5*, 642-646.
- [11] Liu, Y.; Guo, R.; Guo, X. *J. Phys. Chem. B* **2006**, *110*, 784-790.
- [12] Bera, A.; Mandal, A.; Kumar, T. *J. Chem. Eng. Data* **2014**, *59*, 2490-2498.
- [13] Fletcher, P. D. I.; Morris, J. S. *Colloid Surface A* **1995**, *98*, 147-154.
- [14] Fletcher, P. D. I.; Suhling, K. *Langmuir* **1998**, *14*, 4065-4069.
- [15] Jayalakshmi, Y.; Beysens, D. *Phys. Rev. A* **1992**, *45*, 8709-8718.
- [16] Kizilbash, N. A.; Asif, S.; Nazar, M. F.; Shah, S. S.; Alenizi, D. *J. Chem. Soc. Pak.* **2011**, *33*, 1-6.
- [17] Mehta, S. K.; Kawaljit, *Colloid Surface A* **1998**, *136*, 35-41.

- [18] Fanun, M.; Ayad, Z.; Mudalal, S.; Dahoah, S.; Meltzer, D.; Schwarze, M.; Schomacker, R.; Blum, J. *J. Surfactants Deterg.* **2012**, 15, 505-512.
- [19] Kumar, B.; Jain, S. K.; Prajapati, S. K.; Mahor, A.; Kumar, A. *Int. J. Pharm. Sci. Res.* **2010**, 1, 57-74.
- [20] Zala, B. H.; Pandya, R. B.; Prajapat, M. D.; Ramkishan, A.; Parikh, R. K.; Gohel, M. C. *J. Pharm. Sci. Res.* **2011**, 4, 930-933.
- [21] E. Ramadan, T. Borg, G. M. Abdelghani, Saleh, N. M. *Bull. Pharm. Sci.* **2013**, 36, 31-47.
- [22] Basheer, H. S.; Noordin, M. I.; Ghareeb, M. M. *Trop. J. Pharm. Res.* **2013**, 12, 305-310.
- [23] Patel, V.; Kukadiya, H.; Mashru, R.; Surti, N.; Mandal, S. *Iran. J. Pharm. Res.* **2010**, 9, 327-334.
- [24] Goffredi, M.; Liveri, V. T.; Vassallo, G. *J. Solution Chem.* 1993, 22, 941-949.
- [25] Sharma, S. C.; Tsuchiya, K.; Sakai, K.; Sakai, H.; Abe, M. *Langmuir* **2008**, 24, 7658-7662.
- [26] Jahn, W.; Strey, R. *J. Phys. Chem.* **1988**, 92, 2294-2301.
- [27] Jahn, W.; Strey, R. *Physics of Amphiphilic Layers* **1987**, 21, 353-356.
- [28] Senatra, D. *Thermochim. Acta* **2000**, 345, 39-46.
- [29] Senatra, D.; Pratesi, R.; Pieraccini, L. *J. Therm. Anal. Calorim.* **1998**, 51, 79-90.
- [30] Grassi, M.; Grassi, G.; Lapasin, R.; Colombo, I. *Understanding Drug Release and Absorption Mechanisms: A Physical and Mathematical Approach*, Taylor and Francis, CRC press, New York **2007**, 493.
- [31] Quemada, D.; Langevin, D. *J. Theor. Appl. Mech.* **1985**, 201.
- [32] Huang, J. S.; Safran, S. A.; Kim, M. W.; Grest, G. S.; Kotlarchyk, M.; Quirke, N. *Phys. Rev. Lett.* **1984**, 53, 592-595.
- [33] Eicke, H. F.; Bercovec, M.; Das-Gupta B. *J. Phys. Chem.* **1989**, 93, 314-317.
- [34] Ponton, A.; Bose, T. K. *J. Chem. Phys.* **1991**, 94, 6879-6886.
- [35] Kim, M. W.; Huang, J. S. *Phys Rev. A.* **1986**, 34, 719-722.
- [36] Dijk, M. A.; Casteleijn, G.; Joosten, J. G. H.; Levine Y. K. *J. Chem. Phys.* **1986**, 85, 626-631.
- [37] Tsuzuki S.; Tokuda H.; Hayamizu K.; Watanabe M. *J. Phys. Chem. B* **2005**, 109, 16474-16481.
- [38] Pramanik, R.; Ghatak, C.; Rao, V. G.; Sarkar, S.; Sarkar, N. *J. Phys. Chem. B* **2011**, 115, 5971-5979.
- [39] Pramanik, R.; Sarkar, S.; Ghatak, C.; Rao, V. G.; Sarkar, N. *J. Phys. Chem. B* **2011**, 115, 2322-2330.
- [40] Falcone, R. D.; Correa, N. M.; Silber, J. J. *Langmuir* **2009**, 25, 10426-10429.
- [41] Gao, Y. N.; Li, N.; Hilfert, L.; Zhang, S. H.; Zheng, L. Q.; Yu, L. *Langmuir* **2009**, 25, 1360-1365.
- [42] Pramanik, R.; Ghatak, C.; Rao, V. G.; Sarkar, S.; Sarkar, N. *J. Phys. Chem. B* **2011**, 115, 5971-5979. *Phys. Chem. B* 2007, 111, 598-604.
- [43] Pramanik, R.; Sarkar, S.; Ghatak, C.; Rao, V. G.; Sarkar, N. *J. Phys. Chem. B* **2011**, 115, 2322-2330.
- [44] Gao, Y.; Han, S.; Han, B.; Li, G.; Shen, D.; Li, Z.; Du, J.; Hou, W.; Zhang, G. *Langmuir* **2005**, 21, 5681-5684.
- [45] Wei, J.; Su, B.; Xing, H.; Bao, Z.; Yang, Y.; Ren, Q. *Colloid Surface A* **2012**, 396, 213-218.
- [46] Gao, Y.; Zhang, J.; Xu, H.; Zhao X.; Zheng, L.; Li, X.; Yu, L. *ChemPhysChem* **2006**, 7, 1554-1561.

- [47] Gao, Y.; Li, N.; Zheng, L.; Bai, X.; Yu, L.; Zhao, X.; Zhang, J.; Zhao, M.; Li, Z. *J. Phys. Chem. B* **2007**, 111, 2506-2513.
- [48] Qiu, Z.; Texter, J. *Colloid Interface Sci.* **2008**, 13, 252-262.
- [49] Mehta, S. K.; Kaur, K. *Indian J. Chem., Sect A* **2010**, 49, 662-684.
- [50] [59] Łuczak, J.; Hupka, J. *J. Mol. Liq.* **2014**, 199, 552-558.
- [51] [60] Lian, Y.; Zhao, K. *Soft Matter*, **2011**, 7, 8828-8837.
- [52] Tokuda H.; Tsuzuki S.; Susan M. A. B. H.; Hayamizu K.; Watanabe M. *J. Phys. Chem. B* **2006**, 110, 19593-19600.
- [53] Ruff J. K. *Inorg. Chem.* **1965**, 4, 1446-1449.

Abstract

Physicochemical properties of different IL based microemulsions have been studied and compared which were prepared using CTAB as the surfactant and cyclohexane, hydrophilic ILs ([C₂mim][EtSO₄], [C₄mim][MeSO₄], and [C₂mim][MeSO₄]) and 1-butanol as the nonpolar phase, polar phase and cosurfactant, respectively. The conductivity, viscosity and droplet sizes of the microemulsions were found to increase with increasing R . As the anions are varied, conductivities of [C₂mim][EtSO₄] based microemulsions show higher values compared to [C₂mim][MeSO₄] based microemulsions, while the viscosities show an opposite trend. Droplet sizes of [C₂mim][EtSO₄] based microemulsions are larger than [C₂mim][MeSO₄] based ones. During variation of IL cations in the microemulsions, on the other hand, conductivities of [C₄mim][MeSO₄] based microemulsions show higher values compared to those of [C₂mim][MeSO₄] based microemulsions; while the viscosities of the latter were higher, in contrast. [C₄mim][MeSO₄] based microemulsions possess larger droplets than [C₂mim][MeSO₄] based microemulsions. At $R = 1.5424$, the microemulsions show the following trend in surface tension; [C₂mim][MeSO₄] > [C₄mim][MeSO₄] > [C₂mim][EtSO₄]. Density and refractive index increase with increasing R for both cation and anion variations in the IL based microemulsions.

4.1. Introduction

The self-assembly of surfactants in contact with IL or any other polar media can form micelles [1–3], liquid crystals [4, 5], gels [6, 7], vesicles [8], and microemulsions [9, 10]. The incorporation of ILs into micelle cores result in significant changes in the aggregation number, size of the micelles in aqueous solutions and CMC for nonionic [11–13], ionic [14, 15] and zwitterionic surfactants [16].

Microemulsion, an optically isotropic and thermodynamically stable liquid, has received considerable attention due to their special properties (low interfacial tension, low viscosity, high solubilization capacity for both polar and nonpolar substances) and this media has potential applications in chemical, analytical, industrial, pharmaceutical as well as electrochemical processes [17, 18]. To characterize microemulsions different experimental techniques such as DLS, cyclic voltammetry, FEM, SAXS, SANS and differential scanning calorimetry, and measurement of different parameters like conductivity, viscosity, , refractive index, , interfacial tension, density, turbidity have been used [19-41].

For the formation of microemulsions, no cosurfactant is necessary when nonionic surfactants and ionic double chain surfactants such as AOT are used [42]. Surfactants reduce the interfacial tension between polar and nonpolar phases to a very low value in order to form stable microemulsions. For single chain ionic surfactants, cosurfactants (e.g. n -alcohols, n -amines) are necessary to attain the required low interfacial tension for the formation of stable microemulsions [43, 44].

In conventional microemulsion, water corresponds to a polar phase that can contain electrolytes and other additives and non-polar substances such as hydrocarbons, partially or totally chlorinated or fluorinated hydrocarbons, unbranched alkanes, cyclic or aromatic hydrocarbons, triglyceride natural oils which can be used [45] as an oil phase that is immiscible completely or at least to a certain extent with the polar phase. A great variety in microemulsion structure ranging from w/o via bicontinuous to o/w structures depends on the volume fraction of oil, water and amphiphile as well as on the nature of the interfacial film. Water can be replaced by glycerol, glycol, formamide or by a mixture of molten salts (nitrate mixtures of ethylenediamine / ammonia / potassium).

Apart from these classical microemulsions composed of water, oil and surfactant, ILs can be used as both polar and nonpolar phases for preparing microemulsions due to their unique properties. In nonaqueous IL based microemulsions, ILs are used instead of water. In IL/o microemulsion, the volume fraction of IL is low as oil is the continuous phase containing IL droplets; the scenario is opposite for o/IL microemulsions. Bicontinuous microemulsions can be formed at almost equal amounts of IL and oil components which are networks of oil and IL nanodomains separated and stabilized by a surfactant interfacial film with a net curvature close to zero.

Mainly IL/o microemulsions are useful in applications (Section 1.9. of Chapter 1). Highly conductive polar phase exists in IL based microemulsions and the thermal stability range can be expanded if ILs are used in microemulsions. At high R or ϕ_{IL} values of IL/o microemulsions, small channels are formed because two or more reverse micelle droplets coalesce or fuse. The channels make a path for the ions of ILs to move freely which results in high conductance of IL/o based microemulsions compared to the conventional w/o microemulsions. Recently, scientists have also been working on aqueous microemulsions containing ILs as oil the phase to avoid the use of volatile organic compounds (Section 1.9. of Chapter 1).

There have been numerous reports on the preparation and characterization of IL based microemulsions where non-ionic surfactants are used. The properties of such microemulsions have been reported in the literature. Chapter 3 also describes systematic variation of physicochemical properties for change in the structure of ionic liquids and composition for TX-100 microemulsions. The use of ionic surfactants, especially conventional cationic surfactant, CTAB is promising and requires systematic studies.

The goal of the work in this chapter is to study the effect of R , temperature, structure of cation and anion on the physicochemical properties of IL based microemulsions for CTAB. Structural variation has been achieved by increasing the number of carbon atoms in the anion (i.e. from $[\text{MeSO}_4]^-$ to $[\text{EtSO}_4]^-$) or lengthening the side chain of the cation (i.e. from $[\text{C}_2\text{mim}]^+$ to $[\text{C}_4\text{mim}]^+$) of ILs while keeping the cation or the

anion constant. From the analysis of physicochemical properties the interactions involved between different components of microemulsion has been analyzed and attempt has been made to represent a whole picture for the IL based microemulsion systems studied for CTAB.

4.2. Experimental

4.2.1. Materials

CTAB, cyclohexane, 1-butanol and the ILs, [C₂mim][EtSO₄], [C₂mim][MeSO₄] and [C₄mim][MeSO₄] were obtained from Sigma-Aldrich. RBD was received from Sigma Aldrich and the reagent grade ethanol was used to prepare stock solution of RBD. All the chemicals were used as received. The elaborated forms of the abbreviations have been given in Section 1.11. of Chapter 1.

4.2.2. Preparation of Microemulsions

IL based microemulsions with CTAB were prepared with a constant amount of CTAB (5 % wt) with variation of the polar and the nonpolar phases to keep the total weight of the microemulsion constant. Compositions IL based microemulsions with CTAB were discussed briefly in Sections 2.4.3. of Chapter 2.

4.2.3. Measurements

Experimental techniques such as measurement of conductivity, viscosity, density, refractive index, polarity and surface tension were used to characterize microemulsions. DLS measurements were to determine the sizes of microemulsion droplets. were measured by DLS measurement. Measurements have been described in detail in Section 3.2.3. of Chapter 3.

4.3. Results and Discussion

4.3.1. Physicochemical Properties of CTAB/1-Butanol/Cyclohexane/IL Microemulsions

4.3.1.1. Conductivity

4.3.1.1.1. The Influence of *R*

Figure 4.3.1 (a, b) shows the change of conductivity of different series of CTAB microemulsions with increasing *R* at 25 °C (Appendices Tables A43-44.). The conductivities of the microemulsions increase with increasing *R* for all the systems.

At low *R* values, the conductivity is low due to presence of the non-polar (cyclohexane) continuous media in the bulk of the reverse micelle dominated microemulsions. The variation in conductivity can be explained by the ability of migration of charged IL droplets to the non-polar cyclohexane continuous media [46, 47]. The IL droplets acquire charges owing to the fluctuating exchange of anions of IL in the cores of droplets with the charged surfactant heads at the droplet interface. As *R* values further increase in IL based microemulsions, conductivities continue to increase owing to the clustering of IL droplets in microemulsions caused from short range attractive interactions [48-53] and the easy movement of charge particles through the network channel by means of fusion, mass exchange, and subsequent

fission. The sticky droplets are in constant motion and experience collision with one another. With increasing R values furthermore, conductivities increase due to the formation of bicontinuous complex microstructure.

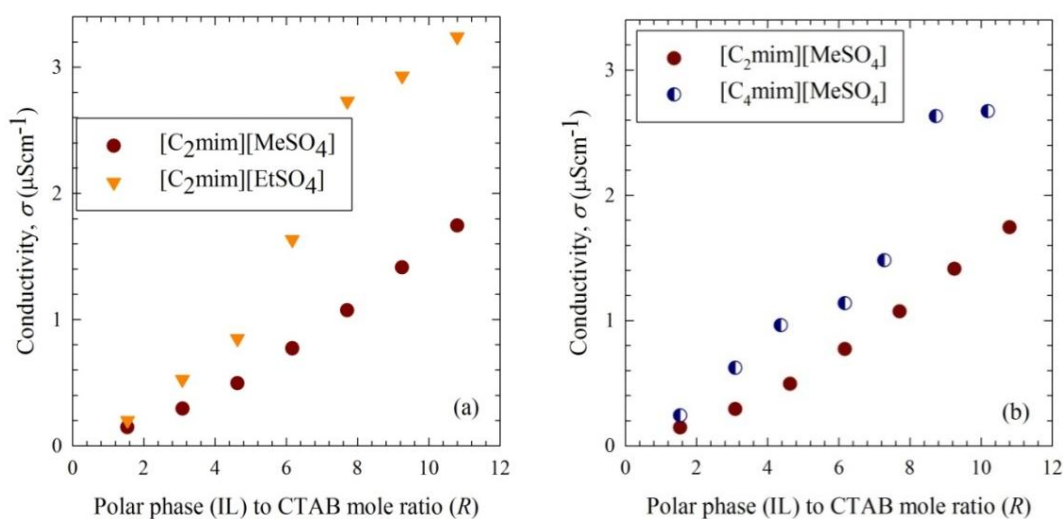


Figure 4.3.1. Variation of conductivity of (a) CTAB/1-butanol/cyclohexane/ $[\text{C}_2\text{mim}][\text{MeSO}_4]$ and CTAB/1-butanol/cyclohexane/ $[\text{C}_2\text{mim}][\text{EtSO}_4]$ (b) CTAB/1-butanol/cyclohexane/ $[\text{C}_2\text{mim}][\text{MeSO}_4]$ and CTAB/1-butanol/cyclohexane/ $[\text{C}_4\text{mim}][\text{MeSO}_4]$ microemulsions as a function of R at 25 °C.

4.3.1.1.2. The Influence of IL Anion

Two different types of ILs, $[\text{C}_2\text{mim}][\text{EtSO}_4]$ and $[\text{C}_2\text{mim}][\text{MeSO}_4]$ with variation of anions, $[\text{MeSO}_4]^-$ and $[\text{EtSO}_4]^-$ with a fixed cation, $[\text{C}_2\text{mim}]^+$ are used to analyze the influence of the structure of the anion on the physicochemical properties (Figure 4.3.1 (a)). The structures of the anions are shown in Scheme 2.1 (a, c, d).

Electrostatic attraction between the cation and anion in $[\text{C}_2\text{mim}][\text{EtSO}_4]$ is comparatively lower than that between the ions of $[\text{C}_2\text{mim}][\text{MeSO}_4]$ due to the relatively bulky size of $[\text{EtSO}_4]^-$ anion. Since the hydrophobic carbon chain in $[\text{EtSO}_4]^-$ anion is longer than that of $[\text{MeSO}_4]^-$ $[\text{EtSO}_4]^-$ possess more asymmetric nature i.e. the negative charge is less centered around $[\text{EtSO}_4]^-$ anion. This results in less electrostatic attraction in $[\text{C}_2\text{mim}][\text{EtSO}_4]$. On the other hand, in $[\text{MeSO}_4]^-$ anion negative charge density is higher due to its less asymmetric structure. So, the more centered negative charge around $[\text{MeSO}_4]^-$ anion results in stronger electrostatic attraction in $[\text{C}_2\text{mim}][\text{MeSO}_4]$. Due to the smaller size and small hydrophobic part of $[\text{MeSO}_4]^-$ anion, stronger electrostatic attraction acts between $[\text{C}_2\text{mim}]^+$ and $[\text{MeSO}_4]^-$ compared to $[\text{C}_2\text{mim}]^+$ and $[\text{EtSO}_4]^-$.

When IL is incorporated in the core of CTAB reverse micelle, anion of IL is attracted to the head group of CTAB due to the more centered positive charge on N atom in CTAB head group rather than the delocalized positive charge in the imidazolium cation (Scheme 4.2). In addition to this, the H atom of terminal -OH group of 1-

butanol also contains partial positive charge. The imidazolium cation stays closer to the anion of IL, while Br^- counterions have some attractive interaction with imidazolium cation.

When $[\text{EtSO}_4]^-$ moves towards the CTAB head group, due to the long alkyl chain of $[\text{EtSO}_4]^-$, the nonpolar tail part of CTAB forms strong hydrophobic-hydrophobic interaction with the ethyl chain of $[\text{EtSO}_4]^-$. $[\text{EtSO}_4]^-$ exposes in the bulk more easily than $[\text{MeSO}_4]^-$ with small alkyl chain. Therefore, conductivity of $[\text{C}_2\text{mim}][\text{EtSO}_4]$ based microemulsion system is larger than $[\text{C}_2\text{mim}][\text{MeSO}_4]$ based microemulsion system (Scheme 4.3 (A)) as shown in Figure 4.3.1 (a). Here, mobility of the anions is the main factor for increasing conductivity.

4.3.1.1.3. The Influence of Alkyl Side Chain Length of Imidazolium Cation

Two different types of ILs, $[\text{C}_4\text{mim}][\text{MeSO}_4]$ and $[\text{C}_2\text{mim}][\text{MeSO}_4]$ with the same anion, $[\text{MeSO}_4]^-$ and different cations, $[\text{C}_4\text{mim}]^+$ and $[\text{C}_2\text{mim}]^+$ were used to study the effect of the length of alkyl side chain of imidazolium cation (Figure 4.3.1 (b)). The structures of the cations used here have been shown in scheme 2.1 (a, b, c).

Electrostatic attraction between the cation and anion of $[\text{C}_4\text{mim}][\text{MeSO}_4]$ is comparatively lower than that between the cation and anion of $[\text{C}_2\text{mim}][\text{MeSO}_4]$ because of the bulky size of $[\text{C}_4\text{mim}]^+$ cation. Due to the longer butyl side chain of $[\text{C}_4\text{mim}]^+$, structural asymmetry is higher in this cation. i.e. the positive charge is less centered around the cation. Moreover, the positive charge density in $[\text{C}_4\text{mim}]^+$ is lower due to the attachment of electron releasing long alkyl butyl side chain. Owing to the longer alkyl side chain, thus the electrostatic attraction is lower between $[\text{C}_4\text{mim}]^+$ and $[\text{MeSO}_4]^-$.

When IL is trapped in the reverse micelle core of CTAB microemulsions, $[\text{MeSO}_4]^-$ of IL is attracted to the head group of CTAB due to the more centered positive charge on the N atom in CTAB head group compared to the delocalized positive charge in the imidazolium cation. Imidazolium cation stays closer to the anion of IL the (Scheme 4.2). Long butyl chain in $[\text{C}_4\text{mim}]^+$ and nonpolar tail part of CTAB form strong hydrophobic-hydrophobic interaction. Butyl side chain of $[\text{C}_4\text{mim}]^+$ is exposed in the bulk more effectively than shorter ethyl side chain of $[\text{C}_2\text{mim}]^+$. So according to Figure 4.3.1 (b) the conductivity for $[\text{C}_4\text{mim}][\text{MeSO}_4]$ based microemulsion system is larger than $[\text{C}_2\text{mim}][\text{MeSO}_4]$ based microemulsion (Scheme 4.3 (B)).

4.3.1.2. Viscosity

4.3.1.2.1. The Influence of R

Figure 4.3.2 (a, b) shows the change of viscosity of different series of CTAB microemulsions with increasing R at 25 °C (Appendices Tables A45-46.). The viscosity of the microemulsions increases with increasing R for all the systems due to the addition of more viscous IL which causes formation of more droplets.

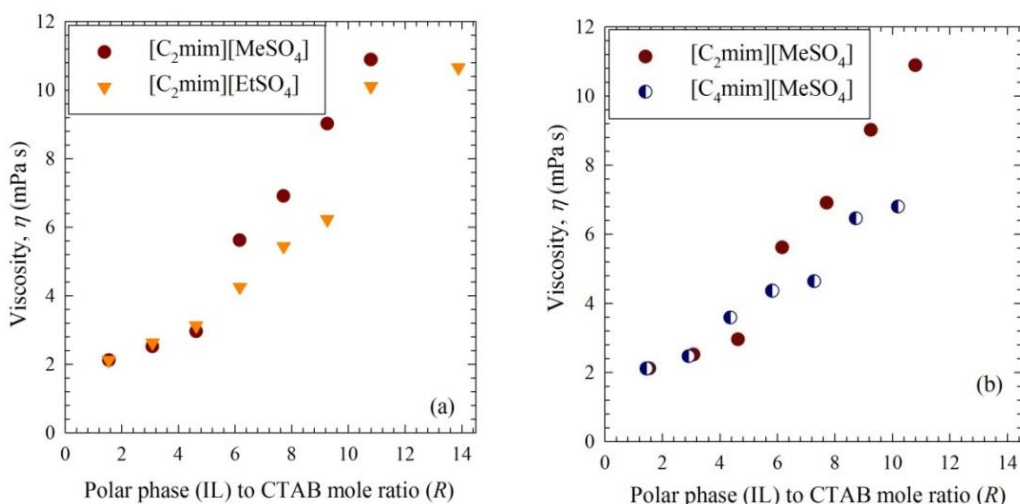


Figure 4.3.2. Variation of viscosity of (a) CTAB/1-butanol/cyclohexane/[C₂mim][MeSO₄] and CTAB/1-butanol/cyclohexane/[C₂mim][EtSO₄] (b) CTAB/1-butanol/cyclohexane/[C₂mim][MeSO₄] and CTAB/1-butanol/cyclohexane/[C₄mim][MeSO₄] microemulsions as a function of R at 25 °C.

At low values of R , where IL/o microemulsion exists, the viscosity is mainly contributed by the continuous cyclohexane medium. At a given temperature the viscosity increases as R value further increases because two or more droplets fuse to create small channels increasing viscosity. Further higher R value creates three dimensional channeling which drastically reduces the flow between layers resulting in steeper increase of viscosity.

4.3.1.2.2. The Influence of IL Anion

Figure 4.3.1 (a) shows that the conductivity of [C₂mim][EtSO₄] based microemulsion system is larger compared to [C₂mim][MeSO₄] microemulsion system. Mobility of anions is the main factor for increasing conductivity. The larger anion in [C₂mim][EtSO₄] makes the charge distribution more diffused in the larger anion and thereby makes the dissociation of the IL easier and causes enhancement of mobility. As mobility increases, layers of [C₂mim][EtSO₄] based microemulsion system can flow easily resulting in a lower viscosity compared to [C₂mim][MeSO₄] based microemulsion system (Figure 4.3.2 (a)).

4.3.1.2.3. The Influence of Alkyl Side Chain Length of Imidazolium Cation

From Figure 4.3.1 (b) we see that conductivity of [C₄mim][MeSO₄] based microemulsion system is higher than that of [C₂mim][MeSO₄] based microemulsion system. Mobility of cations is the main factor here for increasing conductivity (Sec. 4.3.1.3). [C₄mim][MeSO₄] based microemulsion system can flow easily with one another resulting in a lower viscosity compared to [C₂mim][MeSO₄] based microemulsion system (Figure 4.3.2 (b)).

4.3.1.2.4. Effect of Temperature on Viscosity

Figure 4.3.3 (a, b) shows effect of temperature on viscosity of different series of CTAB microemulsions at $R = 1.5424$ (Appendices Tables A47-48.). From Figure 4.3.3 (a, b), it is apparent that the viscosity of the microemulsions decreases with increasing temperature for $R = 1.5424$.

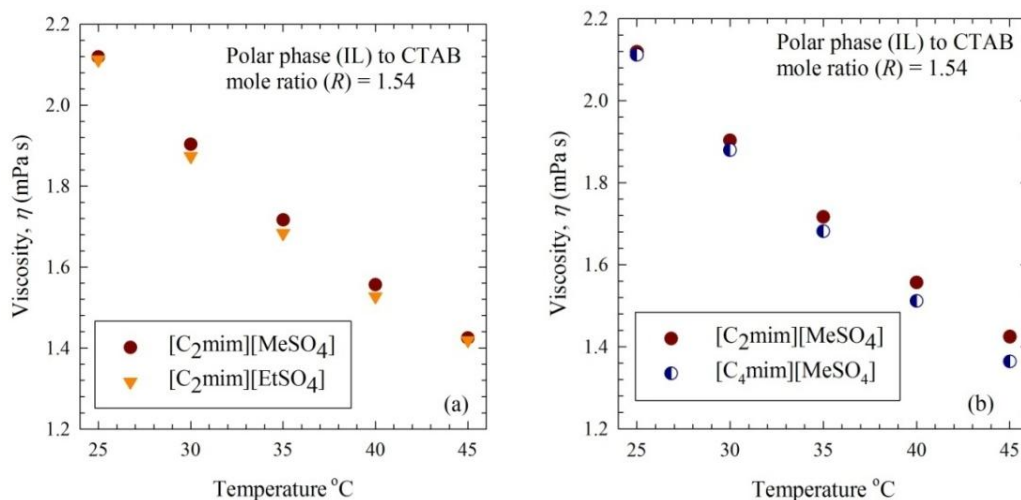


Figure 4.3.3. Effect of temperature on viscosity of (a) CTAB/1-butanol/cyclohexane/ $[C_2mim][MeSO_4]$ and CTAB/1-butanol/cyclohexane/ $[C_2mim][EtSO_4]$ (b) CTAB/1-butanol/cyclohexane/ $[C_2mim][MeSO_4]$ and CTAB/1-butanol/cyclohexane/ $[C_4mim][MeSO_4]$ microemulsions at $R = 1.5424$.

Due to the reduction of attractive interaction for temperature induced gain in kinetic energy among droplets of microemulsion, viscosity continuously decreases with the increase of temperature at constant R for different series of microemulsions.

4.3.1.3. Size and Size Distribution of Droplets

ILs can be encapsulated in reverse micelle droplet cores and the size of the droplets increase with R up to a certain value [54-60]. Concentration of IL, anion structure, and the alkyl side-chain length of cation of IL have a greater effect on the curvature parameter of surfactant [61].

4.3.1.3.1. Influence of IL Anion

Figure 4.3.4 (a, b) shows the variation of size and size distributions of reverse micelle droplets for two different microemulsion systems with increasing R at 25 °C, where the ILs are $[C_2mim][EtSO_4]$ and $[C_2mim][MeSO_4]$. For all the systems there is an increase in the droplets size when R increases (Appendices Table A49.). The size of the droplets increases approximately from 2 and 3 nm to 5 and 6 nm with increasing R from 1.5424 to 6.1697 for $[C_2mim][MeSO_4]$ and $[C_2mim][EtSO_4]$ based microemulsions. For both systems, the sizes of clusters are above 200 nm.

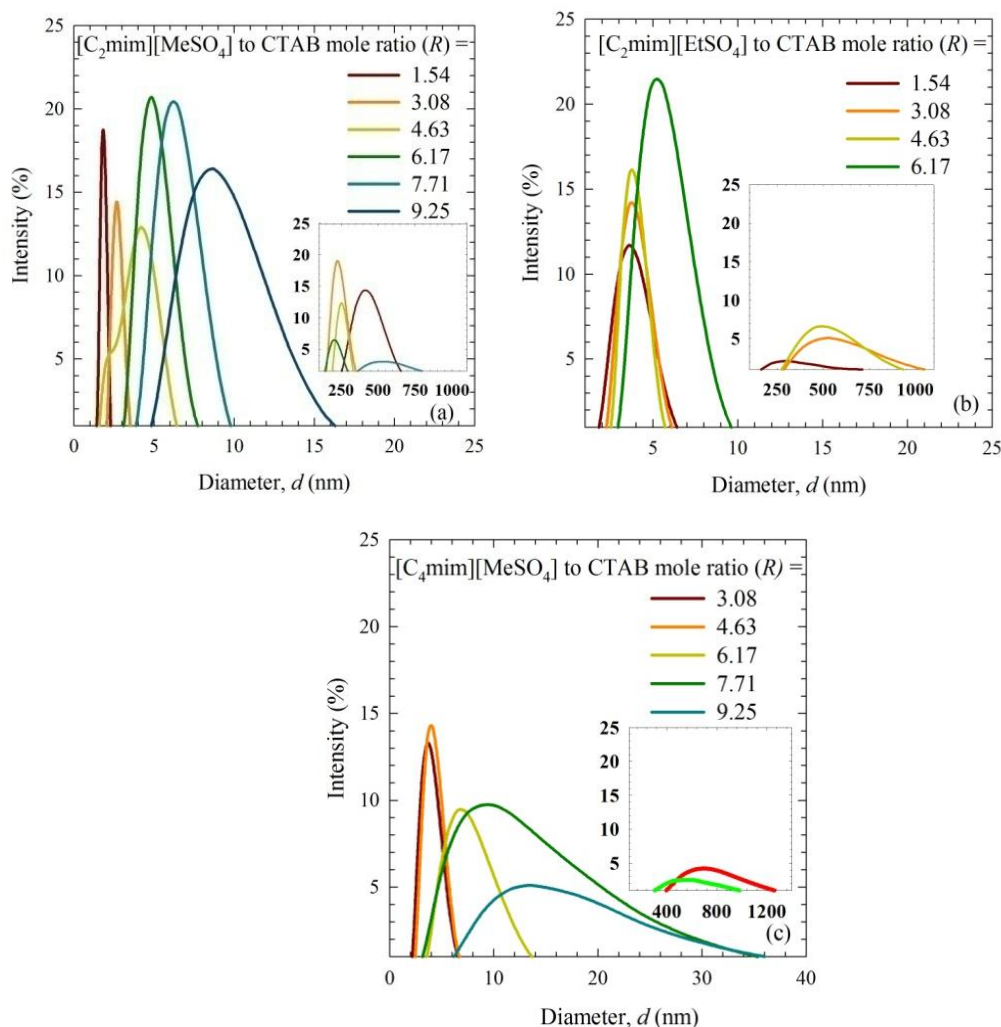


Figure 4.3.4. Size and size distribution of droplets in (a) CTAB/1-butanol/cyclohexane/ $[\text{C}_2\text{mim}][\text{MeSO}_4]$, (b) CTAB/1-butanol/cyclohexane/ $[\text{C}_2\text{mim}][\text{EtSO}_4]$, and (c) CTAB/1-butanol/cyclohexane/ $[\text{C}_4\text{mim}][\text{MeSO}_4]$ microemulsions at different R at 25 °C.

With increasing R , ILs can be encapsulated into the core of reverse micelle droplets and thus the size of the droplets increases. The width of the distributions also increases as R increases. Increasing IL content induces aggregation of droplets to form clusters. Laser beam generally detects both spherical droplets and the clusters which may give hexagonal, cylindrical, rod shape, ellipsoidal, cone-shaped patterns and other structures as well. For these variation in structures of clusters, the hydrodynamic diameter of clusters shows larger distributions. The positive charge is more localized on the N atom of CTAB head group than on the imidazolium cation where the positive charge is not localized. So a stronger interaction between the anions of IL and the CTAB head group can be predicted. Thus, the electrostatic interaction between the cation and anion of IL must be altered when ILs are encapsulated inside the CTAB reverse micelles. Interaction between the ions of $[\text{C}_2\text{mim}][\text{EtSO}_4]$ is comparatively lower than the ions of $[\text{C}_2\text{mim}][\text{MeSO}_4]$ due to the bulky size of $[\text{EtSO}_4]^-$ anion. Thus, as the R values increase, ions of $[\text{C}_2\text{mim}][\text{EtSO}_4]$

penetrates more easily compared to the ions of $[\text{C}_2\text{mim}][\text{MeSO}_4]$ through the surfactant layer and the sizes of $[\text{C}_2\text{mim}][\text{EtSO}_4]$ microemulsions are larger than $[\text{C}_2\text{mim}][\text{MeSO}_4]$ microemulsions.

4.3.1.3.2. Influence of Alkyl Side Chain Length of Imidazolium Cation

The variations of size and size distributions of reverse micelle droplets for two different microemulsion systems are shown in Figure 4.3.4 (b, c) with increasing R values at 25 °C, where the ILs are $[\text{C}_2\text{mim}][\text{MeSO}_4]$ and $[\text{C}_4\text{mim}][\text{MeSO}_4]$ (Appendices Table A49.). In all the systems, there is an increase in the droplet size as R increases. The hydrodynamic size of the aggregates increases approximately from 3 nm to 9 nm and from 3 nm to 14 nm with increasing R values from 3.0849 to 9.2546 for $[\text{C}_2\text{mim}][\text{MeSO}_4]$ and $[\text{C}_4\text{mim}][\text{MeSO}_4]$ based microemulsions respectively (Appendices Table A49). For both systems, sizes of the clusters are found to be above 200 nm. Different shapes of droplets or the fusion of droplets in microemulsions might be the reason for the larger distribution in hydrodynamic diameters. Interaction between the ions of $[\text{C}_4\text{mim}][\text{MeSO}_4]$ is comparatively lower than the ions of $[\text{C}_2\text{mim}][\text{MeSO}_4]$ due to the bulky size of $[\text{C}_4\text{mim}]^+$ cation. Thus, as the R values increases, diameters of $[\text{C}_4\text{mim}][\text{MeSO}_4]$ based microemulsions are thus larger than $[\text{C}_2\text{mim}][\text{MeSO}_4]$ based microemulsions.

4.3.1.4. Density

Figure 4.3.5 shows the change of density of different series of CTAB microemulsions with increasing R at 25 °C (Appendices Tables A50-51). The densities of the microemulsions increase with increasing R for all the systems due to the addition of IL according to Figure 4.3.5.

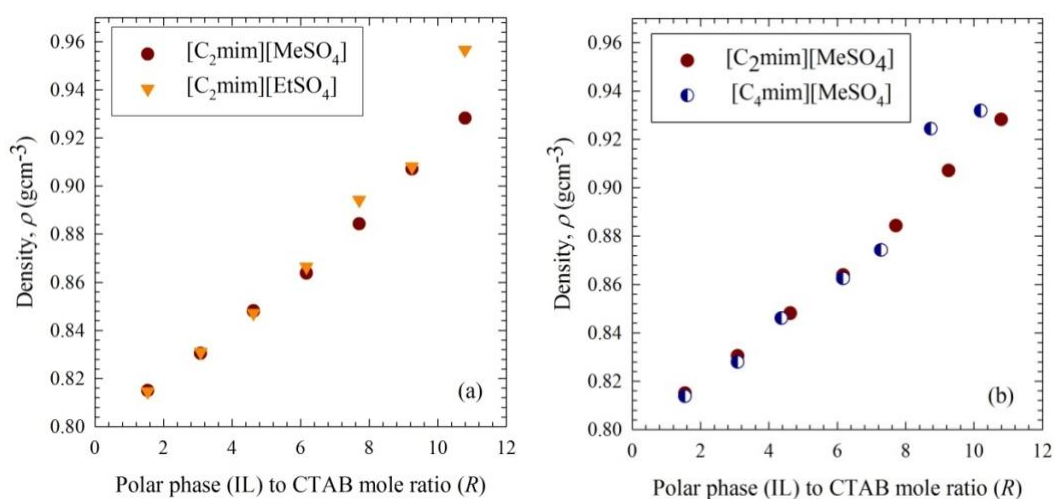


Figure 4.3.5. Density of (a) CTAB/1-butanol/cyclohexane/ $[\text{C}_2\text{mim}][\text{MeSO}_4]$ and CTAB/1-butanol/cyclohexane/ $[\text{C}_2\text{mim}][\text{EtSO}_4]$ (b) CTAB/1-butanol/cyclohexane/ $[\text{C}_2\text{mim}][\text{MeSO}_4]$ and CTAB/1-butanol/cyclohexane/ $[\text{C}_4\text{mim}][\text{MeSO}_4]$ microemulsions as a function of R at 25 °C.

Densities of ILs are higher compared to cyclohexane. In all the microemulsion systems, as the amount of IL is increased, the amount of cyclohexane and 1-butanol (1:1) mixture is simultaneously decreased to keep the total mass of microemulsion constant. So the gradual addition of IL gradually increases the densities and dominate the density of the system, resulting in an increasing trend in density of the microemulsions.

4.3.1.4.1. Effect of Temperature on Density

Figure 4.3.6 (a, b) shows effect of temperature on the densities of different series of CTAB microemulsions at $R = 1.5424$ (Appendices Tables A52-53.). From Figure 4.3.6 (a, b), it can be seen that the density of the microemulsions decrease with increasing temperature for $R = 1.5424$.

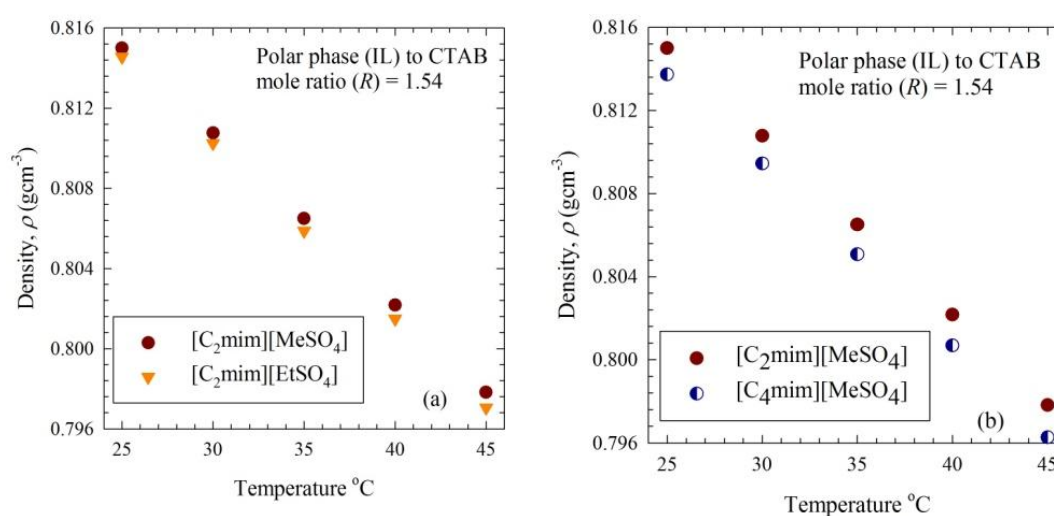


Figure 4.3.6. Effect of temperature on density of (a) CTAB/1-butanol/cyclohexane/[C₂mim][MeSO₄] and CTAB/1-butanol/cyclohexane/[C₂mim][EtSO₄] (b) CTAB/1-butanol/cyclohexane/[C₂mim][MeSO₄] and CTAB/1-butanol/cyclohexane/[C₄mim][MeSO₄] microemulsions at $R = 1.5424$.

As a result of increase in temperature of the system, the mobility of the droplets as well as the volume of the dispersed phase (cyclohexane) increases owing to gain in kinetic energy, thus decrease in the density.

4.3.1.5. Refractive Index

Figure 4.3.7 shows the change of refractive index of different series of CTAB microemulsions with increasing R at 25 °C (Appendices Tables A54-55.). According to Figure 4.3.7 the refractive index of the microemulsions increases with increasing R irrespective of the systems due to the addition of IL.

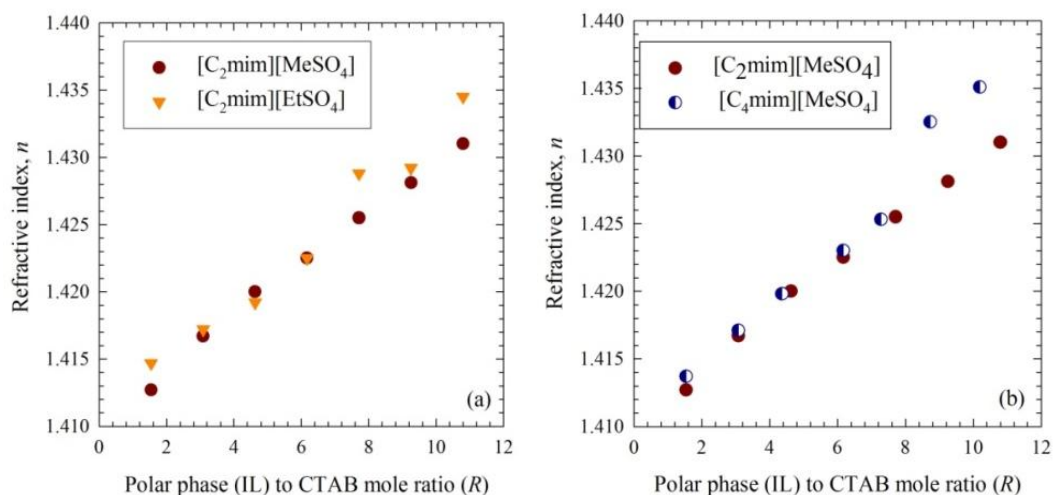


Figure 4.3.7. Refractive index of (a) CTAB/1-butanol/cyclohexane/[C₂mim][MeSO₄] and CTAB/1-butanol/cyclohexane/[C₂mim][EtSO₄] (b) CTAB/1-butanol/cyclohexane/[C₂mim][MeSO₄] and CTAB/1-butanol/cyclohexane/[C₄mim][MeSO₄] microemulsions as a function of R at 25 °C.

With increasing R value the number of ions in the cores of reverse micelle droplets increases, causing formation of aggregation among droplets inside the cores. In a consecutive way, light enters and gets out of these reverse micelle droplets that are dispersed in cyclohexane continuous medium. Ions of ILs and the positive head groups and the negative counterion Br⁻ from cationic CTAB have their own electric field and this field repels the electric field component of light.

4.3.1.5.1. Effect of Temperature on Refractive Index

Figure 4.3.8 (a, b) shows the effect of temperature on the refractive index of different series of CTAB microemulsions at $R = 1.5424$ (Appendices Tables A56-57.). As seen in Figure 4.3.8 (a), refractive index of the microemulsions monotonously decreases with increasing temperature upto 45 °C for CTAB/1-butanol/cyclohexane/[C₂mim][MeSO₄] microemulsions (Figure 4.3.8 (a)).

For CTAB/1-butanol/cyclohexane/[C₂mim][EtSO₄] microemulsions, the refractive index decreases with increasing temperature upto 40 °C and then suddenly increase as the temperature is raised to 45 °C, whereas for CTAB/1-butanol/cyclohexane/[C₂mim][EtSO₄] microemulsions, decrease with increasing temperature upto 40 °C and then remain almost constant at 45 °C

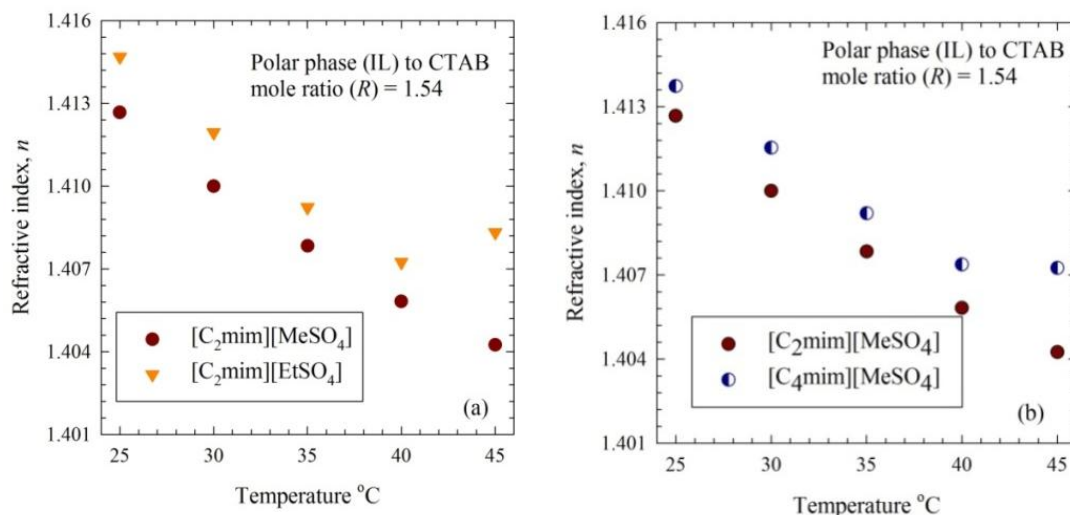


Figure 4.3.8. Effect of temperature on refractive index of (a) CTAB/1-butanol/cyclohexane/[C₂mim][MeSO₄] and CTAB/1-butanol/cyclohexane/[C₂mim][EtSO₄] (b) CTAB/1-butanol/cyclohexane/[C₂mim][MeSO₄] and CTAB/1-butanol/cyclohexane/[C₄mim][MeSO₄] microemulsions at $R = 1.5424$.

4.3.1.6. Polarity

Figure 4.3.9 shows the UV-visible spectra for RBD in different series of CTAB microemulsions with increasing R at 25 °C. From Figure 4.3.9, it can be seen that in the visible range in the absorption spectra of RBD in IL based microemulsion no significant change in absorption is observed.

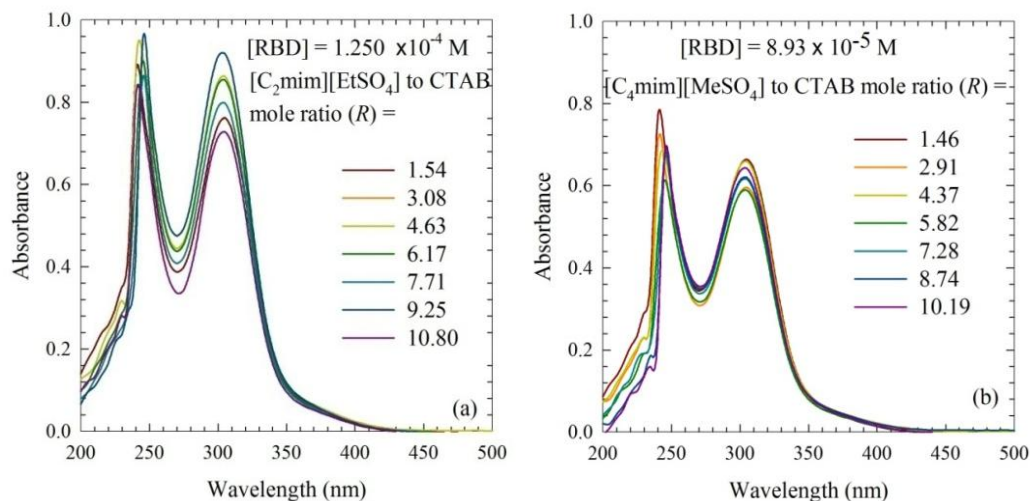


Figure 4.3.9. Absorption spectra of RBD in (a) CTAB/1-butanol/cyclohexane/[C₄mim][MeSO₄] and (b) CTAB/1-butanol/cyclohexane/[C₂mim][EtSO₄] microemulsions at different R values at 25 °C.

Solvatochromic shift in wavelength for absorption maxima (λ_{\max}) of zwitterionic RBD dye (Section 1.10) in the UV-visible absorption spectra has been observed for [C₄mim][MeSO₄] and [C₂mim][EtSO₄] based microemulsion series where the concentrations of RBD were 8.93×10^{-5} M and 1.25×10^{-4} M respectively. No

significant change in absorption band is observed in the visible range in the absorption spectra of RBD in IL based microemulsion due to the intramolecular π - π^* charge transfer transition. IL also exhibits the intramolecular π - π^* charge transfer transition. Therefore, polarity of the microemulsions were not significantly different.

4.3.1.7. Surface Tension

Figure 4.3.10 shows the change in surface tension of CTAB/1-butanol/cyclohexane/[C₂mim][EtSO₄] ($R = 1.5424, 3.0849, 4.6273, 6.1697, 7.7121$), CTAB/1-butanol/cyclohexane/[C₄mim][MeSO₄] ($R = 1.5424$) and CTAB/1-butanol/cyclohexane/[C₂mim][MeSO₄] ($R = 1.5424$) microemulsions as a function of R at 25 °C (Appendices Table A58.).

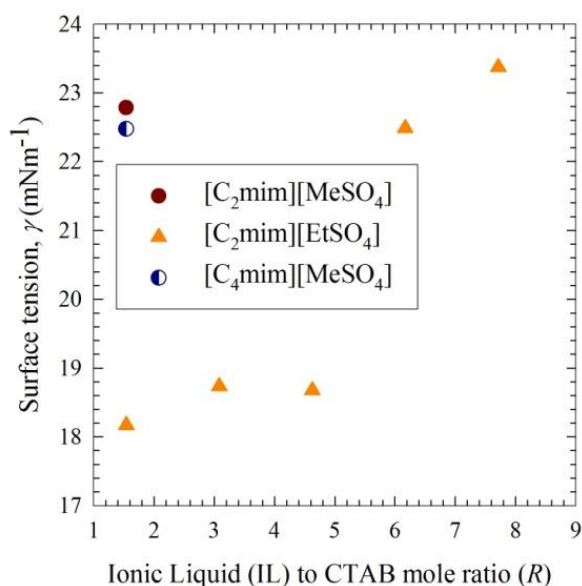
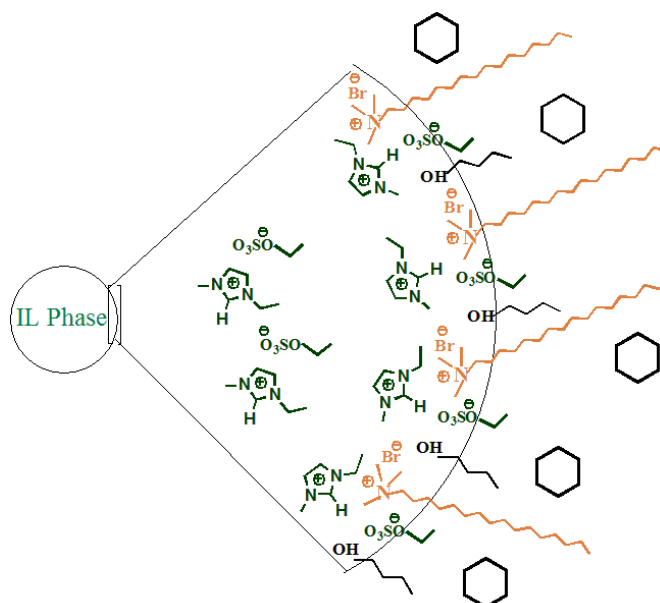


Figure 4.3.10. Surface tension of CTAB/1-butanol/cyclohexane/[C₂mim][EtSO₄] ($R = 1.5424, 3.0849, 4.6273, 6.1697, 7.7121$), CTAB/1-butanol/cyclohexane/[C₄mim][MeSO₄] ($R = 1.5424$) and CTAB/1-butanol/cyclohexane/[C₂mim][MeSO₄] ($R = 1.5424$) as a function of R at 25 °C.

Surface tension of [C₂mim][EtSO₄], [C₄mim][MeSO₄] and [C₂mim][MeSO₄] based microemulsions with $R = 1.5424$ shows the value of 18.170, 22.475 and 22.787 mN m⁻¹ respectively. At the same R value ($R = 1.5424$) [C₂mim][MeSO₄] based microemulsion shows the highest, whereas [C₂mim][EtSO₄] based microemulsion shows the lowest surface tension values.

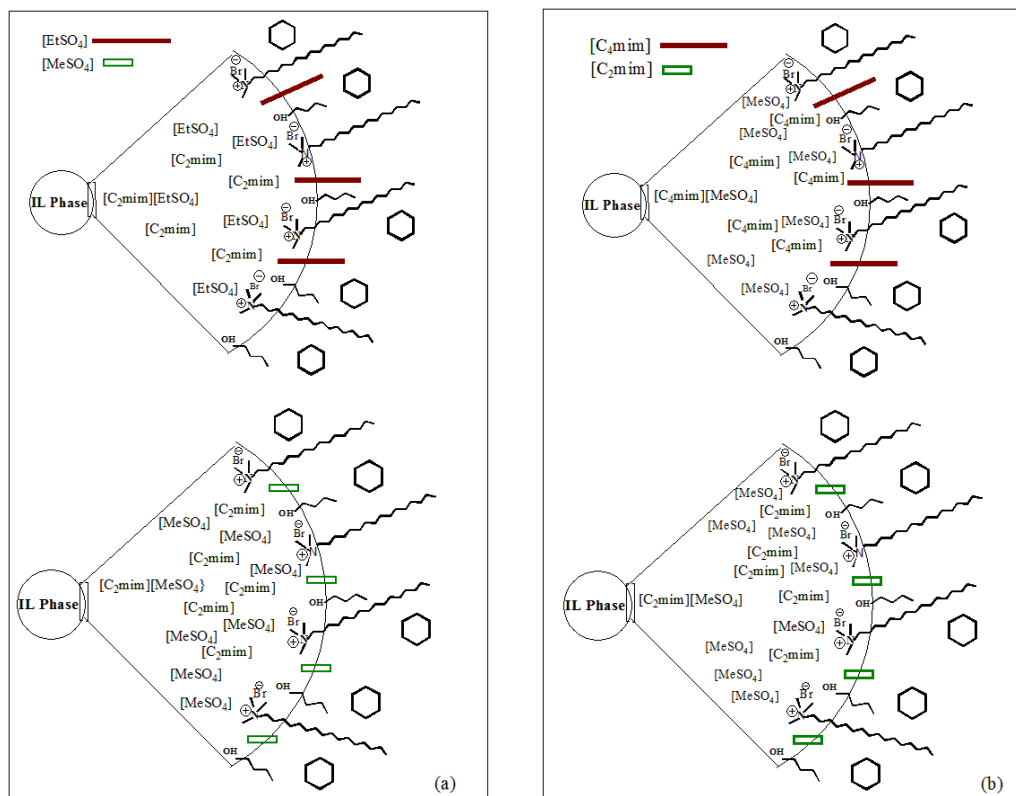
4.3.2. Probable Organization of Different Components in IL/o Microemulsions

Polar phase (IL) can be encapsulated into the core of reverse micelle droplets which can lead to a major packing of the surfactants at the interface, where the nonpolar phase (cyclohexane) remains in the bulk as the continuous medium (Scheme 4.1).



Scheme 4.1. Scheme of the interfacial film layer of inverse CTAB microemulsion droplets.

The positive charge is more localized over the CTAB head group than the imidazolium cation. So the anions of IL form strong Coulombic interactions with the CTAB headgroups than with their own imidazolium cations. Thus, the interaction between the cation and anion of IL must have been altered when they are encapsulated inside the CTAB reverse micelles. The interaction between imidazolium cations and counterions (Br^-) possibly increase thereby. Cosurfactant (1-butanol), integrated into the interfacial layer of reverse microemulsion droplets, has a stabilizing effect on the interfacial layer resulting in increased solubilizing capacity of the interfacial layers. H-bonds may be created between the negatively charged oxygen atoms of anions and the partially positive hydrogen atoms of terminal -OH groups of 1-butanol. When the ions of IL (for any system) move from the core of reverse micelle to the interfacial layer, the nonpolar group of anions and the nonpolar side chain of cations have hydrophobic interactions with the tail part of CTAB. The more carbon atoms are attached with the nonpolar group of anions and the nonpolar side chain of cations, the more hydrophobic interactions form with the tail part of CTAB (Scheme 4.2) The more the hydrophobic interaction of side chain of ions with the CTAB tail group, the more is the tendency of the ions to go to the bulk. Cyclohexane which exists in the bulk forms hydrophobic interaction with the tail part of CTAB.



Scheme 4.2. (a) Strong hydrophobic interaction of $[\text{EtSO}_4]^-$ anion compared to $[\text{MeSO}_4]^-$ anion with the CTAB tail group when the cation is $[\text{C}_2\text{mim}]^+$ and (b) strong hydrophobic interaction of $[\text{C}_4\text{mim}]^+$ cation compared to $[\text{C}_2\text{mim}]^+$ cation with the CTAB tail group when the anion is $[\text{MeSO}_4]^-$.

4.4. Conclusions

Physicochemical properties of CTAB microemulsions have been found to vary with varying R , cations and anions of ILs. The viscosity, conductivity, density, refractive index and droplet size increase as R increases. When structural variation is brought into ILs by varying the cations keeping the anion same, or varying the anions while the cation is fixed, the electrostatic interaction in ILs significantly increases with increase in the side chain of cation, or number of carbon atoms in anion, respectively. This increased electrostatic interaction eventually influences the different physicochemical properties.

References

- [1] Evans, D. F.; Yamauchi, A.; Roman, R.; Casassa, E. Z. *J. Colloid Interface Sci.* **1982**, 88, 89-96.
- [2] Evans, D. F.; Yamauchi, A.; Wei, G. J.; Bloomfield, V. A. *J. Phys. Chem.* **1983**, 87, 3537-3541.
- [3] Fletcher, K. A.; Pandey, S. *Langmuir* **2004**, 20, 33-36.
- [4] Evans, D. F.; Kaler, E. W.; Benton, W. J. *J. Phys. Chem.* **1983**, 87, 533-535.
- [5] Wang, L. J.; Chen, X.; Chai, Y. C.; Hao, J. C.; Sui, Z. M.; Zhuang, W. C.

- Chem. Commun.* **2004**, 2840-2841.
- [6] He, Y.; Lodge, T. P. *Chem. Commun.* **2007**, 2732-2734.
- [7] Lee, J.; Panzer, M. J.; Lodge, T. P.; Frisbie, C. D. *J. Am. Chem. Soc.* **2007**, 129, 4532-4533.
- [8] Hao, J. C.; Song, A. X.; Wang, J. Z.; Chen, X.; Zhuang, W. C.; Shi, F. *Chem. Eur. J.* **2005**, 11, 3936-3940.
- [9] Gao, H.; Li, J.; Han, B.; Chen, W.; Zhang, J.; Zhang, R.; Yan, D. *Phys. Chem. Chem. Phys.* **2004**, 6, 2914-2916.
- [10] Eastoe, J.; Gold, S.; Rogers, S. E.; Paul, A.; Welton, T.; Heenan, R. K.; Grillo, I. *J. Am. Chem. Soc.* **2005**, 127, 7302-7303.
- [11] Gao, Y.; Han, S.; Han, B.; Li, G.; Shen, D.; Li, Z.; Du, J.; Hou, W.; Zhang, G. *Langmuir* **2005**, 21, 5681-5684.
- [12] Li, N.; Gao, Y.; Zheng, L.; Zhang, J.; Yu, L.; Li, X. *Langmuir* **2007**, 23, 1091-1097.
- [13] Li, J.; Zhang, J.; Gao, H.; Han, B.; Gao, L. *Colloid Polym. Sci.* **2005**, 283, 1371-1375.
- [14] Behera, K.; Pandey, S. *J. Phys. Chem. B* **2007**, 111, 13307-13315.
- [15] Behera, K.; Pandey, S. *J. Colloid Interface Sci.* **2007**, 316, 803-814.
- [16] Behera, K.; Pandey, S. *J. Colloid Interface Sci.* **2009**, 331, 196-205.
- [17] Lawrence, M. J.; Rees, G. D. *Adv. Drug Deliver Rev.* **2000**, 45, 89-121.
- [18] Bhargava, H. N.; Narukar, A. Lieb, L. M. *Pharm. Technol.* **1987**, 11, 46-52.
- [19] Sripriya, R.; Raja, K. M.; Santhosh, G; Chandrasekaran, M.; Noel, M. J. *Colloid Interface Sci.* **2007**, 314, 712-717.
- [20] Ruiz, C. C. *Colloid. Polym. Sci.* **1995**, 273, 1033-1040.
- [21] Saha, R.; Rakshit, S.; Mitra, R. ; Pal, S. K. *Langmuir* **2012**, 28, 8309-8317.
- [22] Yang, C. J.; Zeng, Q. R.; Yang, H. J.; Zou, Chin, M. Y. *J. Anal. Chem.* **2006**, 5, 642-646.
- [23] Liu, Y.; Guo, R.; Guo, X. J. *J. Phys. Chem. B* **2006**, 110, 784-790.
- [24] Bera, A.; Mandal, A.; Kumar, T. *J. Chem. Eng. Data* **2014**, 59, 2490-2498.
- [25] Fletcher, P. D. I.; Morris, J. S. *Colloid Surface A* **1995**, 98, 147-154.
- [26] Fletcher, P. D. I.; Suhling, K. *Langmuir* **1998**, 14, 4065-4069.
- [27] Jayalakshmi, Y.; Beysens, D. *Phys. Rev. A* **1992**, 45, 8709-8718.
- [28] Kizilbash, N. A.; Asif, S.; Nazar, M. F.; Shah, S. S.; Alenizi, D. *J. Chem. Soc. Pak.* **2011**, 33, 1-6.
- [29] Mehta, S. K.; Kawaljit, *Colloid Surface A* **1998**, 136, 35-41.
- [30] Fanun, M.; Ayad, Z.; Mudalal, S.; Dahoah, S.; Meltzer, D.; Schwarze, M.; Schomacker, R.; Blum, J. *J. Surfactants Deterg.* **2012**, 15, 505-512.
- [31] Kumar, B.; Jain, S. K.; Prajapati, S. K.; Mahor, A.; Kumar, A. *Int. J. Pharm. Sci. Res.* **2010**, 1, 57-74.
- [32] Zala, B. H.; Pandya, R. B.; Prajapat, M. D.; Ramkishan, A.; Parikh, R. K.; Gohel, M. C. *J. Pharm. Sci. Res.* **2011**, 4, 930-933.
- [33] Ramadan, E.; Borg,; Abdelghani, G. M.; Saleh, N. M. *Bull. Pharm. Sci.* **2013**, 36, 31-47.

- [34] Basheer, H. S.; Noordin, M. I.; Ghareeb, M. M. *Trop. J. Pharm. Res.* **2013**, *12*, 305-310.
- [35] Patel, V.; Kukadiya, H.; Mashru, R.; Surti, N.; Mandal, S. *Iran. J. Pharm. Res.* **2010**, *9*, 327-334.
- [36] Goffredi, M.; Liveri, V. T.; Vassallo, G. *J. Solution Chem.* **1993**, *22*, 941-949.
- [37] Sharma, S. C.; Tsuchiya, K.; Sakai, K.; Sakai, H.; Abe, M. *Langmuir* **2008**, *24*, 7658-7662.
- [38] Jahn, W.; Strey, R. *J. Phys. Chem.* **1988**, *92*, 2294-2301.
- [39] Jahn, W.; Strey, R. *Physics of Amphiphilic Layers* **1987**, *21*, 353-356.
- [40] Senatra, D. *Thermochim. Acta* **2000**, *345*, 39-46.
- [41] Senatra, D.; Pratesi, R.; Pieraccini, L. *J. Therm. Anal. Calorim.* **1998**, *51*, 79-90.
- [42] Angel, L. R.; Evans, D. F. Ninham, B. W. *J. Phys. Chem.* **1983**, *87*, 538-40.
- [43] Bellocq, A. M.; Biais, J.; Bothorel, P.; Clin, B.; Fourche, G.; Lalanne, P.; Lemaire, B.; Lemanceau, B.; Roux, D. *Adv. Colloid Interface Sci.* **1984**, *20*, 167-272.
- [44] Rakshit, A. K.; Moulik, S. P. *Surfactant Science Series* **2009**, *144*, 17-57
- [45] Naouli, N.; Rosano, H. L. *J. Dispersion Sci. Technol.* **2009**, *30*, 370-378.
- [46] Shah, D.O. *Micelles, Microemulsions and Monolayers*, Marcel Dekker, New York **1998**.
- [47] Beitz, T.; Koetz, J.; Wolf, G.; Kleibpeter, E.; Friberg, S. E. *J. Colloid Interface Sci.* **2001**, *240*, 581-589.
- [48] Lemaire, B.; Bothorel, P.; Roux, D. *J. Phys. Chem.* **1983**, *87*, 1023.
- [49] Huang, J. S.; Safran, S. A.; Kim, M. W.; Grest, G. S.; Kotlarchyk, M.; Quirke, N. *Phys. Rev. Lett.* **1984**, *53*, 592-595.
- [50] Eicke, H. F.; Bercovec, M.; Das-Gupta B. *J. Phys. Chem.* **1989**, *93*, 314-317.
- [51] Ponton, A.; Bose, T. K. *J. Chem. Phys.* **1991**, *94*, 6879-6886.
- [52] Kim, M. W.; Huang, J. S. *Phys Rev. A.* **1986**, *34*, 719-722.
- [53] Dijk, M. A.; Casteleijn, G.; Joosten, J. G. H.; Levine Y. K. *J. Chem. Phys.* **1986**, *85*, 626.
- [54] Pramanik, R.; Ghatak, C.; Rao, V. G.; Sarkar, S.; Sarkar, N. *J. Phys. Chem. B* **2011**, *115*, 5971-5979.
- [55] Pramanik, R.; Sarkar, S.; Ghatak, C.; Rao, V. G.; Sarkar, N. *J. Phys. Chem. B* **2011**, *115*, 2322-2330.
- [56] Falcone, R. D.; Correa, N. M.; Silber, J. J. *Langmuir* **2009**, *25*, 10426-10429.
- [57] Gao, Y. N.; Li, N.; Hilfert, L.; Zhang, S. H.; Zheng, L. Q.; Yu, L. *Langmuir* **2009**, *25*, 1360-1365.
- [58] Pramanik, R.; Ghatak, C.; Rao, V. G.; Sarkar, S.; Sarkar, N. *J. Phys. Chem. B* **2011**, *115*, 5971-5979. *Phys. Chem. B* 2007, *111*, 598-604.
- [59] Pramanik, R.; Sarkar, S.; Ghatak, C.; Rao, V. G.; Sarkar, N. *J. Phys. Chem. B* **2011**, *115*, 2322-2330.
- [60] Gao, Y.; Han, S.; Han, B.; Li, G.; Shen, D.; Li, Z.; Du, J.; Hou, W.; Zhang, G. *Langmuir* **2005**, *21*, 5681-5684.

- [61] Wei, J.; Su, B.; Xing, H.; Bao, Z.; Yang, Y.; Ren, Q. *Colloids Surf., A: Physicochem. Eng. Aspects* **2012**, 396, 213–218.
- [62] Falcone, R. D.; Correa, N. M.; Silber, J. J. *Langmuir* **2009**, 25, 10426–10429.

Abstract

Microstructures of IL based microemulsions with TX-100 and CTAB were determined by applying percolation theory on conductivity results. Derived data from density and refractive index further confirmed composition percolation thresholds with the variation of ϕ_w or ϕ_{IL} for IL based microemulsions with TX-100. DLS measurements provided evidence for composition percolation thresholds with the variation of R for different IL based microemulsions with CTAB which are in agreement with those obtained from conductivity measurements. For hydrophilic IL based microemulsions with TX-100, the phase transitions corresponded to the structural change from IL/o to o/IL via bicontinuous microemulsions with increasing ϕ_{IL} and for hydrophobic IL based microemulsions with TX-100, the phase transitions occurred from w/IL to IL/w via bicontinuous microemulsions with increasing ϕ_w . Different types of microstructures such as IL/o and bicontinuous microemulsions were identified by applying percolation theory on hydrophilic IL based microemulsions with CTAB with increasing R .

5.1. Introduction

Microemulsions with different physicochemical properties can be prepared by mixing different polar phase, nonpolar phase, surfactant normally in combination with a cosurfactant at different ratio.. Depending on the ratio of the components, three different microstructures may be formed in a microemulsion system. At high oil content with low amount of water or hydrophilic IL as the polar phase, w/o or IL/o microemulsion is formed which consists of water or IL droplets respectively dispersed in a continuous oil phase. At high water or hydrophilic IL content, o/w or o/IL microemulsion is formed consisting of oil droplets dispersed in a continuous water or IL phase. Not only the organic volatile compound, but also hydrophobic IL can be used as the oil phase in microemulsions. At intermediate ratio of polar and nonpolar component, a bicontinuous phase exists. The microstructure of a microemulsion can be altered from IL/o to a bicontinuous system and from bicontinuous to an o/IL system by increasing the IL content at constant temperature or by increasing the temperature at constant IL content.

Various techniques such as NMR, DLS, dielectric relaxation, SANS, TEM, time-resolved fluorescence quenching (TRFQ), ultrasound, viscosity and electrical conductance can help elucidating the structural transition in microemulsions [1–5]. The application of electrical conductivity measurements has been very popular. From electrical conductivity measurements useful information on micellar interaction could be obtained [6–8]. Water percolation threshold is frequently determined by using electrical conductivity measurements which is an indicator of microstructural transition from w/o to bicontinuous microemulsion [8–10]. Electrical conductivity increases sharply as a function of water content or temperature when microstructural transition occurs from w/o to bicontinuous microemulsion. At water percolation threshold dispersed water droplets are clustering and changing to the continuous water phase [7, 10–14]. Below the water percolation threshold, the conductance medium is

the continuous oil phase which is nonconductive. At the water percolation threshold, the dispersed water phase forms a highly conductive continuous water phase which results in enormous increase in electrical conductivity .

A similar percolation process has been studied extensively for both conventional and IL based microemulsions with either ionic or nonionic surfactants [10–13, 15, 16, 17, 18, 19, 20]. According to percolation phenomenon, an interconnected random structure is formed which spans the total system. This interconnected random structure is governed by universal scaling law (Section 1.4.4. of Chapter 1). After a threshold concentration (ϕ) of water at a constant temperature or after a threshold temperature (θ) at a constant concentration of water in aqueous microemulsion, percolation is occurred. The concentration or temperature at which percolation is occurred is called the percolation threshold. There are two types of percolation phenomenon: static and dynamic percolation (Section 1.4.4. of Chapter 1).

The effective medium theory and scaling law models are used to analyze the conductivity results [10, 12, 13, 15, 17–20]. For reverse microemulsions, water percolation thresholds have been obtained by numerical analysis of the models with adjustment by the least-squares method [10, 12, 13, 15, 21–24]. The application of the scaling law methodology in the estimation of percolation threshold was found to be very complicated. This theoretical models are only valid close to the percolation threshold and they are not applicable to infinite dilution and immediate vicinity of the percolation threshold [8, 26, 27]. Tremendous numerical calculations are required to estimate percolation threshold according to these theoretical models [8, 26, 27].

From the maximum of $d(\log\sigma)/d\phi$ versus ϕ , percolation threshold can also be estimated numerically and the estimated value is relatively close to the final predicted value from the fitting methodology [8, 25–27]. The second methodology of percolation threshold estimation was superior to the first methodology.

In this work, the percolation thresholds for TX-100 microemulsions with both hydrophilic and hydrophobic IL and CTAB microemulsions with hydrophilic IL have been determined by applying percolation theory on conductivity results. Excess volume, V^E vs. ϕ , excess refractive index, n^E vs. ϕ and excess molar refraction, R^E vs. ϕ profiles for TX-100 microemulsions and diameter, d (nm) vs. R profile for CTAB microemulsions have been critically analyzed to establish the structural phase transitions.

5.2. Experimental

5.2.1. Materials

TX-100, CTAB, cyclohexane, 1-butanol and the ILs, [C₂mim][EtSO₄], [C₂mim][BF₄], [C₄mim]BF₄, [C₄mim][MeSO₄], [C₄mim][PF₆] and [C₂mim][TFSI] were obtained from Sigma-Aldrich. They were used without further purification. Further details have

been presented in Section 1.11. of Chapter 1. De-ionized water was used to prepare hydrophobic IL based microemulsions.

5.2.2. Preparation of Microemulsions

TX-100 and CTAB Microemulsions with IL were prepared with a constant amount of TX-100 (70 % wt) and CTAB (5 % wt) with variation of the polar and the nonpolar phases to keep the total weight of the microemulsion constant. Composition and preparation of TX-100 and CTAB microemulsions were discussed in Section 2.4. of Chapter 2.

5.2.3. Measurements

Experimental techniques such as measurement of conductivity, density and refractive index were used to characterize microemulsions. The sizes of microemulsion droplets were measured by DLS measurement. Measurements have been described in detail in Section 3.2.3. of Chapter 3.

5.3. Results and Discussion

5.3.1. Analysis of Microregions of TX-100 Microemulsions by Composition Percolation Theory

Percolation theory describes the formation of long-range connectivity in random systems. Below the threshold a giant connected component does not exist and above the threshold a giant component of the order of system exists. By applying percolation theory different microregions may be identified such as IL/o, bicontinuous and o/IL microemulsions for hydrophilic IL based microemulsions and water/IL, bicontinuous and IL/water microemulsions for hydrophobic IL based microemulsions.

5.3.1.1. Conductivity

Figure 5.3.1. shows the plots of $d\log\sigma/d\phi$ vs. ϕ to determine percolation thresholds of different TX-100 microemulsions with both hydrophilic and hydrophobic ILs (Appendices Tables A59-62.).

Figure 5.3.1. (a). shows that in TX-100/cyclohexane/[C₂mim][EtSO₄] microemulsions, the phase transitions from IL/o to bicontinuous and bicontinuous to o/IL microemulsion occur at $\phi_{IL} \sim 0.1237$ ($R \sim 0.5600$) and $\phi_{IL} \sim 0.1674$ ($R \sim 0.7400$) respectively. Phase transition for TX-100/cyclohexane/[C₂mim][BF₄] system from IL/o to bicontinuous microemulsion occurs at $\phi_{IL} \sim 0.1215$ ($R \sim 0.6765$) and from bicontinuous to o/IL microemulsion may occur at $\phi_{IL} \sim 0.1663$ ($R \sim 0.9020$) which is further confirmed by n^E vs. ϕ_{IL} plot discussed in Section 5.3.1.3.

Phase transitions from IL/o to bicontinuous and bicontinuous to o/IL microemulsion occur at $\phi_{IL} \sim 0.0963$ ($R \sim 0.4510$) and $\phi_{IL} \sim 0.1635$ ($R \sim 0.7400$) respectively in TX-100/cyclohexane/[C₄mim][BF₄] microemulsion and phase transitions from IL/o to bicontinuous and bicontinuous to o/IL microemulsion occur at $\phi_{IL} \sim 0.0517$ ($R \sim 0.2255$) and $\phi_{IL} \sim 0.1647$ ($R \sim 0.6765$) respectively for TX-100/cyclohexane/[C₄mim][MeSO₄] microemulsions (Figure 5.3.1. (b)).

Percolation thresholds for w/IL to bicontinuous and bicontinuous to IL/w microemulsion occur at $\phi_w \sim 0.1157$ ($R \sim 0.4510$, $W_o \sim 5.0731$) and $\phi_w \sim 0.2191$ ($R \sim 0.2255$, $W_o \sim 9.9697$) respectively in TX-100/[C₂mim][TFSI]/water microemulsions (Figure 5.3.1. (c)).

Transitions in TX-100/[C₄mim][PF₆]/water microemulsions from w/IL to bicontinuous and bicontinuous to IL/w, occur at $\phi_w \sim 0.0726$ ($R \sim 0.7400$, $W_o \sim 3.1952$) and $\phi_w \sim 0.1345$ ($R \sim 0.5600$, $W_o \sim 6.0346$) respectively (Figure 5.3.1. (d)).

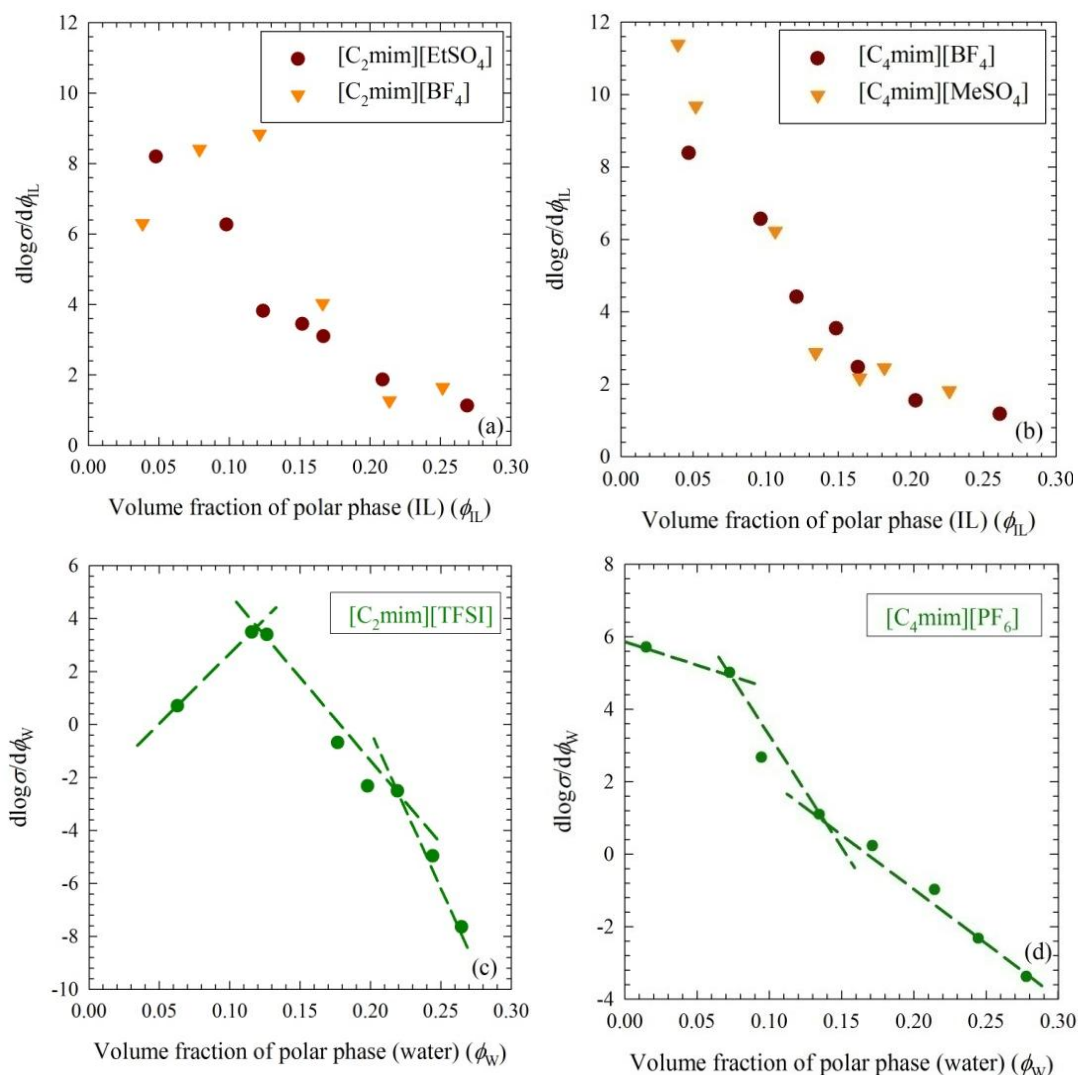


Figure 5.3.1. The $d \log \sigma / d \phi$ of (a) TX-100/cyclohexane/[C₂mim][EtSO₄], TX-100/cyclohexane/[C₂mim][BF₄], (b) TX-100/cyclohexane/[C₄mim][BF₄], TX-100/cyclohexane/[C₄mim][MeSO₄], (c) TX-100/[C₂mim][TFSI]/water, and (d) TX-100/[C₄mim][PF₆]/water microemulsions as a function of ϕ at 25 °C.

5.3.1.2. Excess Volume from Density Results

Figure 3.3.11. shows V^E vs. ϕ plots for different TX-100 microemulsions with both hydrophilic and hydrophobic ILs (Appendices Tables A63-66.). The excess volume of microemulsions were calculated from the following equation,

$$V^E = V_{mic} - \sum_i \phi_i V_i \quad \dots\dots\dots(5.1)$$

where, V^E = the excess volume, V_{mic} = the measured specific volume of the microemulsions, ϕ_i = the volume fraction of component i in the microemulsion and V_i = the specific volume of the component i .

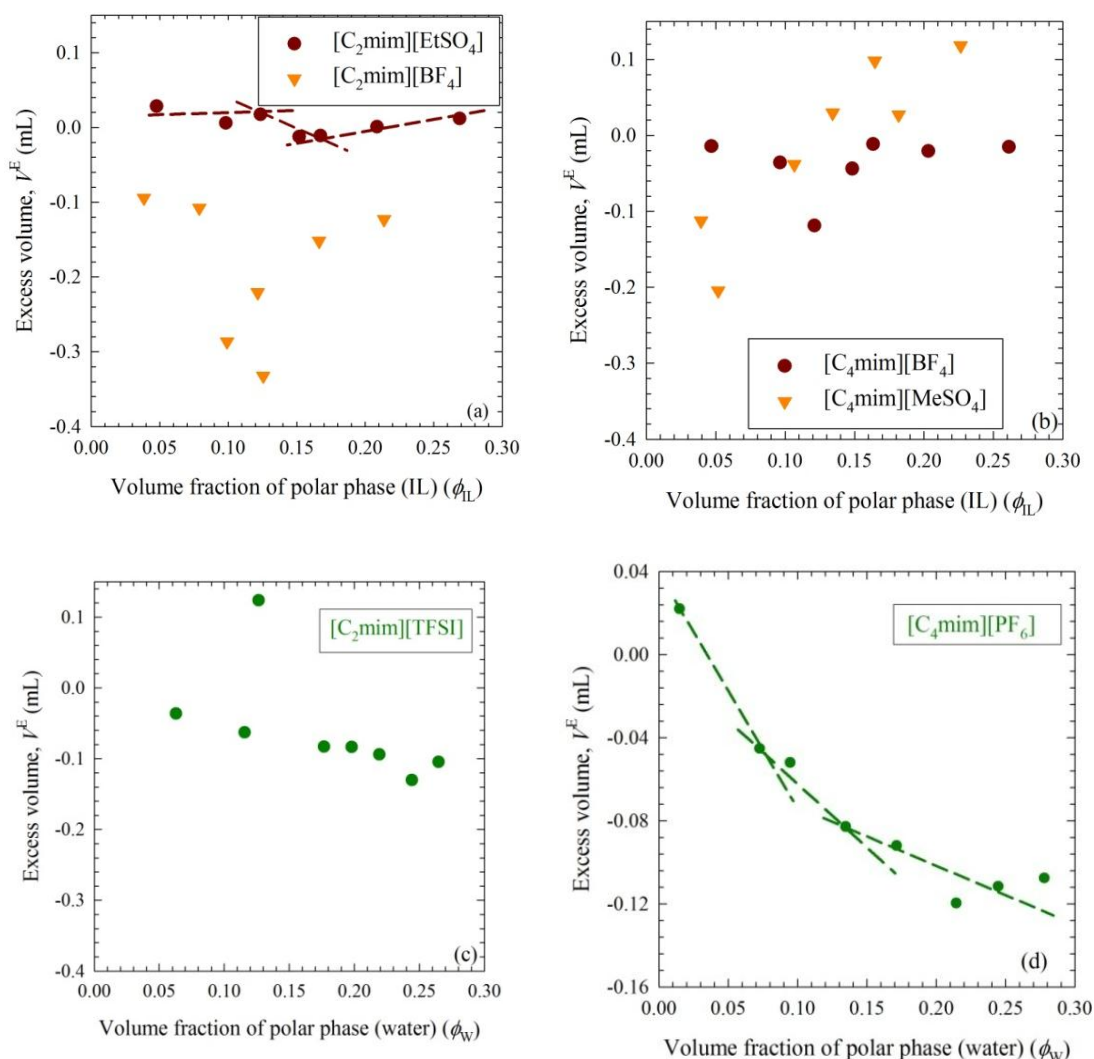


Figure 5.3.2. The V^E of (a) TX-100/cyclohexane/ $[C_2mim][EtSO_4]$, TX-100/cyclohexane/ $[C_2mim][BF_4]$, (b) TX-100/cyclohexane/ $[C_4mim][BF_4]$, TX-100/cyclohexane/ $[C_4mim][MeSO_4]$, (c) TX-100/ $[C_2mim][TFSI]$ /water, and (d) TX-100/ $[C_4mim][PF_6]$ /water microemulsions as a function of ϕ at 25 °C.

The phase transitions from IL/o to bicontinuous and bicontinuous to o/IL microemulsion occurred at $\phi_{IL} \sim 0.1237$ ($R \sim 0.5600$) and $\phi_{IL} \sim 0.1674$ ($R \sim 0.7400$) respectively for [C₂mim][EtSO₄] based microemulsions which are in agreement with conductivity results. From V^E vs. ϕ plot for TX-100/cyclohexane/[C₂mim][BF₄] microemulsion, no information could be obtained about structural transition (Figure 5.3.2. (a)).

Thresholds for IL/o to bicontinuous and bicontinuous to o/IL microemulsion were observed at $\phi_{IL} \sim 0.0963$ ($R \sim 0.4510$) and $\phi_{IL} \sim 0.1635$ ($R \sim 0.7400$) respectively for [C₄mim][BF₄] based microemulsion and at $\phi_{IL} \sim 0.0517$ ($R \sim 0.2255$) and $\phi_{IL} \sim 0.1647$ ($R \sim 0.6765$) respectively for [C₄mim][MeSO₄] based microemulsions (Figure 5.3.2. (b)).

Percolation thresholds were obtained when phase transitions occurred from w/IL to bicontinuous and bicontinuous to IL/w microemulsion occurred at $\phi_w \sim 0.1157$ ($R \sim 0.4510$, $W_o \sim 5.0731$) and $\phi_w \sim 0.2191$ ($R \sim 0.2255$, $W_o \sim 9.9697$) respectively in TX-100/[C₂mim][TFSI]/water microemulsions (Figure 5.3.2. (c), at $\phi_w \sim 0.0726$ ($R \sim 0.7400$, $W_o \sim 3.1952$) and $\phi_w \sim 0.1345$ ($R \sim 0.5600$, $W_o \sim 6.0346$) for [C₄mim][PF₆] microemulsions respectively (Figure 5.3.2. (d)).

All the thresholds obtained from V^E vs. ϕ plots for TX-100 microemulsions are in agreement with the conductivity results.

5.3.1.3. Excess Refractive Index from Refractive Index Results

Figure 3.3.12. shows n^E vs. ϕ plots for different TX-100 microemulsions with both hydrophilic and hydrophobic ILs (Appendices Tables A67-70.). The excess refractive index of microemulsions were calculated from the equation,

$$n^E = n_{mic} - \sum_i \phi_i n_i \dots\dots\dots(5.2)$$

where, n^E = the excess refractive index, n_{mic} = the measured refractive index of the microemulsions and n_i = the refractive index of the component i .

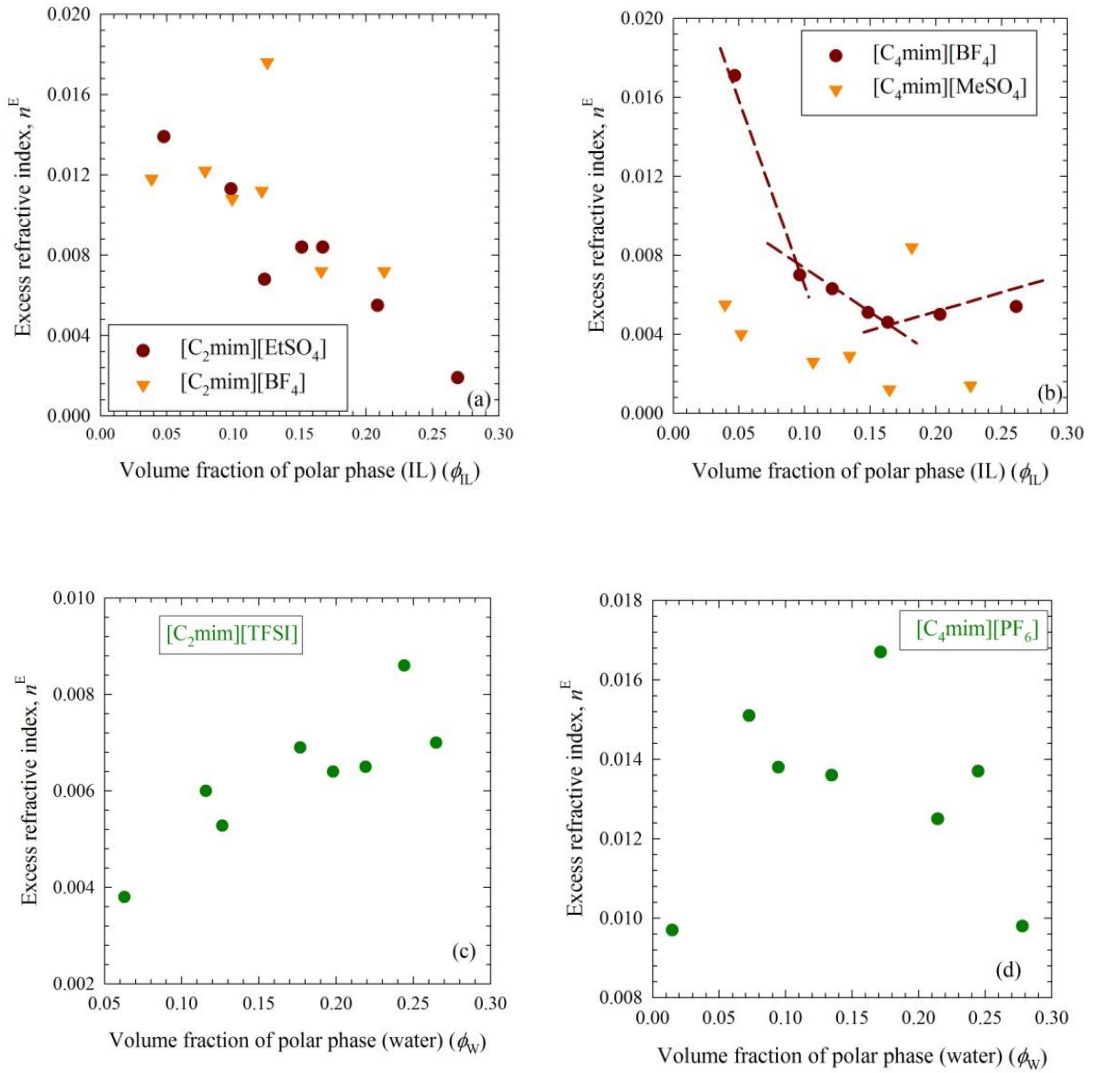


Figure 5.3.3. The n^E of (a) TX-100/cyclohexane/ $[C_2mim][EtSO_4]$, TX-100/cyclohexane/ $[C_2mim][BF_4]$, (b) TX-100/cyclohexane/ $[C_4mim][BF_4]$, TX-100/cyclohexane/ $[C_4mim][MeSO_4]$, (c) TX-100/ $[C_2mim][TFSI]$ /water, and (d) TX-100/ $[C_4mim][PF_6]$ /water microemulsions as a function of ϕ at 25 °C.

Transitions from IL/o to bicontinuous and bicontinuous to o/IL microemulsion occurred at $\phi_{IL} \sim 0.1237$ ($R \sim 0.5600$) and $\phi_{IL} \sim 0.1674$ ($R \sim 0.7400$) respectively for $[C_2mim][EtSO_4]$ based microemulsions and at $\phi_{IL} \sim 0.1215$ ($R \sim 0.6765$) and $\phi_{IL} \sim 0.1663$ ($R \sim 0.9020$) respectively for $[C_2mim][BF_4]$ based microemulsions (Figure 5.3.3. (a))

Thresholds for IL/o to bicontinuous and bicontinuous to o/IL microemulsion were noticeable at $\phi_{IL} \sim 0.0963$ ($R \sim 0.4510$) and $\phi_{IL} \sim 0.1635$ ($R \sim 0.7400$) respectively for $[C_4mim][BF_4]$ based microemulsion and at $\phi_{IL} \sim 0.0517$ ($R \sim 0.2255$) and $\phi_{IL} \sim 0.1647$ ($R \sim 0.6765$) respectively for $[C_4mim][MeSO_4]$ based microemulsions (Figure 5.3.3.

(b)) which are in agreement with the conductivity results and excess volume from density results.

From n^E vs. ϕ plot for TX-100/[C₂mim][TFSI]/water microemulsions, no information was available for phase transition (Figure 5.3.3. (c). For [C₄mim][PF₆] microemulsions phase transition occurred from w/IL to bicontinuous microemulsions at $\phi_W \sim 0.0726$ ($R \sim 0.7400$, $W_o \sim 3.1952$) which is in agreement with the conductivity r and excess volume from density results. No information regarding phase transition from bicontinuous to IL/w microemulsion could be obtained from Figure 5.3.3. (d).

All the thresholds obtained from n^E vs. ϕ plots for TX-100 microemulsions are in agreement with the conductivity and excess volume from density results.

5.3.1.4. Excess Molar Refraction from Refractive Index Results

Figure 3.3.13. shows R^E vs. ϕ plots for different TX-100 microemulsions based on both hydrophilic and hydrophobic ILs (Appendices Tables A71-74.). The excess refractive index of microemulsions were calculated from

$$R^E = R_{mic} - \sum_i \phi_i R_i \dots\dots\dots(5.3)$$

$$R_{mic} = \left[(n^2 - 1) / (n^2 + 2) \right] / V_m \dots\dots\dots(5.4)$$

where, R^E = the excess molar refraction, R_{mic} = the excess molar refraction of the microemulsions, R_i = the molar refraction of component i and V_m = molar volume of the microemulsion.

Percolation thresholds are obtained when transitions occur from IL/o to bicontinuous and bicontinuous to o/IL microemulsion at $\phi_{IL} \sim 0.1237$ ($R \sim 0.5600$) and $\phi_{IL} \sim 0.1674$ ($R \sim 0.7400$) respectively for [C₂mim][EtSO₄] based microemulsions and at $\phi_{IL} \sim 0.1215$ ($R \sim 0.6765$), transitions occur from IL/o to bicontinuous for [C₂mim][BF₄] based microemulsions (Figure 5.3.4. (a)).

Thresholds for IL/o to bicontinuous and bicontinuous to o/IL microemulsion were observed at $\phi_{IL} \sim 0.0963$ ($R \sim 0.4510$) and $\phi_{IL} \sim 0.1635$ ($R \sim 0.7400$) respectively for [C₄mim][BF₄] based microemulsion. The thresholds, although not clearly defined, were at $\phi_{IL} \sim 0.0517$ ($R \sim 0.2255$) and $\phi_{IL} \sim 0.1647$ ($R \sim 0.6765$) respectively for [C₄mim][MeSO₄] based microemulsions (Figure 5.3.4. (b)).

The phase transitions from w/IL to bicontinuous and bicontinuous to IL/w microemulsion occurred at $\phi_W \sim 0.1157$ ($R \sim 0.4510$, $W_o \sim 5.0731$) and $\phi_W \sim 0.2191$ ($R \sim 0.2255$, $W_o \sim 9.9697$) respectively in TX-100/[C₂mim][TFSI]/water microemulsions (Figure 5.3.4. (c), at $\phi_W \sim 0.0726$ ($R \sim 0.7400$, $W_o \sim 3.1952$) and $\phi_W \sim$

0.1345 ($R \sim 0.5600$, $W_o \sim 6.0346$) for $[C_4mim][PF_6]$ based microemulsions respectively (Figure 5.3.4. (d)).

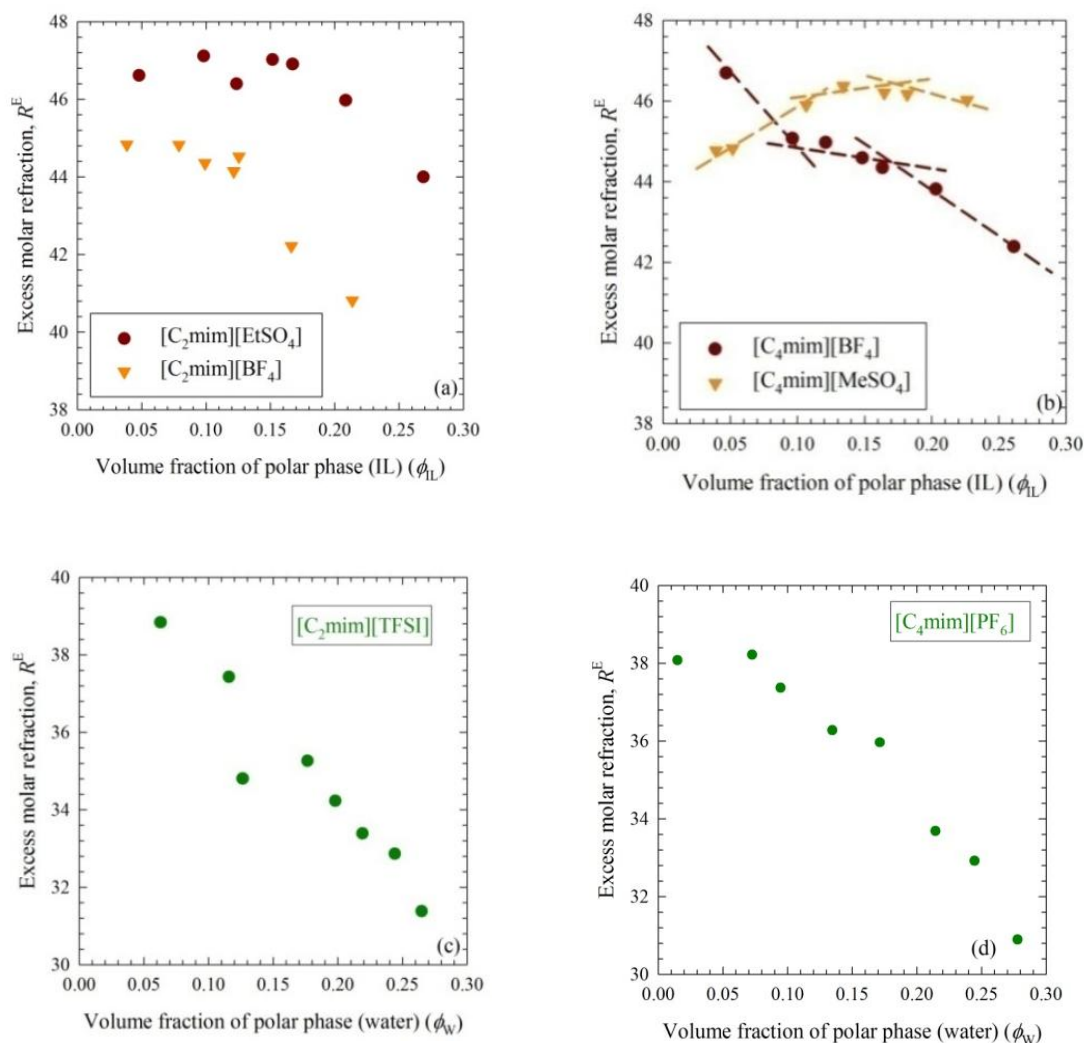


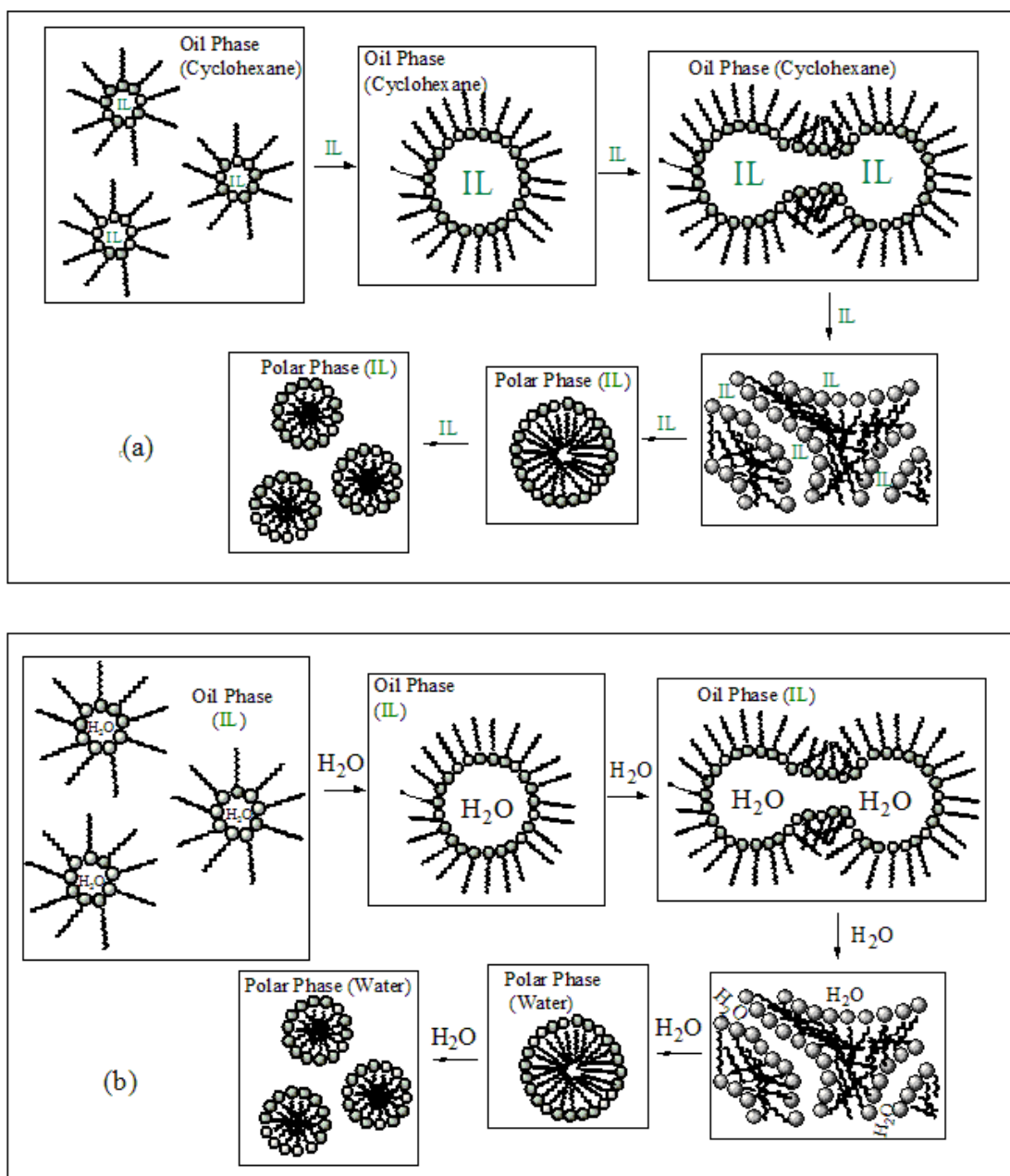
Figure 5.3.4. The R^E of (a) TX-100/cyclohexane/ $[C_2mim][EtSO_4]$, TX-100/cyclohexane/ $[C_2mim][BF_4]$, (b) TX-100/cyclohexane/ $[C_4mim][BF_4]$, TX-100/cyclohexane/ $[C_4mim][MeSO_4]$, (c) TX-100/ $[C_2mim][TFSI]$ /water, and (d) TX-100/ $[C_4mim][PF_6]$ /water microemulsions as a function of ϕ at 25 °C.

All the thresholds obtained from R^E vs. ϕ plots for TX-100 microemulsions are in agreement with the conductivity, excess volume from density, and excess refractive index from refractive index results.

5.3.1.5. Microstructures of Microemulsions

Scheme 5.1. (a) shows that with increasing ϕ_{IL} , for TX-100/cyclohexane/ $[C_2mim][EtSO_4]$, TX-100/cyclohexane/ $[C_2mim][BF_4]$, TX-100/cyclohexane/ $[C_4mim][BF_4]$, and TX-100/cyclohexane/ $[C_4mim][MeSO_4]$ microemulsions IL were encapsulated into the core of reverse micelle droplets and swollen effect occurred. Two or more droplets fuse to create small channels and further increasing ϕ_{IL} , small channels join and form a three dimensional complex

bicontinuous structure. The system further changes to micelle dominated microemulsions with increasing ϕ_{IL} . IL exists in the bulk and cyclohexane is encapsulated in the micelle core. Thus, three different structures of microemulsions can be identified such as, IL/o, bicontinuous and o/IL microemulsions. For TX-100/cyclohexane/[C₂mim][MeSO₄] system may be only IL/o microemulsions are formed due to the lower content of IL in each microemulsions.



Scheme 5.1. (a) Different microstructures of TX-100/cyclohexane/[C₂mim][EtSO₄], TX-100/cyclohexane/[C₂mim][BF₄], TX-100/cyclohexane/[C₄mim][BF₄], and TX-100/cyclohexane/[C₄mim][MeSO₄] microemulsions with increasing ϕ_{IL} and (b) TX-100/[C₂mim][TFSI]/water and TX-100/[C₄mim][PF₆]/water microemulsions with increasing ϕ_w .

Scheme 5.1. (b) shows that with increasing ϕ_w , for TX-100/[C₂mim][TFSI]/water and TX-100/[C₄mim][PF₆]/water microemulsions water encapsulated into the reverse micelle droplets. Small channels are formed when two or more droplets are fused. With further increase in the ϕ_w , small channels join to form bicontinuous complex structure. With increasing ϕ_w , the system further changes to micelle dominated microemulsions. Water exists in the bulk and IL is encapsulated in the micelle core. Different microregions such as, w/IL, bicontinuous and IL/w microemulsions can be identified. Only IL/w microemulsions may exist in TX-100/[C₂mim][PF₆]/water system due to low IL content in each microemulsions.

5.3.2. Analysis of Microregions of CTAB Based Microemulsions by Composition Percolation Theory

The mathematical concept of percolation threshold is related to percolation theory, which describes the formation of long-range connectivity in random systems. A giant connected component does not exist below the threshold and there exists a giant component of the order of system size above the threshold. Different microregions such as IL/o, bicontinuous and o/IL microemulsions may be identified by applying percolation theory in CTAB/1-butanol/cyclohexane/[C₂mim][MeSO₄], CTAB/1-butanol/cyclohexane/[C₂mim][EtSO₄] and CTAB/1-butanol/cyclohexane/[C₄mim][MeSO₄] systems.

5.3.2.1. Conductivity

Figure 5.3.5. shows the plot of $d\log\sigma/dR$ vs. R to determine the composition dependent percolation threshold of different CTAB microemulsions with hydrophilic and ILs (Appendices Tables A75-76.).

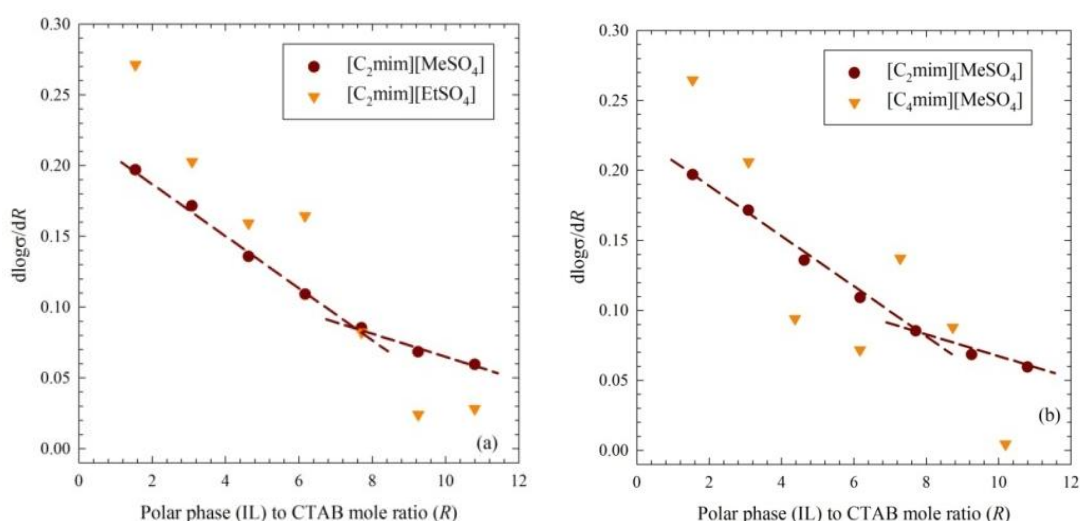


Figure 5.3.5. The $d\log\sigma/dR$ of (a) CTAB/1-butanol/cyclohexane/[C₂mim][MeSO₄], CTAB/1-butanol/cyclohexane/[C₂mim][EtSO₄] and (b) CTAB/1-butanol/cyclohexane/[C₂mim][MeSO₄], CTAB/1-butanol/cyclohexane/[C₄mim][MeSO₄] microemulsions as a function of R at 25 °C.

To get better percolation thresholds $d \log \sigma / dR$ vs. R plots are drawn as shown in Figure 3.3.9. For $[C_2mim][MeSO_4]$ based microemulsion system (Figure 3.3.9. (a)), the phase transition from IL/oil to bicontinuous microemulsion occurred at $R \sim 7.7121$ and for $[C_2mim][EtSO_4]$ based microemulsion system the phase transition from IL/oil to bicontinuous microemulsion occurs at $R \sim 6.1697$. Figure 3.3.9. (b) shows the phase transition for $[C_2mim][MeSO_4]$ based microemulsion system at $R \sim 7.7121$. For $[C_4mim][MeSO_4]$ based microemulsion system the phase transition from IL/oil to bicontinuous microemulsion occurred at $R \sim 7.2800$.

5.3.2.2. Size of Droplets

Figure 5.3.6. shows the plot of reverse micelle droplet size vs. R to determine the composition dependent percolation threshold for different CTAB based microemulsions with hydrophilic ILs (Appendices Tables A77-78.).

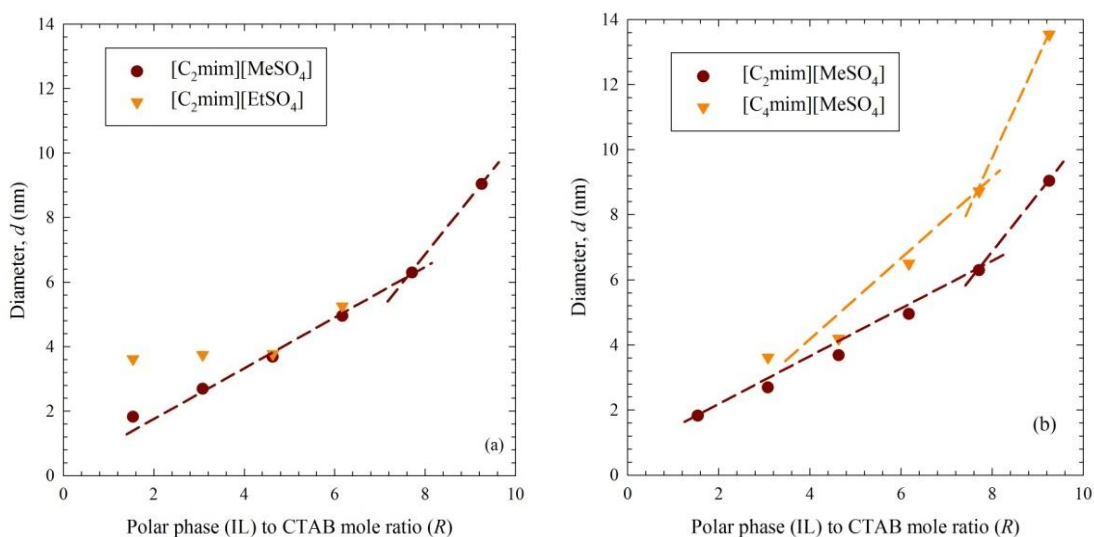
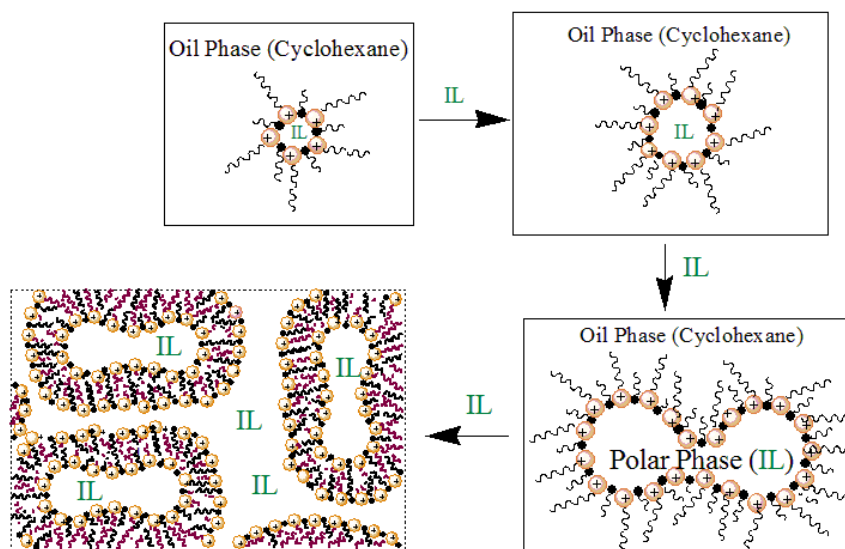


Figure 5.3.6. Diameter of droplets of (a) CTAB/1-butanol/cyclohexane/ $[C_2mim][MeSO_4]$, CTAB/1-butanol/cyclohexane/ $[C_2mim][EtSO_4]$ and (b) CTAB/1-butanol/cyclohexane/ $[C_2mim][MeSO_4]$, CTAB/1-butanol/cyclohexane/ $[C_4mim][MeSO_4]$ microemulsions as a function of R at 25 °C.

Diameter of droplets increases with increasing R value to indicate the formation of clusters of IL droplets and thereby the formation of bicontinuous phase. The phase transition occurred at $R \sim 7.7121$ for $[C_2mim][MeSO_4]$ based microemulsion system which is in agreement with the conductivity results. For $R \sim 4.500$, fusion might occur among IL droplets in $[C_2mim][EtSO_4]$ based microemulsion system (Figure 5.3.6. (a)) and for $R \sim 7.2800$ phase transition occurred for $[C_4mim][MeSO_4]$ based microemulsion system which is in agreement with the conductivity results (Figure 5.3.6. (b)).

5.3.2.3. Microstructures of Microemulsions

Two different structures such as, IL/o and bicontinuous microemulsion can be identified from the analysis of microregions from conductivity results by percolation theory. Thresholds obtained from DLS measurement are in agreement with the conductivity results. With increasing R value swollen effect occurs since IL is entrapped into the reverse micelle droplets. Small channels are formed due to the fusion of droplets and with further increase in the R value small channels join and form a three dimensional complex bicontinuous structure. Scheme 5.2. shows different microstructures of microemulsions with increasing R value.



Scheme 5.2. Different microstructures of CTAB microemulsions with increasing R .

5.4. Conclusions

The microstructures vary interestingly for different microemulsions based on Three different microstructures based on the nature and structure of the ILs and the type of the surfactant as well as the composition. The w/o, bicontinuous, and o/w microemulsions are observed for hydrophobic IL based TX-100 microemulsions; while for hydrophobic IL based TX-100 microemulsions the microstructures were IL/o, bicontinuous, and o/IL microemulsions. The phase transition occurs only from IL/o to bicontinuous microemulsions in the case of CTAB microemulsions with hydrophilic ILs. In w/o or IL/o microemulsions, the interaction between the isolated droplets is relatively weak. With increasing ϕ_w or ϕ_{IL} , the elastic droplets form clusters to form bicontinuous microemulsions. With further increase in the ϕ_w or ϕ_{IL} , the systems form o/w or o/IL microemulsions.

References

- [1] Friberg, S. E.; Bothorel, P. *Microemulsions: Structure and Dynamics*, CRC Press: Boca Raton, **1987**.
- [2] Regev, O.; Ezrahi, S.; Aserin, A.; Garti, N.; Wachtel, E.; Kaler, E.; Khan, A.; Talmon, Y. *Langmuir* **1996**, 12, 668-674.
- [3] Moulik, S. P.; Pal, B. K. *Adv. Colloid Interface Sci.* **1998**, 78, 99-195.

- [4] Yaghmur, A.; Aserin, A.; Antalek, B.; Garti, N. *Langmuir* **2003**, 19, 1063-1068.
- [5] Dong, X.; Erkey, C.; Dai, H. J.; Li, H. C.; Cochran, H. D.; Lin, J. S. *Ind. Eng. Chem. Res.* **2002**, 41, 1038-1042.
- [6] García-Río, L.; Leis, J. R.; López-Fontán, J. L.; Mejuto, J. C.; Mosquera, V.; Rodríguez-Dafonte, P. *J. Colloid Interface Sci.* **2005**, 289, 521-529.
- [7] van Bommel, A.; MacIsaac, G.; Livingstone, N.; Palepu, R. *Fluid Phase Equilib.* **2005**, 237, 59-67.
- [8] Fanun, M. *J. Dispersion Sci. Technol.* **2008**, 29, 1426-1434.
- [9] Mehta, S. K.; Kaur, G.; Mutneja, R.; Bhasin, K. K. *J. Colloid Interface Sci.* **2009**, 338, 542-549.
- [10] Fanun, M. *J. Colloid Interface Sci.* **2010**, 343, 496-503.
- [11] Paul, B. K.; Mitra, R. K. *J. Colloid Interface Sci.* **2006**, 295, 230-242.
- [12] Fanun, M. *J. Mol. Liq.* **2009**, 150, 25-32.
- [13] Li, X.; He, G.; Zheng, W.; Xiao, G. *Colloid Surface A* **2010**, 360, 150-158.
- [14] Paul, B. K.; Mitra, R. K.; Moulik, S. P. *Microemulsions: percolation of conductance and thermodynamics of droplet clustering. In Encyclopedia of Surface and Colloid Science*, ed. Somasundaran, P. Taylor & Francis: New York, **2006**.
- [15] Hattori, Y.; Ushiki, H.; Engl, W.; Courbin, L.; Panizza, P. *Physica A* **2005**, 353, 29-37.
- [16] Cid-Samamed, A.; García-Río, L.; Fernández-Gándara, D.; Mejuto, J. C.; Morales, J.; Pérez-Lorenzo, M. *J. Colloid Interface Sci.* **2008**, 318, 525-529.
- [17] Łuczak, J.; Hupka, J. *J. Mol. Liq.* **2014**, 199, 552-558.
- [18] Gao, Y.; Wang, S.; Zheng, L.; Han, S.; Zhang, X.; Lu, D.; Yu, L.; Ji, Y.; Zhang, G. *J. Colloid Interface Sci.* **2006**, 301, 612-616.
- [19] Naouli, N.; Rosano, H. L. *J. Dispersion Sci. Technol.* **2009**, 30, 370-378.
- [20] Lian, Y.; Zhao, K. *Soft Matter* **2011**, 7, 8828-8837.
- [21] Safran, S. A.; Grest, G. S.; Bug, A.; Webman, I. *Percolation in interacting microemulsions. In Microemulsion Systems*, eds. Rosano, H.; Clause, M. Marcel Dekker Inc.: New York, **1987**.
- [22] Pal, S.; Bisal, S. R.; Moulik, S. P. *J. Phys. Chem.* **1992**, 96, 896-901.
- [23] Garboczi, E. J.; Berryman, J. G. *New effective medium theory for the diffusivity or conductivity of a multi-scale concrete microstructure material*, *Concrete Sci. Eng.* **2000**, vol. 2.
- [24] Weissker, H. Ch.; Furthmiller, J.; Bechstedt, F. *Phys. Rev. B* **2003**, 67, 1653221-1653225.
- [25] Mehta, S. K.; Bala, K. *Fluid Phase Equilib.* **2000**, 172, 197-209.
- [26] Fanun, M. *J. Mol. Liq.* **2008**, 139, 14-22.
- [27] Fanun, M. *J. Mol. Liq.* **2008**, 142, 103-110.

Abstract

Physicochemical properties, such as viscosity, conductivity, density, and refractive index of different microemulsions prepared by varying polar phase, nonpolar phase and surfactant have been compared with focus on the similarities and contrastive features for variation of the nature and structure of the IL, type of the surfactant used, and composition, in particular R or W_o . The viscosity has been found to increase with increasing R in TX-100/cyclohexane/[C₂mim][EtSO₄] microemulsions; while viscosity initially decreases and after reaching a minimum value increases with increasing W_o for TX-100/[C₂mim][TFSI]/water microemulsions. With increasing W_o for TX-100/cyclohexane/water microemulsions the viscosity increases for both w/o and o/w microemulsions. The density increases with increasing R and W_o for TX-100/cyclohexane/[C₂mim][EtSO₄] and TX-100/cyclohexane/water microemulsions respectively and for TX-100/[C₂mim][TFSI]/water microemulsions it decreases with increasing W_o . The refractive index changes with increasing R for TX-100/cyclohexane/[C₂mim][EtSO₄] microemulsions; decreases with increasing W_o for TX-100/[C₂mim][TFSI]/water microemulsions and refractive index decreases with increasing W_o for both w/o and o/w microemulsions for TX-100/cyclohexane/water system. Physicochemical properties of CTAB/1-butanol/cyclohexane/water microemulsions have also been compared with CTAB/1-butanol/cyclohexane/[C₂mim][EtSO₄] microemulsions by using [C₂mim][EtSO₄] as the polar phase instead of water. The viscosity increases with increasing R for CTAB/1-butanol/cyclohexane/[C₂mim][EtSO₄] microemulsions. On the other hand, the viscosity slightly increases with increasing W_o for w/o microemulsions and initially increases and then decreases with increasing W_o for o/w microemulsions in CTAB/1-butanol/cyclohexane/water system. The shows any increase with increasing R and W_o for CTAB/1-butanol/cyclohexane/[C₂mim][EtSO₄] and CTAB/1-butanol/cyclohexane/water microemulsions respectively. The refractive index increases with increasing R for CTAB/1-butanol/cyclohexane/[C₂mim][EtSO₄] microemulsions and for CTAB/1-butanol/cyclohexane/water microemulsions the refractive index only changes slightly. Physicochemical properties of TX-100/cyclohexane/[C₂mim][EtSO₄] and CTAB/1-butanol/cyclohexane/[C₂mim][EtSO₄] microemulsions have been compared with each other. For both systems conductivity, viscosity, and density increase with increasing R . For CTAB/1-butanol/cyclohexane/[C₂mim][EtSO₄] and TX-100/cyclohexane/[C₂mim][EtSO₄] microemulsions, the refractive index increases with increasing R . Finally, the strategy to tune physicochemical properties of IL based microemulsions by controlling different parameters has been developed.

6.1. Introduction

Microemulsions consist of sphere-shaped droplets of a disperse phase separated by a layer of surfactant from a continuous phase [1]. They can dissolve both hydrophobic and hydrophilic compounds simultaneously for the presence of both organic and aqueous environments. A variety of phases such as w/o to o/w through bicontinuous phase can exist in equilibrium with one another [2, 3]. Molecular structure,

temperature, salinity, nature of the surfactant and cosurfactant, the water/oil to surfactant ratio, and nature of the oil affect the phase transition between different types of microemulsions [4-8]. Reverse micelles and w/o microemulsions have attracted significant attention as a result of their capability to host hydrophilic components in nonpolar solvents. These systems act like “nanoreactors” for a variety of chemical and biological reactions that involve hydrophobic and hydrophilic reactants [9, 10].

Cationic surfactant ,BHDC was reported to form reverse micelles in nonpolar solvents without the addition of a cosurfactant [11-13]. In fact, nonionic surfactant, TX-100 was widely used for preparation of reverse micelle without the use of a cosurfactant [14-16]. In recent years, attempts have been made to prepare waterless reverse micelles by the use of polar solvents, which have relatively high dielectric constant [17]. These nonaqueous reverse micelles are essentially oil continuous [18] and have attracted much interest from both theoretical and practical viewpoints [19-23]. ILs are attractive as an influential substitute to conventional organic solvents [24-27]. Nonaqueous IL based microemulsions are interesting since they provide hydrophobic or hydrophilic nanodomains expanding the potential uses of the ILs in microheterogeneous systems as reaction, separation, and/or extraction media [28-31].

Useful information about the possible structures of microemulsions can be obtained from the study of physicochemical properties of microemulsions such as conductivity, viscosity, density, refractive index etc. [32-34]. Very few studies have been made for comparative studies of physicochemical properties of microemulsions containing ILs. Rao et al. [35] characterized $[C_4mim][AOT]/benzene/ILs$ microemulsions by performing a phase behavior study, DLS measurements, and 1H NMR measurements. Area of single phase region was found to increase with increase in alkyl chain length of the cation of ILs which followed the trend $[C_6mim][TFSI] > [C_4mim][TFSI] > [C_2mim][TFSI]$ and increased with decrease in the cation-anion interaction strength of added ILs and followed the trend $[C_4mim][TFSI] > [C_4mim][PF_6] > [C_4mim][BF_4]$. The size increased with increasing R value and followed the trend $[C_2mim][TFSI] > [C_4mim][TFSI] > [C_6mim][TFSI]$. The size increase was almost the same with increase in R value in the case of ILs with different anions. IL/o microemulsions are highly thermally stable compared to those of aqueous microemulsions. From DLS measurements it could be observed that the aggregates in microemulsions remained monodisperse in nature with increasing temperature at $R = 1.0$ and in all the cases with increasing temperature, the size of aggregates in microemulsions decreased [35]. The added water in IL/o microemulsions has a prominent effect on the microstructure of the microemulsions. A clear picture of locations of the ILs in $[C_4mim][AOT]/benzene/ILs$ microemulsions and the added water molecules in microemulsions could be obtained by 1H NMR spectra. Using the solvatochromic behavior of 1-methyl-8-oxyquinolinium betaine (QB) as an absorption probe and DLS technique Falcone et al. [36] studied the microenvironment of the polar core of

different IL reverse micelle systems. The reverse micelle of surfactant/benzene/IL systems consist of two different ILs ($[C_4mim][BF_4]$ and $[C_4mim][TFSI]$) sequestered by TX-100 and BHDC. To characterize these nonaqueous reverse micelles, the effect of the variation of R on the QB spectroscopy was studied. DLS studies showed that with increasing R the droplet size increases which confirm the formation of IL reverse micelles [36].

The aim of this work is to compare studies of physicochemical properties of IL based microemulsions with conventional microemulsions for both TX-100 and CTAB. Physicochemical properties, such as viscosity, conductivity, density, and refractive index of different microemulsions been compared contrasted for variation of the nature and structure of the IL, type of the surfactant used, and composition, in particular R or W_o . prepared In these microemulsions, hydrophilic $[C_2mim][EtSO_4]$ was used as the polar phase instead of water and hydrophobic $[C_2mim][TFSI]$ was used as the nonpolar phase instead of cyclohexane. Physicochemical properties of TX-100 and CTAB based microemulsions with $[C_2mim][EtSO_4]$ and cyclohexane as polar and nonpolar phase respectively were also compared. Attempts have been made to tune physicochemical properties of IL based microemulsions by controlling different parameters for desirable chemistry.

6.2. Experimental

6.2.1. Materials

TX-100, CTAB, cyclohexane, 1-butanol and the ILs, $[C_2mim][EtSO_4]$ and $[C_2mim][TFSI]$ were obtained from Sigma-Aldrich. De-ionized water was used to prepare conventional TX-100 and CTAB microemulsions and hydrophobic IL based microemulsions of TX-100. The elaborated forms of the abbreviations have been given in Section 1.11. of Chapter 1.

6.2.2. Preparation of Microemulsions

Conventional and IL based microemulsions with TX-100 and CTAB were prepared with a constant amount of TX-100 (70 % wt) and CTAB (5 % wt) with variation of the polar and the nonpolar phases to keep the total weight of the microemulsion constant. Compositions of conventional and IL based microemulsions were discussed briefly in Sections 2.3. and 2.4. of Chapter 2 respectively.

6.2.3. Measurements

Viscosity, density and refractive index were measured to characterize the microemulsions. All the measurements have been described in detail in Section 3.2.3. of Chapter 3.

6.3. Results and Discussions

6.3.1. Comparative Study of Physicochemical Properties of Conventional vs. IL Based Microemulsions of TX-100

6.3.1.1. Viscosity

Figure 6.3.1. shows the change of viscosity of different series of TX-100 microemulsions with increasing R or W_o at 25 °C (Appendices Table A79.). For TX-100/cyclohexane/[C₂mim][EtSO₄] microemulsions, the viscosity increases with increasing R . The viscosity, on the hand, initially decreases and after reaching a minimum value viscosity increases with increasing W_o for TX-100/[C₂mim][TFSI]/water microemulsions. For TX-100/cyclohexane/water microemulsions, the viscosity increases for both w/o and o/w microemulsions with increasing W_o .

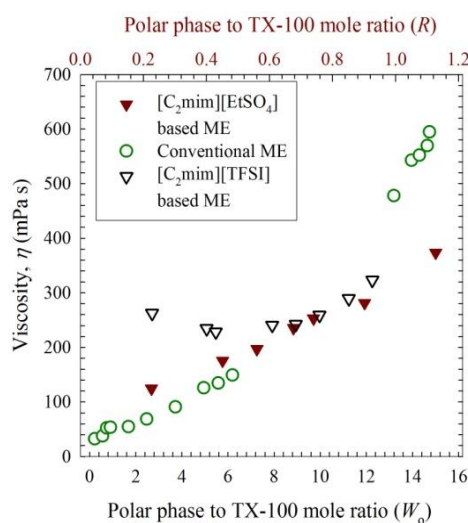


Figure 6.3.1. Viscosity of TX-100/cyclohexane/[C₂mim][EtSO₄], TX-100/[C₂mim][TFSI]/water and TX-100/cyclohexane/water microemulsions as a function of R or W_o at 25 °C. R value at the top is for clarity for TX-100/cyclohexane/[C₂mim][EtSO₄] microemulsions.

TX-100/cyclohexane/[C₂mim][EtSO₄] system changes from IL/o to bicontinuous and bicontinuous to o/IL microemulsion at $\phi_{IL} \sim 0.1237$ ($R \sim 0.5600$) and $\phi_{IL} \sim 0.1674$ ($R \sim 0.7400$) respectively with increasing R . Polar phase is IL and oil phase is cyclohexane. On the other hand, TX-100/[C₂mim][TFSI]/water system changes from w/IL to bicontinuous and bicontinuous to IL/w microemulsions at $\phi_w \sim 0.1157$ ($R \sim 0.4510$, $W_o \sim 5.0731$) and $\phi_w \sim 0.2191$ ($R \sim 0.2255$, $W_o \sim 9.9697$) respectively with increasing W_o (Section 5.3.1.1.). Here polar phase is water and oil phase is IL. For conventional microemulsions, only o/w and w/o microemulsions are formed. Water is the polar phase and cyclohexane is the oil phase. W_o from 6.9385 to 12.3903 i.e. with TX-100, cyclohexane and water at 70.0000 %, 16.0000-5.0000 % and 14.0000-25.0000 % respectively gel formation occurred (Section 2.3.1.).

TX-100/cyclohexane/[C₂mim][EtSO₄] system with low R , viscosity mainly depends on the continuous cyclohexane medium. (Figure 3.3.2. (a, b)). With the addition of

more viscous IL, the size of reverse micelle droplets increase due to the encapsulation of IL into reverse micelle droplets. With further increase in R , the viscosity increases due to the formation of three dimensional channels among droplet clusters at a given temperature. When the system changes to o/IL microemulsions with increasing R , IL is the continuous medium and cyclohexane is encapsulated into the core of micelles and the viscosity further increases.

For TX-100/[C₂mim][TFSI]/water microemulsions with low W_o , the continuous medium is aggregated IL of w/IL microemulsions and thus viscosity is high. Strong Coulombic attraction exists in aggregated IL in the bulk. With increasing W_o , the mobility of ions of IL increases since water dissociates the aggregated IL in the bulk and the viscosity decreases. The size of reverse micelle droplets increase and simultaneously clustering of water droplets in microemulsions occurs with increasing W_o and the ions of IL can easily move through the small channels. When bicontinuous complex microemulsions are formed, the viscosity has the lowest value due to the increased mobility of ions of IL in the channels. In IL/w microemulsions water exists in the bulk and IL is encapsulated in the core of micelles where the mobility of ions of IL decreases. In the bulk H-bond formation may occur among water molecules and thus viscosity further increases.

For conventional w/o microemulsions, the size of reverse micelle increases and simultaneously clustering of water droplets in microemulsions occurs with increasing W_o and thus viscosity increases. In the core of both droplets and cluster of droplets water molecules may form H-bonds. For conventional o/w microemulsions water exists in the bulk of micelle dominated microemulsions. In the bulk strong H-bonds may form among water molecules and the viscosity sharply increases.

6.3.1.2. Density

Figure 6.3.2. shows the change of density of different series of TX-100 microemulsions with increasing R or W_o at 25 °C (Appendices Table A80.). For TX-100/cyclohexane/[C₂mim][EtSO₄] microemulsions the density shows an increase with increasing R . For TX-100/[C₂mim][TFSI]/water microemulsions, the density on the other hand, decreases with increasing W_o and for TX-100/cyclohexane/water microemulsions density increases for both w/o and o/w microemulsions with increasing W_o .

Density of [C₂mim][EtSO₄] (1.2356 gcm⁻³) was higher compared to cyclohexane (0.7781 gcm⁻³). Therefore, it is expected that the addition of the IL would dominate overall density of the system. With an increase in the amount of IL, the density also increases.

For TX-100/[C₂mim][TFSI]/water microemulsions, the amount of water is increased with increasing W_o and simultaneously the amount of IL is decreased. With the decrease of the amount of IL density also decreases. It may be worth comparing the density of [C₂mim][TFSI] and water as 1.5186 gcm⁻³ and 0.99705 gcm⁻³ respectively.

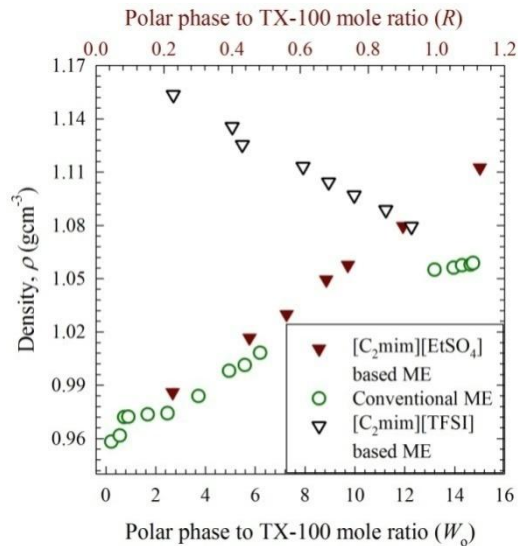


Figure 6.3.2. Density of TX-100/cyclohexane/[C₂mim][EtSO₄], TX-100/[C₂mim][TFSI]/water and TX-100/cyclohexane/water microemulsions as a function of R or W_0 at 25 °C. R value at the top is for clarity for TX-100/cyclohexane/[C₂mim][EtSO₄] microemulsions.

Density of water is higher compared to cyclohexane. With increasing W_0 , the amount of water is increased and simultaneously the amount of cyclohexane is decreased in conventional microemulsions. As a consequence, with the increase in the amount of water density also increases.

6.3.1.3. Refractive Index

Figure 6.3.3. shows the change of refractive index of different series of TX-100 microemulsions with increasing R or W_0 at 25 °C (Appendices Table A81.).

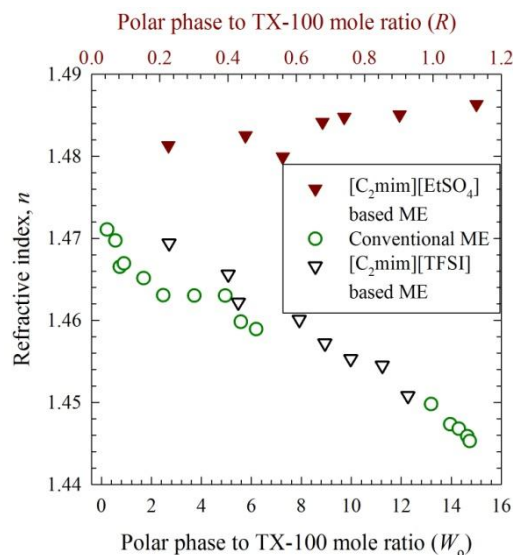


Figure 6.3.3. Refractive index of TX-100/cyclohexane/[C₂mim][EtSO₄], TX-100/[C₂mim][TFSI]/water and TX-100/cyclohexane/water microemulsions as a function of R or W_0 at 25 °C. R value at the top is for clarity for TX-100/cyclohexane/[C₂mim][EtSO₄] microemulsions.

For TX-100/cyclohexane/[C₂mim][EtSO₄] microemulsions, the refractive index does not change significantly with increasing *R*; for TX-100/[C₂mim][TFSI]/water microemulsions refractive index decreases with increasing *W*₀ and for TX-100/cyclohexane/water microemulsions refractive index decreases with increasing *W*₀ for both w/o and o/w microemulsions with increasing *W*₀. For conventional microemulsions refractive index decreases with increasing *W*₀ for both w/o and o/w microemulsions.

6.3.2. Comparative Study of Physicochemical Properties of Conventional vs. IL Based Microemulsions of CTAB

6.3.2.1. Viscosity

Figure 6.3.4. shows the change of the viscosity for different series of CTAB microemulsions with increasing *R* or *W*₀ at 25 °C (Appendices Table A82.). It is apparent that for CTAB/1-butanol/cyclohexane/[C₂mim][EtSO₄] microemulsions, the viscosity increases with increasing *R*. For w/o microemulsions in CTAB/1-butanol/cyclohexane/water system, the viscosity slightly increases with increasing *W*₀ and for o/w microemulsions in CTAB/1-butanol/cyclohexane/water system viscosity initially increases and then decreases with increasing *W*₀.

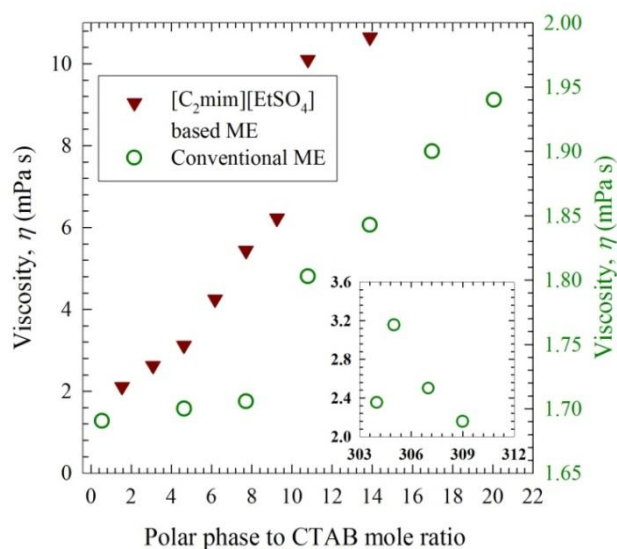


Figure 6.3.4. Viscosity of CTAB/1-butanol/cyclohexane/[C₂mim][EtSO₄] and CTAB/1-butanol/cyclohexane/water microemulsions as a function of polar phase to CTAB mole ratio at 25 °C. Viscosity at the right side is for clarity for CTAB/1-butanol/cyclohexane/water microemulsions.

For [C₂mim][EtSO₄] based microemulsion system, the phase transition from IL/oil to bicontinuous microemulsion occurs at *R* ~ 6.1697 (Section 5.3.2.1.). For conventional microemulsions, only o/w and w/o microemulsions are formed. *W*₀ from 25.0001 to 302.0001 i.e. with CTAB, cyclohexane:butanol (1:1) and water at 5.0000 %, 88.8212-20.3605 % and 6.1788-74.6395 % respectively the solution became turbid (Section 2.3.2.).

At low value of R , IL/o microemulsion exists for $[\text{C}_2\text{mim}][\text{EtSO}_4]$ based microemulsions. Here cyclohexane is the continuous medium. In IL/o microemulsion viscosity mainly depends on the continuous cyclohexane medium. With increasing R i.e. increasing IL content the viscosity increases since two or more IL droplets fuse to create small channels which reduce the flow between layers of microemulsions. The viscosity of the IL is higher than cyclohexane. For further increase in R value three dimensional network of channels occurs which drastically reduce the flow between layers resulting in the steeper increase of viscosity.

For conventional w/o microemulsions, cyclohexane is the continuous medium. With increasing W_o i.e. increasing water content the viscosity slightly increases for w/o microemulsions. Water is encapsulated into the reverse micelle droplets and the size of water droplets increases. Water droplets can aggregate with one another and thus the viscosity increases

For conventional o/w microemulsions, water is the continuous medium. Initially with increasing W_o , H-bond formation may occur among water molecules and viscosity increases. But further increasing W_o may be the mobility of counter ions (Br^-) in the water continuous medium increases and thus viscosity decreases.

As the viscosity of IL is higher compared to water, the viscosity of IL based microemulsions increases sharply compared to the conventional microemulsions.

6.3.2.2. Density

Figure 6.3.5. shows the change of density of different series of CTAB microemulsions with increasing R or W_o at 25 °C (Appendices Table A83.).

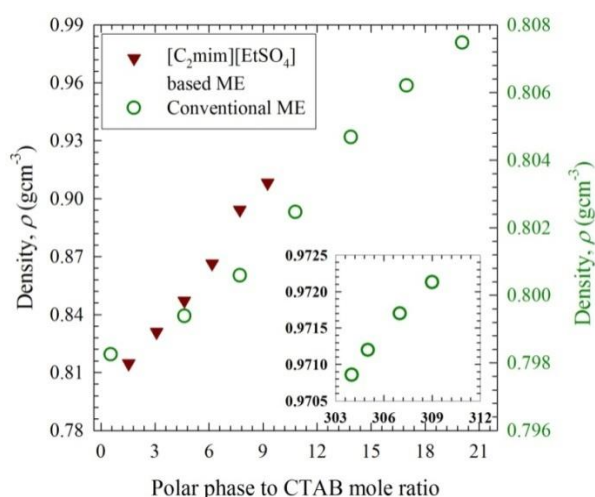


Figure 6.3.5. Density of CTAB/1-butanol/cyclohexane/ $[\text{C}_2\text{mim}][\text{EtSO}_4]$ and CTAB/1-butanol/cyclohexane/water microemulsions as a function of polar phase to CTAB mole ratio at 25 °C. Density at the right side is for clarity for CTAB/1-butanol/cyclohexane/water microemulsions.

For CTAB/1-butanol/cyclohexane/[C₂mim][EtSO₄] and CTAB/1-butanol/cyclohexane/water microemulsions, the density increases with increasing R and W_0 . Density of IL in IL based microemulsions is higher compared to water in conventional microemulsions. For both the system cyclohexane is the oil phase. Addition of the polar phase (IL or water) and simultaneously decreasing cyclohexane content for both the systems results in an increase in density.

6.3.2.3. Refractive Index

Figure 6.3.6. shows the change of refractive index of different series of CTAB microemulsions with increasing R or W_0 at 25 °C (Appendices Table A84.). The refractive index increases with increasing R for CTAB/1-butanol/cyclohexane/[C₂mim][EtSO₄] microemulsions. For conventional CTAB microemulsions, refractive index show only slight from 1.3506 to 1.4098.

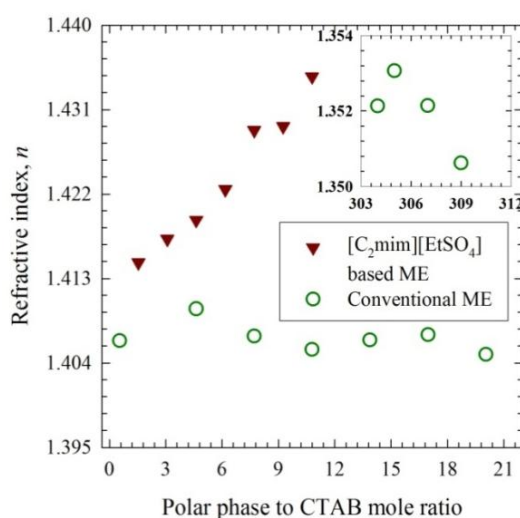


Figure 6.3.6. Refractive index of CTAB/1-butanol/cyclohexane/[C₂mim][EtSO₄] and CTAB/1-butanol/cyclohexane/water microemulsions as a function of polar phase to CTAB mole ratio at 25 °C.

The number of ions of IL in the core of reverse micelle droplets increases with increasing R in IL based microemulsions. At the same time aggregation occurs among IL droplets. Cations and anions of ILs, positive head group and the negative counterion Br⁻ of CTAB have their own electric field which repel to the electric vector of light. As a result, the angle of refraction of light through the droplets in microemulsions increases.

6.3.3. Comparative Study of Physicochemical Properties of IL Based Microemulsions with TX-100 and CTAB

6.3.3.1. Conductivity

Figure 6.3.7. shows the change of conductivity of TX-100/cyclohexane/[C₂mim][EtSO₄] and CTAB/1-butanol/cyclohexane/[C₂mim][EtSO₄] microemulsions with increasing R at 25 °C

(Appendices Table A85.). For both systems, the conductivity increases with increasing R .

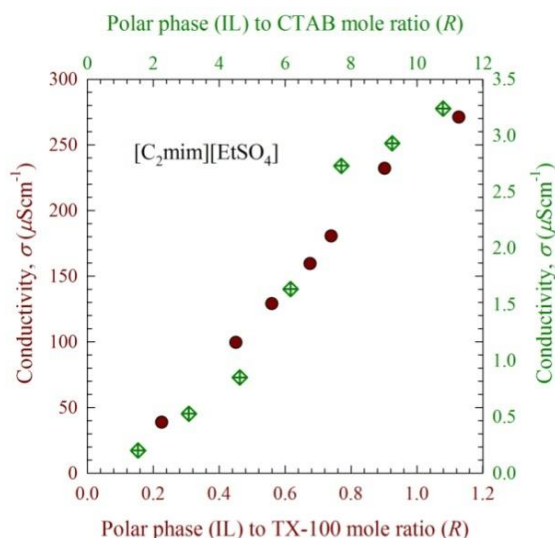


Figure 6.3.7. Conductivity of TX-100/cyclohexane/[C₂mim][EtSO₄] and CTAB/1-butanol/cyclohexane/[C₂mim][EtSO₄] microemulsions as a function of R at 25 °C. Conductivity at the left and R value at the bottom is for TX-100/cyclohexane/[C₂mim][EtSO₄] microemulsions.

The conductivity of TX-100 microemulsions (70.0000 % wt TX-100, 24.0321-0.1610 % wt cyclohexane, 5.9680-29.8390 % wt [C₂mim][EtSO₄] (Section 2.4.1.)). show much higher value compared to CTAB based microemulsions (5.0000 % wt CTAB, 90.0000-60.0000 % wt cyclohexane:butanol (1;1), 5.0000-35.0000 % wt [C₂mim][EtSO₄] (Section 2.4.3.)). With increasing R , TX-100 microemulsions undergo transition from IL/o to o/IL microemulsions via bicontinuous microemulsions and CTAB microemulsions change from IL/o to bicontinuous microemulsions.

As the value of R increases, IL can encapsulate into TX-100 reverse micelle core and the size of the droplets increase. [EtSO₄]⁻ of [C₂mim][EtSO₄] can interact with hydrogen of terminal hydroxide of head group of TX-100. Cations stay close to the anions. The mobility of [EtSO₄]⁻ may be the main factor for increasing conductivity in IL/o microemulsions. In bicontinuous microemulsions, due to the formation of three dimensional channels conductivity further increases for the mobility of both the [C₂mim]⁺ and [EtSO₄]⁻ of the IL in the system. With further increases in R , the mobility of [C₂mim]⁺ may be the main factor for increasing conductivity in micelle dominated microemulsions. The nonpolar part of [EtSO₄]⁻ and the tail part of TX-100 in micelle core have hydrophobic attraction. The mobility of [C₂mim]⁺ may increases in the bulk.

On the other hand, the positive charge in CTAB head group is more localized than [C₂mim]⁺ in [C₂mim][EtSO₄] based microemulsions of CTAB. Therefore, a strong Coulombic interaction arises between [EtSO₄]⁻ and the CTAB head group than with

its own $[\text{C}_2\text{mim}]^+$. The interaction between $[\text{C}_2\text{mim}]^+$ and counterions (Br^-) may increase. H-bond may exist between the negatively charged oxygen of $[\text{EtSO}_4]^-$ and the partially positive hydrogen of terminal OH- group of 1-butanol. In the interface of CTAB surfactant, ions of IL and counter ions of CTAB may stuck and the mobility of ions decreases as compared to TX-100 microemulsions. Thus the conductivity of CTAB microemulsions shows much lower value compared to TX-100 microemulsions.

6.3.3.2. Viscosity

Figure 6.3.8. shows the change of viscosity of TX-100/cyclohexane/ $[\text{C}_2\text{mim}][\text{EtSO}_4]$ and CTAB/1-butanol/cyclohexane/ $[\text{C}_2\text{mim}][\text{EtSO}_4]$ microemulsions with increasing R at 25 °C (Appendices Table A86.). The viscosity for both systems has been found to increase with increasing R .

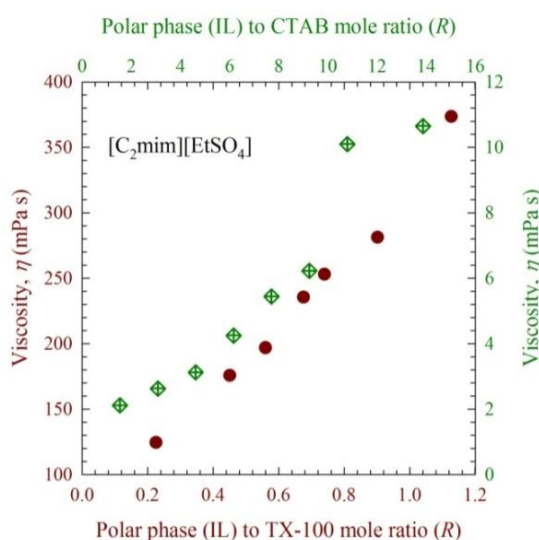


Figure 6.3.8. Viscosity of TX-100/cyclohexane/ $[\text{C}_2\text{mim}][\text{EtSO}_4]$ and CTAB/1-butanol/cyclohexane/ $[\text{C}_2\text{mim}][\text{EtSO}_4]$ microemulsions as a function of R at 25 °C.

The mobility of ions of IL in CTAB microemulsions decreases as compared to TX-100 microemulsions. Formation of channels may occur with ease in TX-100 microemulsions compared to CTAB microemulsions. Thus the viscosity of TX-100 based microemulsions is much higher compared to CTAB microemulsions. In o/IL microemulsions of TX-100, IL exists in the bulk and the viscosity further increases.

6.3.3.3. Density

Figure 6.3.9. shows the change of density of TX-100/cyclohexane/ $[\text{C}_2\text{mim}][\text{EtSO}_4]$ and CTAB/1-butanol/cyclohexane/ $[\text{C}_2\text{mim}][\text{EtSO}_4]$ microemulsions with increasing R at 25 °C (Appendices Table A87.). An increase in the value of R brings about an increase in density for both systems. For both the system, cyclohexane is the oil phase and IL is the polar phase. With increasing R , the density increases for both the systems. Addition of the IL contributes to the densities and it dominates the system.

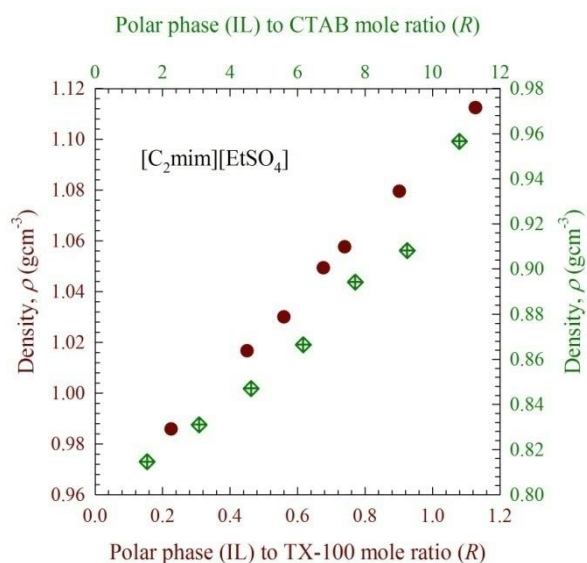


Figure 6.3.9. Density of TX-100/cyclohexane/[C₂mim][EtSO₄] and CTAB/1-butanol/cyclohexane/[C₂mim][EtSO₄] microemulsions as a function of R at 25 °C. Density at the left and R value at the bottom is for TX-100/cyclohexane/[C₂mim][EtSO₄] microemulsions.

6.3.3.4. Refractive Index

Figure 6.3.10. shows the change of refractive index for TX-100/cyclohexane/[C₂mim][EtSO₄] and CTAB/1-butanol/cyclohexane/[C₂mim][EtSO₄] microemulsions with increasing R at 25 °C (Appendices Table A88.).

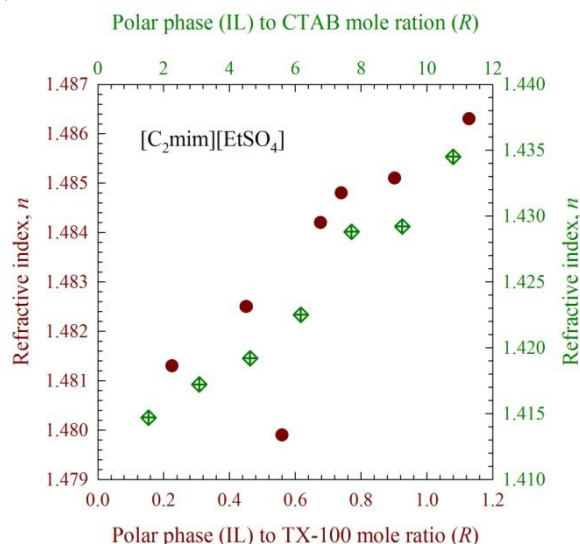


Figure 6.3.10. Refractive index of TX-100/cyclohexane/[C₂mim][EtSO₄] and CTAB/1-butanol/cyclohexane/[C₂mim][EtSO₄] microemulsions as a function of R at 25 °C. Conductivity at the left and R value at the bottom are for TX-100/cyclohexane/[C₂mim][EtSO₄] microemulsions.

For CTAB/1-butanol/cyclohexane/[C₂mim][EtSO₄] and TX-100/cyclohexane/[C₂mim][EtSO₄], the refractive index increases with increasing R . With increasing R in IL based microemulsions, the number of ions of IL increases in the systems. At $\phi_{IL} \sim 0.1237$ ($R \sim 0.5600$) the system changes from IL/o to bicontinuous microemulsions for TX-100 microemulsions.

6.4. Conclusions

TX-100/cyclohexane/[C₂mim][EtSO₄] microemulsions change from IL/o to o/IL microemulsions via bicontinuous microemulsions with increasing R . IL droplets aggregate and channel formation occurs with increasing R . Aggregation of IL droplets and channel formation also occur with increasing R for CTAB/1-butanol/cyclohexane/[C₂mim][EtSO₄] microemulsions. H-bond and enhancement of mobility of counter ions also increase in the continuous medium at high R values. The physicochemical properties, such as density, viscosity, and refractive index are dictated by the microenvironment in the microemulsions which is strongly dependent on the type of the surfactant, structure of the ionic liquids and composition. Microemulsions with desirable properties may thus be prepared by controlling the composition and careful choice of the polar and nonpolar phase. Ionic liquids are definitely better choices as both the polar and nonpolar phases and the structure of ionic liquids may be widely varied by changing the structure of the cation and the anion to fine tune physicochemical properties of microemulsions.

References

- [1] Fanun, M. *Microemulsions: Properties and application*, Surfactant science series, vol. 144, CRC press.
- [2] Bera, A.; Ojha, K.; Kumar, T.; Mandal, A. *J. Chem. Eng. Data* **2012**, 57, 1000-1006.
- [3] Bera, A.; Mandal, A.; Kumar, T. *J. Chem. Eng. Data* **2014**, 59, 2490-2498.
- [4] Chai, J. L.; Zhao, J. R.; Gao, Y. H.; Yang, X. D.; Wu, C. *Colloid Surface A* **2007**, 302, 31-35.
- [5] Chen, L.; Shang, Y.; Liu, H.; Hu, Y. *Colloid Surface A* **2007**, 305, 29-35.
- [6] Aarra, M. G.; Hoiland, H.; Skauge, A. *J Colloid Interf. Sci.* **1999**, 215, 201-215.
- [7] Nakamae, M.; Abe, M.; Ogino, K. *J Colloid Interf. Sci.* **1988**, 31, 466-472.
- [8] Sripriya, R.; Raja, K. M.; Santhosh, G.; Chandrasekaran, M.; Noel, M. *J Colloid Interf. Sci.* **2007**, 314, 712-717.
- [9] De, T. K.; Maitra, A. *Adv. Colloid Interface Sci.* **1995**, 59, 95-193.
- [10] Silber, J. J.; Biasutti, M. A.; Abuin, E.; Lissi, E. *Adv. Colloid Interface Sci.* **1999**, 82, 189-252.
- [11] Correa, N. M.; Biasutti, M. A.; Silber, J. J. *J. Colloid Interf. Sci.* **1996**, 184, 570-578.
- [12] McNeil, R.; Thomas, J. K. *J. Colloid Interf. Sci.* **1981**, 83, 57.
- [13] Novaira, M.; Biasutti, M. A.; Silber, J. J.; Correa, N. M. *J. Phys. Chem. B* **2007**, 111, 748-759.

- [14] Zhu, D.; Schelly, Z. A. *Langmuir* **1992**, 8, 48-50.
- [15] Gu, J.; Schelly, Z. A. *Langmuir* **1997**, 13, 4256-4266.
- [16] Zhu, D. M.; Wu, X.; Schelly, Z. A. *J. Phys. Chem.* **1992**, 96, 7121-7126.
- [17] Martino, A.; Kaler, E. W. *J. Phys. Chem.* **1990**, 94, 1627-1631.
- [18] Ray, S.; Moulik, S. P. *Langmuir* **1994**, 10, 2511-2515.
- [19] Fletcher, P. D. I.; Galal, M. F.; Robinson, B. H. *J. Chem. Soc., Faraday Trans. I* **1984**, 80, 3307-3314.
- [20] López-Cornejo, P.; Costa, S. M. B. *Langmuir* **1998**, 14, 2042-2049.
- [21] Das, K. P.; Ceglie, A.; Lindman, B. *J. Phys. Chem.* **1987**, 91, 2938-2946.
- [22] Arcoleo, V.; Aliotta, F.; Goffredi, M.; La Manna, G.; Turco Liveri, V. *Mater. Sci. Eng. C* **1997**, 5, 47-53.
- [23] Riter, R. E.; Kimmel, J. R.; Undiks, E. P.; Levinger, N. E. *J. Phys. Chem. B* **1997**, 101, 8292-8297.
- [24] Sheldon, R. *Chem. Commun.* **2001**, 2399-2407.
- [25] Welton, T.; Wasserscheid, P. *Ionic Liquids in Synthesis*, VCH-Wiley, Weinheim, Germany, **2002**.
- [26] Welton, T. *Coord. Chem. Rev.* **2004**, 248, 2459-2477.
- [27] Freemantle, M. *Chem. Eng. News* **1998**, 76, 32-37.
- [28] Cheng, S.; Zhang, J.; Zhang, Z.; Han, B. *Chem. Commun.* **2007**, 2497-2499.
- [29] Moniruzzaman, M.; Kamiya, N.; Goto, M. *Langmuir* **2009**, 25, 977-982.
- [30] Gao, H. X.; Li, J. C.; Han, B. X.; Chen, W. N.; Zhang, J. L.; Zhang, R.; Yan, D. D. *Phys. Chem. Chem. Phys.* **2004**, 6, 2914-2916.
- [31] Eastoe, J.; Gold, S.; Rogers, S. E.; Paul, A.; Welton, T.; Heenan, R. K.; Grillo, I. *J. Am. Chem. Soc.* **2005**, 127, 7302-7303.
- [32] Zielinska, K.; Wilk, K. A.; Jezierski, A.; Jesionowski, T. *J. Colloid Interf. Sci.* **2008**, 321, 408-417.
- [33] Patidar, V.; Chandra, A.; Singh, M.; Kale, R. K. *International Journal of Renewable and Sustainable Energy* **2014**, 3, 13-19.
- [34] Kestin, J.; Sokolov, M.; Wakeham, W. A. *J. Phys. Chem. Ref. Data* **1978**, 7, 941-948.
- [35] Rao, V. G.; Mandal, S.; Ghosh, S.; Banerjee, C.; Sarkar, N. *J. Phys. Chem. B* **2013**, 117, 1480-1493.
- [36] Falcone, R. D.; Correa, N. M.; Silber, J. J. *Langmuir* **2009**, 25, 10426-10429.

Abstract

Lipase catalyzed hydrolysis of *p*-NPB was investigated in aqueous medium, w/o, w/C₄mim][PF₆], and bicontinuous [C₄mim][PF₆] based microemulsions to evaluate the catalytic efficiency of lipase under optimum conditions. Kinetic parameters were evaluated from Michaelis-Menten and Lineweaver-Burk plots. The W_o of the microemulsions affects the catalytic activity of lipase. Among the different reaction media, IL based microemulsion at $W_o = 4.20$ showed the highest catalytic activity due to the presence of bicontinuous phase. The presence of volatile organic compound in conventional microemulsions makes the system unstable and such system shows lower catalytic activity compared to aqueous medium.

7.1. Introduction

The catalytic efficiency of enzymes can be improved significantly by the use of ILs due to their unique physicochemical properties (Section 1.5. of Chapter 1). ILs with negligible vapor pressure can be used as a replacement for organic solvents to reduce volatile organic compound emissions [1].

The catalytic activity of enzyme in general, increases by an IL with low coordination ability of the anion. The dissolution of the enzyme in the ILs increases but the risk of the denaturation of the enzyme in the medium increases by the use of ILs with the anions of strong nucleophilicity or hydrogen-bond basicity [2]. The catalytic activity of lipase depends not only on the coordination ability of the anion of an IL but also on the hydrophobicity of the IL [3, 4]. The catalytic efficiency and steadiness of lipase in a hydrophobic IL with [PF₆]⁻ has been reported to be better than those in the hydrophilic IL with [BF₄]⁻ and thus lipase is usually suspended in the hydrophobic IL medium [4, 5]. Enzymes are not soluble in most ILs. Through the weak hydrogen bonding interactions, some ILs can dissolve enzymes. The conformational structure of the enzyme changes in ILs and thus the dissolved enzymes show low catalytic activity in ILs [6]. The inactivation of enzymes can also occur when it is stirred or shaken vigorously in ILs to interact with substrates. The solubility of enzymes in ILs can improve to conjugate lipase with polyethylene glycol through chemical modification which shows good solubility in ILs but such a modification is time consuming [7, 8].

The insolubility of enzymes in ILs can be overcome by the use of a w/IL microemulsion without the loss of their catalytic activity [1, 9–12]. Solubilized enzymes in such water pools are protected from the unfavorable effect of organic solvents by the surfactant layer.

Moniruzzaman et al. reported that the water pool in AOT/1-hexanol/[C₈mim][TFSI]/water microemulsion is very suitable for enzymatic reactions in ILs. In this work lipase-catalyzed hydrolysis of *p*-PNB has been used as a model reaction [1]. Xue et al. showed that the laccase hosted in the water pool of AOT/TX-100/[C₄mim][PF₆]/water microemulsion exhibited catalytic activity and the activity could be regulated by the composition of the interfacial membrane [13]. The catalytic

efficiency of lipase in a novel water/[C₄mim][PF₆] microemulsion stabilized by both AOT and TX-100 was studied by Xue et al. [14].

The objective of the present study is to observe the lipase catalyzed hydrolysis of 4-nitrophenyl butyrate (*p*-PNB) as a model reaction in aqueous medium, w/o, w/[C₄mim][PF₆] and bicontinuous [C₄mim][PF₆] based microemulsions. The catalytic activity of lipase in different media has been compared and explained with the microstructures and microenvironment of the systems. Kinetic parameters of lipase catalyzed hydrolysis of *p*-NPB in aqueous medium have been evaluated. The ultimate goal is to explore the prospect of IL based microemulsions for development of suitable media to control the rate of reactions and stabilize reactive reagents or reaction intermediates.

7.2. Experimental

7.2.1. Materials

Lipase from porcine pancreas (Type II, 100-400 units mg⁻¹ protein (using olive oil (30 min incubation)), 30-90 units mg⁻¹ protein (using triacetin)), substrate, *p*-NPB (≥ 98 %) and tris(hydroxymethyl)aminomethane (Tris) were obtained from Sigma-Aldrich. TX-100, cyclohexane and [C₄mim][PF₆] were also obtained from Sigma-Aldrich. Further details are given in Section 1.11. of Chapter 1. Double distilled de-ionized water from HPLC grade water purification systems (BOECO, BOE 8082060 Germany) were used. Conductivity was 0.0550 μS cm⁻¹ at 25 °C.

7.2.2. Preparation of Tris-HCl Buffer

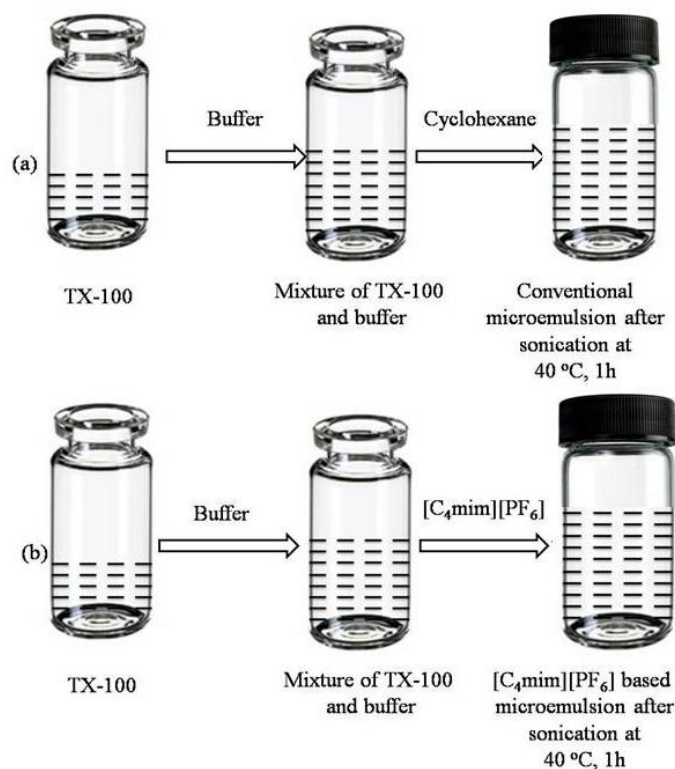
The Tris-HCl buffer was used to prepare the solutions. It may be worth mentioning that phosphate buffer could not be used since the microemulsions are not stable in phosphate buffer. Tris buffer could maintain a stable pH when working with solution. The kinetic runs were carried out at pH = 8.3 (50 mM Tris-HCl buffer). Xue et al. earlier reported that the lipase hosted in water/[C₄mim][PF₆] microemulsion stabilized by both AOT and TX-100 shows the maximum activity at pH = 8.3 and the buffer concentration below 50 mM in microemulsion does not show better activity [14].

Stock solution of 100 mL 50 mM (pH = 8.3) Tris-HCl buffer was prepared at 25 °C. To prepare the stock solution, 80 mL of deionized water was taken to a graduated cylinder and the water was transferred to a 250 mL beaker. 0.6057 gm of Tris powder was added into a beaker and was magnetically stirred to get a clear solution. The pH was adjusted to desired pH by using 5 M HCl solution. Prepared buffer solution was transferred to a 100 mL volumetric flask. Deionized water was added to get the final volume of 100 mL.

7.2.3. Preparation of Microemulsions

TX-100/cyclohexane/water ($W_o = 2.5000, 3.2000, 4.2000, 4.9600, 5.5000, 6.1953$) and TX-100/[C₄mim][PF₆]/water ($W_o = 2.5000, 3.2000, 4.2000, 4.9600, 5.5000,$

6.1953) microemulsions were prepared at pH 8.3 (50 mM Tris-HCl) (Scheme 7.1). Tris-HCl buffer (polar phase) was used instead of double distilled de-ionized water to prepare the microemulsions. Cyclohexane and $[C_4mim][PF_6]$ were used as the nonpolar phase for conventional and IL based microemulsions respectively. Microemulsions were prepared at a fixed TX-100 composition (70.0000 %). The amount of polar and nonpolar phases were varied to keep the total weight of microemulsions constant.



Scheme 7.1. Preparation of (a) TX-100/cyclohexane/water and (b) TX-100/ $[C_4mim][PF_6]$ /water microemulsions at pH 8.3 (50 mM Tris-HCl).

7.2.4. Determination of the Catalytic Activity of Lipase

The hydrolysis of *p*-NPB was chosen as a model reaction to characterize the catalytic efficiency of lipase in aqueous medium, w/o, w/ $[C_4mim][PF_6]$, and bicontinuous $[C_4mim][PF_6]$ based microemulsions. Lipase was taken in two quartz cells each with optical path length of 1 cm. The concentration of lipase in both aqueous solution (50 mM Tris-HCl) and microemulsions (50 mM Tris-HCl) was 2 mgmL^{-1} . Cells were placed in ice bath. 2.5 mL of aqueous solution or microemulsion was taken in each cells with a micropipette. Cells were shaken well for the mixing of lipase in aqueous solution or microemulsion. Cells with aqueous solution or microemulsion were incubated for 5 min at 37 °C to initiate the reaction by adding *p*-NPB. An appropriate amount of *p*-NPB was added to the sample cell and the resulting solution was thoroughly mixed by shaking (2 min for microemulsion and 5 s for aqueous solution). In microemulsions with different W_o , concentration of *p*-NPB was 10.87 mM and in aqueous solution different concentration of *p*-NPB was used for the kinetic runs. The

cells were transferred into the sample chamber of the spectrophotometer to monitor the time-dependent change of the absorbance of the hydrolysis product 4-nitrophenol (*p*-NP) of *p*-NPB at 410 nm. The activity of lipase was expressed as the initial rate (v) of the enzymatic reaction in $\text{mgmL}^{-1}\text{min}^{-1}$.

The reaction product is *p*-NP, which exists in two forms (ionized and non-ionized). Xue et al. reported that there exist an isosbestic point in the absorption spectra of the 4-nitrophenol/4-nitrophenolate couple which interferes the absorption band of the substrate *p*-NPB. The ionized *p*-NP absorbs light at 410 nm and the substrate *p*-NPB does not interfere with the absorbance measurement of ionized *p*-NP at 410 nm [14]. The kinetic runs in this work were carried out at 410 nm to avoid any interference from the substrate (Figures 7.3.1., 7.3.5. and 7.3.7.)

7.2.5. Methods

The pH of the Tris-HCl buffer solutions and microemulsions were measured with cyberscan 500 pH meter. Magnetism heating mixture (79-1, Innovation Scientific International) was used to get homogeneous mixture of buffer solutions. An analytical balance, UB-110/0.0001 g) UNILAB, U. S. A.) was used for weighing samples. A digital ultrasonic bath (UNILAB UET-1080) was used to get homogeneous mixture of microemulsions.

Kinetic measurements and spectral analysis were made by using a double beam Shimadzu UV-visible spectrophotometer (Model: UVD 3500, Labomed, USA). Rectangular quartz cells of path length 1 cm were used throughout the investigation. It was equipped with spectral data processing facilities and the sensitivity was 0.001 absorbance unit at a signal to noise ratio of 1. The reaction of hydrolysis of *p*-NPB catalyzed by lipase in aqueous solution, conventional and IL based microemulsions of TX-100 was followed by observing the increase in absorbance at 410 nm as a function of time. Microemulsions (50 mM Tris-HCl) with different W_o , concentration of *p*-NPB was 10.87 mM for the kinetic runs. In aqueous solution (50 mM Tris-HCl) different concentration of *p*-NPB was used for the kinetic runs. Kinetic parameters in aqueous solution were measured by using Michaelis-Menten and Lineweaver-Burk plots (Section 1.8 of Chapter 1).

7.3. Results and Discussion

7.3.1. Influence of Different Media on Lipase Catalyzed Hydrolysis of *p*-NPB

7.3.1.1. Influence of Aqueous Medium on Lipase Catalyzed Hydrolysis of *p*-NPB

7.3.1.1.1. Absorption Spectrum of Lipase Catalyzed Hydrolysis of *p*-NPB in Aqueous Medium

Figure 7.3.1. shows absorption spectrum for the product *p*-NP from the hydrolysis of *p*-NPB in aqueous medium. Product *p*-NP is partially in the form of *p*-nitrophenolate anion which absorbs light at 410 nm. Absorbance at 400 nm is not considered to avoid any interference from the substrate [14]. Kinetic studies were carried out by recording the absorbance at 410 nm as a function of time.

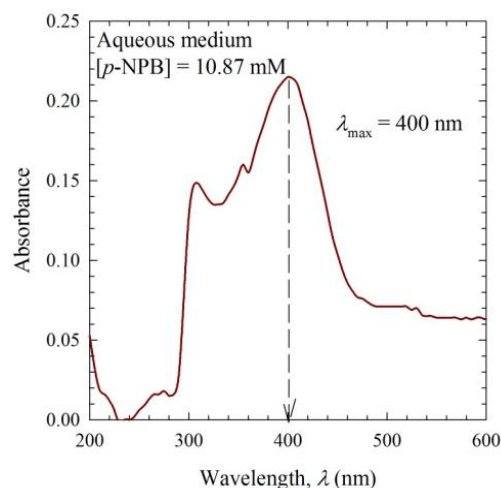


Figure 7.3.1. Absorption spectra of *p*-NP (10.87 mM) in aqueous medium at pH = 8.3 (50 mM Tris-HCl) at 37 °C.

7.3.1.1.2. Influence of the Concentration of *p*-NPB on the Catalytic Activity of Lipase in Aqueous Medium

Fig 7.3.2. shows (a) absorbance vs. *t* profiles and (b) effect of the concentration of *p*-NPB on the *v* of the lipase catalyzed hydrolysis of *p*-NPB in aqueous medium. The *v* has been determined from the slope of the absorbance vs. *t* profile obtained by least squares fitting. The *v* changed significantly with concentration of *p*-NPB (Appendices Table A89.).

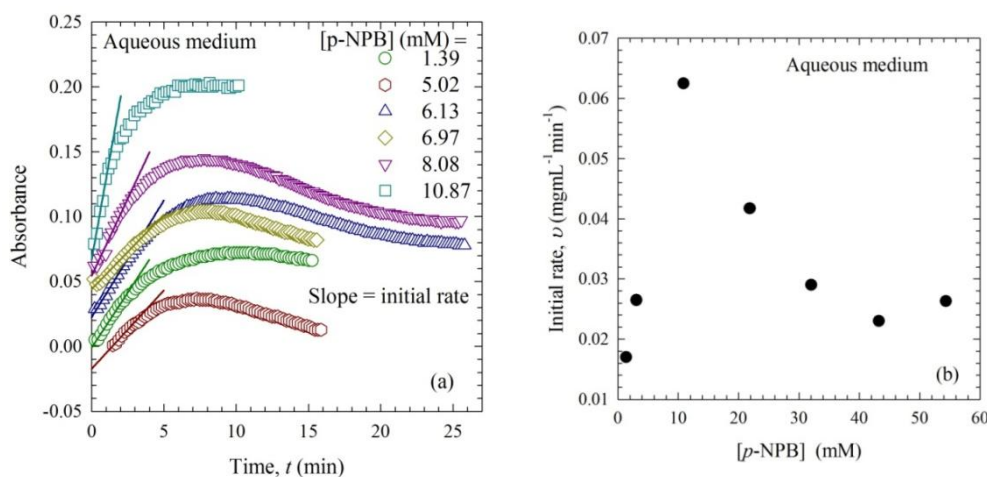


Figure 7.3.2. (a) Absorbance as a function of *t* and (b) effect of the concentration of *p*-NPB on the *v* of the lipase catalyzed hydrolysis of *p*-NPB in aqueous medium at 37 °C. Conditions were: [lipase] = 2 mgmL⁻¹, pH = 8.3 (50 mM Tris-HCl), λ = 410 nm.

The *v* of the lipase catalyzed hydrolysis of *p*-NPB in aqueous medium increases with increase in the concentration of *p*-NPB up to 10.87 mM. After that the *v* decreases with the increase in the concentration of *p*-NPB. Due to the formation of enzyme-substrate complex, the *v* initially increases which follows Michaelis-Menten

mechanism. According to this mechanism the increase in the concentration of *p*-NPB increases the concentration of enzyme-substrate complex and the v increases. At higher *p*-NPB concentration the v should be constant. But in this work the v decreases with increase in the concentration of *p*-NPB which clearly deviates from the above mechanism. Reed et al. explained the mechanism of substrate inhibition for this type of behavior where the v rises to a maximum as the substrate concentration increases and then descends either to zero or to a non-zero asymptote. At high substrate concentrations, the substrate molecule binds to an enzyme in a spot different from the active site for another substrate molecule and inhibits to the formation of products from the enzyme-substrate complex [15].

7.3.1.1.3. Kinetic Parameters of Lipase Catalyzed Hydrolysis of *p*-NPB in Aqueous Medium

To determine K_m , V_m and K_{cat} (Section 1.8. of Chapter 1) of the lipase-catalyzed hydrolysis of *p*-NPB in aqueous medium, the v vs. [*p*-NPB] profile was plotted by using the data from appendices Table A89. The plot was then fitted according to Michaelis-Menten equation (Section 1.8. of Chapter 1, Equation 1.5). For the better fit the concentration ranging from 1.3900-21.8400 mM was considered (Figure 7.3.3.).

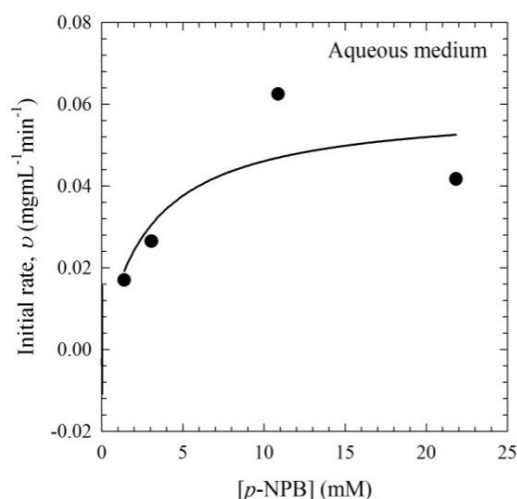


Figure 7.3.3. The v as a function of [*p*-NPB]. Conditions were: [lipase] = 2 mgmL⁻¹, pH = 8.3 (50 mM Tris-HCl), λ = 410 nm.

From Lineweaver-Burk equation (Section 1.8. of Chapter 1, Equation 1.7) kinetic parameters can also be determined. The double reciprocal plot or Lineweaver-Burk plot of $1/v$ vs. $1/[p\text{-NPB}]$ will be linear according to Equation 1.7. (Figure 7.3.4.). Kinetic parameters, K_m and V_m can be calculated by using the slope and intercept respectively.

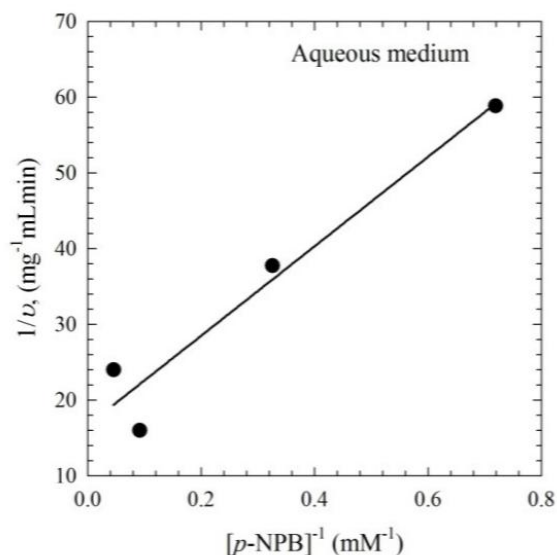


Figure. 7.3.4. The $1/v$ as a function of $1/[p\text{-NPB}]$. Conditions were: $[\text{lipase}] = 2 \text{ mg mL}^{-1}$, $\text{pH} = 8.3$ (50 mM Tris-HCl), $\lambda = 410 \text{ nm}$.

The values of K_m , V_m and k_{cat} obtained both from Michaelis-Menten and Lineweaver-Burk plots are listed in Table 7.1.

Table 7.1. Kinetic parameters of lipase-catalyzed hydrolysis of $p\text{-NPB}$ in aqueous medium

Plots	K_m , mM	V_m , Mg mL^{-1} min^{-1}	k_{cat} , $\text{g mol}^{-1} \text{ min}^{-1}$	r^2
Michaelis-Menten plot	2.92 ± 3.09	0.06 ± 0.02	20.55	0.82
Lineweaver-Burk plot	3.55 ± 2.50	0.06 ± 0.24	16.90	0.97

7.3.1.2. Influence of TX-100/Cyclohexane/Water Microemulsions on Lipase Catalyzed Hydrolysis of $p\text{-NPB}$

7.3.1.2.1. Absorption Spectra of Lipase Catalyzed Hydrolysis of $p\text{-NPB}$ in TX-100/Cyclohexane/Water Microemulsions

Figure 7.3.5. shows absorption spectra for the product $p\text{-NP}$ in conventional microemulsion at $W_o = 4.20$. Kinetic studies were carried out by recording the absorbance at 410 nm as a function of time because product $p\text{-NP}$ which is partially in the form of $p\text{-NP}$ anion absorbs light at 410 nm.

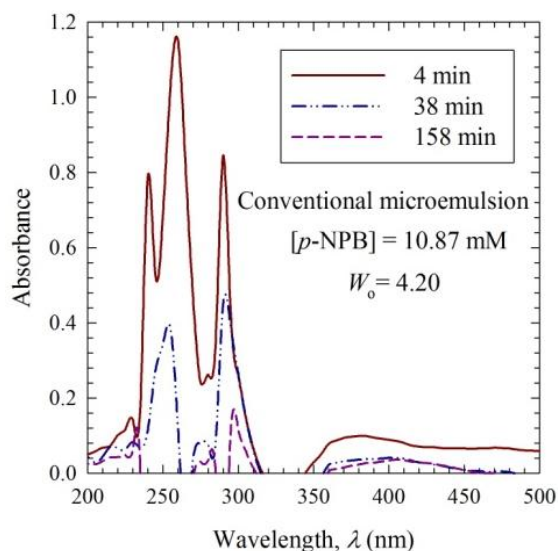


Figure 7.3.5. Absorption spectra of *p*-NP (10.87 mM) in conventional microemulsion at $W_o = 4.20$, pH = 8.3 (50 mM Tris-HCl) at 37 °C.

7.3.1.2.2. Influence of W_o on the Catalytic Activity of Lipase in TX-100/Cyclohexane/Water Microemulsions

Figure 7.3.6. shows (a) Absorbance vs. t profiles and (b) effect of the W_o on the ν of the lipase catalyzed hydrolysis of *p*-NPB in conventional microemulsions. The ν has been found to change significantly with W_o of conventional microemulsions (Appendices Table A90.).

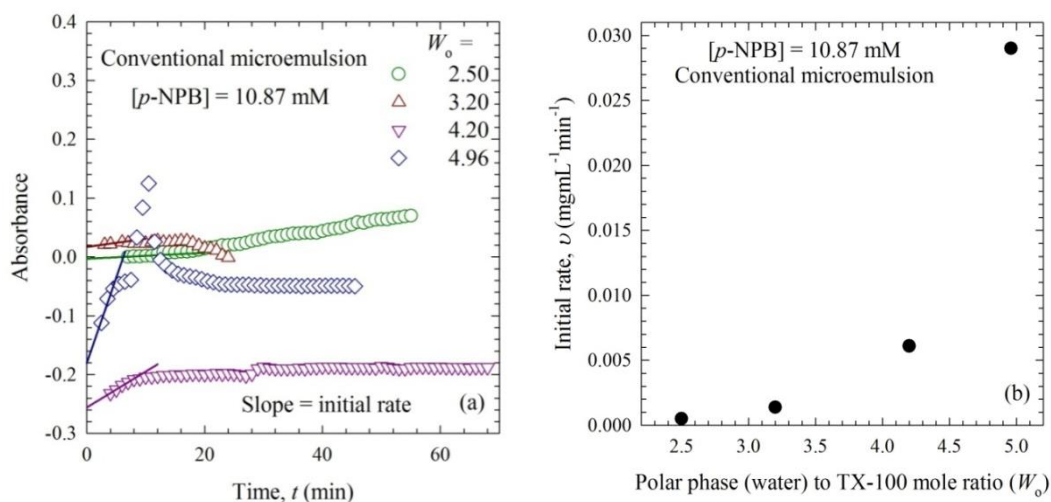


Figure 7.3.6. (a) Absorbance as a function of t and (b) effect of W_o on the ν of the lipase catalyzed hydrolysis of *p*-NPB in conventional microemulsions at 37 °C. Conditions were: [lipase] = 2 mgmL⁻¹, [p-NPB] = 10.87 mM, pH = 8.3 (50 mM Tris-HCl), $\lambda = 410$ nm.

The ν at W_o lower than 2.50 could be hardly determined spectrophotometrically. May be lipase cannot disperse in the w/o microemulsion properly due to low water content and such a system is not favorable for product formation. With increasing W_o , a microemulsion droplet may encapsulate lipase in the water pool of the microemulsions and the catalytic activity increases. A larger water pool at $W_o = 4.96$ can encapsulate satisfactory amount of lipase and this system shows highest catalytic activity. With further increase in the the water content ($W_o > 4.96$), the microstructure of the microemulsion may change and no catalytic activity is observed.

7.3.1.3. Influence of TX-100/[C₄mim][PF₆]/Water Microemulsions on Lipase Catalyzed Hydrolysis of *p*-NPB

7.3.1.3.1. Absorption Spectrum of Lipase Catalyzed Hydrolysis of *p*-NPB in TX-100/[C₄mim][PF₆]/Water Microemulsions

Figure 7.3.7. shows absorption spectrum for the product *p*-NP in IL based microemulsion at $W_o = 4.20$. Absorbance vs. t profiles were monitored by recording the absorbance at 410 nm as a function of time.

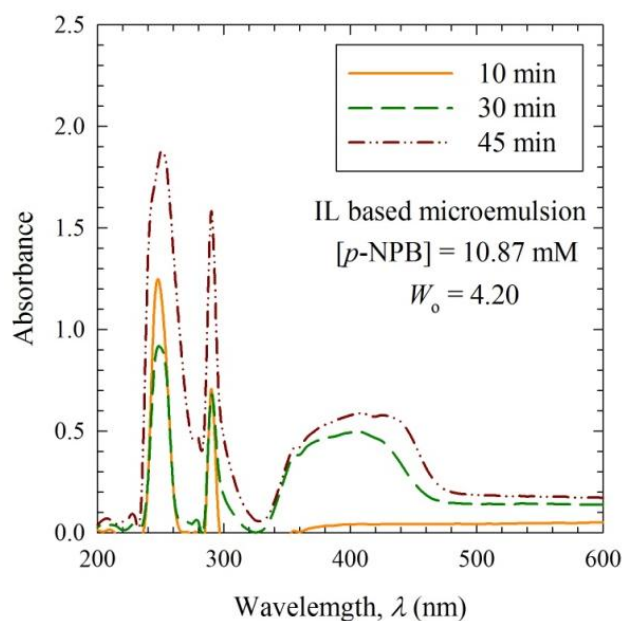


Figure 7.3.7. Absorption spectra of *p*-NP (10.87 mM) in IL based microemulsion at $W_o = 4.20$, pH = 8.3 (50 mM Tris-HCl) at 37 °C.

7.3.1.3.2. Influence of W_o on the Catalytic Activity of Lipase in TX-100/[C₄mim][PF₆]/Water Microemulsions

Figure 7.3.8. shows (a) Absorbance vs. t profiles and (b) effect of W_o on the ν of the lipase catalyzed hydrolysis of p -NPB in IL based microemulsions. The ν significantly changes with W_o of IL based microemulsions (Appendices Table A91.).

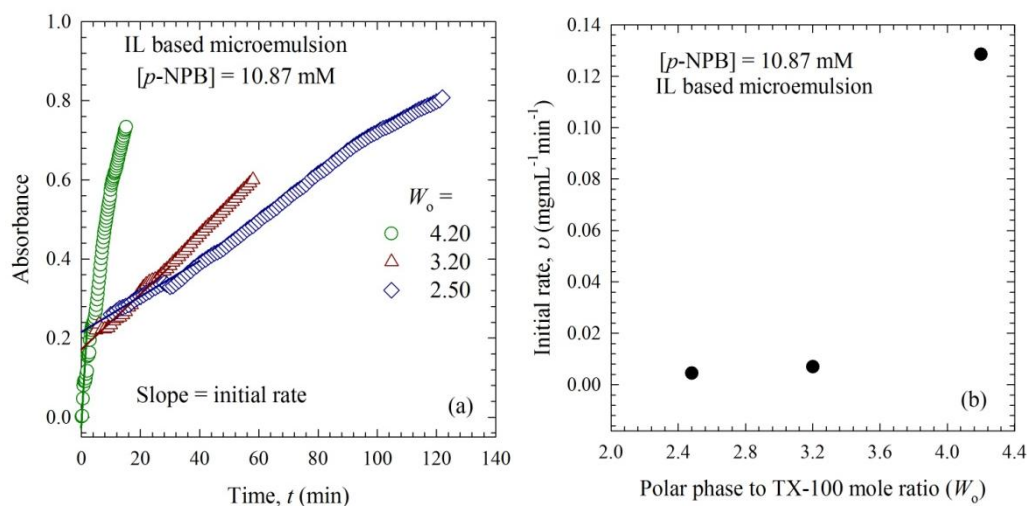


Figure 7.3.8. (a) Absorbance as a function of t and (b) effect of W_o on the ν of the lipase catalyzed hydrolysis of p -NPB in IL based microemulsions at 37 °C. Conditions were: [lipase] = 2 mg mL⁻¹, [p -NPB] = 10.87 mM, pH = 8.3 (50 mM Tris- HCl), λ = 410 nm.

The ν at W_o lower than 2.50 could not be determined accurately. Lower water content cannot break the association of IL in the bulk and lipase cannot disperse properly in such a system to initiate the reaction. As the W_o increases, the water breaks the association of IL in the bulk and the water pool in the microemulsion may encapsulate lipase and the catalytic activity increases. Bicontinuous microemulsion is formed at $W_o = 4.20$ (Section 5.3.1.1. of Chapter 5) where both the w/IL and IL/w droplets coexist. In such a system lipase can disperse in the microemulsion properly and this system shows highest catalytic activity (Scheme 7.1.). With further increase in the water content ($W_o > 4.20$), the microstructure of the microemulsion may change and no catalytic activity is observed.

7.3.2. Comparative Study of the Catalytic Activity of Lipase in Different Media

7.3.2.1. Comparative Study of the Catalytic Activity of Lipase in Aqueous Medium and TX-100/Cyclohexane/Water Microemulsions

Figure 7.3.9. shows absorbance vs. t profiles for lipase catalyzed hydrolysis of p -NPB in aqueous medium and conventional microemulsion at $W_o = 4.96$ and ν for aqueous medium and conventional microemulsions with different W_o . The ν significantly changes with different media (Appendices Table A92.).

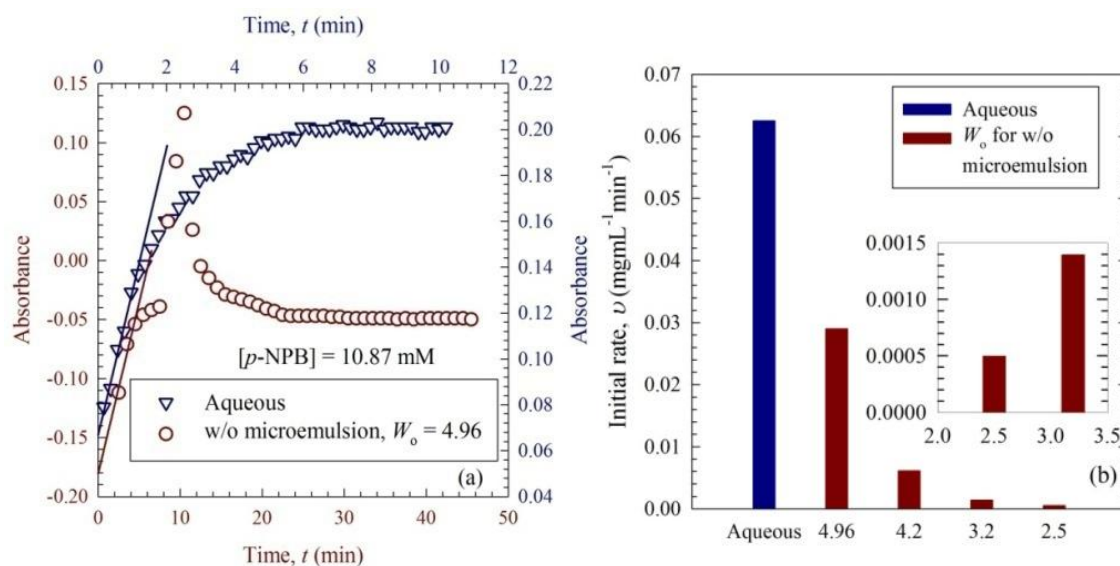


Figure 7.3.9. (a) Absorbance as a function of t for lipase catalyzed hydrolysis of p -NPB in aqueous medium (dark blue) and conventional microemulsion (dark red) at $W_o = 4.96$ and (b) v for aqueous medium and conventional microemulsions with different W_o at 37°C . In Figure (a) absorbance in the left side and t in bottom is for conventional microemulsion and absorbance in the right side and t in the top is for aqueous medium. Conditions were: $[\text{lipase}] = 2 \text{ mg mL}^{-1}$, $[p\text{-NPB}] = 10.87 \text{ mM}$, $\text{pH} = 8.3$ (50 mM Tris-HCl), $\lambda = 410 \text{ nm}$.

The catalytic efficiency of lipase in aqueous medium is higher than that in the conventional microemulsions. Lipase can disperse in aqueous medium. On the other hand, the water pool of w/o reverse microemulsions has the ability to solubilize enzymes which are protected from the unfavorable effect of organic solvents by the surfactant layer [1, 14]. But organic solvents emits volatile organic compound. Such w/o microemulsions are not stable and do not show good catalytic activity compared to aqueous medium.

7.3.2.2. Comparative Study of the Catalytic Activity of Lipase in TX-100/Cyclohexane/Water and TX-100/[C₄mim][PF₆]/Water Microemulsions

Figure 7.3.10. shows absorbance vs. t profiles of the lipase catalyzed hydrolysis of p -NPB in conventional microemulsion at $W_o = 4.96$ and IL based microemulsion at $W_o = 4.20$ and v for conventional and IL based microemulsions with different W_o . The v significantly changes with different media (Appendices Table A93.).

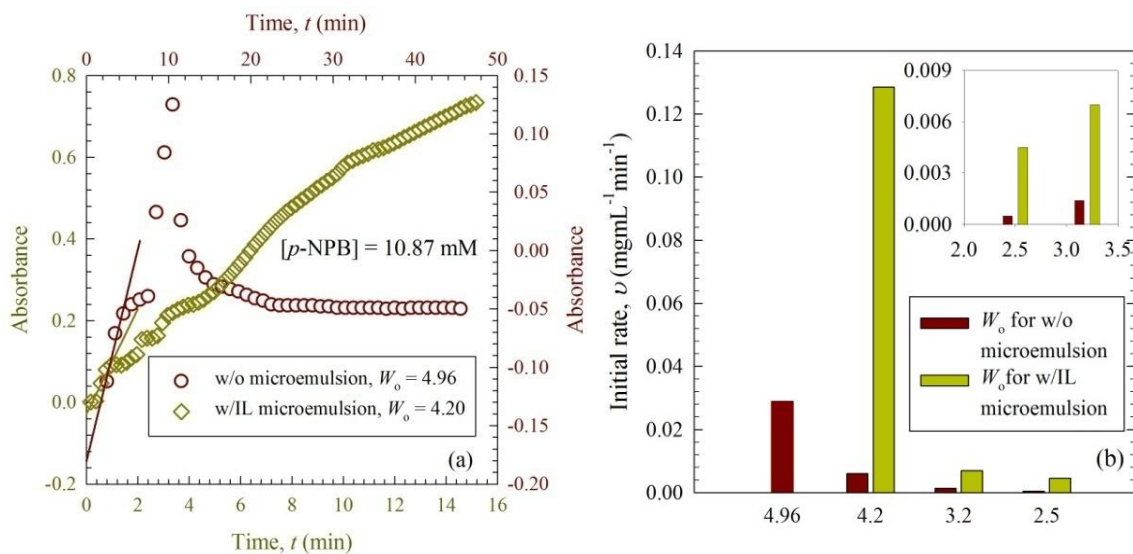


Figure 7.3.10. (a) Absorbance as a function of t of the lipase catalyzed hydrolysis of p -NPB in conventional microemulsion (dark red) at $W_o = 4.96$ and IL based microemulsion (dark yellow) at $W_o = 4.20$ and (b) ν for conventional and IL based microemulsions with different W_o at 37 °C. In Figure (a) absorbance in left side and t in bottom is for IL based microemulsion and absorbance in right side and t in top is for conventional microemulsion. Conditions were: [lipase] = 2 mg mL $^{-1}$, [p-NPB] = 10.87 mM, pH = 8.3 (50 mM Tris-HCl), $\lambda = 410 \text{ nm}$.

The catalytic efficiency of lipase in the IL based microemulsions are higher than that in the conventional microemulsions because IL based microemulsion have some advantages over conventional microemulsions. Volatile compounds are released from organic solvents. ILs are useful as a replacement for ordinary organic solvents to reduce volatile organic compound release because of their negligible vapor pressure. Due to the stable interface, high water activity, full dispersion of lipase in microemulsion and probably the activating effect of the imidazolium cation in the water pool, the IL based microemulsion is demonstrated to be a promising medium for the lipase catalyzed hydrolytic reaction [14]. The solubilized imidazolium cation in the water pool has an activating effect on the hydrolytic enzymes by improving the nucleophilicity of water in the vicinity of the enzyme through hydrogen bonding [14, 16, 17]. At $W_o = 4.20$, catalytic efficiency of lipase in the IL based microemulsions shows the highest efficiency (Scheme 7.1.). In such a bicontinuous IL based microemulsion system where both the w/IL and IL/w droplets coexist, lipase can disperse in the microemulsion properly and this system shows highest catalytic activity. No catalytic activity is observed at $W_o > 4.20$ because the microstructure of the microemulsion may changes.

7.3.2.3. Comparative Study of the Catalytic Activity of Lipase in Aqueous Medium, TX-100/Cyclohexane/Water and TX-100/[C₄mim][PF₆]/Water Microemulsion

Figure 7.3.10. shows (a) absorbance vs. t profiles of the lipase catalyzed hydrolysis of p -NPB in aqueous medium, conventional microemulsion at $W_o = 4.96$ and IL based microemulsion at $W_o = 4.20$ and (b) ν for aqueous medium, conventional and IL based microemulsions with different W_o . The ν significantly changes for different media (Appendices Table A94.).

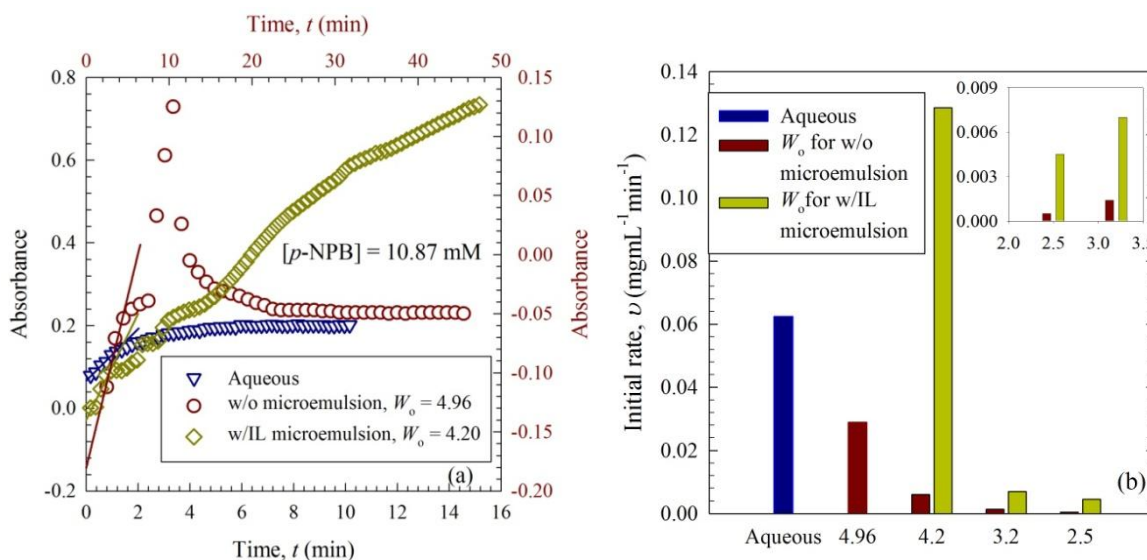


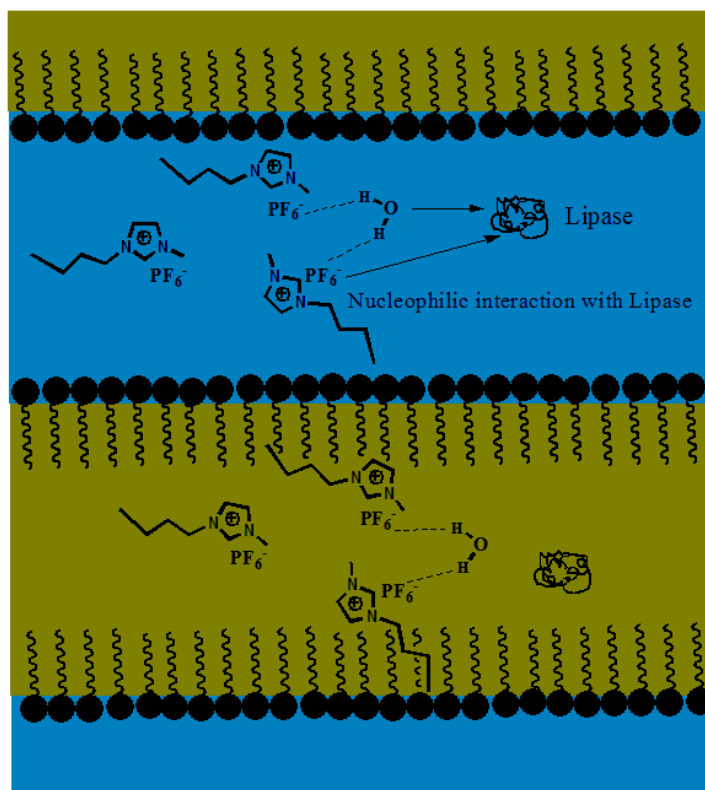
Figure 7.3.11. (a) Absorbance as a function of t of the lipase catalyzed hydrolysis of p -NPB in aqueous medium (dark blue), conventional microemulsion (dark red) at $W_o = 4.96$ and IL based microemulsion (dark yellow) at $W_o = 4.20$ and (b) ν for aqueous medium, conventional and IL based microemulsions with different W_o at 37 °C. In Figure (a) absorbance in the left side and t in bottom is for aqueous medium and IL based microemulsion and absorbance in the right side and t in the top is for conventional microemulsion. Conditions were: [lipase] = 2 mg mL⁻¹, [p -NPB] = 10.87 mM, pH = 8.3 (50 mM Tris-HCl), $\lambda = 410$ nm.

Among the three systems IL based microemulsion at $W_o = 4.20$ shows the highest catalytic activity due to the presence of bicontinuous phase (Scheme 7.1.). Aqueous medium shows higher activity compared to conventional microemulsions. Due to the presence of volatile organic compound in conventional microemulsions, these systems are not stable.

7.3.3. Probable Organization of Different Components in Bicontinuous TX-100/[C₄mim][PF₆]/Water Microemulsion

The activity of lipase can be enhanced in presence of imidazolium cation [17]. Water can dissociate the aggregation of the IL. In bicontinuous microemulsion both water and IL are continuous phases. In such a system both the w/IL and IL/w droplets coexist and lipase can disperse in the microemulsion properly. The solubilized

imidazolium cation in the bicontinuous microemulsion has an activating effect on lipase because the nucleophilicity of water increases in the vicinity of the enzyme through hydrogen bonding (Scheme 7.2) [16, 17].



Scheme 7.2. Schematic representation of the activating effect of $[C_2mim][PF_6]$ on lipase in presence of water in bicontinuous IL based microemulsion. Dark blue color represents polar (water) phase and dark yellow color represents oil ($[C_2mim][PF_6]$) phase.

7.4. Conclusion

IL based microemulsions could have advantages over aqueous medium and conventional microemulsions as reaction media for the lipase catalyzed hydrolysis of *p*-NPB. The catalytic activity of lipase is affected by the W_o of the microemulsions. Due to the presence of bicontinuous phase, IL based microemulsion at $W_o = 4.20$ shows the highest catalytic activity among the different reaction media. The IL based microemulsion is established to be a potential medium for the lipase catalyzed hydrolytic reaction due to the stable interface, full dispersion of lipase in microemulsion and may be due to the activating effect of the imidazolium cation in the bicontinuous phase.

References

- [1] Moniruzzaman, M.; Kamiya, N.; Nakashima, K.; Goto, M. *Green Chem.* **2008**, 10, 497–500.
- [2] Zhao, H. J. *J. Chem. Technol. Biotechnol.* **2010**, 85, 891-907.
- [3] Kaar, J. L.; Jesionowski, A. M.; Berberich, J. A.; Moulton, R.; Russell, A. J. *J. Am. Chem. Soc.* **2003**, 125, 4125-4131.
- [4] Nara, S. J.; Harjani, J. R.; Salunkhe, M. M. *Tetrahedron Lett.* **2002**, 43, 2979-2982.
- [5] Sunitha, S.; Kanjilal, S.; Reddy, P. S.; Prasad, R. B. N. *Biotechnol. Lett.* **2007**, 29, 1881-1885.
- [6] Turner, M. B.; Spear, S. K.; Huddleston, J. G.; Holbrey, J. D.; Rogers, R. D. *Green Chem.* **2003**, 5, 443–447.
- [7] Ohno, H.; Suzuki, C.; Fukumoto, K.; Yoshizawa, M.; Fujita, K. *Chem. Lett.* **2003**, 32, 450–451.
- [8] Nakashima, K.; Maruyama, T.; Kamiya, N.; Goto, M. *Chem. Commun.* **2005**, 4297–4299.
- [9] Zhang, Y.; Huang, X. R.; Huang, F.; Li, Y. Z.; Qu, Y. B.; Gao, P. J. *Colloid Surface B* **2008**, 65, 50-53.
- [10] Zhou, G. P.; Zhang, Y.; Huang, X. R.; Shi, C. H.; Liu, W. F.; Li, Y. Z.; Qu, Y. B.; Gao, P. J. *Colloid Surface B* **2008**, 66, 146-149.
- [11] Moniruzzaman, M.; Kamiya, N.; Goto, M. *Langmuir* **2009**, 25, 977-982.
- [12] Shome, A.; Roy, S.; Das, P. K. *Langmuir* **2007**, 23, 4130–4136.
- [13] Xue, L.; Qiu, H.; Li, Y.; Lu, L.; Huang, X.; Qu, Y. *Colloid Surface B* **2011**, 82, 432-437.
- [14] Xue, L.; Li, Y.; Zou, F.; Lu, L.; Zhao, Y.; Huang, X.; Qu, Y. *Colloid Surface B* **2012**, 92, 360– 366.
- [15] Reed, M. C.; Lieb, A.; Nijhout, H. F. *Bioessays.* **2010**, 32, 422-429.
- [16] Das, D.; Das, D.; Das, P. K. *Biochimie* **2008**, 90, 820-829.
- [17] Debnath, S.; Das, D.; Dutta, S.; Das, P. K. *Langmuir* **2010**, 26, 4080-4086.

8.1. General Conclusions

Series of IL/w, w/IL, and bicontinuous IL microemulsions with TX-100 could be prepared by varying R or W_o . Variation of R in a wide range of compositions also yielded series of w/IL and bicontinuous IL microemulsions for CTAB. Gel formation is noticed for conventional TX-100 based microemulsions at W_o ranging from 6.9385 to 12.3903; while bicontinuous microemulsions could not be achieved for conventional CTAB based microemulsions. Anionic surfactant, SDS did not give microemulsions for any of the ILS in this study even with the assistance of cosurfactant of varying chain length. Hydrophilic and hydrophobic ILS could efficiently replace water and volatile organic phase, respectively in IL based microemulsions.

Physicochemical properties of IL based microemulsions varied interestingly with change in the nature of the surfactant, structure of the cation or the anion of the ILS, hydrophilicity or hydrophobicity of the ILS, the R or W_o values and other parameters controlling microemulsions. Different microregions could be established by applying percolation theory on conductivity results on TX-100 based microemulsions based on ILS with increasing volume fraction of water (ϕ_w) or volume fraction of IL (ϕ_{IL}) respectively. The phase transitions corresponded to the structural change from IL/o to o/IL via bicontinuous microemulsions with increasing ϕ_{IL} and from w/IL to IL/w via bicontinuous microemulsions with increasing ϕ_w . With increase in the R or W_o values, microemulsion droplets aggregate due to the hydrophobic interactions of the tail parts of surfactants and channel formation occurs. Through the channels in bicontinuous microemulsions, ions can easily move. With further increase in the R or W_o values, o/IL or IL/w microemulsions are formed. By applying percolation theory on conductivity results, percolation thresholds are confirmed. Only reverse micelle and micelle dominated microemulsions exist for $[C_2mim][MeSO_4]$ and $[C_2mim][PF_6]$ based microemulsions with TX-100 respectively.

Increasing the nonpolar side chain of the cation or anion of the IL, electrostatic interaction decreases and a competition arises between the electrostatic forces and the inductive, dispersive forces. Loosely bonded ions of ILS can penetrate the surfactant layer easily. Cation of the IL can easily combine with or separate from the spherical anion of the IL. These properties of IL play an important role in the physicochemical properties such as conductivity, viscosity and dynamic light scattering measurement of IL microemulsions with the variation of the cation and the anion of the IL. Three dimensional complex channel formation occurs easily in TX-100 microemulsions based on IL compared to CTAB microemulsions based on ILS. At the interface of CTAB surfactant, ions of IL and counter ions of CTAB may stuck and mobility of ions decreases compared to nonionic TX-100 based microemulsions. Therefore, the conductivity and viscosity values of IL based microemulsions of TX-100 are much higher compared to IL based microemulsions of CTAB.

IL based microemulsion is a potential reaction medium for lipase catalyzed hydrolysis of *p*-NPB over aqueous medium and conventional microemulsions. W_o of the microemulsions affect the

catalytic activity of lipase. Bicontinuous IL based microemulsion at $W_o = 4.20$ shows the highest catalytic activity and the interface was considered to be very stable. Full dispersion of lipase in microemulsion and the activating effect of the imidazolium cation in the bicontinuous phase associated with the stable interface gave bicontinuous IL based microemulsion higher efficiency for enzyme catalysis.

8.2. Outlook

Surfactant based organized media, in other words, supramolecular self-assembly, such as w/IL (reverse micelle dominated) or IL/w (micelle dominated), and bicontinuous IL microemulsions can offer essential contribution as a new kind of reaction media as they can solubilize both the polar and nonpolar substrate. Since the physicochemical properties vary interestingly with change in the nature of the surfactant as well as the structure of ionic liquids and other parameters controlling the formation of microemulsions, IL-based microemulsions may be prepared with desirable chemistry for task specific applications. The microstructures of various microemulsions may be carefully tuned and selected for specific applications. This would open up new routes for application of such systems for diverse applications selectively. The industrial effectiveness of enzymes may also be enhanced significantly by their use in ILs rather than in volatile organic solvents or in their natural aqueous reaction media due to their unusual solvent characteristics. As IL microemulsions can accelerate a reaction, alter the course of a reaction in limited quarters, perturb equilibrium, contort conformations and either stabilize reactive reagents or reaction intermediates, this novel microemulsions are used for diverse applications such as nanoparticle preparation, organic and bioorganic synthesis, material science, pollution control, food and pharmaceutical industry, cosmetics and drug delivery systems.

Appendices

Table A1. The σ for TX-100/cyclohexane/[C₂mim][MeSO₄], TX-100/cyclohexane/[C₂mim][EtSO₄] and TX-100/cyclohexane/[C₂mim][BF₄] microemulsions with increasing R at 25 °C.

R for [C ₂ mim][MeSO ₄] based microemulsion	σ ($\mu\text{S cm}^{-1}$)	R for [C ₂ mim][EtSO ₄] based microemulsion	σ ($\mu\text{S cm}^{-1}$)	R for [C ₂ mim][BF ₄] based microemulsion	σ ($\mu\text{S cm}^{-1}$)
0.1400	6.6900	0.2255	38.7000	0.2255	37.9000
0.1728	8.7200	0.4510	99.4000	0.4510	68.1000
0.2000	10.1600	0.5600	128.9000	0.6765	191.0000
0.2255	10.7900	0.6765	159.4000	0.9020	400.0000
0.2855	19.6800	0.7400	180.5000	1.1275	441.0000
0.4510	54.0000	0.9020	232.0000	1.3000	509.0000
0.5600	67.4000	1.1275	271.0000		

Table A2. The σ for TX-100/cyclohexane/[C₄mim][MeSO₄] and TX-100/cyclohexane/[C₄mim][BF₄] microemulsions with increasing R at 25 °C.

R for [C ₄ mim][MeSO ₄] based microemulsion	σ ($\mu\text{S cm}^{-1}$)	R for [C ₄ mim][BF ₄] based microemulsion	σ ($\mu\text{S cm}^{-1}$)
0.1728	16.7300	0.2255	30.1000
0.2255	23.1000	0.4510	78.1000
0.4510	63.1000	0.5600	102.4000
0.5600	84.0000	0.6765	132.2000
0.6765	91.7000	0.7400	146.9000
0.7400	103.5000	0.9020	175.2000
0.9020	124.8000	1.1275	205.0000

Table A3. The σ for TX-100/[C₂mim][TFSI]/water and TX-100/[C₂mim][PF₆]/water microemulsions with decreasing W_o at 25 °C.

W_o for [C ₂ mim][TFSI] based microemulsion	σ ($\mu\text{S cm}^{-1}$)	W_o for [C ₂ mim][PF ₆] based microemulsion	σ ($\mu\text{S cm}^{-1}$)
12.2614	256.0000	14.0421	152.5000
11.2404	368.0000	13.1624	266.0000
9.9697	420.0000	12.4514	336.0000
8.9428	480.0000	11.6622	408.0000
7.9179	527.0000	10.9897	429.0000
5.4715	496.0000	10.3186	472.0000
5.0731	425.0000	9.3874	516.0000
2.7041	390.0000		

Table A4. The η for TX-100/cyclohexane/[C₂mim][MeSO₄], TX-100/cyclohexane/[C₂mim][EtSO₄] and TX-100/cyclohexane/[C₂mim][BF₄] microemulsions with increasing R at 25 °C.

R for [C ₂ mim][MeSO ₄] based microemulsion	η (mPa s)	R for [C ₂ mim][EtSO ₄] based microemulsion	η (mPa s)	R for [C ₂ mim][BF ₄] based microemulsion	η (mPa s)
0.1400	139.6900	0.2255	124.5400	0.2255	71.4240
0.1728	139.6900	0.4510	175.6400	0.4510	111.4700
0.2000	153.9700	0.5600	196.9000	0.5600	146.9000
0.2255	177.5800	0.6765	235.5300	0.6765	195.0700
0.2855	195.0000	0.7400	253.1000	0.7000	224.0000
0.4510	208.3000	0.9020	281.3300	0.9020	280.8100
0.5600	246.4900	1.1275	373.5400	1.1275	377.6800
				1.3000	441.0000

Table A5. The η for TX-100/cyclohexane/[C₄mim][MeSO₄] and TX-100/cyclohexane/[C₄mim][BF₄] microemulsions with increasing R at 25 °C.

R for [C ₄ mim][MeSO ₄] based microemulsion	η (mPa s)	R for [C ₄ mim][BF ₄] based microemulsion	η (mPa s)
0.1728	157.0700	0.2255	62.4100
0.2255	170.2300	0.4510	108.7200
0.4510	195.7400	0.5600	158.6900
0.5600	195.8700	0.6765	172.4100
0.6765	201.2400	0.7400	178.1500
0.7400	208.8600	0.9020	254.9500
0.9020	244.9300	1.1275	419.4300

Table A6. The η for TX-100/[C₂mim][TFSI]/water and TX-100/[C₂mim][PF₆]/water microemulsions with decreasing W_o at 25 °C.

W_o for [C ₂ mim][TFSI] based microemulsion	η (mPa s)	W_o for [C ₂ mim][PF ₆] based microemulsion	η (mPa s)
12.2614	323.1100	14.0421	507.8000
11.2404	289.2890	13.1624	440.1700
9.9697	258.8800	12.4514	413.5300
8.9428	242.3300	11.6622	378.1800
7.9179	240.3900	10.9897	357.3300
5.4715	228.1800	10.3186	337.6400
5.0731	234.4500	9.3874	329.4500
2.7041	262.4000		

Table A7. The η for TX-100/cyclohexane/[C₂mim][MeSO₄], TX-100/cyclohexane/[C₂mim][EtSO₄] and TX-100/cyclohexane/[C₂mim][BF₄] microemulsions with increasing temperature at $R = 0.2255$.

Temperature (°C)	η (mPa s) for [C ₂ mim][MeSO ₄] based microemulsion	η (mPa s) for [C ₂ mim][EtSO ₄] based microemulsion	η (mPa s) for [C ₂ mim][BF ₄] based microemulsion
25.0000	177.5800	124.5400	71.4240
30.0000	129.6800	93.5340	54.0500
35.0000	96.1170	72.7500	42.8600
40.0000	74.1230	58.3000	33.8630
45.0000	59.8460	48.2450	26.6610

Table A8. The η for TX-100/cyclohexane/[C₄mim][MeSO₄] and TX-100/cyclohexane/[C₄mim][BF₄] microemulsions with increasing temperature at $R = 0.2255$.

Temperature (°C)	η (mPa s) for [C ₄ mim][MeSO ₄] based microemulsion	η (mPa s) for [C ₄ mim][BF ₄] based microemulsion
25.0000	157.0700	62.4100
30.0000	107.0910	48.1170
35.0000	87.3240	38.5350
40.0000	66.2500	31.3900
45.0000	53.2260	25.8740

Table A9. The diameter of droplets of TX-100/cyclohexane/[C₂mim][MeSO₄], TX-100/cyclohexane/[C₂mim][EtSO₄], TX-100/cyclohexane/[C₂mim][BF₄], TX-100/cyclohexane/[C₄mim][MeSO₄], TX-100/cyclohexane/[C₄mim][BF₄], TX-100/[C₂mim][PF₆]/water, TX-100/[C₄mim][PF₆]/water and TX-100/[C₂mim][TFSI]/water microemulsions at different R or W_o at 25 °C.

Microemulsion	Polar phase to TX-100 mole ratio (R or W_o)	Diameter of droplet, d (nm)	Diameter of cluster, d (nm)
[C ₂ mim][MeSO ₄] based	0.1400	5	130
	0.1728	6	29
	0.2000	8	×
	0.2255	11	×
	0.2855	-	-
	0.4510	-	-
	0.5600	-	-

	0.2255	13	142
[C ₂ mim][EtSO ₄] based	0.4510	17	295
	0.5600	23	308
	0.6765	24	555
	0.7400	-	-
	0.9020	-	-
	1.1275	-	-
	0.2255	164	×
[C ₂ mim][BF ₄] based	0.4510	295	×
	0.5600	319	×
	0.6765	484	×
	0.7000	503	×
	0.9020	-	-
	1.1275	-	-
	0.1728	13	×
[C ₄ mim][MeSO ₄] based	0.2255	15	155
	0.4510	31	×
	0.5600	58	×
	0.6765	-	-
	0.7400	-	-
	0.9020	-	-
	0.2255	142	×
[C ₄ mim][BF ₄] based	0.4510	182	×
	0.5600	208	×
	0.6765	245	×
	0.7400	-	-
	0.9020	-	-
	1.1275	-	-
	14.0421	3	59
[C ₂ mim][PF ₆] based	13.1624	5	130
	12.4514	5	132
	11.6622	7	29
	9.3874	8	×
	12.2614	5	106
[C ₂ mim][TFSI] based	11.2404	7	120
	9.9697	8	110
	8.9428	9	113
	7.9179	-	-
	5.4715	-	-
	5.0731	-	-
	2.7041	-	-
	12.9756	6	118
[C ₄ mim][PF ₆] based	11.3113	8	153
	9.8265	9	149
	7.7538	11	169

Table A10. The ρ for TX-100/cyclohexane/[C₂mim][MeSO₄], TX-100/cyclohexane/[C₂mim][EtSO₄] and TX-100/cyclohexane/[C₂mim][BF₄] microemulsions with increasing R at 25 °C.

R for [C ₂ mim][MeSO ₄] based microemulsion	ρ (g cm ⁻³)	R for [C ₂ mim][EtSO ₄] based microemulsion	ρ (g cm ⁻³)	R for [C ₂ mim][BF ₄] based microemulsion	ρ (g cm ⁻³)
0.1400	0.9751	0.2255	0.9859	0.2255	0.9949
0.1728	0.9777	0.4510	1.0167	0.4510	1.0219
0.2000	0.9787	0.5600	1.0299	0.5600	1.0543
0.2255	0.9833	0.6765	1.0494	0.6765	1.0615
0.2855	1.0031	0.7400	1.0577	0.7000	1.0738
0.4510	1.0253	0.9020	1.0796	0.9020	1.0826
0.5600	1.0340	1.1275	1.1124	1.1275	1.1094
				1.3000	1.1214

 Table A11. The ρ for TX-100/cyclohexane/[C₄mim][MeSO₄] and TX-100/cyclohexane/[C₄mim][BF₄] microemulsions with increasing R at 25 °C.

R for [C ₄ mim][MeSO ₄] based microemulsion	ρ (g cm ⁻³)	R for [C ₄ mim][BF ₄] based microemulsion	ρ (g cm ⁻³)
0.1728	0.9937	0.2255	0.9876
0.2255	1.0097	0.4510	1.0156
0.4510	1.0224	0.5600	1.0375
0.5600	1.0300	0.6765	1.0438
0.6765	1.0387	0.7400	1.0482
0.7400	1.0554	0.9020	1.0700
0.9020	1.0686	1.1275	1.0997

 Table A12. The ρ for TX-100/[C₂mim][TFSI]/water and TX-100/[C₂mim][PF₆]/water microemulsions with decreasing W_o at 25 °C.

W_o for [C ₂ mim][TFSI] based microemulsion	ρ (g cm ⁻³)	W_o for [C ₂ mim][PF ₆] based microemulsion	ρ (g cm ⁻³)
12.2614	1.0793	14.0421	1.0656
11.2404	1.0887	13.1624	1.0726
9.9697	1.0969	12.4514	1.0773
8.9428	1.1043	11.6622	1.0830
7.9179	1.1130	10.9897	1.0877
5.4715	1.1254	10.3186	1.0928
5.0731	1.1354	9.3874	1.0984
2.7041	1.1535		

Table A13. The ρ for TX-100/cyclohexane/[C₂mim][MeSO₄], TX-100/cyclohexane/[C₂mim][EtSO₄] and TX-100/cyclohexane/[C₂mim][BF₄] microemulsions with increasing temperature at $R = 0.2255$.

Temperature (°C)	ρ (g cm ⁻³) for [C ₂ mim][MeSO ₄] based microemulsion	ρ (g cm ⁻³) for [C ₂ mim][EtSO ₄] based microemulsion	ρ (g cm ⁻³) for [C ₂ mim][BF ₄] based microemulsion
25.0000	1.0031	0.9859	0.9949
30.0000	0.9989	0.9817	0.9906
35.0000	0.9947	0.9775	0.9867
40.0000	0.9903	0.9734	0.9821
45.0000	0.9858	0.9692	0.9790

Table A14. The ρ for TX-100/cyclohexane/[C₄mim][MeSO₄] and TX-100/cyclohexane/[C₄mim][BF₄] microemulsions with increasing temperature at $R = 0.2255$.

Temperature (°C)	ρ (g cm ⁻³) for [C ₄ mim][MeSO ₄] based microemulsion	ρ (g cm ⁻³) for [C ₄ mim][BF ₄] based microemulsion
25.0000	1.0097	0.9876
30.0000	1.0046	0.9834
35.0000	1.0004	0.9791
40.0000	0.9957	0.9746
45.0000	0.9921	0.9685

Table A15. The n for TX-100/cyclohexane/[C₂mim][MeSO₄], TX-100/cyclohexane/[C₂mim][EtSO₄] and TX-100/cyclohexane/[C₂mim][BF₄] microemulsions with increasing R at 25 °C.

R for [C ₂ mim][MeSO ₄] based microemulsion	n	R for [C ₂ mim][EtSO ₄] based microemulsion	n	R for [C ₂ mim][BF ₄] based microemulsion	n
0.1400	1.4709	0.2255	1.4813	0.2255	1.4757
0.1728	1.4705	0.4510	1.4825	0.4510	1.4764
0.2000	1.4693	0.5600	1.4799	0.5600	1.4752
0.2255	1.4731	0.6765	1.4842	0.6765	1.4759
0.2855	1.4694	0.7400	1.4848	0.7000	1.4775
0.4510	1.4759	0.9020	1.4851	0.9020	1.4721
0.5600	1.4765	1.1275	1.4863	1.1275	1.4733
				1.3000	1.4723

Table A16. The σ for n data of TX-100/cyclohexane/[C₄mim][MeSO₄] and TX-100/cyclohexane/[C₄mim][BF₄] microemulsions as a function of R at 25 °C.

R for [C ₄ mim][MeSO ₄] based microemulsion	n	R for [C ₄ mim][BF ₄] based microemulsion	n
0.1728	1.4721	0.2255	1.4815
0.2255	1.4714	0.4510	1.4723
0.4510	1.4744	0.5600	1.4721
0.5600	1.4768	0.6765	1.4714
0.6765	1.4774	0.7400	1.4712
0.7400	1.4784	0.9020	1.4723
0.9020	1.4823	1.1275	1.4738

Table A17. The n for TX-100/[C₂mim][TFSI]/water and TX-100/[C₂mim][PF₆]/water microemulsions with decreasing W_o at 25 °C.

W_o for [C ₂ mim][TFSI] based microemulsion	n	W_o for [C ₂ mim][PF ₆] based microemulsion	n
12.2614	1.4508	14.0421	1.4466
11.2404	1.4545	13.1624	1.4491
9.9697	1.4553	12.4514	1.4501
8.9428	1.4572	11.6622	1.4514
7.9179	1.4601	10.9897	1.4523
5.4715	1.4622	10.3186	1.4533
5.0731	1.4656	9.3874	1.4544
2.7041	1.4694		

Table A18. The n for TX-100/cyclohexane/[C₂mim][MeSO₄], TX-100/cyclohexane/[C₂mim][EtSO₄] and TX-100/cyclohexane/[C₂mim][BF₄] microemulsions with increasing temperature at $R = 0.2255$.

Temperature (°C)	n for [C ₂ mim][MeSO ₄] based microemulsion	n for [C ₂ mim][EtSO ₄] based microemulsion	n for [C ₂ mim][BF ₄] based microemulsion
25.0000	1.4731	1.4813	1.4757
30.0000	1.4720	1.4794	1.4734
35.0000	1.4711	1.4783	1.4714
40.0000	1.4702	1.4764	1.4718
45.0000	1.4674	1.4747	1.4713

Table A19. The n for TX-100/cyclohexane/[C₄mim][MeSO₄] and TX-100/cyclohexane/[C₄mim][BF₄] microemulsions with increasing temperature at $R = 0.2255$.

Temperature (°C)	n for [C ₄ mim][MeSO ₄] based microemulsion	n for [C ₄ mim][BF ₄] based microemulsion
25.0000	1.4714	1.4815
30.0000	1.4709	1.4801
35.0000	1.4710	1.4791
40.0000	1.4717	1.4781
45.0000	1.4718	1.4771

Table A20. The γ for da TX-100/cyclohexane/[C₂mim][MeSO₄] and TX-100/cyclohexane/[C₂mim][EtSO₄] microemulsions with increasing R at 25 °C.

R for [C ₂ mim][MeSO ₄] based microemulsion	γ (mN m ⁻¹)	R for [C ₂ mim][EtSO ₄] based microemulsion	γ (mN m ⁻¹)
0.2255	19.9070	0.1728	21.7770
		0.2255	22.0880
		0.4510	22.2220
		0.5600	23.5030
		0.6765	24.9510

Table A21. The γ for TX-100/cyclohexane/[C₂mim][PF₆] and TX-100/cyclohexane/[C₂mim][TFSI] microemulsions with decreasing W_o at 25 °C.

W_o for [C ₂ mim][TFSI] based microemulsion	γ (mN m ⁻¹)	W_o for [C ₂ mim][PF ₆] based microemulsion	γ (mN m ⁻¹)
9.9697	27.987	14.0421	27.122
		13.1624	28.245
		11.6622	28.092
		10.9897	28.534
		10.3186	28.495
		9.9697	28.500

Table A22. The σ for TX-100/cyclohexane/[C₂mim][MeSO₄] and TX-100/cyclohexane/[C₄mim][MeSO₄] microemulsions with increasing R at 25 °C.

R for [C ₂ mim][MeSO ₄] based microemulsion	σ ($\mu\text{S cm}^{-1}$)	R for [C ₄ mim][MeSO ₄] based microemulsion	σ ($\mu\text{S cm}^{-1}$)
0.1400	6.6900	0.1728	16.7300
0.1728	8.7200	0.2255	23.1000
0.2000	10.1600	0.4510	63.1000
0.2255	10.7900	0.5600	84.0000
0.2855	19.6800	0.6765	91.7000
0.4510	54.0000	0.7400	103.5000
0.5600	67.4000	0.9020	124.8000

Table A23. The σ for TX-100/cyclohexane/[C₂mim][BF₄] and TX-100/cyclohexane/[C₄mim][BF₄] microemulsions with increasing R at 25 °C.

R for [C ₂ mim][BF ₄] based microemulsion	σ ($\mu\text{S cm}^{-1}$)	R for [C ₄ mim][BF ₄] based microemulsion	σ ($\mu\text{S cm}^{-1}$)
0.2255	37.9000	0.2255	30.1000
0.4510	68.1000	0.4510	78.1000
0.6765	191.0000	0.5600	102.4000
0.9020	400.0000	0.6765	132.2000
1.1275	441.0000	0.7400	146.9000
1.3000	509.0000	0.9020	175.2000
		1.1275	205.0000

Table A24. The σ for TX-100/[C₂mim][PF₆]/water and TX-100/[C₄mim][PF₆]/water microemulsions with decreasing W_0 at 25 °C.

W_0 for [C ₂ mim][PF ₆] based microemulsion	σ ($\mu\text{S cm}^{-1}$)	W_0 for [C ₄ mim][PF ₆] based microemulsion	σ ($\mu\text{S cm}^{-1}$)
14.0421	152.5000	12.9756	199.3000
13.1624	266.0000	11.3113	258.0000
12.4514	336.0000	9.8205	282.0000
11.6622	408.0000	7.7538	302.0000
10.9897	429.0000	6.0346	274.0000
10.3186	472.0000	4.1968	249.0000
9.3874	516.0000	3.1952	200.0000
		0.6398	93.5000

Table A25. Walden plot data of TX-100/cyclohexane/[C₂mim][BF₄] and TX-100/cyclohexane/[C₄mim][BF₄] microemulsions.

$\log[\eta^{-1}(\text{Pa s}^{-1})]$ [C ₂ mim][BF ₄] based microemulsion	$\log[A(\text{S cm}^2 \text{mol}^{-1})]$	$\log[\eta^{-1}(\text{Pa s}^{-1})]$ [C ₄ mim][BF ₄] based microemulsion	$\log[A(\text{S cm}^2 \text{mol}^{-1})]$
1.1462	-2.0570	1.2047	-2.1453
0.9528	-1.7785	0.9637	-1.6976
0.7098	-1.3084	0.7995	-1.5653
0.5516	-0.9536	0.7634	-1.4299
0.4229	-0.8744	0.7492	-1.3704
0.3556	-0.7769	0.5935	-1.2604
		0.3773	-1.1371

Table A26. Walden plot data of TX-100/[C₂mim][PF₆]/water and TX-100/[C₄mim][PF₆]/water microemulsions.

$\log[\eta^{-1}(\text{Pa s}^{-1})]$ [C ₂ mim][PF ₆] based microemulsion	$\log[A(\text{S cm}^2 \text{mol}^{-1})]$	$\log[\eta^{-1}(\text{Pa s}^{-1})]$ [C ₄ mim][PF ₆] based microemulsion	$\log[A(\text{S cm}^2 \text{mol}^{-1})]$
0.2943	-2.0727	0.4234	-1.9287
0.3564	-1.8096	0.4859	-1.7697
0.3835	-1.6895	0.5403	-1.6841
0.4223	-1.5833	0.5500	-1.5757
0.4469	-1.5420		
0.4715	-1.4798		
0.48226	-1.4097		

Table A27. The η for TX-100/cyclohexane/[C₂mim][MeSO₄] and TX-100/cyclohexane/[C₄mim][MeSO₄] microemulsions with increasing R at 25 °C.

R for [C ₂ mim][MeSO ₄] based microemulsion	η (mPa s)	R for [C ₄ mim][MeSO ₄] based microemulsion	η (mPa s)
0.1400	139.6900	0.1728	157.0700
0.1728	139.6900	0.2255	170.2300
0.2000	153.9700	0.4510	195.7400
0.2255	177.5800	0.5600	195.8700
0.2855	195.0000	0.6765	201.2400
0.4510	208.3000	0.7400	208.8600
0.5600	246.4900	0.9020	244.9300

Table A28. The η for TX-100/cyclohexane/[C₂mim][BF₄] and TX-100/cyclohexane/[C₄mim][BF₄] microemulsions with increasing R at 25 °C.

R for [C ₂ mim][BF ₄] based microemulsion	η (mPa s)	R for [C ₄ mim][BF ₄] based microemulsion	η (mPa s)
0.2255	71.4240	0.2255	62.4100
0.4510	111.4700	0.4510	108.7200
0.5600	146.9000	0.5600	158.6900
0.6765	195.0700	0.6765	172.4100
0.7000	224.0000	0.7400	178.1500
0.9020	280.8100	0.9020	254.9500
1.1275	377.6800	1.1275	419.4300
1.3000	441.0000		

Table A29. The η for TX-100/[C₂mim][PF₆]/water and TX-100/[C₄mim][PF₆]/water microemulsions with decreasing W_o at 25 °C.

W_o for [C ₂ mim][PF ₆] based microemulsion	η (mPa s)	W_o for [C ₄ mim][PF ₆] based microemulsion	η (mPa s)
14.0421	14.0421	12.9756	377.2200
13.1624	13.1624	11.3113	326.6600
12.4514	12.4514	9.8205	288.2300
11.6622	11.6622	7.7538	281.8300
10.9897	10.9897	6.0346	294.2200
10.3186	10.3186	4.1968	345.5600
9.3874	9.3874	3.1952	391.1800
		0.6398	604.2000

Table A30. The η for TX-100/cyclohexane/[C₂mim][MeSO₄] and TX-100/cyclohexane/[C₄mim][MeSO₄] microemulsions with increasing temperature at $R = 0.2255$.

Temperature (°C)	η (mPa s) for [C ₂ mim][MeSO ₄] based microemulsion	η (mPa s) for [C ₄ mim][MeSO ₄] based microemulsion
25.0000	177.5800	157.0700
30.0000	129.6800	123.7600
35.0000	96.1170	87.3240
40.0000	75.3400	72.1200
45.0000	59.8460	53.2260

Table A31. The η for TX-100/cyclohexane/[C₂mim][BF₄] and TX-100/cyclohexane/[C₄mim][BF₄] microemulsions with increasing temperature at $R = 0.2255$.

Temperature (°C)	η (mPa s) for [C ₂ mim][BF ₄] based microemulsion	η (mPa s) for [C ₄ mim][BF ₄] based microemulsion
25.0000	71.4240	62.4100
30.0000	54.0500	48.1170
35.0000	42.8600	38.5350
40.0000	33.8630	31.3900
45.0000	26.6610	25.8740

Table A32. The ρ for TX-100/cyclohexane/[C₂mim][MeSO₄] and TX-100/cyclohexane/[C₄mim][MeSO₄] microemulsions with increasing R at 25 °C.

R for [C ₂ mim][MeSO ₄] based microemulsion	ρ (g cm ⁻³)	R for [C ₄ mim][MeSO ₄] based microemulsion	ρ (g cm ⁻³)
0.1400	0.9751	0.1728	0.9937
0.1728	0.9777	0.2255	1.0097
0.2000	0.9787	0.4510	1.0224
0.2255	0.9833	0.5600	1.0300
0.2855	1.0031	0.6765	1.0387
0.4510	1.0253	0.7400	1.0554
0.5600	1.0340	0.9020	1.0686

Table A33. The ρ for TX-100/cyclohexane/[C₂mim][BF₄] and TX-100/cyclohexane/[C₄mim][BF₄] microemulsions with increasing R at 25 °C.

R for [C ₂ mim][BF ₄] based microemulsion	ρ (g cm ⁻³)	R for [C ₄ mim][BF ₄] based microemulsion	ρ (g cm ⁻³)
0.2255	0.9949	0.2255	0.9876
0.4510	1.0219	0.4510	1.0156
0.5600	1.0543	0.5600	1.0375
0.6765	1.0615	0.6765	1.0438
0.7000	1.0738	0.7400	1.0482
0.9020	1.0826	0.9020	1.0700
1.1275	1.1094	1.1275	1.0997
1.3000	1.1214		

Table A34. The ρ for TX-100/[C₂mim][PF₆]/water and TX-100/[C₄mim][PF₆]/water microemulsions with decreasing W_o at 25 °C.

W_o for [C ₂ mim][PF ₆] based microemulsion	ρ (g cm ⁻³)	W_o for [C ₄ mim][PF ₆] based microemulsion	ρ (g cm ⁻³)
14.0421	1.0656	12.9756	1.0707
13.1624	1.0726	11.3113	1.0817
12.4514	1.0773	9.8205	1.0923
11.6622	1.0830	7.7538	1.1026
10.9897	1.0877	6.0346	1.1130
10.3186	1.0928	4.1968	1.1217
9.3874	1.0984	3.1952	1.1278
		0.6398	1.1371

Table A35. The ρ for TX-100/cyclohexane/[C₂mim][MeSO₄] and TX-100/cyclohexane/[C₄mim][MeSO₄] microemulsions with increasing temperature at $R = 0.2255$.

Temperature (°C)	ρ (g cm ⁻³) for [C ₂ mim][MeSO ₄] based microemulsion	ρ (g cm ⁻³) for [C ₄ mim][MeSO ₄] based microemulsion
25.0000	1.0031	1.0097
30.0000	0.9989	1.0046
35.0000	0.9947	1.0004
40.0000	0.9903	0.9957
45.0000	0.9858	0.9921

Table A36. The ρ for TX-100/cyclohexane/[C₂mim][BF₄] and TX-100/cyclohexane/[C₄mim][BF₄] microemulsions with increasing temperature at $R = 0.2255$.

Temperature (°C)	ρ (g cm ⁻³) for [C ₂ mim][BF ₄] based microemulsion	ρ (g cm ⁻³) for [C ₄ mim][BF ₄] based microemulsion
25.0000	0.9876	0.9949
30.0000	0.9834	0.9906
35.0000	0.9791	0.9867
40.0000	0.9746	0.9821
45.0000	0.9685	0.9790

Table A37. The n for TX-100/cyclohexane/[C₂mim][MeSO₄] and TX-100/cyclohexane/[C₄mim][MeSO₄] microemulsions with increasing R at 25 °C.

R for [C ₂ mim][MeSO ₄] based microemulsion	n	R for [C ₄ mim][MeSO ₄] based microemulsion	n
0.1400	1.4709	0.1728	1.4721
0.1728	1.4705	0.2255	1.4714
0.2000	1.4693	0.4510	1.4744
0.2255	1.4731	0.5600	1.4768
0.2855	1.4694	0.6765	1.4774
0.4510	1.4759	0.7400	1.4784
0.5600	1.4765	0.9020	1.4823

Table A38. The n for TX-100/cyclohexane/[C₂mim][BF₄] and TX-100/cyclohexane/[C₄mim][BF₄] microemulsions with increasing R at 25 °C.

R for [C ₂ mim][BF ₄] based microemulsion	n	R for [C ₄ mim][BF ₄] based microemulsion	n
0.2255	1.4757	0.2255	1.4815
0.4510	1.4764	0.4510	1.4723
0.5600	1.4752	0.5600	1.4721
0.6765	1.4759	0.6765	1.4714
0.7000	1.4775	0.7400	1.4712
0.9020	1.4721	0.9020	1.4723
1.1275	1.4733	1.1275	1.4738
1.3000	1.4723		

Table A39. The n for TX-100/[C₂mim][PF₆]/water and TX-100/[C₄mim][PF₆]/water microemulsions with decreasing W_o at 25 °C.

W_o for [C ₂ mim][PF ₆] based microemulsion	n	W_o for [C ₄ mim][PF ₆] based microemulsion	n
14.0421	1.4466	12.9756	1.4504
13.1624	1.4491	11.3113	1.4562
12.4514	1.4501	9.8205	1.4568
11.6622	1.4514	7.7538	1.4635
10.9897	1.4523	6.0346	1.4625
10.3186	1.4533	4.1968	1.4651
9.3874	1.4544	3.1952	1.4678
		0.6398	1.4658

Table A40. The n for TX-100/cyclohexane/[C₂mim][MeSO₄] and TX-100/cyclohexane/[C₄mim][MeSO₄] microemulsions with increasing temperature at $R = 0.2255$.

Temperature (°C)	n for [C ₂ mim][MeSO ₄] based microemulsion	n for [C ₄ mim][MeSO ₄] based microemulsion
25.0000	1.4731	1.4714
30.0000	1.4720	1.4709
35.0000	1.4711	1.4710
40.0000	1.4702	1.4717
45.0000	1.4674	1.4718

Table A41. The n for TX-100/cyclohexane/[C₂mim][BF₄] and TX-100/cyclohexane/[C₄mim][BF₄] microemulsions with increasing temperature at $R = 0.2255$.

Temperature (°C)	n for [C ₂ mim][BF ₄] based microemulsion	n for [C ₄ mim][BF ₄] based microemulsion
25.0000	1.4757	1.4815
30.0000	1.4734	1.4801
35.0000	1.4714	1.4791
40.0000	1.4718	1.4781
45.0000	1.4713	1.4771

Table A42. The γ for TX-100/[C₂mim][PF₆]/water and TX-100/[C₄mim][PF₆]/water microemulsions with decreasing W_o at 25 °C.

W_o for [C ₂ mim][PF ₆] based microemulsion	γ (mN m ⁻¹)	W_o for [C ₄ mim][PF ₆] based microemulsion	γ (mN m ⁻¹)
14.0421	27.122	11.3113	28.324
13.1624	28.245		
11.6622	28.092		
10.9897	28.534		
10.3186	28.495		
9.9697	28.500		

Table A43. The σ for CTAB/1-butanol/cyclohexane/[C₂mim][MeSO₄] and CTAB/1-butanol/cyclohexane/[C₂mim][EtSO₄] microemulsions with increasing R at 25 °C.

R for [C ₂ mim][MeSO ₄] based microemulsion	σ ($\mu\text{S cm}^{-1}$)	R for [C ₂ mim][EtSO ₄] based microemulsion	σ ($\mu\text{S cm}^{-1}$)
1.5424	0.1460	1.5424	0.2010
3.0849	0.2940	3.0849	0.5270
4.6273	0.4940	4.6273	0.8490
6.1697	0.7710	6.1697	1.6340
7.7121	1.0730	7.7121	2.7300
9.2546	1.4130	9.2546	2.9300
10.7970	1.7450	10.7970	3.2400

Table A44. The σ for CTAB/1-butanol/cyclohexane/[C₂mim][MeSO₄] and CTAB/1-butanol/cyclohexane/[C₄mim][MeSO₄] microemulsions with increasing R at 25 °C.

R for [C ₂ mim][MeSO ₄] based microemulsion	σ ($\mu\text{S cm}^{-1}$)	R for [C ₄ mim][MeSO ₄] based microemulsion	σ ($\mu\text{S cm}^{-1}$)
1.5424	0.1460	1.5424	0.2430
3.0849	0.2940	3.0849	0.6220
4.6273	0.4940	4.3680	0.9620
6.1697	0.7710	6.1697	1.1380
7.7121	1.0730	7.2800	1.4810
9.2546	1.4130	8.7359	2.6300
10.7970	1.7450	10.1918	2.6700

Table A45. The η for CTAB/1-butanol/cyclohexane/[C₂mim][MeSO₄] and CTAB/1-butanol/cyclohexane/[C₂mim][EtSO₄] microemulsions with increasing R at 25 °C.

R for [C ₂ mim][MeSO ₄] based microemulsion	η (mPa s)	R for [C ₂ mim][EtSO ₄] based microemulsion	η (mPa s)
1.5424	2.1121	1.5424	2.1190
3.0849	2.6281	3.0849	2.5194
4.6273	3.1216	4.6273	2.9539
6.1697	4.2497	6.1697	5.6134
7.7121	5.4389	7.7121	6.9015
9.2546	6.2267	9.2546	9.0145
10.7970	10.1030	10.7970	10.8870
13.8818	10.6505		

Table A46. The η for CTAB/1-butanol/cyclohexane/[C₂mim][MeSO₄] and CTAB/1-butanol/cyclohexane/[C₄mim][MeSO₄] microemulsions with increasing R at 25 °C.

R for [C ₂ mim][MeSO ₄] based microemulsion	η (mPa s)	R for [C ₄ mim][MeSO ₄] based microemulsion	η (mPa s)
1.5424	2.1190	1.4560	2.1113
3.0849	2.5194	2.9120	2.4638
4.6273	2.9539	4.3679	3.5876
6.1697	5.6134	5.8239	4.3618
7.7121	6.9015	7.2799	4.6337
9.2546	9.0145	8.7359	6.4584
10.7970	10.8870	10.1918	6.7960

Table A47. The η for CTAB/1-butanol/cyclohexane/[C₂mim][MeSO₄] and CTAB/1-butanol/cyclohexane/[C₂mim][EtSO₄] microemulsions with increasing temperature at $R = 1.5424$.

Temperature (°C)	η (mPa s) for [C ₂ mim][MeSO ₄] based microemulsion	η (mPa s) for [C ₂ mim][EtSO ₄] based microemulsion
25.0000	2.1190	2.1121
30.0000	1.9030	1.8740
35.0000	1.7161	1.6839
40.0000	1.5566	1.5275
45.0000	1.4243	1.4191

Table A48. The η for CTAB/1-butanol/cyclohexane/[C₂mim][MeSO₄] and CTAB/1-butanol/cyclohexane/[C₄mim][MeSO₄] microemulsions with increasing temperature at $R = 1.5424$.

Temperature (°C)	η (mPa s) for [C ₂ mim][MeSO ₄] based microemulsion	η (mPa s) for [C ₄ mim][MeSO ₄] based microemulsion
25.0000	2.1190	2.1113
30.0000	1.9030	1.8794
35.0000	1.7161	1.6815
40.0000	1.5566	1.5111
45.0000	1.4243	1.3640

Table A49. Diameter of droplets of CTAB microemulsions at different R at 25 °C.

Microemulsion	R	Diameter of droplet, d (nm)	Diameter of cluster, d (nm)
[C ₂ mim][MeSO ₄] based	1.5424	2	420
	3.0849	3	233
	4.6273	4	254
	6.1697	5	208
	7.7121	6	566
	9.2546	9	982
[C ₂ mim][EtSO ₄] based	1.5424	3	295
	3.0849	4	531
	4.6273	5	493
	6.1697	6	x
[C ₄ mim][MeSO ₄] based	3.0849	3	x
	4.6273	4	712
	6.1697	7	531
	7.7121	9	x
	9.2546	14	x

Table A50. The ρ for CTAB/1-butanol/cyclohexane/[C₂mim][MeSO₄] and CTAB/1-butanol/cyclohexane/[C₂mim][EtSO₄] microemulsions with increasing R at 25 °C.

R for [C ₂ mim][MeSO ₄] based microemulsion	ρ (g cm ⁻³)	R for [C ₂ mim][EtSO ₄] based microemulsion	ρ (gc m ⁻³)
1.5424	0.8150	1.5424	0.8146
3.0849	0.8305	3.0849	0.8310
4.6273	0.8481	4.6273	0.8471
6.1697	0.8638	6.1697	0.8664
7.7121	0.8843	7.7121	0.8942
9.2546	0.9071	9.2546	0.9081
10.7970	0.9282	10.7970	0.9566

Table A51. The ρ for CTAB/1-butanol/cyclohexane/[C₂mim][MeSO₄] and CTAB/1-butanol/cyclohexane/[C₄mim][MeSO₄] microemulsions with increasing R at 25 °C.

R for [C ₂ mim][MeSO ₄] based microemulsion	ρ (g cm ⁻³)	R for [C ₄ mim][MeSO ₄] based microemulsion	ρ (g cm ⁻³)
1.5424	0.8150	1.5424	0.8137
3.0849	0.8305	3.0849	0.8279
4.6273	0.8481	4.3679	0.8461
6.1697	0.8638	6.1697	0.8624
7.7121	0.8843	7.2799	0.8742
9.2546	0.9071	8.7359	0.9244
10.7970	0.9282	10.1918	0.9318

Table A52. The ρ for CTAB/1-butanol/cyclohexane/[C₂mim][MeSO₄] and CTAB/1-butanol/cyclohexane/[C₂mim][EtSO₄] microemulsions with increasing temperature at $R = 1.5424$.

Temperature (°C)	ρ (g cm ⁻³) for [C ₂ mim][MeSO ₄] based microemulsion	ρ (g cm ⁻³) for [C ₂ mim][EtSO ₄] based microemulsion
25.0000	0.8150	0.8146
30.0000	0.8108	0.8103
35.0000	0.8065	0.8059
40.0000	0.8022	0.8015
45.0000	0.7978	0.7971

Table A53. The ρ for CTAB/1-butanol/cyclohexane/[C₂mim][MeSO₄] and CTAB/1-butanol/cyclohexane/[C₄mim][MeSO₄] microemulsions with increasing temperature at $R = 1.5424$.

Temperature (°C)	ρ (g cm ⁻³) for [C ₂ mim][MeSO ₄] based microemulsion	ρ (g cm ⁻³) for [C ₄ mim][MeSO ₄] based microemulsion
25.0000	0.8150	0.8137
30.0000	0.8108	0.8094
35.0000	0.8065	0.8051
40.0000	0.8022	0.8007
45.0000	0.7978	0.7963

Table A54. The n for CTAB/1-butanol/cyclohexane/[C₂mim][MeSO₄] and CTAB/1-butanol/cyclohexane/[C₂mim][EtSO₄] microemulsions with increasing R at 25 °C.

R for [C ₂ mim][MeSO ₄] based microemulsion	n	R for [C ₂ mim][EtSO ₄] based microemulsion	n
1.5424	1.4127	1.5424	1.4147
3.0849	1.4167	3.0849	1.4172
4.6273	1.4200	4.6273	1.4192
6.1697	1.4225	6.1697	1.4225
7.7121	1.4255	7.7121	1.4288
9.2546	1.4281	9.2546	1.4292
10.7970	1.4310	10.7970	1.4345

Table A55. The n for CTAB/1-butanol/cyclohexane/[C₂mim][MeSO₄] and CTAB/1-butanol/cyclohexane/[C₄mim][MeSO₄] microemulsions with increasing R at 25 °C.

R for [C ₂ mim][MeSO ₄] based microemulsion	n	R for [C ₄ mim][MeSO ₄] based microemulsion	n
1.5424	1.4127	1.5424	1.4137
3.0849	1.4167	3.0849	1.4171
4.6273	1.4200	4.3679	1.4198
6.1697	1.4225	6.1697	1.4230
7.7121	1.4255	7.2799	1.4253
9.2546	1.4281	8.7359	1.4325
10.7970	1.4310	10.1918	1.4351

Table A56. The n for CTAB/1-butanol/cyclohexane/[C₂mim][MeSO₄] and CTAB/1-butanol/cyclohexane/[C₂mim][EtSO₄] microemulsions with increasing temperature at $R = 1.5424$.

Temperature (°C)	n for [C ₂ mim][MeSO ₄] based microemulsion	n for [C ₂ mim][EtSO ₄] based microemulsion
25.0000	1.4127	1.4147
30.0000	1.4100	1.4119
35.0000	1.4078	1.4092
40.0000	1.4058	1.4072
45.0000	1.4042	1.4083

Table A57. The n for CTAB/1-butanol/cyclohexane/[C₂mim][MeSO₄] and CTAB/1-butanol/cyclohexane/[C₄mim][MeSO₄] microemulsions with increasing temperature at $R = 1.5424$.

Temperature (°C)	n for [C ₂ mim][MeSO ₄] based microemulsion	n for [C ₄ mim][MeSO ₄] based microemulsion
25.0000	1.4127	1.4137
30.0000	1.4100	1.4115
35.0000	1.4078	1.4092
40.0000	1.4058	1.4074
45.0000	1.4042	1.4073

Table A58. The γ for CTAB/1-butanol/cyclohexane/[C₂mim][MeSO₄], CTAB/1-butanol/cyclohexane/[C₂mim][EtSO₄] and CTAB/1-butanol/cyclohexane/[C₄mim][MeSO₄] microemulsions with increasing R at 25 °C.

R for [C ₂ mim][MeSO ₄] based microemulsion	γ (mN m ⁻¹)	R for [C ₂ mim][EtSO ₄] based microemulsion	γ (mN m ⁻¹)	R for [C ₄ mim][MeSO ₄] based microemulsion	γ (mN m ⁻¹)
1.5424	22.787	1.5424	18.170	1.5424	22.475
		3.0849	18.734		
		4.6273	18.675		
		6.1697	22.488		
		7.7121	23.375		

Table A59. The $d\log\sigma/d\phi$ for TX-100/cyclohexane/[C₂mim][EtSO₄] and TX-100/cyclohexane/[C₂mim][BF₄] microemulsions as a function of ϕ at 25 °C.

ϕ_{IL} (IL = [C ₂ mim][EtSO ₄])	$d\log\sigma/d\phi_{IL}$	ϕ_{IL} (IL = [C ₂ mim][BF ₄])	$d\log\sigma/d\phi_{IL}$
0.0480	8.1940	0.0385	6.2995
0.0980	6.2682	0.0789	8.4068
0.1240	3.8176	0.1215	8.8408
0.1520	3.4464	0.1663	4.0299
0.1670	3.0976	0.2137	1.2681
0.2090	1.8601	0.2516	1.6438
0.2690	1.1250		

Table A60. The $d\log\sigma/d\phi$ for TX-100/cyclohexane/[C₄mim][BF₄] and TX-100/cyclohexane/[C₄mim][MeSO₄] microemulsions as a function of ϕ at 25 °C.

ϕ_{IL} (IL = [C ₄ mim][BF ₄])	$d\log\sigma/d\phi_{IL}$	ϕ_{IL} (IL = [C ₄ mim][MeSO ₄])	$d\log\sigma/d\phi_{IL}$
0.0469	8.3826	0.0394	11.3902
0.0963	6.5623	0.0517	9.6769
0.1211	4.4096	0.1065	6.2254
0.1483	3.5452	0.1342	2.8683
0.1635	2.4701	0.1647	2.1687
0.2032	1.5523	0.1817	2.4535
0.2612	1.1776	0.2264	1.8188

Table A61. The $d\log\sigma/d\phi$ for TX-100/[C₂mim][TFSI]/water microemulsions as a function of ϕ at 25 °C.

ϕ_w (IL = [C ₂ mim][TFSI])	$d\log\sigma/d\phi_w$
0.2648	-7.6505
0.2442	-4.9687
0.2191	-2.5178
0.1980	-2.3275
0.1767	-0.6916
0.1264	3.3970
0.1157	3.4887
0.0629	0.7064

Table A62. The $d\log\sigma/d\phi$ for TX-100/[C₄mim][PF₆]/water microemulsions as a function of ϕ at 25 °C.

ϕ_w (IL = [C ₄ mim][PF ₆])	$d\log\sigma/d\phi_w$
0.2779	-3.3765
0.2447	-2.3231
0.2143	-0.9814
0.1713	0.2300
0.1347	1.0965
0.0947	2.6739
0.0726	5.0103
0.0148	5.7128

Table A63. The V^E for TX-100/cyclohexane/[C₂mim][EtSO₄] and TX-100/cyclohexane/[C₂mim][BF₄] microemulsions as a function of ϕ at 25 °C.

ϕ_{IL} (IL = [C ₂ mim][EtSO ₄])	V^E	ϕ_{IL} (IL = [C ₂ mim][BF ₄])	V^E
0.0479	0.0284	0.0385	-0.0942
0.0983	0.0060	0.0789	-0.1076
0.1237	0.0173	0.0992	-0.2863
0.1518	-0.0124	0.1215	-0.2205
0.1674	-0.0112	0.1256	-0.3321
0.2086	0.0010	0.1663	-0.1519
0.2690	0.0119	0.2137	-0.1229

Table A64. The V^E for TX-100/cyclohexane/[C₄mim][BF₄] and TX-100/cyclohexane/[C₄mim][MeSO₄] microemulsions as a function of ϕ at 25 °C.

ϕ_{IL} (IL = [C ₄ mim][BF ₄])	V^E	ϕ_{IL} (IL = [C ₄ mim][MeSO ₄])	V^E
0.0469	-0.0143	0.0394	-0.1125
0.0963	-0.0357	0.0517	-0.2044
0.1211	-0.1188	0.1065	-0.0380
0.1483	-0.0438	0.1342	0.0298
0.1635	-0.0114	0.1647	0.0979
0.2032	-0.0207	0.1817	0.0272
0.2612	-0.0152	0.2264	0.1180

Table A65. The V^E for TX-100/[C₂mim][TFSI]/water microemulsions as a function of ϕ at 25 °C.

ϕ_w (IL = [C ₂ mim][TFSI])	V^E
0.2648	-0.1045
0.2442	-0.1301
0.2191	-0.0940
0.1980	-0.0836
0.1767	-0.0832
0.1264	0.1237
0.1157	-0.0627
0.0629	-0.0362

Table A66. The V^E for TX-100/[C₄mim][PF₆]/water microemulsions as a function of ϕ at 25 °C.

ϕ_W (IL = [C ₄ mim][PF ₆])	V^E
0.2779	-0.1076
0.2447	-0.1116
0.2143	-0.1197
0.1713	-0.0920
0.1347	-0.0828
0.0947	-0.0519
0.0726	-0.0452
0.0148	0.0221

Table A67. The n^E for TX-100/cyclohexane/[C₂mim][EtSO₄] and TX-100/cyclohexane/[C₂mim][BF₄] microemulsions as a function of ϕ at 25 °C.

ϕ_{IL} (IL = [C ₂ mim][EtSO ₄])	n^E	ϕ_{IL} (IL = [C ₂ mim][BF ₄])	n^E
0.0479	0.0139	0.0385	0.0118
0.0983	0.0113	0.0789	0.0122
0.1237	0.0068	0.0992	0.0108
0.1518	0.0084	0.1215	0.0112
0.1674	0.0084	0.1256	0.0176
0.2086	0.0055	0.1663	0.0072
0.2690	0.0019	0.2137	0.0072

Table A68. The n^E for TX-100/cyclohexane/[C₄mim][BF₄] and TX-100/cyclohexane/[C₄mim][MeSO₄] microemulsions as a function of ϕ at 25 °C.

ϕ_{IL} (IL = [C ₄ mim][BF ₄])	n^E	ϕ_{IL} (IL = [C ₄ mim][MeSO ₄])	n^E
0.0469	0.0171	0.0394	0.0055
0.0963	0.0070	0.0517	0.0040
0.1211	0.0063	0.1065	0.0026
0.1483	0.0051	0.1342	0.0029
0.1635	0.0046	0.1647	0.0012
0.2032	0.0050	0.1817	0.0084
0.2612	0.0054	0.2264	0.0014

Table A69. The n^E for TX-100/[C₂mim][TFSI]/water microemulsions as a function of ϕ at 25 °C.

ϕ_w (IL = [C ₂ mim][TFSI])	n^E
0.2648	0.0070
0.2442	0.0086
0.2191	0.0065
0.1980	0.0064
0.1767	0.0069
0.1264	0.0053
0.1157	0.0060
0.0629	0.0038

Table A70. The n^E for TX-100/[C₄mim][PF₆]/water microemulsions as a function of ϕ at 25 °C.

ϕ_w (IL = [C ₄ mim][PF ₆])	n^E
0.2779	0.0098
0.2447	0.0137
0.2143	0.0125
0.1713	0.0167
0.1347	0.0136
0.0947	0.0138
0.0726	0.0151
0.0148	0.0097

Table A71. The R^E for TX-100/cyclohexane/[C₂mim][EtSO₄] and TX-100/cyclohexane/[C₂mim][BF₄] microemulsions as a function of ϕ at 25 °C.

ϕ_{IL} (IL = [C ₂ mim][EtSO ₄])	R^E	ϕ_{IL} (IL = [C ₂ mim][BF ₄])	R^E
0.0479	46.6121	0.0385	44.8336
0.0983	47.1102	0.0789	44.8274
0.1237	46.4015	0.0992	44.3565
0.1518	47.0215	0.1215	44.1485
0.1674	46.9045	0.1256	44.5266
0.2086	45.9732	0.1663	42.2160
0.2690	43.9972	0.2137	40.8159

Table A72. The R^E for TX-100/cyclohexane/[C₄mim][BF₄], TX-100/cyclohexane/[C₄mim][MeSO₄] microemulsions as a function of ϕ at 25 °C.

ϕ_{IL} (IL = [C ₄ mim][BF ₄])	R^E	ϕ_{IL} (IL = [C ₄ mim][MeSO ₄])	R^E
0.0469	46.6971	0.0394	44.7745
0.0963	45.0705	0.0517	44.8228
0.1211	44.9703	0.1065	45.9018
0.1483	44.5867	0.1342	46.3705
0.1635	44.3469	0.1647	46.2080
0.2032	43.8150	0.1817	46.1697
0.2612	42.3853	0.2264	46.0228

Table A73. The R^E for TX-100/[C₂mim][TFSI]/water microemulsions as a function of ϕ at 25 °C.

ϕ_w (IL = [C ₂ mim][TFSI])	R^E
0.2648	31.3786
0.2442	32.8615
0.2191	33.3913
0.1980	34.2278
0.1767	35.2637
0.1264	34.8051
0.1157	37.4297
0.0629	38.8391

Table A74. The R^E for TX-100/[C₄mim][PF₆]/water microemulsions as a function of ϕ at 25 °C.

ϕ_w (IL = [C ₄ mim][PF ₆])	R^E
0.2779	30.8898
0.2447	32.9134
0.2143	33.6811
0.1713	35.9643
0.1347	36.2794
0.0947	37.3653
0.0726	38.2191
0.0148	38.0790

Table A75. The $d\log\sigma/dR$ for CTAB/1-butanol/cyclohexane/[C₂mim][MeSO₄] and CTAB/1-butanol/cyclohexane/[C₂mim][EtSO₄] microemulsions as a function of R at 25 °C.

R (IL = [C ₂ mim][MeSO ₄])	$d\log\sigma/d\phi_R$	R (IL = [C ₂ mim][EtSO ₄])	$d\log\sigma/d\phi_R$
1.5424	0.1970	1.5424	0.2714
3.0849	0.1716	3.0849	0.2028
4.6273	0.1358	4.6273	0.1593
6.1697	0.1092	6.1697	0.1645
7.7121	0.0853	7.7121	0.0822
9.2546	0.0685	9.2546	0.0241
10.7970	0.0595	10.7970	0.0283

Table A76. The $d\log\sigma/dR$ for CTAB/1-butanol/cyclohexane/[C₂mim][MeSO₄] and CTAB/1-butanol/cyclohexane/[C₄mim][MeSO₄] microemulsions as a function of R at 25 °C.

R (IL = [C ₂ mim][MeSO ₄])	$d\log\sigma/d\phi_R$	R (IL = [C ₄ mim][MeSO ₄])	$d\log\sigma/d\phi_R$
1.5424	0.1970	1.5424	0.2646
3.0849	0.1716	3.0849	0.2061
4.6273	0.1358	4.3680	0.0940
6.1697	0.1092	6.1697	0.0718
7.7121	0.0853	7.2800	0.1372
9.2546	0.0685	8.7359	0.0879
10.7970	0.0595	10.1918	0.0045

Table A77. Diameter of droplets for CTAB/1-butanol/cyclohexane/ [C₂mim][MeSO₄] and CTAB/1-butanol/cyclohexane/[C₂mim][EtSO₄] microemulsions as a function of R at 25 °C.

R (IL = [C ₂ mim][MeSO ₄])	d (nm)	R (IL = [C ₂ mim][EtSO ₄])	d (nm)
1.5400	1.8200	1.5400	3.6200
3.0800	2.6900	3.0800	3.7500
4.6300	3.6800	4.6300	3.7700
6.1700	4.9500	6.1700	5.2500
7.7100	6.3000		
9.2500	9.0400		

Table A78. Diameter of droplets for CTAB/1-butanol/cyclohexane/[C₂mim][MeSO₄], CTAB/1-butanol/cyclohexane/[C₄mim][MeSO₄] microemulsions as a function of R at 25 °C.

R (IL = [C ₂ mim][MeSO ₄])	d (nm)	R (IL = [C ₄ mim][MeSO ₄])	d (nm)
1.5400	1.8200	3.0800	3.6200
3.0800	2.6900	4.6300	4.1900
4.6300	3.6800	6.1700	6.5000
6.1700	4.9500	7.7100	8.7200
7.7100	6.3000	9.2500	13.5400
9.2500	9.0400		

Table A79. The η for TX-100/cyclohexane/[C₂mim][EtSO₄], TX-100/[C₂mim][TFSI]/water and TX-100/cyclohexane/water microemulsions as a function of R or W_o at 25 °C.

R for [C ₂ mim][EtSO ₄] based microemulsion	η (mPa s)	W_o for [C ₂ mim][TFSI] based microemulsion	η (mPa s)	W_o for conventional microemulsion	η (mPa s)
0.2255	124.5400	12.2614	323.1100	0.2255	32.2780
0.4510	175.6400	11.2404	289.2890	0.5600	37.6460
0.5600	196.9000	9.9697	258.8800	0.7400	52.1180
0.6765	235.5300	8.9428	242.3300	0.9020	53.4470
0.7400	253.1000	7.9179	240.3900	1.6901	54.4490
0.9020	281.3300	5.4715	228.1800	2.4781	68.4920
1.1275	373.5400	5.0731	234.4500	3.7172	90.8840
		2.7041	262.4000	4.9562	125.9800
				5.5758	134.7600
				6.1953	149.1000
				13.2010	477.9800
				13.9661	542.3700
				14.3085	551.9500
				14.6431	569.5500
				14.7444	594.3200

Table A80. The ρ for TX-100/cyclohexane/[C₂mim][EtSO₄], TX-100/[C₂mim][TFSI]/water, and TX-100/cyclohexane/water microemulsions as a function of R or W_o at 25 °C.

R for [C ₂ mim][EtSO ₄] based microemulsion	ρ (g cm ⁻³)	W_o for [C ₂ mim][TFSI] based microemulsion	ρ (g cm ⁻³)	W_o for conventional microemulsion	ρ (g cm ⁻³)
0.2255	0.9859	12.2614	1.0793	0.2255	0.9581
0.4510	1.0167	11.2404	1.0887	0.5600	0.9616
0.5600	1.0299	9.9697	1.0969	0.7400	0.9720
0.6765	1.0494	8.9428	1.1043	0.9020	0.9722
0.7400	1.0577	7.9179	1.1130	1.6901	0.9735
0.9020	1.0796	5.4715	1.1254	2.4781	0.9742
1.1275	1.1124	5.0731	1.1354	3.7172	0.9839
		2.7041	1.1535	4.9562	0.9981
				5.5758	1.0014
				6.1953	1.0082
				13.2010	1.0550
				13.9661	1.0561
				14.3085	1.0575
				14.6431	1.0579
				14.7444	1.0587

Table A81. The n for TX-100/cyclohexane/[C₂mim][EtSO₄], TX-100/[C₂mim][TFSI]/water, and TX-100/cyclohexane/water microemulsions as a function of R or W_o at 25 °C.

R for [C ₂ mim][EtSO ₄] based microemulsion	n	W_o for [C ₂ mim][TFSI] based microemulsion	n	W_o for conventional microemulsion	n
0.2255	1.4813	12.2614	1.4508	0.2255	1.4711
0.4510	1.4825	11.2404	1.4545	0.5600	1.4697
0.5600	1.4799	9.9697	1.4553	0.7400	1.4665
0.6765	1.4842	8.9428	1.4572	0.9020	1.4669
0.7400	1.4848	7.9179	1.4601	1.6901	1.4651
0.9020	1.4851	5.4715	1.4622	2.4781	1.4631
1.1275	1.4863	5.0731	1.4656	3.7172	1.4630
		2.7041	1.4694	4.9562	1.4630
				5.5758	1.4598
				6.1953	1.4589
				13.2010	1.4498
				13.9661	1.4473
				14.3085	1.4468
				14.6431	1.4459
				14.7444	1.4453

Table A82. The η for CTAB/1-butanol/cyclohexane/[C₂mim][EtSO₄] and CTAB/1-butanol/cyclohexane/water microemulsions as a function of R or W_o at 25 °C.

R for [C ₂ mim][EtSO ₄] based microemulsion	η (mPa s)	W_o for conventional microemulsion	η (mPa s)
1.5424	2.1121	0.5424	1.6906
3.0849	2.6281	4.6273	1.7001
4.6273	3.1216	7.7121	1.7058
6.1697	4.2497	10.7970	1.8030
7.7121	5.4389	13.8818	1.8430
9.2546	6.2267	16.9667	1.9000
10.7970	10.1030	20.0515	1.9400
13.8818	10.6505	304.0000	2.3531
		305.0000	3.1568
		307.0000	2.5008
		309.0000	2.1590

Table A83. The ρ for CTAB/1-butanol/cyclohexane/[C₂mim][EtSO₄] and CTAB/1-butanol/cyclohexane/water microemulsions as a function of R or W_o at 25 °C.

R for [C ₂ mim][EtSO ₄] based microemulsion	ρ (g cm ⁻³)	W_o for conventional microemulsion	ρ (g cm ⁻³)
1.5424	0.8146	0.5424	0.7983
3.0849	0.8310	4.6273	0.7994
4.6273	0.8471	7.7121	0.8006
6.1697	0.8664	10.7970	0.8025
7.7121	0.8942	13.8818	0.8047
9.2546	0.9081	16.9667	0.8062
10.7970	0.9566	20.0515	0.8075
		304.0000	0.9709
		305.0000	0.9712
		307.0000	0.9717
		309.0000	0.9721

Table A84. The n for CTAB/1-butanol/cyclohexane/[C₂mim][EtSO₄] and CTAB/1-butanol/cyclohexane/water microemulsions as a function of R or W_o at 25 °C.

R for [C ₂ mim][EtSO ₄] based microemulsion	n	W_o for conventional microemulsion	n
1.5424	1.4147	0.5424	1.4064
3.0849	1.4172	4.6273	1.4098
4.6273	1.4192	7.7121	1.4069
6.1697	1.4225	10.7970	1.4054
7.7121	1.4288	13.8818	1.4064
9.2546	1.4292	16.9667	1.4070
10.7970	1.4345	20.0515	1.4049
		304.0000	1.3521
		305.0000	1.3531
		307.0000	1.3521
		309.0000	1.3506

Table A85. The σ for TX-100/cyclohexane/[C₂mim][EtSO₄] and CTAB/1-butanol/cyclohexane/[C₂mim][EtSO₄] microemulsions as a function of R at 25 °C.

R for TX-100 based microemulsions	σ ($\mu\text{S cm}^{-1}$)	R for CTAB based microemulsions	σ ($\mu\text{S cm}^{-1}$)
0.2255	38.7000	1.5424	0.2010
0.4510	99.4000	3.0849	0.5270
0.5600	128.9000	4.6273	0.8490
0.6765	159.4000	6.1697	1.6340
0.7400	180.5000	7.7121	2.7300
0.9020	232.0000	9.2546	2.9300
1.1275	271.0000	10.7970	3.2400

Table A86. The η for TX-100/cyclohexane/[C₂mim][EtSO₄] and CTAB/1-butanol/cyclohexane/[C₂mim][EtSO₄] microemulsions as a function of R at 25 °C.

R for TX-100 based microemulsions	η (mPa s)	R for CTAB based microemulsions	η (mPa s)
0.2255	124.5400	1.5424	2.1121
0.4510	175.6400	3.0849	2.6281
0.5600	196.9000	4.6273	3.1216
0.6765	235.5300	6.1697	4.2497
0.7400	253.1000	7.7121	5.4389
0.9020	281.3300	9.2546	6.2267
1.1275	373.5400	10.7970	10.1030
		13.8818	10.6505

Table A87. The ρ for TX-100/cyclohexane/[C₂mim][EtSO₄] and CTAB/1-butanol/cyclohexane/[C₂mim][EtSO₄] microemulsions as a function of R at 25 °C.

R for TX-100 based microemulsions	ρ (g cm ⁻³)	R for CTAB based microemulsions	ρ (g cm ⁻³)
0.2255	0.9859	1.5424	0.8146
0.4510	1.0167	3.0849	0.8310
0.5600	1.0299	4.6273	0.8471
0.6765	1.0494	6.1697	0.8664
0.7400	1.0577	7.7121	0.8942
0.9020	1.0796	9.2546	0.9081
1.1275	1.1124	10.7970	0.9566

Table A88. The n for TX-100/cyclohexane/[C₂mim][EtSO₄] and CTAB/1-butanol/cyclohexane/[C₂mim][EtSO₄] microemulsions as a function of R at 25 °C.

R for TX-100 based microemulsions	n	R for CTAB based microemulsions	n
0.2255	1.4813	1.5424	1.4147
0.4510	1.4825	3.0849	1.4172
0.5600	1.4799	4.6273	1.4192
0.6765	1.4842	6.1697	1.4225
0.7400	1.4848	7.7121	1.4288
0.9020	1.4851	9.2546	1.4292
1.1275	1.4863	10.7970	1.4345

Table A89. The v as a function of [p -NPB] for lipase catalyzed hydrolysis of p -NPB in aqueous medium.

[p -NPB] (mM)	v (mgmL ⁻¹ min ⁻¹)
1.3900	0.0170
3.0700	0.0265
10.8700	0.0625
21.8400	0.0417
32.0500	0.0290
43.2000	0.0230
54.3500	0.0263

Table A90. The v as a function of W_o lipase catalyzed hydrolysis of *p*-NPB in conventional microemulsions.

W_o	v (mgmL ⁻¹ min ⁻¹)
2.5000	0.0005
3.2000	0.0014
4.2000	0.0061
4.9600	0.0290

Table A91. The v as a function of W_o of the lipase catalyzed hydrolysis of *p*-NPB in IL microemulsions.

W_o	v (mg mL ⁻¹ min ⁻¹)
4.2000	0.1285
3.2000	0.0070
2.4800	0.0045

Table A92. The v for aqueous medium and conventional microemulsions as a function of W_o .

	v (mg mL ⁻¹ min ⁻¹)	W_o	v (mg mL ⁻¹ min ⁻¹)
Aqueous medium	0.0625	4.9600	0.0290
		4.2000	0.0061
		3.2000	0.0014
		2.5000	0.0005

Table A93. The v for conventional and IL microemulsions as a function of W_o .

W_o (conventional microemulsion)	v (mg mL ⁻¹ min ⁻¹)	W_o (IL microemulsion)	v (mg mL ⁻¹ min ⁻¹)
4.9600	0.0290	4.2000	0.1285
4.2000	0.0061	3.2000	0.0070
3.2000	0.0014	2.5000	0.0045
2.5000	0.0005		

Table A94. The v for aqueous medium, conventional and IL microemulsions as a function of W_o .

	v (mg mL ⁻¹ min ⁻¹)	W_o (conventional microemulsion)	v (mgmL ⁻¹ min ⁻¹)	W_o (IL microemulsion)	v (mg mL ⁻¹ min ⁻¹)
Aqueous medium	0.0625	4.9600	0.0290	4.2000	0.1285
		4.2000	0.0061	3.2000	0.0070
		3.2000	0.0014	2.5000	0.0045
		2.5000	0.0005		

List of Publications

1. **Shaila Alam**, M. Yousuf Ali Mollah, M. Muhibur Rahman, Md. Abu Bin Hasan Susan, "*Mechanism of Electrical Percolation of Ionic Liquid-in-Oil Microemulsions of CTAB with the Variation of Cations and Anions of Ionic Liquids*", in preparation.
2. **Shaila Alam**, M. Yousuf Ali Mollah, M. Muhibur Rahman, Md. Abu Bin Hasan Susan, "*Comparative Study of Physicochemical Properties of Hydrophilic Ionic Liquid Based Microemulsions of TX-100 with the Variation of Cations and Anions of Ionic Liquids through Electrical Percolation*", in preparation.
3. **Shaila Alam**, M. Yousuf Ali Mollah, M. Muhibur Rahman, Md. Abu Bin Hasan Susan, "*Comparative Study of Physicochemical Properties of Hydrophobic Ionic Liquid Based Microemulsions of TX-100 with the Variation of Cations and Anions of Ionic Liquids through Electrical Percolation*", in preparation.
4. **Shaila Alam**, M. Yousuf Ali Mollah, M. Muhibur Rahman, Md. Abu Bin Hasan Susan, "*Comparative Study of Physicochemical Properties of 1-Ethyl-3 Methylimidazolium Ethyl Sulfate Based Microemulsions with TX-100 and CTAB* ", in preparation.
5. **Shaila Alam**, M. Yousuf Ali Mollah, M. Muhibur Rahman, Md. Abu Bin Hasan Susan, "*Comparative Study of Physicochemical Properties of Conventional, 1-Ethyl-3 Methylimidazolium Ethyl Sulfate and 1-Ethyl-3-Methylimidazolium Bis(trifluoromethylsulfonyl)imide Based Microemulsions with TX-100* ", in preparation.
6. **Shaila Alam**, M. Yousuf Ali Mollah, M. Muhibur Rahman, Md. Abu Bin Hasan Susan, "*Comparative Study of Physicochemical Properties of Conventional and 1-Ethyl-3 Methylimidazolium Ethyl Sulfate Based Microemulsions with CTAB* ", in preparation.

List of Attended Seminars

1. Seminar on Supramolecular systems, organized by the Higher Education Quality Enhancement Project (HEQEP) of the University Grants Commission of Bangladesh, November 15, 2012, Department of Chemistry, University of Dhaka, Bangladesh
2. Bangladesh Chemical Congress, December 07-09, 2012, Dhaka, Bangladesh
3. Seminar on Electrochemistry for Material Science, organized by the Higher Education Quality Enhancement Project (HEQEP) of the University Grants Commission of Bangladesh, December 10, 2012, Department of Chemistry, University of Dhaka, Bangladesh
4. International Bose Conference, February 04, 2013, Dhaka, Bangladesh
5. 19th Conference of Islamic World Academy of Sciences, May 06-10, 2013 in Dhaka, Bangladesh
6. Seminar on *Air Quality and Its Consequence: Bangladesh Perspective*, organized by Establishing Air Quality Monitoring Centre (CP-2196), Dhaka, Bangladesh, 28 December, 2013.

7. Seminar on *Tandem Mass Spectrometry and its Application for Analysis of Chemical Contaminants in Food Stuff*, Dhaka, Bangladesh, 02 June, 2015.
8. Seminar on *3D Gel Printer and Future Life Innovation*, organized by the Material Chemistry Research Laboratory, Department of Chemistry, University of Dhaka, Dhaka, 30 August, 2015.
9. Seminar on *New Trophological States of Quantum Matter*, organized by Bose Centre for Advanced Study and Research in Natural Sciences, University of Dhaka, Dhaka, 25 November, 2015.
10. Seminar on *New Insight into the Chemistry on Carbon Nanotubes and Graphene Oxide and Boron Oxide Nanotubes*, organized by Department of Microbiology, University of Dhaka, Dhaka, 10 December, 2015.

List of Workshops Attended

1. Preparation and Characterization of Novel Functional Materials with Emphasis on Electrochemistry, Dhaka, Bangladesh, 12 February, 2012.
2. Black Carbon Emission from Brick Kilns in Bangladesh, Department of Chemistry, University of Dhaka, 16 November, 2014.

Abstracts Published as Contribution in the Scientific Meetings

1. **Shaila Alam**, M. Yousuf Ali Mollah, Md. Abu Bin Hasan Susan, *Structural Studies of 1-Butyl-3-methylimidazolium Hexafluorophosphate/TX-100/Water Ionic Liquid Microemulsions*, 37th Annual Conference of Bangladesh Chemical Society (ACBCS), Comilla University, Comilla, Bangladesh, 11 April, 2015. (Oral presentation)
2. **Shaila Alam**, M. Yousuf Ali Mollah, Md. Abu Bin Hasan Susan, *Analysis of Microregions in Cyclohexane/Triton X-100/Hydrophilic Ionic Liquid Microemulsions by Percolation Theory*, 2nd International Bose Conference, Dhaka, Bangladesh, 3-4 December 2015. (Oral presentation)
3. **Shaila Alam**, M. Yousuf Ali Mollah, Md. Abu Bin Hasan Susan, *Analysis of Microregions in Water/Triton X-100/Hydrophobic Ionic Liquid Microemulsions by Percolation Theory*, 16th Assian Chemical Congress (16 ACC), Dhaka, Bangladesh, 16-19 March, 2016. (Oral presentation)
4. **Shaila Alam**, M. Yousuf Ali Mollah, Md. Abu Bin Hasan Susan, *Analysis of Microregions of a Cationic Surfactant Based Microemulsions with the Variation of the Structure of Ionic Liquids*, 1st Symposium on Chemistry for Global Solidarity, Jagannath University, Dhaka, Bangladesh, 02 September, 2016. (Oral presentation)